Main Group and Transition Metal Complexes Supported by Multidentate Tripodal Ligands that Feature Nitrogen, Oxygen and Sulfur Donors: Synthesis, Structural Characterization and Applications

Yi Rong

Submitted in partial fulfillment of the
requirements for the degree of
Doctor of Philosophy
in the Graduate School of Arts and Sciences

COLUMBIA UNIVERSITY
2014

ABSTRACT

Main Group and Transition Metal Complexes Supported by Multidentate Tripodal Ligands that Feature Nitrogen, Oxygen and Sulfur Donors: Synthesis, Structural Characterization and Applications

Yi Rong

Chapter 1 focuses on the computational study of $Zr(CH_2Ph)_4$ and chapter 2 discusses synthesis, characterization and density functional study of 2-imidazolethione. Chapters 3 – 6 describe the synthesis, structural characterization several multidentate tripodal ligands, namely *tris*(mercaptoimidazolyl)-hydroborato ligand, [Tm^R], *tris*(2-pyridylseleno)methyl ligand, [Tpsem], *bis*(2-pyridonyl)(pyridine-2-yloxy)methyl ligand, [*O*-poBpom] and allyl-*tris*(3-t-butylpyrazolyl)borato ligand, [allylTp^{Bu^t}], and their application to main group and transition metals.

Chapter 1 describes the analysis of a monoclinic modification of $Zr(CH_2Ph)_4$ by single crystal X–ray diffraction, which reveals that the Zr–CH_2–Ph bond angles in this compound span a range of 25.1° that is much larger than previously observed for the orthorhombic form (12.1°). In accord with this large range, density functional theory calculations demonstrate that little energy is required to perturb the Zr–CH_2–Ph bond angles in this compound. Furthermore, density functional theory calculations on Me_3ZrCH_2Ph indicate that bending of the Zr–CH_2–Ph moiety in the monobenzyl compound is also facile, thereby demonstrating that a benzyl ligand attached to zirconium is intrinsically flexible, such that its bending does not require a buffering effect involving another benzyl ligand.

Chapter 2 describes the structure of 1-t-butyl-1,3-dihydro-2*H*-benzimidazole-2-thione which has been determined by X-ray diffraction. The compound exists in the chalcogenone form instead of chalcogenol form, which is similar to its oxo and selone counterparts. Comparison of 2-imidazolone, 2-imidazolethione and 2-imidazoleselone compounds shows that two N–C–E bond angles in the chalcogenone forms are not symmetric, and the differences between the two angles decrease in the sequence of Se > S > O. This trend can be reproduced by density functional theory calculations. Additionally, H(mbenzim$^{Bu^t}$) has intermolecular hydrogen bonding interactions, whereas its selenium counterpart does not. The C–E bond lengths of 2-imidazolone, 2-imidazolethione and 2-imidazoleselone compounds are intermediate between those of formal C–E single and double bonds, which is in accord with the notion that zwitterionic structures that feature single C^+–E^- dative covalent bonds provide an important contribution in such molecules. Furthermore, NBO analysis of the bonding in H(*x*im$^{Bu^t}$) derivatives demonstrates that the doubly bonded C=E resonance structure is most significant for the oxygen derivative, whereas singly bonded C^+–E^- resonance structures dominate for the tellurium derivative. This result appears to be counterintuitive, based on the fact that it opposes the trend that one would expect on the basis of electronegativity difference, however, studies on XC(E)NH_2 derivatives provide solid support for it. In this regard, the C~E bonding in these compounds is significantly different to that in chalcogenoformaldehyde derivatives for which the bonding is well represented by a H_2C=E double bonded resonance structure.

Chapter 3 describes the computational study on [Tm^{MeBenz}] anion and the synthesis and characterization of [Tm$^{Bu^tBenz}$]Na, [Tm$^{Bu^tBenz}$]Tl and [Tm$^{Bu^tBenz}$]Tl. It is worth noting that the two thallium compounds are the first structurally characterized monovalent monomeric [Tm^R]Tl complexes.

Chapter 4 describes the synthesis and characterization of a few [Tm^{R}]M (M = Ti, Zr, Hf) complexes, including (*i*) Cp[Tm^{Bu^t}]$TiCl_2$ and Cp[Tm^{Bu^t}]$ZrCl_2$, which are analogues of Cp_2TiCl_2 and Cp_2ZrCl_2; (*ii*) [Tm^{Bu^t}]$Zr(CH_2Ph)_3$ and (*iii*) [Tm^{Bu^t}]$Hf(CH_2Ph)_3$ and [Tm^{Ad}]$Hf(CH_2Ph)_3$, which are the first structurally characterized [Tm^{R}]Hf complexes.

Chapter 5 describes two multidentate, L_3X type ligands, which feature [CN_3] and [CNO_2] donors, namely *tris*(2-pyridylseleno)methane, [Tpsem]H, and *bis*(2-pyridonyl)(pyridin-2-yloxy)methane, [*O*-poBpom]H. They have been synthesized, characterized, and employed in the synthesis of zinc and cadmium complexes. Specifically, [Tpsem]H has been employed to synthesize the *bis*(trimethylsilyl)amido zinc complex, [κ^3-Tpsem]$ZnN(SiMe_3)_2$. The latter compound provides access to a variety of other [Tpsem]ZnX derivatives, which include the isocyanate complex [κ^4-Tpsem]ZnNCO, the hydrosulfido complex [κ^3-Tpsem]ZnSH, the sulfido complex {[κ^3-Tpsem]Zn}$_2$(μ–S), the 2:1 complex [κ^2-Tpsem]$_2$Zn and the pyridyl-2-selenolate complex [κ^4-Tpsem]Zn(κ^2–SeC_6H_4N), thereby demonstrating that the [Tpsem] ligand can exhibit κ^2-, κ^3- and κ^4-coordination modes. Variable temperature ^{1}H NMR spectroscopic studies demonstrate that [κ^3-Tpsem]$ZnN(SiMe_3)_2$, [κ^3-Tpsem]ZnSH and {[κ^3-Tpsem]Zn}$_2$(μ–S) are fluxional on the NMR timescale. Similarly, [*O*-poBpom]H has been employed to synthesize the *bis*(trimethylsilyl)amido zinc complex, [κ^4-*O*-poBpom]$ZnN(SiMe_3)_2$, and the *bis*(trimethylsilyl)amido cadmium complex, [κ^4-*O*-poBpom]$CdN(SiMe_3)_2$. Both structures were characterized by X-ray diffraction, which demonstrate a new [CNO_2] coordination environment.

Chapter 6 describes the synthesis and structural characterization of a new [Tp] ligand featuring an allyl substituent on the central boron atom, namely [allylTp$^{Bu^t}$]Li is reported. The compound reacts steadily with CH_3CH_2SH under 350 nm UV light *via* a thiol-ene click reaction. The resulting

$[CH_3CH_2S(CH_2)_3Tp^{Bu^t}]Li$ complex can further react with metal halide. For example, the reaction of $[CH_3CH_2S(CH_2)_3Tp^{Bu^t}]Li$ with ZnI_2 produced $[CH_3CH_2S(CH_2)_3Tp^{Bu^t}]ZnI$ at room temperature. This study provides a simple model on the immobilization of [Tp] metal complexes to the polymer chains with –SH terminals.

TABLE OF CONTENTS

LIST OF FIGURES

accompanied by an increased interaction with the phenyl group, while increasing the angle is accompanied by the formation of agostic interactions with the CH_2 group. The geometries have approximate Cs symmetry such that at acute angles the benzyl ligand approaches η^4 rather than η^3 coordination.

LIST OF TABLES

LIST OF SCHEMES

ACKNOWLEDGEMENTS

First, I would like to thank Professor Gerard Parkin, for his mentorship and enthusiasm and for him giving me the opportunity to do research in his group. I always feel lucky to be in his group for my graduate study. Ged is a great advisor and one of the smartest people I have known. He has taught me about X-ray crystallography and Schlenk techniques when I first joined the group. He always gave good suggestions and encouraged me to explore different areas. In addition, he gave me the opportunities to be in charge of our important activities outside of lab. I have been fortunate to have Ged as my guide during the past five years. Many thanks, Professor Parkin!

Next, I would like to thank my Graduate Committee for their great help throughout the phases of my graduate study. Professor Jack Norton has been supportive as my graduate committee and thesis defense chair. In addition, it is a fun experience to be your teaching assistant. Professor Jonathan Owen has served on my graduate committee and my thesis defense committee. Professor Nicholas Turro served on my committee and gave valuable feedback during my second-year report. I also would like to thank Professor Roberto Sánchez-Delgado and Professor Jun Shin for taking the time to read my thesis and serve on my thesis defense committee.

Now it is time for our excellent twin brothers, Wesley Sattler and Aaron Sattler. They are the best graduate students I have ever met. During the four years when we worked together, they taught me everything they know about research and answered lots of my questions with patience. They are my best friends and families in US. I wish them good luck in their career!

Many thanks to the Parkin Group members for the support and help during my graduate study and for editing my thesis. In particular, I would like to thank

Ahmed Al-Harbi, without whom, I cannot learn so many computer skills. Ahmed is of great personality and always ready to help both inside and outside of lab. We have worked together a lot and he is a chemist with lots of new ideas. Thank you to Ashley Zuzek, for the help of synthesizing selenolpyridine and Neena Chakrabarti and Ava Kreider-Mueller for all the pleasant conversations about chemistry and life. I wish the three girls good luck in finishing up at school! Julia Oktawiec, our undergraduate student, has been such a wonderful desk-mate and a friend. Dr. Kevin Yurkerwich, Dr. Joshua Palmer, Serge Ruccolo and and Michelle Neary are all supportive labmates. Wish everyone in Parkin Group all the best.

I also would like to thank technical and administrative staff members in this department. Specifically, thank Dr. John Decatur and Michael Appel, for their help with solid state NMR spectroscopy; Dr. Yushiro Itagaki for assistance with mass spectroscopy; Dr. Calman Lobel for the help with computational work; Dr. Steffen Jockush and Dr. Yongjun Li for the photochemistry experiments; Jeffrey Lancaster for the help with Mendeley. Jay Kirschenbaum, Robert Rutherford, Christopher Cecillio, Daniel Lugo and Bill Reynolds have also been important members for maintenance of lab and our packages. In addition, I would like to thank Alix Lamia, Dani Farrell and Carlos Garcia for facilitating administrative tasks.

I would like to acknowledge the U.S. National Science Foundation, the U.S. Department of Energy (Office of Basic Energy Sciences) and the United Technologies Research Center (Department of Energy ARPA-E program) for supporting portions of the research described in this thesis.

Finally, I would like to thank my family. I thank my parents for their endless support and love. They are always there providing the encouragement, direction and driving force to me. I also thank Lai Jiang for his positive attitude

and support during my graduate study. The people I love have made me recognize my five years graduate experience as a wonderful one of learning and growth.

For my parents

CHAPTER 1

Highly Variable Zr–CH_2–Ph Bond Angles in Tetrabenzylzirconium: Analysis of Benzyl Ligand Coordination Modes

Table of Contents

Reproduced in part from:

Rong, Y.; Al-Harbi, A.; Parkin, G. *Organometallics* **2012**, *31*, 8208–8217.

1.1 Introduction

1.1.1 Coordination Modes of Benzyl Ligands towards Transition Metals

Benzyl ligands can coordinate to transition metal centers in a manifold of ways (Figure 1). In addition to η^1–coordination, η^2, η^3, η^4, and η^7–coordination modes, which feature interactions *via* the phenyl group, have also been discussed in literature.[1] It is worth noting that although there are no η^5–benzyl compounds listed in the Cambridge Structural Database (CSD),[2] pentamethyl $CH_2C_6Me_5$ counterparts are known.[3] The coordination mode of a benzyl ligand has influences not only on the intrinsic reactivity of the M–CH_2Ph bond but also on the reactivity associated with other sites in the molecule, being a non-innocent "spectator".

1.1.2 Different Coordination Modes of Benzyl Ligands in $Zr(CH_2Ph)_4$

Tetrabenzylzirconium has been widely used as a precursor towards the synthesis of a variety of zirconium derivatives since its first report in 1969.[4] Most of the benzyl zirconium complexes have found practical application as olefin polymerization catalysts.[5,6,7,8] For example, $[Zr(CH_2Ph)_3]^+[B(CH_2Ph)(C_6F_5)_3]^-$, formed by the reaction between $Zr(CH_2Ph)_4$ and $B(C_6F_5)_3$ was identified as the first non-metallocene ionic complex, which functions as a single site olefin polymerization catalyst.[9]

In the previously reported crystal structure of $Zr(CH_2Ph)_4$, the four benzyl ligands exhibit different coordination modes,[10] with Zr–C–C bond angles that range from 87.0(3)° to 99.1(3)°.[10a] However, researcher Ahmed Al-Harbi in our

group was able to obtain another crystalline form, in which the molecule exhibits an even greater range of Zr–C–C bond angles, from 81.6(1)° to 106.7(2)°.

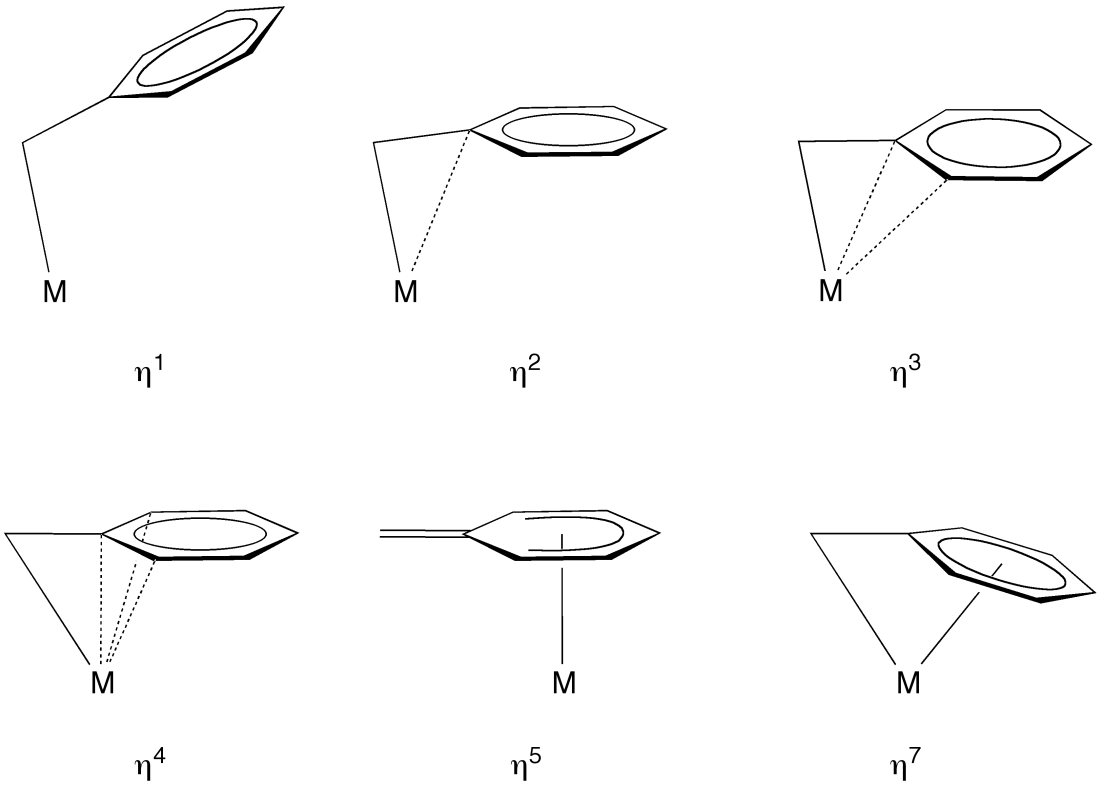

Figure 1. Benzyl ligand coordination modes discussed in the literature.

To understand the influences of the benzyl group coordination mode, we have applied density functional theory calculations to evaluate the energy required to perturb the Zr–CH_2–Ph bond angles in $Zr(CH_2Ph)_4$ and $Me_3Zr(CH_2Ph)$. In addition, we have also analyzed the occurrence of the various types of benzyl coordination modes using Cambridge Structural Database.

1.2 Comparison of Two Different Crystalline Forms of $Zr(CH_2Ph)_4$

Previous X-ray diffraction studies have revealed that $Zr(CH_2Ph)_4$ exists as orthorhombic crystals, with space group *Pbca*. However, the compound obtained

by Ahmed Al-Harbi was in a monoclinic crystalline form. The crystal data of two different forms are summarized in Table 1 and the monoclinic $Zr(CH_2Ph)_4$ structure has been characterized by X-ray diffraction and solved by Ahmed Al-Harbi.[11]

Table 1. Crystallographic data for polymorphs of $Zr(CH_2Ph)_4$.

Reference	10a	10b,c	this work[a]
Crystallization method	*n*–heptane at –25˚C	toluene at –25˚C	toluene at room temperature
lattice	orthorhombic	orthorhombic	monoclinic
space group	*Pbca*	*Pbca*	$P2_1$
a/Å	16.387(1)	19.945(6)	10.2238(10)
b/Å	20.022(1)	13.716(7)	9.6635(9)
c/Å	13.758(6)	16.306(5)	11.2356(11)
α/˚	90	90	90
β/˚	90	90	101.295(1)
γ/˚	90	90	90
V/Å^3	4514(2)	4461	1088.6(2)
d/g cm^{-3}	1.341	1.36	1.390
Temp/K	293(2)	233	150(2)

(a) crystal structural data are from Ahmed Al-Harbi's work.

The monoclinic structure differs from the previously reported orthorhombic structure in some significant ways. First, the conformation of the benzyl ligands in orthorhombic $Zr(CH_2Ph)_4$ are arranged as to give an approximate S_4 molecular symmetry while the molecular structure of the monoclinic one deviates

significantly from this high symmetry and idealized geometry, as illustrated in Figure 2. The two features that eliminate the S_4 symmetry in the monoclinic structure are: (*i*) one of the benzyl ligands points away from the zirconium center in a direction which destroys the C_2 axis and (*ii*) the dihedral angle between the two [C–Zr–C] planes, which contain the axis that corresponds most closely to a molecular S_4 axis, is reduced from 90˚ to 69˚.[12] Secondly, the zirconium–benzyl interactions in the two polymorphs are also different as supported by metrical data in Table 2. The Zr–CH_2–Ph bond angles of the monoclinic form span a range of 25.1˚, whereas those in the orthorhombic form only span a range of 12.1˚. Furthermore, monoclinic $Zr(CH_2Ph)_4$ exhibits Zr–CH_2–Ph bond angles that are both more acute (81.6˚) and more obtuse (106.7˚) than the observed for the orthorhombic form, for which the four Zr–CH_2–Ph bond angles fall into the region of 87.0˚ – 99.1˚.

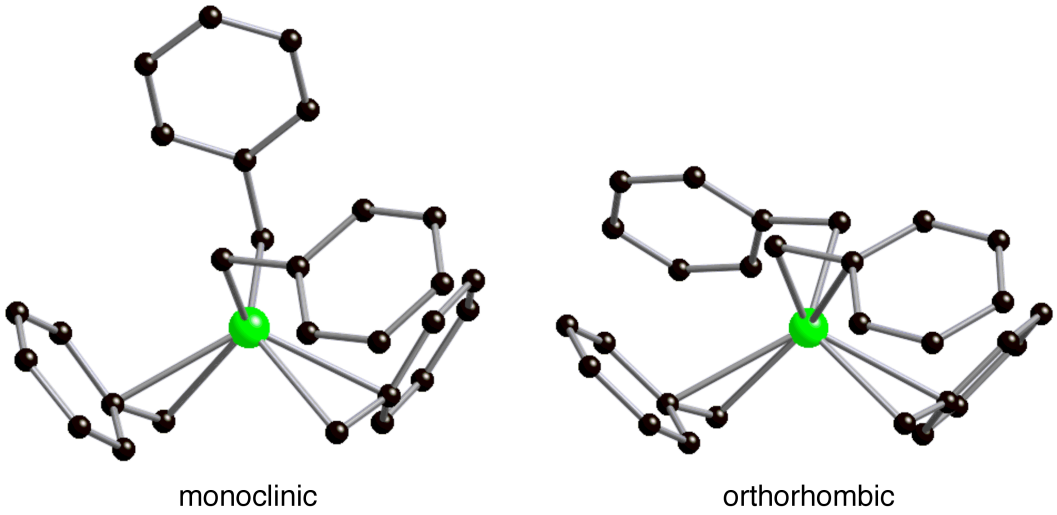

Figure 2. Comparison of the molecular structure of monoclinic (left) and orthorhombic (right) forms of $Zr(CH_2Ph)_4$. Hydrogen atoms omitted for clarity.

Table 2. Metrical data for polymorphs of $Zr(CH_2Ph)_4$.

	Zr–CH_2–Ph/°	**Zr–CH_2/Å**	**Zr···C_{ipso}/Å**	**Zr···$C_{ortho\text{-}short}$/Å**	**Zr···$C_{ortho\text{-}long}$/Å**	**δ_{ipso}/Å**	**$\delta_{ortho(short)}$/Å**	**$\delta_{ortho(long)}$/Å**
Monoclinic[a]								
C11	81.63(14)	2.270(2)	2.509(2)	3.022(2)	3.089(2)	0.24	0.75	0.82
C21	82.36(13)	2.278(2)	2.533(2)	2.969(3)	3.174(2)	0.26	0.69	0.90
C31	98.67(15)	2.262(3)	2.873(2)	3.472(2)	3.628(2)	0.61	1.21	1.37
C41	106.73(15)	2.2929(19)	3.063(2)	3.774(2)	3.820(2)	0.77	1.48	1.53
Orthorhombic[b]								
C1	87.0(3)	2.259(5)	2.614(4)	3.072(5)	3.347(6)	0.36	0.81	1.09
C2	90.2(3)	2.248(5)	2.684(4)	3.249(4)	3.361(5)	0.44	1.00	1.11
C3	93.9(3)	2.255(5)	2.773(3)	3.298(5)	3.535(4)	0.52	1.04	1.28
C4	99.1(3)	2.258(4)	2.879(4)	3.519(5)	3.589(6)	0.62	1.26	1.33

(a) Ahmed Al-Harbi's work

(b) reference 10a

1.3 Classification of Benzyl Ligands in $Zr(CH_2Ph)_4$: Criteria for Identifying the Benzyl Ligand Coordination Mode

1.3.1 Basic Considerations

Using M–CH_2–Ph bond angle, one can distinguish whether a benzyl ligand coordinates in an η^1 manner (with an idealized value of 109.5°) or an η^x manner ($x > 1$). However, differentiation between the various expanded hapticities requires analysis of the M•••C distances involving carbons from the phenyl group.[1a,b,10a] As the hapticity increases, the *ipso*, *ortho*, *meta* and *para* carbon atoms approach the metal center thus it is reasonable to compare the M•••C_{ipso}, M•••C_{ortho}, M•••C_{meta} and M•••C_{para} distances relative to the M–CH_2 bond length, *i.e.* δ_{ipso}, δ_{ortho}, δ_{meta}, and δ_{para} (Figure 3), an approach that has been reported by Andersen and co-workers.[1a]

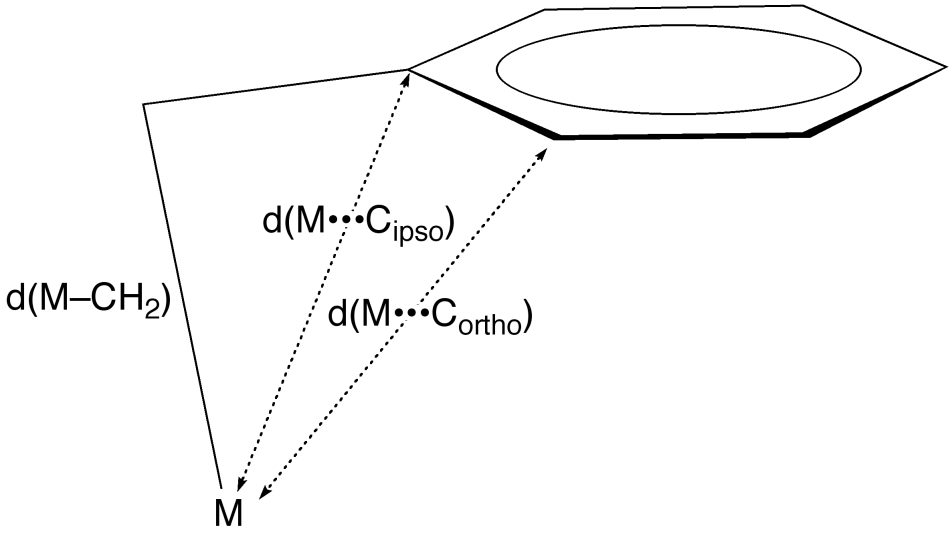

$$\delta_{ipso} = d(M\bullet\bullet\bullet C_{ipso}) - d(M–CH_2)$$

$$\delta_{ortho} = d(M\bullet\bullet\bullet C_{ortho}) - d(M–CH_2)$$

Figure 3. Definition of δ_{ipso} and δ_{ortho}.

1.3.2 Idealized Situations

To better interpret the defined values on classifying the coordination mode of a benzyl ligand, it is pertinent to consider some idealized situations (Table 3). In the case of η^1– coordination, an idealized M–CH_2–Ph tetrahedral angle is 109.5°, which is characterized by a δ_{ipso} value of 0.84 Å, while an η^2–benzyl ligand with a M–CH_2–Ph angle of 90.0° is characterized by a δ_{ipso} value of 0.44 Å. An idealized η^3–benzyl ligand has the M–CH_2–Ph angle < 90.0° and *one* of the *ortho* carbon atoms approaches the metal center within a distance that is comparable to that of the methylene carbon, *i.e.* δ_{ipso} and $\delta_{ortho(short)}$ have values of 0.0 Å while the other *ortho* carbon atom has a non–zero value for $\delta_{ortho(long)}$. An idealized η^4–benzyl ligand requires *both* δ_{ortho} values to be 0.0 Å, similarly in an idealized η^7–benzyl ligand situation, where all δ_{meta} and δ_{para} values are required to be 0.0 Å.

It should be noted that the classification of the coordination modes of benzyl ligand in a compound is, nevertheless, a subjective issue. For example, in a brief examination of literature, one can find that a compound with a M–CH_2–Ph angle as small as 97.1° has been classified as η^1,[13] while a compound with a M–CH_2–Ph angle as large as 97.5° has been classified as η^2.[14,15] However, all other compounds listed in the Cambridge Structural Database that have been assigned η^2-benzyl coordination have M–CH_2–Ph angles less than 97°.[16]

Table 3. Metrical data for selected benzyl ligand coordination modes.

	M–CH_2–Ph/°	**δ_{ipso}/Å**	**$\delta_{ortho(short)}$/Å**	**$\delta_{ortho(long)}$/Å**	**$\delta_{meta(short)}$/Å**	**$\delta_{meta(long)}$/Å**	**δ_{para}/Å**	**Notes**
η^1	109.5	0.84	0.85 – 1.58	1.58 – 2.21	2.20 – 2.75	2.75 –3.23	3.24	a
η^2	90.0	0.44	1.10	1.10	2.14	2.14	2.57	b
η^2	97.0	0.59	1.27	1.27	2.36	2.36	2.81	c
η^3	69.3	0	0	1.14	1.14	1.96	1.96	d
η^4	57.4	-0.42	0	0	0.69	0.69	0.98	e
η^7	62.1	-0.30	-0.12	-0.10	-0.03	-0.02	-0.10	f

(a) Derived values for an idealized value of M–CH_2–Ph = 109.5° obtained by using the CSD average values of *d*(M–CH_2Ph) = 2.195 Å and *d*(CH_2–C_{ipso}) = 1.483 Å for η^1-benzyl compounds. The range for δ_{ortho} and δ_{meta} correspond to rotation about the C–Ph bond.

(b) Derived values for an idealized value of M–CH_2–Ph = 90.0° obtained by obtained using the CSD average value of *d*(M–CH_2Ph) = 2.300 Å for η^2-benzyl compounds and *d*(CH_2–C_{ipso}) = 1.483 Å. Values for δ_{ortho} and δ_{meta} are for a M–C–C–C torsion angle of 90°.

(Cont.)

(c) Derived values for a value of M–CH_2–Ph = 97.0° obtained by obtained using the CSD average value of d(M–CH_2Ph) = 2.300 Å for η^2-benzyl compounds and d(CH_2–C_{ipso}) = 1.483 Å. Values for δ_{ortho} and δ_{meta} are for a M–C–C–C torsion angle of 90°.

(d) Derived values obtained assuming that d(M–CH_2Ph) = 2.090 Å, which is the average of known η^3 compounds, and that d(M–CH_2Ph) = d(M–$C_{ortho(short)}$).

(e) Derived values obtained assuming a d(M–CH_2Ph) = 2.653 Å, corresponding to that in the only known η^7 compound and that d(M–CH_2Ph) = d(M–$C_{ortho(short)}$) = d(M–$C_{ortho(long)}$).

(f) Values listed are for the only structurally reported η^7 compound.

1.3.3 Proposed Criteria

In order to classify better the benzyl coordination modes, we propose criteria listed in Table 4. These criteria are based on examination of the majority of compounds with benzyl ligands reported in literature, but it should be noted that such distinctions have little meaning at the borderline.

Specifically, compounds with M–CH_2–Ph bond angles ≤ 97° are classified as η^2 coordination. Those with values of $\delta_{ortho(short)} \leq 0.5$ Å have an η^3-benzyl group coordinated. The value of 0.5 Å was obtained based on the fact that the Zr–arene bond lengths[17] may be up to *ca*. 0.5 Å longer than the mean Zr–CH_2Ph bond length for compounds listed in the Cambridge Structural Database. η^4-benzyl coordination mode is distinguishable by possessing values of $\delta_{ipso} \leq 0.0$ Å. Criteria for higher coordination modes, *i.e.* η^5- to η^7-benzyl coordination, are not listed in Table 4 since such cases are rare and not enough data have been reported.

Table 4. Criteria for assigning benzyl ligand coordination modes.

	M–CH_2–Ph / °	δ_{ipso} / Å	$\delta_{ortho(short)}$ / Å	$\delta_{ortho(long)}$ / Å
η^1	> 97°	> 0.5	–	–
η^2	≤ 97°	≤ 0.5	–	–
η^3	≤ 97°	≤ 0.5	≤ 0.5	> 0.5
η^4	<< 90	< 0.0	≤ 0.5	≤ 0.5

1.3.4 Distribution Analysis of Known M-CH_2-Ph Compounds

To determine the distribution of reported M-CH_2-Ph, an analysis was performed. A plot of M–CH_2–Ph bond angle *versus* $\delta_{ortho(short)}$ (Figure 4) illustrates the

regions that correspond to η^1, η^2 and η^3 benzyl coordination modes, and examples of compounds that belong to these classes are provided in Table 5. [18–33]

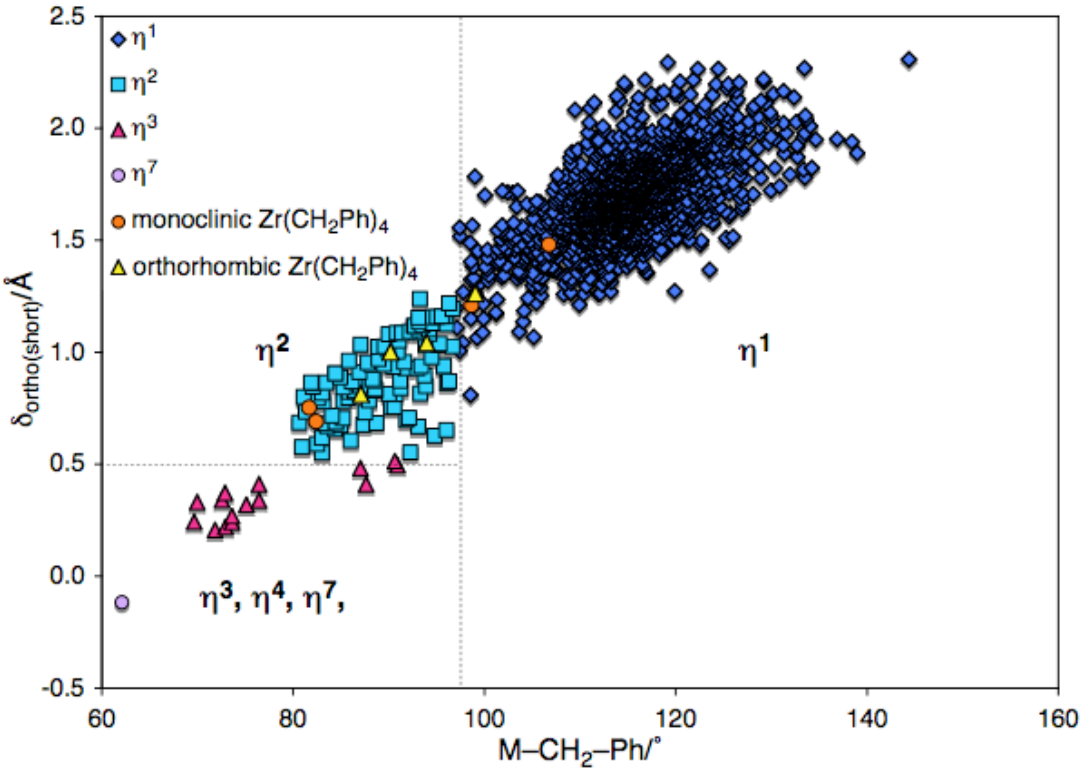

Figure 4. Classification of benzyl ligands according to M–CH_2–Ph bond angle and δ_{ortho}. η^1-coordination (92.9 %) is the most prevalent, followed by η^2 (6.1 %), η^3 (0.9 %) and η^7 (0.1 %).

Table 5. Examples of benzyl compounds classified according to their coordination mode (note that compounds with multiple benzyl ligands have an entry for each structurally different benzyl ligand).

Compound	M–CH_2–Ph	δ_{ipso}/Å	$\delta_{ortho(short)}$/Å	$\delta_{ortho(long)}$/Å	Ref.
η^1					
(η^2-3,5-Me_2Pz)$_2$Zr(η^1-CH_2Ph)(η^2-CH_2Ph)	97.1	0.59	1.11	1.39	13
[OONO]Zr(η^1–CH_2Ph)$_2$	98.6	0.62	1.19	1.41	15
[η^3–MeC(NC_7H_6)CHC(N-*p*-Tol)Me]Zr(η^1-CH_2Ph)(η^2-CH_2Ph)	99.6	0.64	1.31	1.35	21
{[2,6-$CH_2N(C_6F_5)$]$_2$$NC_5H_3$}$_2$Zr($\eta^1$–$CH_2$Ph)($\eta^2$–$CH_2$Ph)	104.2	0.73	1.19	1.69	19
[η^2–N(CHMePh)(PPh_2)]Zr(η^1–CH_2Ph)$_2$(η^2–CH_2Ph)	108.3	0.80	1.26	1.78	20
[NNO]Zr(η^1–CH_2Ph)(η^2–CH_2Ph)	106.7	0.77	1.37	1.61	16c
[η^2–N(CHMePh)(PPh_2)]Zr(η^1–CH_2Ph)$_2$(η^2–CH_2Ph)	115.8	0.94	1.67	1.74	20
(pyCMe_2O)$_2$Zr(η^1–CH_2Ph)(η^2–CH_2Ph)	116.6	0.95	1.61	1.81	16d

(Cont.)

$(Cp^{1,2,4\text{-}Bu^t_3})CeCH_2Ph$	130.4	1.12	1.82	2.03	35
$Tp^*Zr(\eta^1\text{-}CH_2Ph)_3$	144.4	1.31	2.02	2.31	18
η^2					
$[\eta^2\text{–}N(CHMePh)(PPh_2)]Zr(\eta^1\text{–}CH_2Ph)_2(\eta^2\text{–}CH_2Ph)$	82.5	0.25	0.59	0.99	20
$Cp^*Mo(NO)(CH_2SiMe_3)(\eta^2\text{–}CH_2Ph)$	83.0	0.29	0.82	0.98	1d
$[\eta^3\text{–}MeC(NC_7H_6)CHC(N\text{-}p\text{-}Tol)Me]Zr(\eta^1\text{-}CH_2Ph)(\eta^2\text{-}CH_2Ph)$	83.6	0.28	0.67	0.98	21
$Cp^*Th(\eta^2\text{–}CH_2Ph)_3$	84.1	0.25	0.72	0.97	23
$[Cp_2Zr(CH_3CN)(\eta^2\text{-}CH_2Ph)][(BPh_4]$	84.4	0.31	0.91	0.93	22
$\{[2,6\text{–}CH_2N(C_6F_5)]_2NC_5H_3\}_2Zr(\eta^1\text{–}CH_2Ph)(\eta^2\text{–}CH_2Ph)$	84.5	0.31	0.69	1.04	19
$Cp^*U(\eta^2\text{–}CH_2Ph)_3$	85.4	0.29	0.88	0.95	24
$Cp^*Th(\eta^2\text{–}CH_2Ph)_3$	85.8	0.31	0.80	0.92	23
$Cp^*U(\eta^2\text{–}CH_2Ph)_3$	87.1	0.32	0.89	0.97	24
$Cp^*U(\eta^2\text{–}CH_2Ph)_3$	87.3	0.34	0.90	0.94	24

(Cont.)					
$Cp^*Th(\eta^2–CH_2Ph)_3$	90.3	0.40	0.75	1.25	23
$(Cp^{1,2,4\text{-}Bu^t_3})CeCH_2Ph$	93.1	0.44	0.67	1.41	35
(Cont.)					
$[NNO]Zr(\eta^1–CH_2Ph)(\eta^2–CH_2Ph)$	95.8	0.55	0.94	1.47	16c
$(pyCMe_2O)_2Zr(\eta^1–CH_2Ph)(\eta^2–CH_2Ph)$	96.1	0.55	1.13	1.31	16d
η^3					
$Ni(PMe_3)(\eta^1–CH_2Ph)(\eta^3–CH_2Ph)$	69.7	0.02	0.24	0.82	30
$Ni(PMe_3)(\eta^1–CH_2Ph)(\eta^3–CH_2Ph)$	70.0	0.03	0.33	0.76	30
$\{\kappa^2–C,N–(Ar)N=C(Me)C(CH_2)[OB(C_6F_5)_3]\}Ni(\eta^3–CH_2Ph)$ (Ar = 2,6-$Pr^i_2C_6H_3$)	71.8	0.07	0.21	0.98	32
$[\kappa^2–P,O–2–P(Cy)_2–4–Me–C_6H_3(SO_3)]Ni(\eta^3–CH_2Ph)$	72.6	0.10	0.34	0.94	33
$[P(OCH_3)_3]_3Co(\eta^3–CH_2Ph)$	72.9	0.08	0.37	1.01	27
$[Pr^i_2P(CH_2)_3PPr^i_2]Rh(\eta^3–CH_2Ph)$	72.9	0.06	0.22	0.95	28

(Cont.)

[κ²–P,C–2–P(2–OMePh)₂–4–Me–C₆H₃(SO₃)]Ni(η³–CH₂Ph)	73.6	0.12	0.24	1.09	33
[κ²-N,O-PhC(O)C₆H₄N=C(Ph)OB(C₆F₅)₃]Ni(η³-CH₂Ph)	75.1	0.17	0.32	1.00	31
{[NH(Me)CH₂CH₂(η⁵–C₅H₄)] (CO)Re(η³–CH₂Ph)}⁺ReO₄⁻	76.4	0.14	0.34	1.01	26
(NHC-2,6-Prⁱ₂-C₆H₃)(CF₃SO₃)Ni (η³-CH₂Ph)	76.4	0.20	0.41	1.13	29
[Cp*Zr(η³–CH₂Ph)(η⁷–CH₂Ph)][B(CH₂Ph)(C₆F₅)₃]	87.7	0.36	0.41	1.44	1f
[(Me₃Si)₂NC(NCy)₂]₂Er(η³–CH₂Ph)	90.6	0.38	0.51	1.39	24
[(Me₃Si)₂NC(NCy)₂]₂Y(η³–CH₂Ph)	90.9	0.41	0.50	1.49	24
η⁷					
[Cp*Zr(η³–CH₂Ph)(η⁷–CH₂Ph)][B(CH₂Ph)(C₆F₅)₃]	62.1	-0.30	-0.12	-0.10	1f

Among all of these coordination modes, η^1 is the most prevalent (92.9 %), followed by η^2 (6.1 %) and η^3 (0.9 %). η^4-Benzyl coordination requires small values for both $\delta_{ortho(short)}$ and $\delta_{ortho(long)}$. Interestingly, despite the fact that η^4-benzyl complexes are frequently considered in literature,[1,10a] there are no benzyl compounds listed in the Cambridge Structural Database that can be clearly assigned such a coordination mode according to the criteria listed in Table 4. Therefore the η^3-compound that most closely approaches η^4-coordination listed in the Cambridge Structural Database is $Me_3PNi(CH_2Ph)_2$, for which $\delta_{ortho(short)} = 0.33$ Å and $\delta_{ortho(long)} = 0.76$ Å.[30] There is only one structure with values of both $\delta_{ortho(short)}$ and $\delta_{ortho(long)} < 0.5$ Å that is reported in Cambridge Structural Database (Figure 5), which is an η^7-benzyl complex $[Cp^*Zr(CH_2Ph)_2]^+$.[1f]

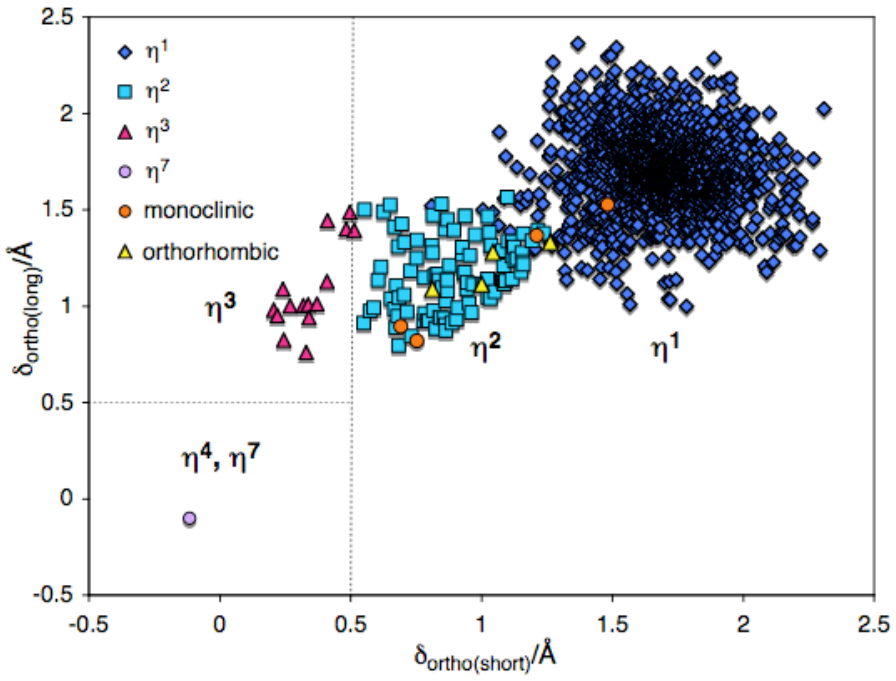

Figure 5. Classification of benzyl ligands according to $\delta_{ortho(short)}$ and $\delta_{ortho(long)}$

1.3.5 Classification of Benzyl Ligands in $Zr(CH_2Ph)_4$

In the monoclinic form of $Zr(CH_2Ph)_4$, two of the benzyl ligands are coordinated in an η^1–manner, while two are coordinated in an η^2–manner (Table 2) according to the criteria listed in Table 4 and Figure 4. Specifically, the two η^1-benzyl ligands have obtuse Zr–CH_2–Ph angles of 98.7(2)˚ and 106.7(2)˚, while the two η^2-benzyl ligands have acute Zr–CH_2–Ph angles of 81.6(1)˚ and 82.4(1)˚ and values for $\delta_{ortho(short)}$ in the two η^2-benzyl ligands are 0.75 Å and 0.69 Å, which indicate there is little η^3-character associated with the interaction.

In the orthorhombic form of $Zr(CH_2Ph)_4$, only one of the benzyl ligands is coordinated in an η^1–manner with a Zr–CH_2–Ph angle of 99.1(3)˚ as illustrated in Figure 4, while the other three are coordinated in an η^2–manner with a Zr–CH_2–Ph angle of 87.0(3)˚, 90.2(3)˚, and 93.9(3)˚, respectively.

1.3.6 Flexibility of Benzyl Ligands in M-CH_2-Ph Compounds

It is worth noting that the flexibility of benzyl ligands is by no means restricted to $Zr(CH_2Ph)_4$. Examination of structurally characterized benzyl zirconium compounds shows that Zr–CH_2–Ph bond angles range from 62.1˚[1f] to 144.4˚.[18] Arnold and co-workers have reported that crystal packing forces are able to influence zirconium benzyl interactions. Specifically, the compound they studied $\{CyNC[N(SiMe_3)_2]NCy\}Zr(CH_2Ph)_3$ exists as two polymorphs with Zr–CH_2–Ph bond angles that span the ranges 88.7(4)˚ – 123.2(4)˚ and 104.6(2)˚ – 115.9(2)˚.[1g,34] Another particularly interesting example of the flexibility of the benzyl ligand is provided by the observation that $(Cp^{1,2,4\text{-}But_3})CeCH_2Ph$ exists with

two distinctly different geometries in the asymmetric unit, with Ce–CH_2–Ph angles of 93.1(4)° and 130.4(3)°.[35]

1.3.7 NMR Spectroscopic Study on $Zr(CH_2Ph)_4$

A solid-state NMR[36] spectroscopic study of $Zr(CH_2Ph)_4$ was carried out on a Bruker 400 Cyber-enabled Avance III spectrometer. The $^{13}C\{^1H\}$ NMR spectrum exhibits a 1:1:2 set of signals, rather than a singlet for the four methylene carbon atoms at 76.4, 74.2 and 70.9 ppm, respectively (Figure 6), which is consistent with the inequivalent nature of the benzyl ligands in the solid state structure of $Zr(CH_2Ph)_4$. However, in solution, the benzyl ligands are chemically equivalent on the NMR time-scale,[37] as illustrated in Figure 7 and Figure 8. According to reported spectroscopic data for benzyl ligands, η^1–coordination is associated with $\delta H_{ortho} > 6.5$, $\delta C_{ipso} \approx 150$, and $^1J_{C–H}$ for the CH_2 group of ≈ 120 Hz, while η^2–coordination is identified by $\delta H_{ortho} < 6.5$, $\delta C_{ipso} \approx 140$, and $^1J_{C–H}$ for the CH_2 group of ≈ 135 Hz.[38] In our case, $Zr(CH_2Ph)_4$ is characterized by $\delta H_{ortho} = 6.38$, $\delta C_{ipso} = 139.5$ and $^1J_{C–H} = 135$ for the CH_2 group, which support the presence of η^2–benzyl ligands. It is worth clarifying that although these values are in accord with the presence of some degree of η^2-benzyl coordination in solution, they do not distinguish between a situation in which the η^2-benzyl ligands are equivalent, and one in which the molecule is fluxional and exchange between η^2- and η^1-benzyl ligands is facile.[37a]

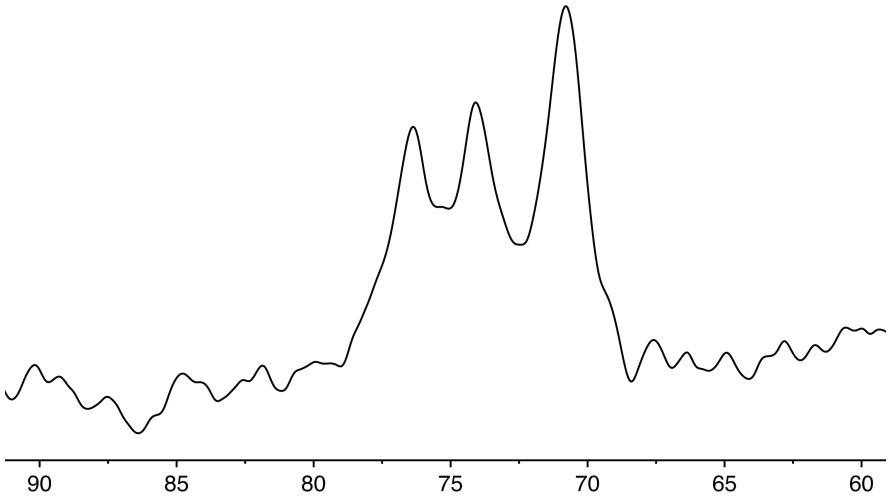

Figure 6. Solid state ^{13}C NMR spectrum of $Zr(CH_2Ph)_4$ (only methylene region is shown).

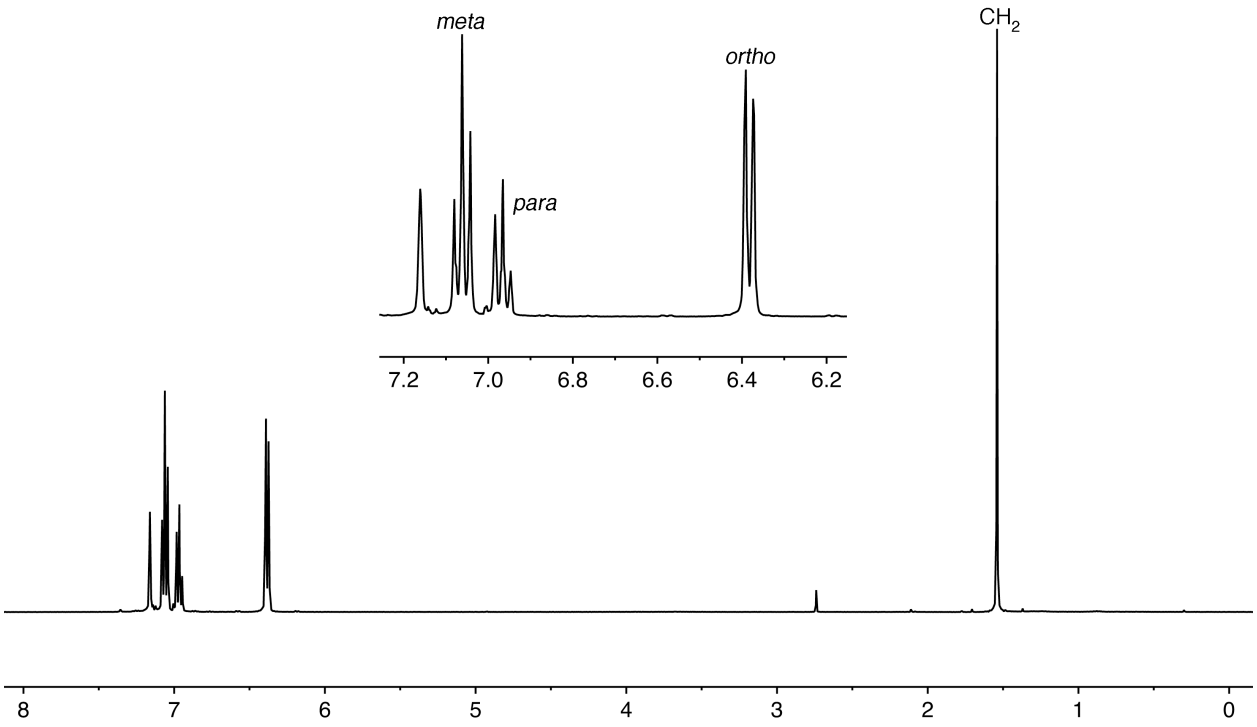

Figure 7. ^{1}H NMR spectrum of $Zr(CH_2Ph)_4$.

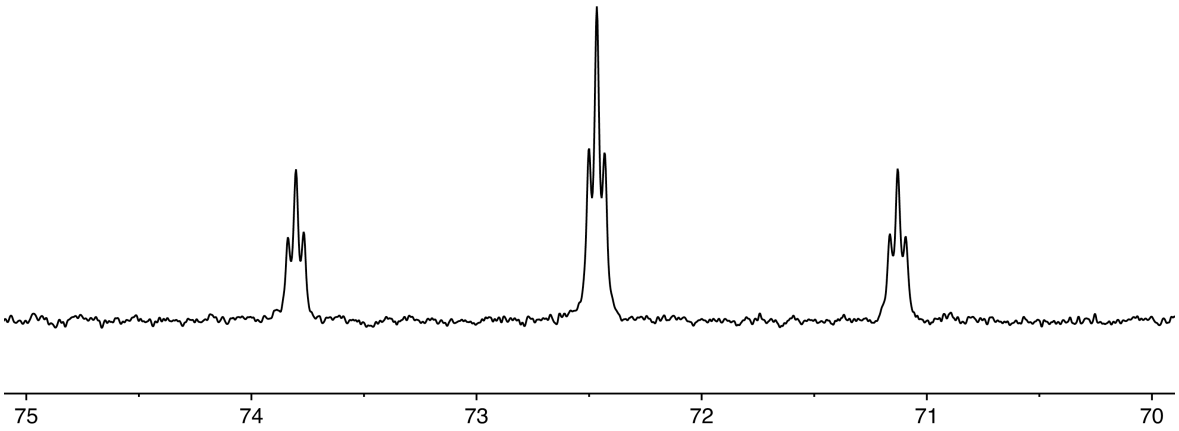

Figure 8. ^{13}C NMR spectrum of $Zr(CH_2Ph)_4$ (only methylene region is shown). $^{1}J_{C–H}$ = 135Hz, $^{3}J_{C–H_{ortho}}$ = 4 Hz.

1.4 Computational Evaluation of the Flexibility of Benzyl Ligands Attached to Zirconium

1.4.1 Density Functional Theory Study on $Zr(CH_2Ph)_4$

The molecular structure of $Zr(CH_2Ph)_4$ was studied using density functional theory geometry optimization calculations (B3LYP). To investigate the nature of $Zr(CH_2Ph)_4$ in the gas phase, the calculations were performed using *(i)* constrained Zr–CH_2–Ph bond angles that correspond to the monoclinic and orthorhombic structures, *(ii)* S_4 symmetry[39] and *(iii)* no constraints. The optimization results are significant. Specifically, despite the fact that the Zr–C–C angles vary significantly between the structures (Table 6), the energies of each of these geometry-optimized structures differ by less than 2 kcal mol^{-1} (Figure 9). The small difference in energies is consistent with the observation that in solid state, $Zr(CH_2Ph)_4$ could exist in two different ways.

Furthermore, the S_4 symmetric structure was geometry optimized subject to constraining one of the Zr–C–C bond angles to a series of values that range from 70˚ to 150˚. The results provide further significance of the energetic penalty associated with bending the Zr–C–C bonds. The data in Figure 10 and Table 7 indicates that changing one of the Zr–C–C bond angles would not exert a significant energetic penalty. As is presented in the data plot (Figure 10), the energy of the molecule fluctuates by < 1.5 kcal mol^{-1} over the range 85˚ –120˚. Also constraining one of the Zr–C–C bond angles to a specific value is accompanied by changes in the other benzyl ligands to accommodate the induced perturbation, as illustrated by the variation in the range of Zr–C–C bond angles for each structure (Table 6). For this reason, the energy profile is not characterized by a single minimum.

Table 6. Geometry optimized structures for $Zr(CH_2Ph)_4$.

	Zr–C–C/°	**Zr–C–C/°**	**Zr–C–C/°**	**Zr–C–C/°**	**Relative energy/ kcal mol^{-1}**
No constraints	87.7	87.9	105.1	106.1	0.00
S_4 symmetry	100.2	100.2	100.2	100.2	0.69
Monoclinic	81.7	82.4	98.6	106.7	1.04
Zr–CH_2–Ph angle constraints					
Orthorhombic	87.1	90.2	93.9	99.0	1.93
Zr–CH_2–Ph angle constraints					

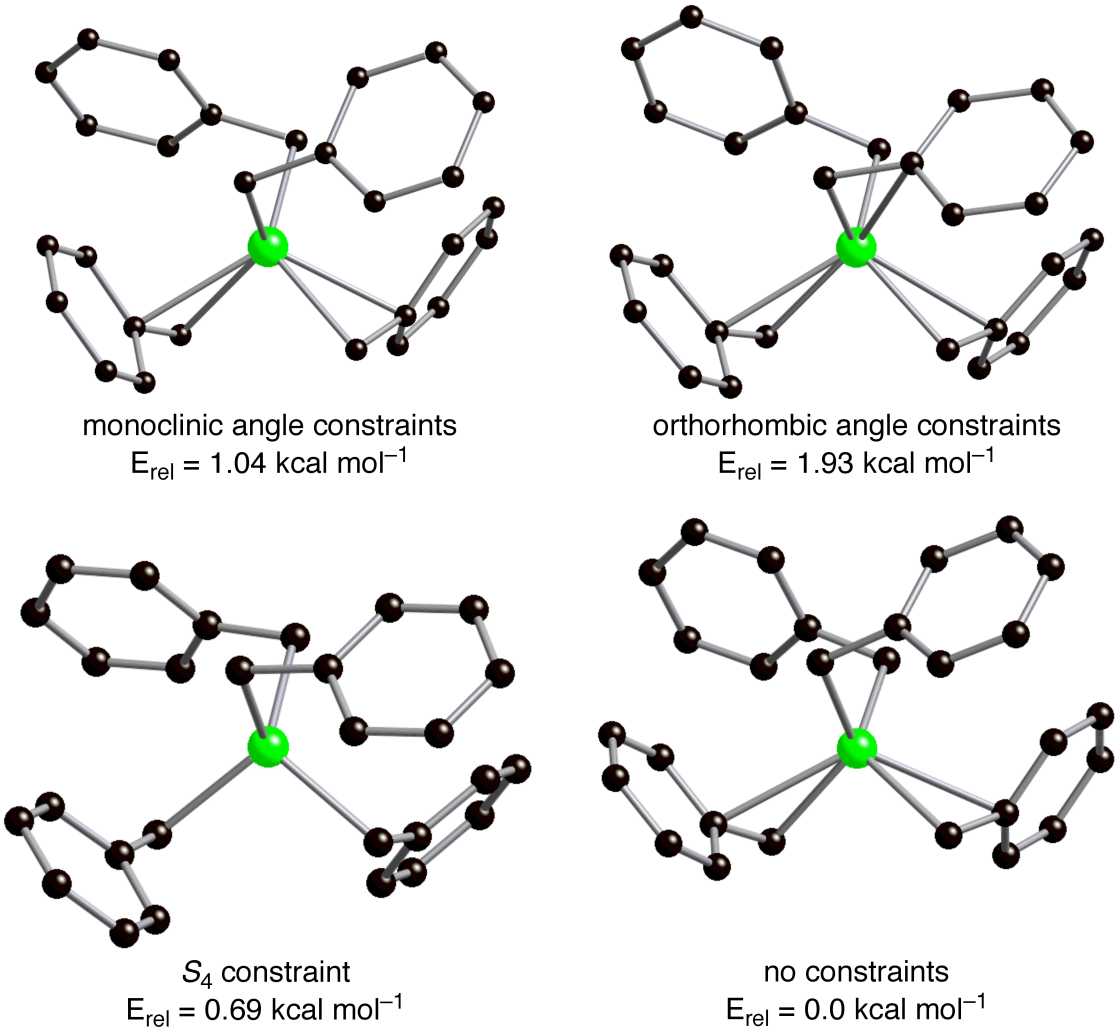

Figure 9. Geometry optimized structures of $Zr(CH_2Ph)_4$ subject to various constraints.

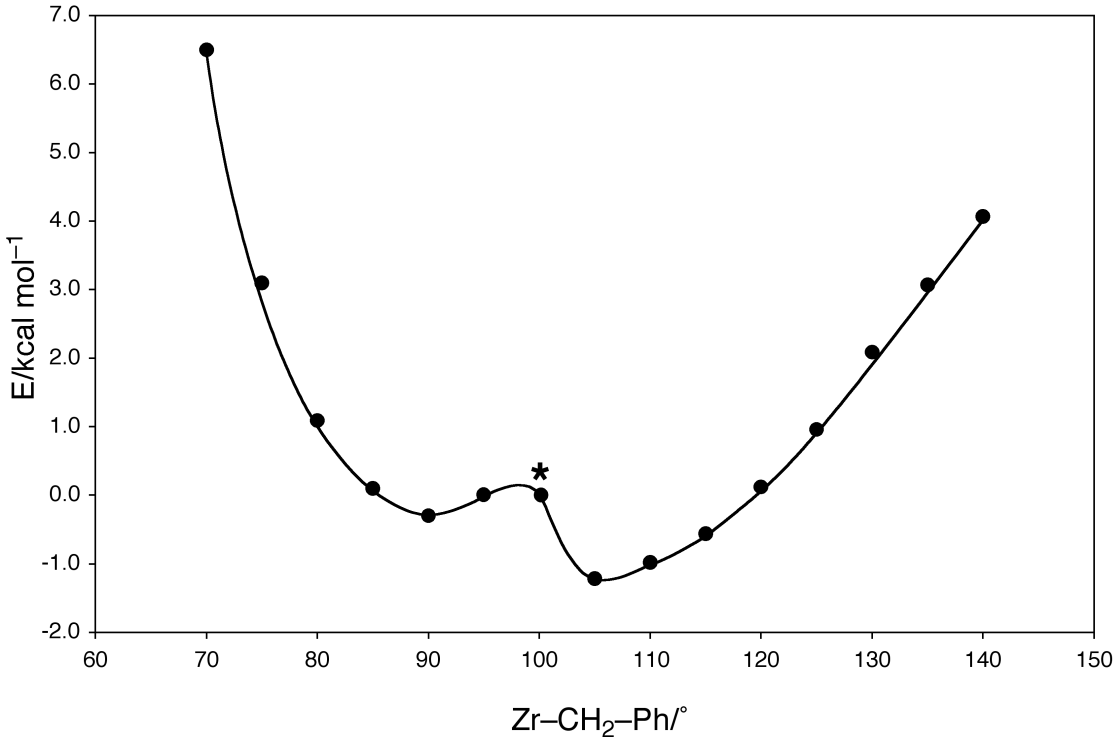

Figure 10. Variation in energy of $Zr(CH_2Ph)_4$ as a function of varying a single Zr–CH_2–Ph bond angle after allowing the geometry to re-optimize. The energies are relative to that of the S_4 constrained geometry, as indicated with an asterisk.

Table 7. Energy changes associated with bending the Zr–C–C angle of one of the benzyl ligands (#1) in $Zr(CH_2Ph)_4$.

Zr–C–C/° #1 constrained	Zr–C–C/° #2	Zr–C–C/° #3	Zr–C–C/° #4	Bond angle distribution/°	Bond angle range/°	Relative energy/ kcal mol^{-1}
70.0	93.4	104.3	106.8	70.0 – 106.8	36.8	6.50
75.0	93.3	105.4	105.8	75.0 – 105.8	30.8	3.10
80.0	93.4	106.4	105.3	80.0 – 106.4	26.4	1.09
85.0	94.0	109.0	104.8	85.0 – 109.0	24.0	0.10
90.0	93.8	109.3	104.6	90.0 – 109.3	19.3	-0.30
95.0	93.9	110.3	104.5	93.9 – 110.3	16.4	-0.09
100.0	93.4	111.5	104.2	93.4 – 111.5	18.1	0.31
100.2*	100.2*	100.2*	100.2*	100.2	0.0	0.00
105.0	105.7	88.0	87.5	87.5 – 105.7	18.2	-1.22
110.0	105.7	87.4	88.2	87.4 – 110.0	22.6	-0.98
115.0	105.3	86.2	88.8	86.2 – 115.0	28.8	-0.56
120.0	105.1	86.1	89.6	86.1 – 120.0	33.9	0.12

(Cont)

Zr–C–C/° #1 constrained	Zr–C–C/° #2	Zr–C–C/° #3	Zr–C–C/° #4	Bond angle distribution/°	Bond angle range/°	Relative energy/ kcal mol^{-1}
125.0	105.7	89.3	91.1	89.3 – 125.0	35.7	0.96
130.0	105.4	91.8	94.5	91.8 – 130.0	38.2	2.09
135.0	98.9	101.7	88.8	88.8 – 135.0	46.2	3.07
140.0	102.7	95.9	88.0	88.0 – 140.0	52.0	4.07

* Geometry optimized value when constrained to S_4 symmetry.

1.4.2 Density Functional Theory Study on Me_3ZrCH_2Ph

Density functional theory geometry optimizations were also performed on Me_3ZrCH_2Ph, with the purpose of eliminating the buffering effect provided by the other benzyl groups as in the case of $Zr(CH_2Ph)_4$. The energy of the molecule changes by less than 2 kcal mol^{-1} over the range of 80 – 125°, with the most stable geometry optimized structure possessing a Zr–C–C bond angle of 92.8°, as illustrated in Figure 11. Comparison of the calculations on Me_3ZrCH_2Ph and $Zr(CH_2Ph)_4$ shows that the flexibility of the benzyl ligands in $Zr(CH_2Ph)_4$ is not merely attributable to a buffering effect due to the presence of other benzyl ligands, but is intrinsic to the Zr–CH_2–Ph moiety. Specifically, the energy required to decrease the Zr–CH_2–Ph bond angle is compensated by interaction of the phenyl group with the electronically unsaturated zirconium center, while the energy required to increase the Zr–CH_2–Ph bond angle is compensated by the formation of agostic interactions with the methylene group,[40] as illustrated in Figure 12. Such interactions between metal center and benzyl ligand has been reported in literature. For example, in compound $Cp^*Ti(CH_2Ph)_3$, the large Ti–CH_2–Ph angle (139.0°) and short Ti•••H interactions (2.32 and 2.37 Å) for one of the benzyl ligands have been interpreted in terms of a double agostic interaction.[41] Furthermore, species with α-agostic interactions have also been proposed as intermediates in olefin polymerization catalyzed by $[Cp_2Zr(CH_2Ph)]^+$.[8k]

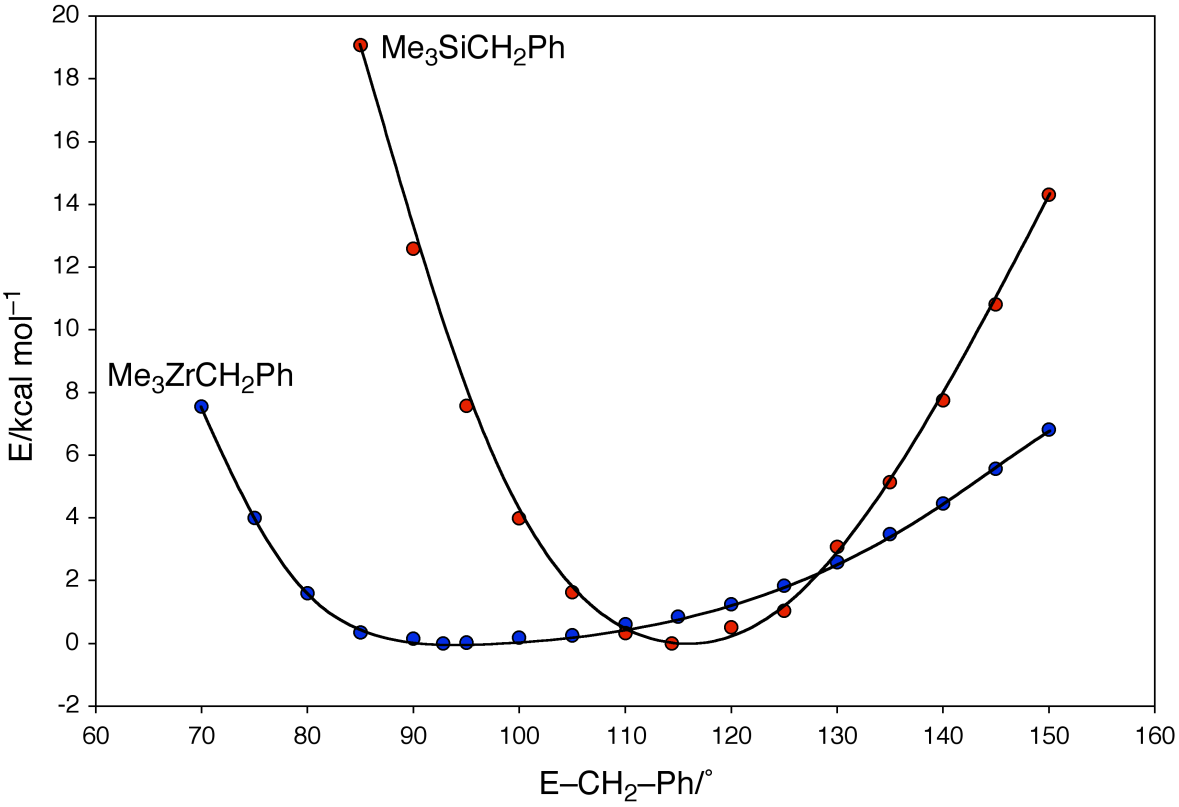

Figure 11. Variation in energy of Me_3ECH_2Ph as a function of the E–CH_2–Ph bond angle after allowing the geometry to re-optimize. (E = Zr, Si).

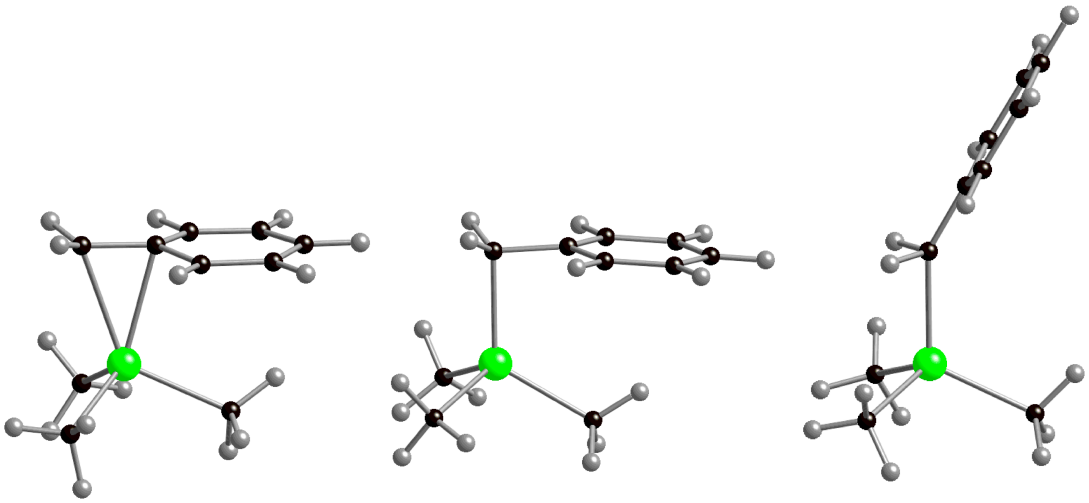

Figure 12. Geometry optimized structures of Me_3ZrCH_2Ph. Reducing the Zr–CH_2–Ph bond angle from that in the fully optimized structure (92.8°) is accompanied by an increased interaction with the phenyl group, while increasing the angle is accompanied by the formation of agostic interactions with the CH_2 group. The geometries have approximate C_s symmetry such that at acute angles the benzyl ligand approaches η^4 rather than η^3 coordination.

1.4.3 Density Functional Theory Study on Me_3SiCH_2Ph

To further understand if the secondary interactions with zirconium metal center are responsible for the flexibility of the benzyl ligand of Me_3ZrCH_2Ph, DFT geometry optimization calculations were carried out on the silicon counterpart, Me_3SiCH_2Ph. According to the literature, silicon does not form benzyl compounds with a very large range of Si–CH_2–Ph bond angles.[42,43] As presented in Figure 11, the Si–CH_2–Ph bond angle for the most stable structure (114.4°) is much larger than the corresponding value for the zirconium compound (92.8°). Furthermore, as

the Si–CH_2–Ph bond angle deviates from the most stable structure, the energy of the molecule increases substantially. Specifically, reducing the Si–CH_2–Ph bond angle to 85˚ increases the energy of the molecule by 19.1 kcal mol^{-1}, while increasing the angle to 150˚ increases the energy to 14.3 kcal mol^{-1}, both of which are much greater than the corresponding values of 0.4 kcal mol^{-1} and 6.8 kcal mol^{-1} for the zirconium system.

1.5 Summary and Conclusions

In summary, the monoclinic crystal form of $Zr(CH_2Ph)_4$ obtained by our group has Zr–CH_2–Ph bond angles that span a much larger range (25.1˚) than those previously reported in the literature for the orthorhombic form (12.1˚). In order to classify the coordination modes for benzyl ligands, we proposed the following criteria to distinguish the different coordination modes: (*i*) if M–CH_2–Ph bond angle ≥ 97˚, it is classified as η^1 coordination; (*ii*) if M–CH_2–Ph bond angle ≤ 97˚, and $\delta_{ortho(short)} \geq 0.5$ Å, the compound is identified as η^2 coordination; (*iii*) if M–CH_2–Ph bond angle ≤ 97˚, and $\delta_{ortho(short)} \leq 0.5$ Å, but $\delta_{ortho(long)} \geq 0.5$ Å the compound is identified as η^3 coordination; (*iv*) for compounds that do not meet any of the above criteria, they should be investigated case by case, since not much data have been reported to use as references. It should be noted that such distinctions have little meaning at the borderline but are based on examination of the majority of compounds with benzyl ligands reported in literature.

According to our proposed criteria, two of the benzyl ligands in the monoclinic form of $Zr(CH_2Ph)_4$ are coordinated in an η^1–manner and two are coordinated in an η^2–manner. In the orthorhombic form, three of the benzyl ligands are classified as η^1 coordination and one as η^2 coordination.

NMR spectroscopic studies of $Zr(CH_2Ph)_4$ were carried out in the solid state and in solution. The solid-state NMR exhibits a 1:1:2 set of peaks, which is consistent with the observation that the four benzyl ligands are chemically inequivalent in solid state. The solution $^{13}C\{^1H\}$ NMR spectrum shows one singlet, which indicates that all benzyl ligands are chemically equivalent on the NMR time-scale.

Density functional theory geometry optimization calculations demonstrate that little energy is required to perturb the Zr–CH_2–Ph bond angles in $Zr(CH_2Ph)_4$. Furthermore, bending of the Zr–CH_2–Ph moiety in the monobenzyl compound Me_3ZrCH_2Ph is facile, thereby demonstrating that a benzyl ligand attached to zirconium is intrinsically flexible, such that its bending does not require a buffering effect involving another benzyl ligand. This flexibility of the benzyl ligand could provide a means to protect a metal center during a catalytic transformation.[6,8k] Despite this flexibility, however, the majority of structurally characterized benzyl compounds features η^1–coordination modes with a prevalence of 92.9 %, followed by η^2 (6.1 %) and η^3 (0.9 %).

1.6 Experimental Section

1.6.1 General Considerations

All manipulations were performed using a combination of glovebox, high vacuum, and Schlenk techniques under an argon atmosphere unless otherwise specified.[44] Solvents were purified and degassed by using standard procedures. ^1H NMR spectra were measured on Bruker 400 Cyber-enabled Avance III and Bruker 500 DMX spectrometers. ^1H chemical shifts are reported in ppm relative to $SiMe_4$ ($\delta = 0$) and were referenced internally with respect to the protio solvent

impurity (δ 7.16 for C_6D_5H).[45] ^{13}C NMR spectra are reported in ppm relative to $SiMe_4$ (δ = 0) and were referenced internally with respect to the solvent (δ 128.06 for C_6D_6).[45] Coupling constants are given in hertz. Solid-state $^{13}C\{^1H\}$ NMR experiments were performed on a Bruker 400 Cyber-enabled Avance III at a field of 9.40 T (corresponding to a ^{13}C resonance frequency of 100.62 MHz) using the CP-MAS pulse sequence, with an acquisition time of 0.03 seconds and a spin rate of 10^4 Hz. Solid-state ^{13}C NMR spectra are reported in ppm relative to $SiMe_4$ (δ = 0) and were referenced externally to the methylene peak of adamantane (δ = 38.5).[46]

1.6.2 Computational Details

Calculations were carried out using DFT as implemented in the Jaguar 7.6 (release 110) suite of *ab initio* quantum chemistry programs.[47] Geometry optimizations were performed with the B3LYP density functional[48] using the 6-31G** (C, H and Si) and LACVP (Zr) basis sets.[49]

1.7 References and Notes

(1) (a) Edwards, P. G.; Andersen, R. A.; Zalkin, A. *Organometallics* **1984**, *3*, 293-298.

(b) Legzdins, P.; Jones, R. H.; Phillips, E. C.; Yee, V. C.; Trotter, J.; Einstein, F. W. B. *Organometallics* **1991**, *10*, 986-1002.

(c) Carmona, E.; Marin, J. M.; Paneque, M.; Poveda, M. L. *Organometallics* **1987**, *6*, 1757-1765.

(d) Dryden, N. H.; Legzdins, P.; Trotter, J.; Yee, V. C. *Organometallics* **1991**, *10*, 2857-2870.

(e) Scholz, J.; Rehbaum, F.; Thiele, K. H.; Goddard, R.; Betz, P.; Kruger, C. *J. Organomet. Chem.* **1993**, *443*, 93-99.

(f) Pellecchia, C.; Immirzi, A.; Pappalardo, D.; Peluso, A. *Organometallics* **1994**, *13*, 3773-3775.

(g) Giesbrecht, G. R.; Whitener, G. D.; Arnold, J. *Organometallics* **2000**, *19*, 2809-2812.

(2) Cambridge Structural Database (Version 5.33). *3D Search and Research Using the Cambridge Structural Database*, Allen, F. H.; Kennard, O. *Chemical Design Automation News* **1993**, *8* (1), pp 1 & 31-37.

(3) (a) Hamon, J. R.; Astruc, D.; Roman, E.; Batail, P.; Mayerle, J. J. *J. Am. Chem. Soc.* **1981**, *103*, 2431-2433.

(b) Moler, J. L.; Eyman, D. P.; Nielson, J. M.; Morken, A. M.; Schauer, S. J.; Synder, D. B. *Organometallics* **1993**, *12*, 3304-3315.

(4) (a) Zucchini, U.; Giannini, U.; Albizzati, E.; D'Angelo, R. *J. Chem. Soc. D, Chem. Commun.* **1969**, 1174-1175.

(b) Zucchini, U.; Albizzati, E.; Giannini, U. *J. Organomet. Chem.* **1971**, *26*, 357-372.

(5) Schrock, R. R.; Parshall, G. W. *Chem. Rev.* **1976**, *76*, 243-268.

(6) Pedeutour, J. N.; Radhakrishnan, K.; Cramail, H.; Deffieux, A. *Macromol. Rapid Commun.* **2001**, *22*, 1095-1123.

(7) (a) Morton, C.; Munslow, I. J.; Sanders, C. J.; Alcock, N. W.; Scott, P. *Organometallics* **1999**, *18*, 4608-4613.

(b) Gendler, S.; Segal, S.; Goldberg, I.; Goldschmidt, Z.; Kol, M. *Inorg. Chem.* **2006**, *45*, 4783-4790.

(c) Tonzetich, Z. J.; Schrock, R. R.; Hock, A. S.; Muller, P. *Organometallics* **2005**, *24*, 3335-3342.

(d) Turculet, L.; Tilley, T. D. *Organometallics* **2004**, *23*, 1542-1553.

(e) Covert, K. J.; Mayol, A. R.; Wolczanski, P. T. *Inorg. Chim. Acta* **1997**, *263*, 263-278.

(f) Scott, M. J.; Lippard, S. J. *Inorg. Chim. Acta* **1997**, *263*, 287-299.

(g) Lubben, T. V.; Wolczanski, P. T.; Vanduyne, G. D. *Organometallics* **1984**, *3*, 977-983.

(h) Felten, J. J.; Anderson, W. P. *J. Organomet. Chem.* **1972**, *36*, 87-92

(8) (a) Chen, C.; Lee, H.; Jordan, R. F. *Organometallics* **2010**, *29*, 5373-5381.

(b) Martin, A.; Uhrhammer, R.; Gardner, T. G.; Jordan, R. F.; Rogers, R. D. *Organometallics* **1998**, *17*, 382-397.

(c) Pellecchia, C.; Grassi, A.; Zambelli, A. *J. Mol Catal.* **1993**, *82*, 57-65.

(d) Pellecchia, C.; Grassi, A.; Immirzi, A. *J. Am. Chem. Soc.* **1993**, *115*, 1160-1162.

(e) Ahn, H.; Nicholas, C. P.; Marks, T. J. *Organometallics* **2002**, *21*, 1788-1806.

(f) Cohen, A.; Kopilov, J.; Goldberg, I.; Kol, M. *Organometallics* **2009**, *28*, 1391-1405.

(g) Cuomo, C.; Milione, S.; Grassi, A. *Macromol. Rapid Commun.* **2006**, *27*, 611-618.

(h) Gauvin, R. M.; Kress, J. *J. Mol. Catal. A-Chem.* **2002**, *182*, 411-417.

(i) Duchateau, R.; Abbenhuis, H. C. L.; van Santen, R. A.; Meetsma, A.; Thiele, S. K. H.; van Tol, M. F. H. *Organometallics* **1998**, *17*, 5663-5673.

(j) Chen, Y. X.; Fu, P. F.; Stern, C. L.; Marks, T. J. *Organometallics* **1997**, *16*, 5958-5963.

(k) Bochmann, M.; Lancaster, S. J. *Organometallics* **1993**, *12*, 633-640.

(9) Pellecchia, C.; Grassi, A.; Immirzi, A. *J. Am. Chem. Soc.* **1993**, *115*, 1160–1162.

(10) (a) Tedesco, C.; Immirzi, A.; Proto, A. *Acta Crystallogr. Sect. B, Struct. Sci.* **1998**, *B54*, 431-437.

(b) Davies, G. R.; Jarvis, J. A. J.; Kilbourn, B. T. *J. Chem. Soc., Chem. Commun.* **1971**, 1511-1512.

(c) Davies, G. R.; Jarvis, J. A. J.; Kilbourn, B. T.; Pioli, A. J. P. *J. Chem. Soc. D., Chem. Commun.* **1971**, 677.

(11) Rong, Y.; Al-Harbi, A.; Parkin, G. *Organometallics* **2012**, *31*, 8208–8217.

(12) The dihedral angles between the other two pairs of planes are 68˚ and 88˚ respectively.

(13) Sanz, M.; Mosquera, M. E. G.; Cuenca, T.; de Arellano, C. R.; Schormann, M.; Bochmann, M. *Polyhedron* **2007**, *26*, 5339-5348.

(14) Beckerle, K.; Manivannan, R.; Spaniol, T. P.; Okuda, J. *Organometallics* **2006**, *25*, 3019-3026.

(15) Furthermore, a benzyl compound with a bond angle of 98.6˚ was described as possessing partial η^2 character. See: Groysman, S.; Goldberg, I.; Kol, M.; Genizi, E.; Goldschmidt, Z. *Organometallics* **2003**, *22*, 3013-3015.

(16) Other large M–CH_2–Ph bond angles that have been assigned to η^2-coordination include 94.5˚,[a] 95.3˚,[b] 95.8˚,[c] 96.1,[d] 96.3,[e] and 96.7.[f]

(a) reference 1d.

(b) Natrajan, L. S.; Wilson, C.; Okuda, J.; Arnold, P. L. *Eur. J. Inorg. Chem.* **2004**, 3724-3732.

(c) Cariou, R.; Gibson, V. C.; Tomov, A. K.; White, A. J. P. *J. Organomet. Chem.* **2009**, *694*, 703-716.

(d) Tsukahara, T.; Swenson, D. C.; Jordan, R. F. *Organometallics* **1997**, *16*, 3303-3313.

(e) Chan, M. C. W.; Kui, S. C. F.; Cole, J. M.; McIntyre, G. J.; Matsui, S.; Zhu, N. Y.; Tam, K. H. *Chem. Eur. J.* **2006**, *12*, 2607-2619.

(f) Irwin, L. J.; Reibenspies, J. H.; Miller, S. A. *Polyhedron* **2005**, *24*, 1314-1324.

(17) Mean = 2.685 Å; range = 2.592 – 2.762 Å.

(18) Lee, H.; Jordan, R. F. *J. Am. Chem. Soc.* **2005,** *127*, 9384-9385.

(19) Ziniuk, Z.; Goldberg, I.; Kol, M. *Inorg. Chem. Commun.* **1999,** *2*, 549-551.

(20) Wiecko, M.; Girnt, D.; Rastatter, M.; Panda, T. K.; Roesky, P. W. *Dalton Trans.* **2005**, 2147-2150.

(21) Qian, B. X.; Scanlon, W. J.; Smith, M. R.; Motry, D. H. *Organometallics* **1999,** *18*, 1693-1698.

(22) Jordan, R. F.; Lapointe, R. E.; Baenziger, N.; Hinch, G. D. *Organometallics* **1990,** *9*, 1539-1545.

(23) Mintz, E. A.; Moloy, K. G.; Marks, T. J.; Day, V. W. *J. Am. Chem. Soc.* **1982,** *104*, 4692-4695.

(24) Kiplinger, J. L.; Morris, D. E.; Scott, B. L.; Burns, C. J. *Organometallics* **2002**, *21*, 5978-5982.

(25) Zhang, Z.; Zhang, L.; Li, Y.; Hong, L.; Chen, Z.; Zhou, X. *Inorg Chem* **2010,** *49*, 5715-5722.

(26) Wang, T.-F.; Hwu, C.-C.; Tsai, C.-W.; Wen, Y.-S. *J. Chem. Soc., Dalton Trans.* **1998**, 2091-2096.

(27) Bleeke, J. R.; Burch, R. R.; Coulman, C. L.; Schardt, B. C. *Inorg. Chem.* **1981,** *20*, 1316-1318.

(28) Fryzuk, M. D.; McConville, D. H.; Rettig, S. J. *J. Organomet. Chem.* **1993,** *445*, 245-256.

(29) Sujith, S.; Noh, E. K.; Lee, B. Y.; Han, J. W. *J. Organomet. Chem.* **2008,** *693*, 2171-2176.

(30) Wasilke, J.-C.; Ziller, J. W.; Bazan, G. C. *Adv. Synth. Catal.* **2005,** *347*, 405-408.

(31) Shim, C. B.; Kim, Y. H.; Lee, B. Y.; Shin, D. M.; Chung, Y. K. *J. Organomet. Chem.* **2003,** *675*, 72-76.

(32) Chen, Y.; Boardman, B. M.; Wu, G.; Bazan, G. C. *J. Organomet. Chem.* **2007,** *692*, 4745-4749.

(33) Zhou, X.; Bontemps, S.; Jordan, R. F. *Organometallics* **2008,** *27*, 4821-4824.

(34) For a recent review of crystal packing effects on bond lengths, see: Minasian, S. G.; Krinsky, J. L.; Arnold, J. *Chem. Eur. J.* **2011**, *17*, 12234-12245.

(35) Werkema, E. L.; Andersen, R. A.; Maron, L.; Eisenstein, O. *Dalton Trans.* **2010**, *39*, 6648-6660.

(36) John Decatur (PhD), Michael Appel, Wenbo Li and Ahmed Al-Harbi are thanked for the help with solid state NMR.

(37) (a) Latesky, S. L.; McMullen, A. K.; Niccolai, G. P.; Rothwell, I. P.; Huffman, J. C. *Organometallics* **1985**, *4*, 902-908.

(b) Scholz, J.; Schlegel, M.; Thiele, K. H. *Chem. Ber. Recl.* **1987**, *120*, 1369-1374.

(38) Oulié, P.; Freund, C.; Saffon, N.; Martin-Vaca, B.; Maron, L.; Bourissou, D. *Organometallics* **2007**, *26*, 6793-6804.

(39) The geometry optimized S_4 geometry is characterized by a τ_4 parameter of 0.8, where $\tau_4 = [360 - (\alpha + \beta)]/141$ and $\alpha + \beta$ is the sum of the two largest angles. For comparison, a tetrahedral geometry has a τ_4 parameter of 1.0. See: Yang, L.; Powell, D. R.; Houser, R. P. *Dalton Trans.* **2007**, 955.

(40) (a) Brookhart, M.; Green, M. L. H.; Parkin, G. *Proc. Natl. Acad. Sci. U. S. A.* **2007**, *104*, 6908-6914.

(b) Brookhart, M.; Green, M. L. H.; Wong, L. L. *Prog. Inorganic Chem.* **1988**, *36*, 1-124.

(c) Brookhart, M.; Green, M. L. H. *J. Organomet. Chem.* **1983**, *250*, 395-408.

(41) Mena, M.; Pellinghelli, M. A.; Royo, P.; Serrano, R.; Tiripicchio, A. *Chem. Commun.* **1986**, 1118-1119.

(42) The mean Si–CH_2–Ph bond angle for compounds listed in the Cambridge Structural Database is 115.0˚, with a range of 106.3˚ – 120.8˚.

(43) Calculations were performed on Me_3SiCH_2Ph rather than Me_3CCH_2Ph because silicon is capable of adopting coordination numbers greater than 4, which is required if the benzyl ligand is to adopt an expanded hapticity.

(44) (a) McNally, J. P.; Leong, V. S.; Cooper, N. J. in *Experimental Organometallic Chemistry*, Wayda, A. L.; Darensbourg, M. Y., Eds.; American Chemical Society: Washington, DC, 1987; Chapter 2, pp 6-23.

(b) Burger, B.J.; Bercaw, J. E. in *Experimental Organometallic Chemistry*;

Wayda, A. L.; Darensbourg, M. Y., Eds.; American Chemical Society: Washington, DC, 1987; Chapter 4, pp 79-98.

(c) Shriver, D. F.; Drezdzon, M. A.; *The Manipulation of Air-Sensitive Compounds*, 2nd Edition; Wiley-Interscience: New York, 1986.

(45) Gottlieb, H. E.; Kotlyar, V.; Nudelman, A. *J. Org. Chem.* **1997**, *62*, 7512-7515.

(46) Morcombe, C. R.; Zilm, K. W. *J. Magn. Reson.* **2003,** *162*, 479-486.

(47) Jaguar 7.6, Schrödinger, LLC, New York, NY 2009.

(48) (a) Becke, A. D. *J. Chem. Phys.* **1993**, *98*, 5648-5652.

(b) Becke, A. D. *Phys. Rev. A* **1988**, *38*, 3098-3100.

(c) Lee, C. T.; Yang, W.; Parr, R. G. *Phys. Rev. B* **1988**, *37*, 785-789.

(d) Vosko, S. H.; Wilk, L.; Nusair, M. *Can. J. Phys.* **1980**, *58*, 1200-1211.

(e) Slater, J. C. *Quantum Theory of Molecules and Solids, Vol. 4: The Self-Consistent Field for Molecules and Solids*; McGraw-Hill: New York, 1974.

(49) (a) Hay, P. J.; Wadt, W. R. *J. Chem. Phys.* **1985**, *82*, 270-283.

(b) Wadt, W. R.; Hay, P. J. *J. Chem. Phys.* **1985**, *82*, 284-298.

(c) Hay, P. J.; Wadt, W. R. *J. Chem. Phys.* **1985**, *82*, 299-310.

CHAPTER 2
Structural Characterization and Computational Study of 2-Imidazolethione: Comparison with its Chalcogen Counterparts

Table of Contents

Reproduced in part from:

Rong, Y.; Al-Harbi, A.; Kriegel, B.; Parkin, G. *Inorg. Chem.* **2013**, *52*, 7172–7182

2.1 Introduction

2.1.1 Biological Activity of Imidazolones, Imidazolethiones and Imidazoleselones

2-Imidazolones[1] belong to a class of 5 membered heterocyclic nitrogen compounds which feature exocyclic C=O functional group. They have been extensively studied due to their various biological activities.[2] For example, 1-ethyl-2-benzimidazolinone is a direct activator of K_{Ca} channels in epithelial cells and is potentially valuable for studying cellular hyperpolarization.[2d] 2-Imidazole-thiones[3] belong to the same class but feature an exocyclic C=S functional group, and one of their methyl derivatives, methimazole (tapazole), is a widely used antithyroid drug.[3,4] The selenium analogues of this family, imidazoleselones,[5,6,7] have also received attention with respect to potential antithyroid activity,[5,8] and a derivative has been discovered in the blood of bluefin tuna.[9] In addition to these chalcogenone forms,[10] the molecules also have

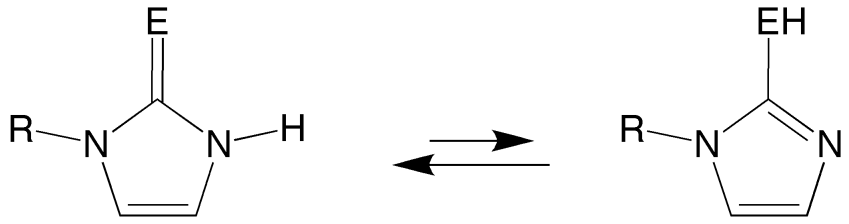

E = O (imidazolone)
E = S (imidazolethione)
E = Se (imidazoleselone)

Figure 1. Tautomers of 2-imidazolones, 2-imidazolethiones and 2-imidazoleselones.

potential for existing in equilibrium with their chalcogenol tautomers (Figure 1),[11,12] although the latter forms are typically less stable.[1,3,5,6,13,14,15]

2.1.2 Imidazolone, Imidazolethiones and Imidazoleselones as Building Blocks in Preparation of Multidentate Ligands

In inorganic chemistry, 2-imidazolones,[16] 2-imidazolethiones[17,18] and 2-imidazoleselones[6b] are also used as building blocks in preparation of multidentate ligands, due to their ability of coordinating to metals. It has been one of our interests to convert these compounds into tripodal ligands, namely *tris*(2-oxo-imidazolyl)hydroborato, [To^{R}],[19] *tris*(2-mercaptoimidazolyl)hydroborato, [Tm^{R}],[20,21] and *tris*(2-selenoimidazolyl)hydroborato ligands, [Tse^{R}],[21,22,23] which respectively provide [O_3], [S_3] and [Se_3] donor arrays.[24]

In this chapter, we report the molecular structure of 1-t-butyl-1,3-dihydro-2*H*-benzimidazol-2-thione [H(mbenzim$^{Bu^t}$)],[25] as illustrated in Figure 2, and compare it with its oxo and selone counterparts, H(obenzim^{R}) (R = Me, Bu^{t})[26,27] and H(sebenzim$^{Bu^t}$).[6b] In addition, computational analyses were performed on 2-imidazolethiones and their chacolgen counterparts using density functional theory (DFT) methods.

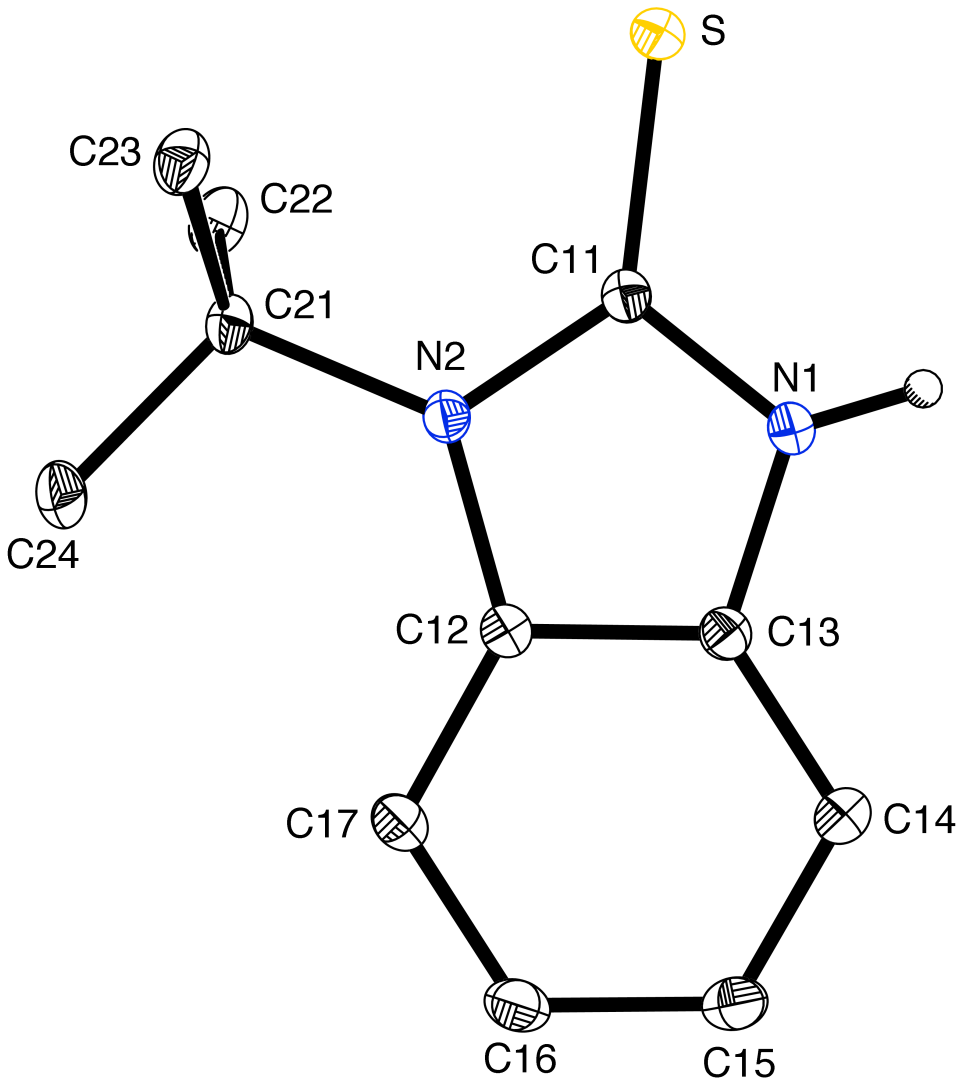

Figure 2. Molecular structure of H(mbenzim^{But}).

2.2 Structural Comparison of 2-Imidazolone, 2-Imidazolethione and 2-Imidazoleselone Compounds

2.2.1 Unusual Structural Features of H(sebenzim^{But})

1-t-butyl-1,3-dihydro-2*H*-benzimidazole-2-selone, H(sebenzim^{But}), has been synthesized, structurally characterized, and reported recently by our group.[6b] The compound exists as the selone tautomer, which is in accord with other

derivatives.[5d,5g,6a] However, the observation that there is no intermolecular N–H•••Se hydrogen bonding interactions is unexpected[6b] since other 2-imidazole-selones exhibit such interactions.[5d,5g,6a] Another interesting feature of H(sebenzim^{But}) is that the two Se–C–N angles are substantially different [120.7(2)° and 132.1(2)°].

2.2.2 Structural Features of H(mbenzim^{But})

Regarding these unusual features of the structure of H(sebenzim^{But}) , it is of interest to compare them with those of the sulfur and oxygen counterparts, 1-t-butyl-1,3-dihydro-2*H*-benzimidazole-2-thione, H(mbenzim^{But}) and 1-t-butyl-1,3-dihydro-2*H*-benzimidazol-2-one, H(obenzim^{But}).[28]

Comparison of the structure of H(mim^{But})[17a] with that of H(mbenzim^{But}) demonstrates that annulation has little effect on the metrical parameters associated with the [N_2C=S] moiety (Table 1). Similarly, there is little difference in the [N_2C=O] moieties of the oxygen derivatives. Also the two S–C–N angles are different by 8.9°.

Table 1. Metrical data for 2-imidazolone, 2-imidazolethione and 2-imidazoleselone Derivatives.

	C=E/Å	C–N$_1$/Å[d]	C–N$_2$/Å[e]	N$_1$–C–E/°[d]	N$_2$–C–E/°[e]	Δθ/°[f]	C–N–C(R)/°	NH···E/Å	N···E/Å	Nature of hydrogen bonding
H(*x*benzim$^{Bu^t}$)										
O[a]	1.2372(12)	1.3926(12	1.3690(12)	127.87(9)	124.95(9)	3.0	127.26(8)	1.88	2.71	dimer
S	1.6851(10)	1.3821(12	1.3517(12)	130.66(7)	121.83(7)	8.9	123.17(8)	2.50	3.34	dimer
Se[b]	1.845(2)	1.370(3)	1.349(3)	132.13(18)	120.69(18)	10.4	122.8(2)	–	–	monomer
H(*x*im$^{Bu^t}$)										
O[a]	1.2468(19)	1.368(2)	1.356(2)	127.43(15)	126.35(16)	1.0	124.01(14)	1.80	2.76	dimer
	1.2438(18)	1.373(2)	1.360(2)	127.55(15)	126.56(15)	1.0	123.50(13)	1.853	2.78	
S[c]	1.7003(15)	1.3632(18	1.3484(19)	130.08(11)	123.88(11)	6.2	127.05(12)	2.38	3.27	dimer

(a) data taken from reference 28; (b) data taken from reference 6b; (c) data taken from reference 17a; (d) N_1 is the nitrogen atom that is attached to R; (e) N_2 is the nitrogen atom that is attached to H; (f) $\Delta\theta = [N_1–C–E] – [N_2–C–E]$.

In contrast to the H(sebenzim^{But}),[6b] the 2-imidazolethione derivative, H(mbenzim^{But}), exists as a hydrogen bonded dimer as illustrated in Figure 3. The N•••S distance is [3.3422(9) Å], which is in the range of typical N–H•••S hydrogen bonding interactions.[29]

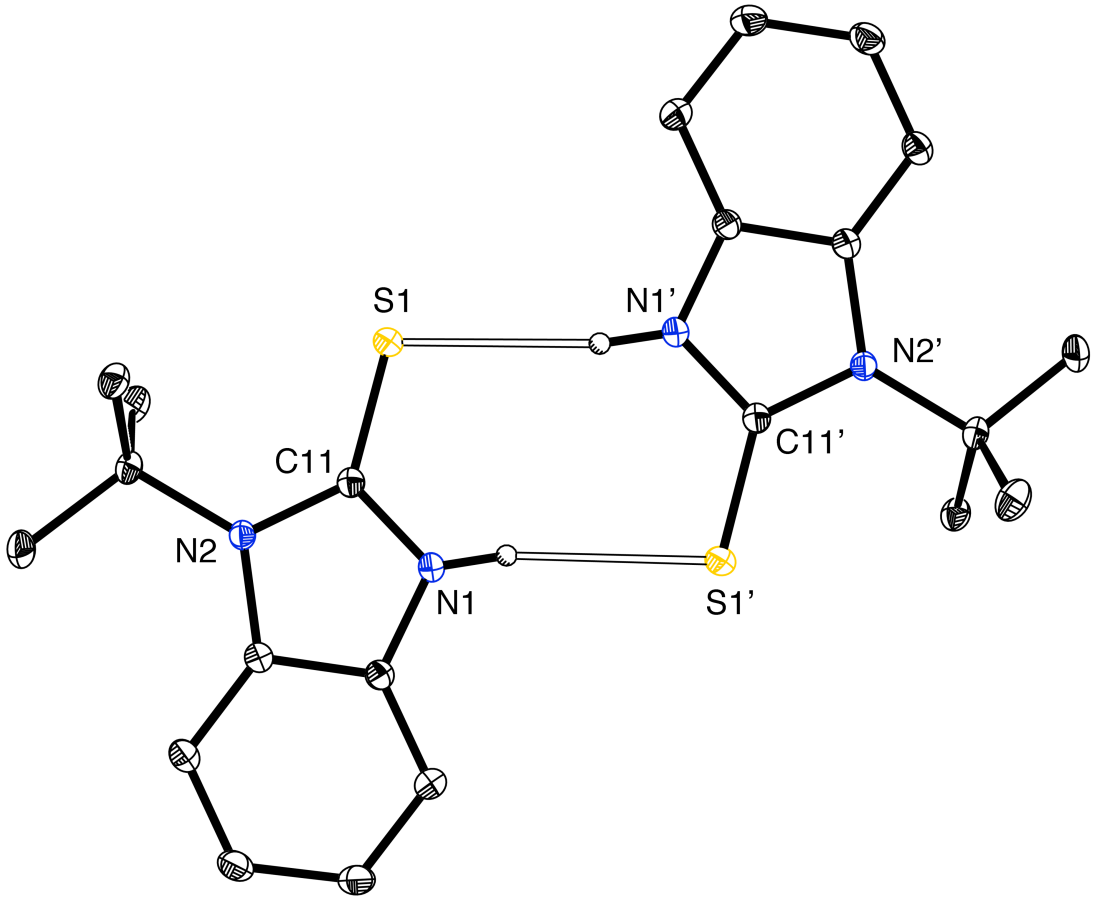

Figure 3. Hydrogen bonded dimeric structure of H(mbenzim^{But}). Hydrogen bonding distance: *d*(N1•••S1′) = 3.3422(9) Å.

2.2.3 Chalcogenones *vs* Chalcogenol Tautomers

As presented in Figure 2, H(mbenzim$^{Bu^t}$) exists in its chalcogenone form, which is inconsistent with the thiol tautomer reported in literature,[25a] while its chalcogen counterparts exist as chalcogenone tautomers that are consistent with other studies regarding the tautomerism of this type of molecule. Therefore, further density functional theory (DFT) calculations were carried out and the results are in accord with the experimental observations. Specifically, the chalcogenone tautomers of both H(obenzim$^{Bu^t}$) and H(mbenzim$^{Bu^t}$) are calculated to be more stable than their chalcogenol forms, as represented in Figure 4 and Table 2. In addition, comparison of H(*x*benzim$^{Bu^t}$) and H(*x*benzim^{Me}) systems (*x* = o, m, se) demonstrates that the chalcogenone tautomer is more favored for the methyl-subsitituted H(*x*benzim^{Me}) system than for the t-butyl-substituted H(*x*benzim$^{Bu^t}$) system, as illustrated in Table 2. Furthermore, it is worth noting that the H(*x*benzim^{R}) compounds can exist with a variety of different conformations, which differ according to the location of the hydrogen on the chalcogen. To investigate the stabilities of these chalcogenol tautomers, density functional theory geometry optimization calculations were carried out by rotating the hydrogen attached to chalcogen atom to three different positions relative to the R substituent (R = Me or Bu^t), *i.e*. towards the R substituent, within the aromatic ring plane, perpendicular to the plane or away from the R substituent. Among all the test results, the most stable conformation is the orientation in which the hydrogen on chalcogen is directed away from the R substituents, *i.e. exo* position. The preferential adoption of an *exo* could be explained as a consequence of steric interactions between the R substituents and the EH functional groups.

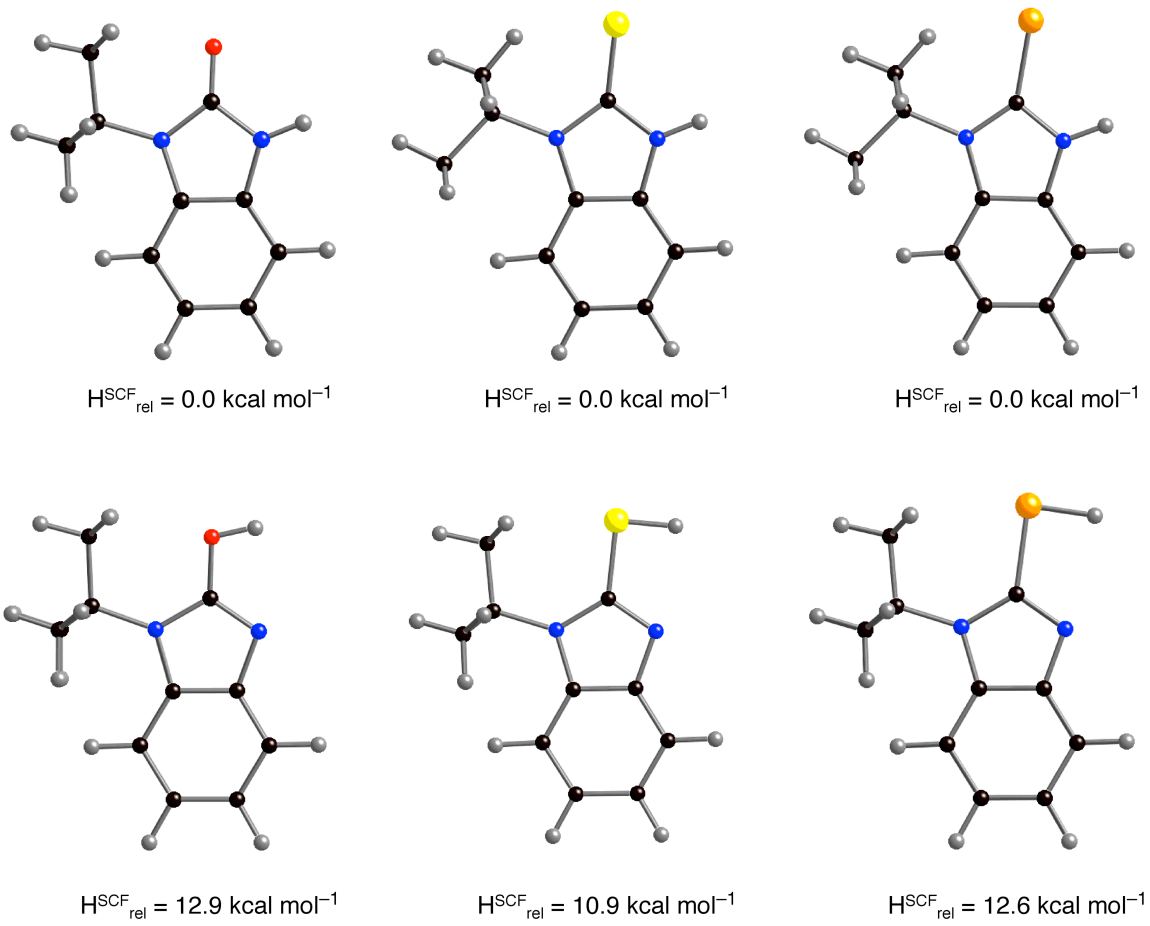

Figure 4. Geometry optimized structures of chalcogenone and chalcogenol tautomers of H(*x*benzim^{But}) (*x* = o, left; m, center; se, right).

Table 2. H_{SCF} values (kcal mol^{-1}) of various conformations of the chalcogenol tautomers relative to that of the chalcogenone tautomer.

	EH(*exo*)	**EH(*endo*)**	**EH(90°)**	**EH(endo) – EH(exo)**	**H···H distance/Å**
H(*x*benzim^{But})					
O	12.9	21.2	20.4[b]	8.3	1.86[c]
S	10.9	16.0	15.6[b]	5.1	1.96[c]
Se	12.6	16.9	16.7[b]	4.3	2.03[c]
H(*x*benzim^{Me})					
O	14.1	21.6[a]	20.7[b]	7.5	1.94
S	13.7	16.6[a]	15.8[b]	2.9	1.95
Se	16.0	17.6[a]	17.0[b]	0.4	2.01

(a) N–C–E–H torsion angle constrained to 180°.

(b) N–C–E–H torsion angle constrained to 90°.

(c) average value for the two close interactions.

For each chacogenol tautomer, the relative stability of the *exo* and *endo* conformers depends strongly on the chalcogen, with *endo* conformer increasing in stability in the sequence of O < S < Se. Moreover, the relative energies of the *exo* conformers correlate with the shortest nonbonding distance between the chalcogenol hydrogen and the hydrogens of the R substituent within the *endo* conformer, as illustrated in Table 2. This observation provides further support to the notion that steric interactions play a role in determining the stabilities of the chalcogenol tautomers. Another observation of note is that the difference in energies of the *endo* and *exo* conformers is smaller for the methyl-subsitituted H(*x*benzim^{Me}) system than for the t-butyl-subsitituted H(*x*benzim^{But}) system, as

illustrated in Table 2 and Figure 5, which provides further evidence for the importance of steric interactions destabilizing the *endo* isomers.

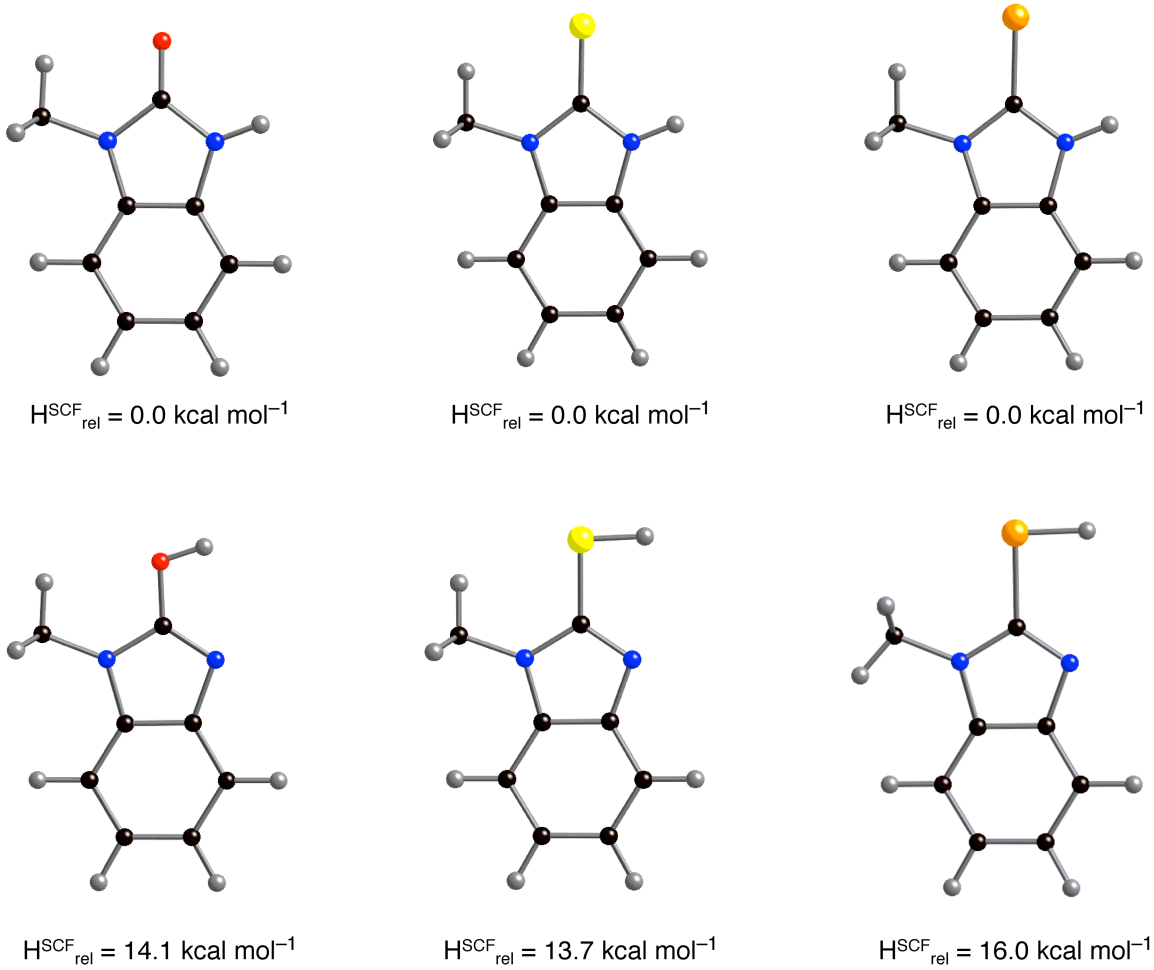

Figure 5. Geometry optimized structures of chalcogenone and chalcogenol tautomers of H(*x*benzim^{Me}) (*x* = o, left; m, center; se, right).

2.2.4 Asymmetry in Chalcogenone Forms

As mentioned above, in the structure of H(sebenzim^{But}), the two Se–C–N angles are substantially different [120.7(2)° and 132.1(2)°]. This asymmetry in the two N–C–E bond angles is also observed in the oxygen and sulfur analogues.

The X-ray diffraction studies on H(obenzim^{But}),[28] H(mbenzim^{But}) and H(sebenzim^{But})[6b] demonstrate that the asymmetry in the two N–C–E bond angles of the selenium compound, which differ by 10.4˚, is reduced for the sulfur (Δθ = 8.9˚) and oxygen (Δθ = 3.0˚) counterparts, as shown in Table 1. DFT calculations reproduced this trend nicely, as illustrated in Figure 4 and Table 3. One reasonable explanation for this is that the steric interactions between the t-butyl group and the chalcogen increasing with the size of the chalcogen. To examine this suggestion, DFT calculations were also carried out on the methyl-substituted system, and the results show that H(*x*benzim^{Me}), exhibits less asymmetry than does the t-butyl system H(*x*benzim^{But}), as illustrated in Figure 5 and Table 3. Specifically, whereas Δθ for H(*x*benzim^{But}) ranges from 4.8˚ to 14.3˚, Δθ for H(*x*benzim^{Me}) only ranges from –0.4˚ to 3.3˚ (Table 3).

Table 3. Asymmetry of N–C–E bond angles for DFT geometry optimized chalcogenone isomers of H(*x*benzim^{R}).

	N_1–C–E/˚[a]	N_2–C–E/˚[b]	Δθ/˚[c]
H(*x*benzim^{But})			
O	129.7	124.9	4.8
S	132.6	121.3	11.3
Se	133.9	119.6	14.3
H(*x*benzim^{Me})			
O	127.4	127.8	–0.4
S	128.7	126.1	2.6
Se	128.9	125.6	3.3

(a) N_1 is the nitrogen atom that is attached to R.

(b) N_2 is the nitrogen atom that is attached to H.

(c) Δθ = [N_1–C–E] – [N_2–C–E].

2.2.5 Asymmetry in Chalcogenol Forms

Similarly, the chalcogenol tautomers of H(*x*benzim$^{Bu^t}$) also exhibit asymmetry in the two N–C–E bond angles, but the range of Δθ (–1.0˚ to 10.4˚) is smaller than that for the corresponding chalcogenone tautomer (4.8˚ to 14.3˚), as shown in Table 4. In addition, the asymmetry for the chalcogenol tautomers of H(*x*benzim^{Me}) is less than that for H(*x*benzim$^{Bu^t}$), as expected on the basis of the comparison of the chalcogenone forms of H(*x*benzim^{Me}) and H(*x*benzim$^{Bu^t}$).

Table 4. Asymmetry of N–C–E bond angles for DFT geometry optimized chalcogenol isomers of H(*x*benzim^{R}).

	N_1–C–E/°[a]	N_2–C–E/°[b]	Δθ/°[c]
H(*x*benzim$^{Bu^t}$)			
O	121.5	122.5	–1.0
S	126.9	118.6	8.3
Se	127.9	117.5	10.4
H(*x*benzim^{Me})			
O	118.5	125.8	–7.3
S	121.2	124.4	–3.2
Se	120.2	125.0	–4.8

(a) N_1 is the nitrogen atom that is attached to R.

(b) N_2 is the nitrogen atom that has no substituent.

(c) $\Delta\theta = [N_1\text{–C–E}] - [N_2\text{–C–E}]$.

2.3 Electronic Structure of the Chalcogenone Compounds

2.3.1 Analysis of C=E Bond Lengths

A summary of various C=E bond lengths for the chalcogenone compounds, H(oim$^{Bu^t}$) and H(*x*benzim^{R}) is represented in Figure 6, and for comparison, the average C–E single bond length data for compounds listed in the Cambridge

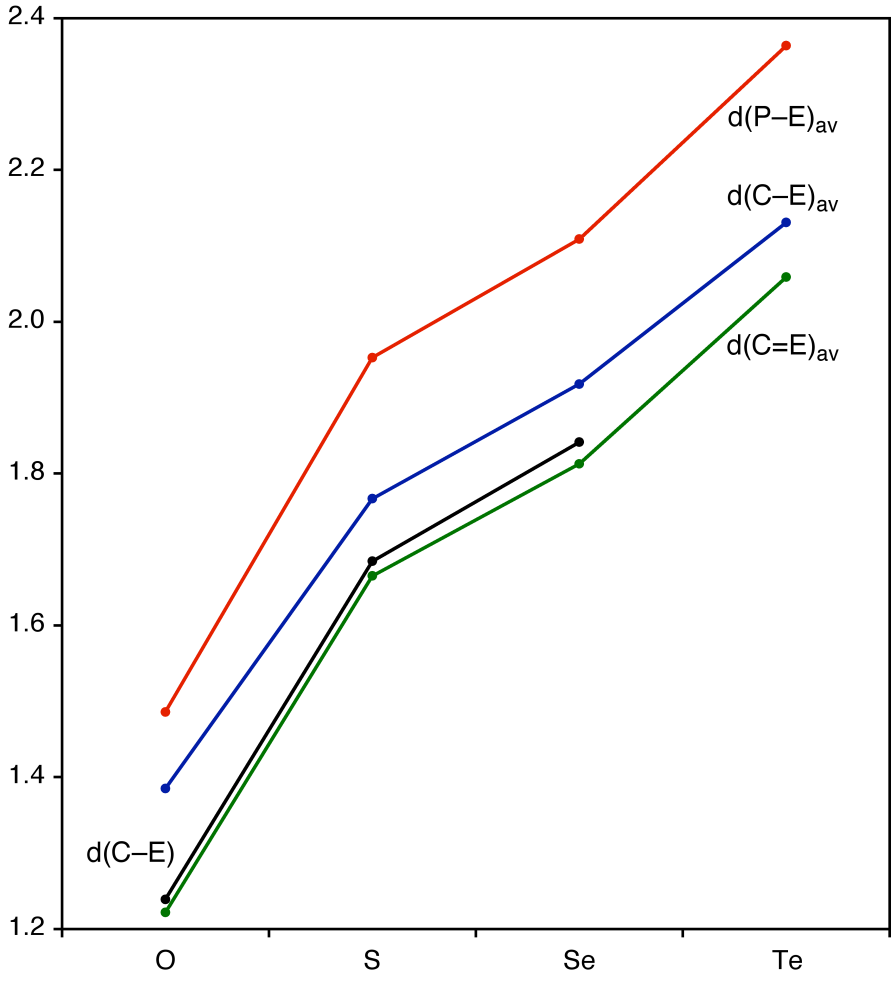

Figure 6. Variation of average C–E bond lengths in H(oim$^{Bu^t}$) and H(*x*benzim^{R}) (black line). For comparison, CSD average data for C–E single and double bonds, together with P–E data for R_3PE compounds, are also included.

Structural Database (CSD)[30] is also included, together with the bond lengths for $X_2C{=}E$ compounds. From Figure 6, we notice that the C–E bonds in these chalcogenones are 0.017 Å – 0.029 Å longer than the CSD average for other $X_2C{=}E$ compounds, which indicates that the zwitterionic resonance structures, which feature single C^+–E^- dative covalent bonds,[31] provide an important contribution to the chalcogenone compounds, as illustrated in Figure 7. [32]

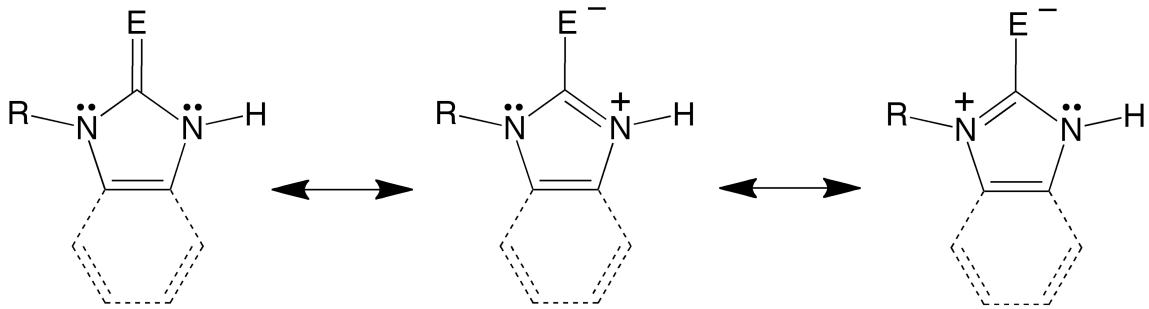

Figure 7. Three principal resonance structures for 2-imidazolechalcogenones. Other resonance structures also exist.

2.3.2 Nature of C–E Interactions

Analysis of the difference between the observed C–E bond lengths and the CSD average C–E single bond lengths as a function of the chalcogens provides further insight into the nature of the C–E interactions within these chalcogenones (Table 5). Specifically, based on the data we examined, the C–E bond lengths in oxygen derivatives have the greatest variation from the corresponding C–E single bond lengths. Figure 8 is another illustration of the differences provided by the variation of C–E bond lengths that have been normalized to the value for the oxygen derivative. Basically, the C–E bonds in the chalcogenones do not parallel the changes in CSD average C–E single bond lengths. As illustrated in Figure 8, compared to the oxygen derivative, the C–S and C–Se bonds of the chalcogenone

compounds are longer than expected. In another word, the C–O bonds may be viewed as being anomalously short.

Table 5. Comparison of C–E bond lengths in H(oim$^{Bu^t}$) and H(*x*benzim^{R}) with CSD mean C–E single and double bonds.

	***d*(C–E)/Å**[a]	**CSD mean single bond *d*′(C–E)/Å**	**CSD mean *d*(C=E)/Å**	***d*′(C–E)/Å – *d*(C–E)/Å**
O	1.239	1.385	1.222	0.146
S	1.685	1.767	1.665	0.082
Se	1.842	1.918	1.813	0.076

(a) average value for H(oim$^{Bu^t}$) and H(*x*benzim^{R}) derivatives.

A simple and straightforward explanation for the exceptionally short C–O bond length in the oxo compound, could be that the doubly bonded resonance structure has a greater contribution, as shown in Figure 7. However, the observation that R_3PE compounds also exhibit anomalously short P–O bond lengths, indicates that such an argument is overly simplistic. It is well known that R_3PE is better represented as possessing a P^+–E^- zwitterionic interaction rather than a P=E double bond, which would be associated with an expanded octet.[33] Thus, the unusually short P–O bond in R_3PO derivatives cannot be explained with a greater contribution of a doubly bonded P=O resonance structure. Therefore, the short C–O bond length in the 2-imidazolone compounds may not solely be a consequence of a doubly bonded C=O resonance structure, but may also be an indication of an ionic component to the bonding.[34]

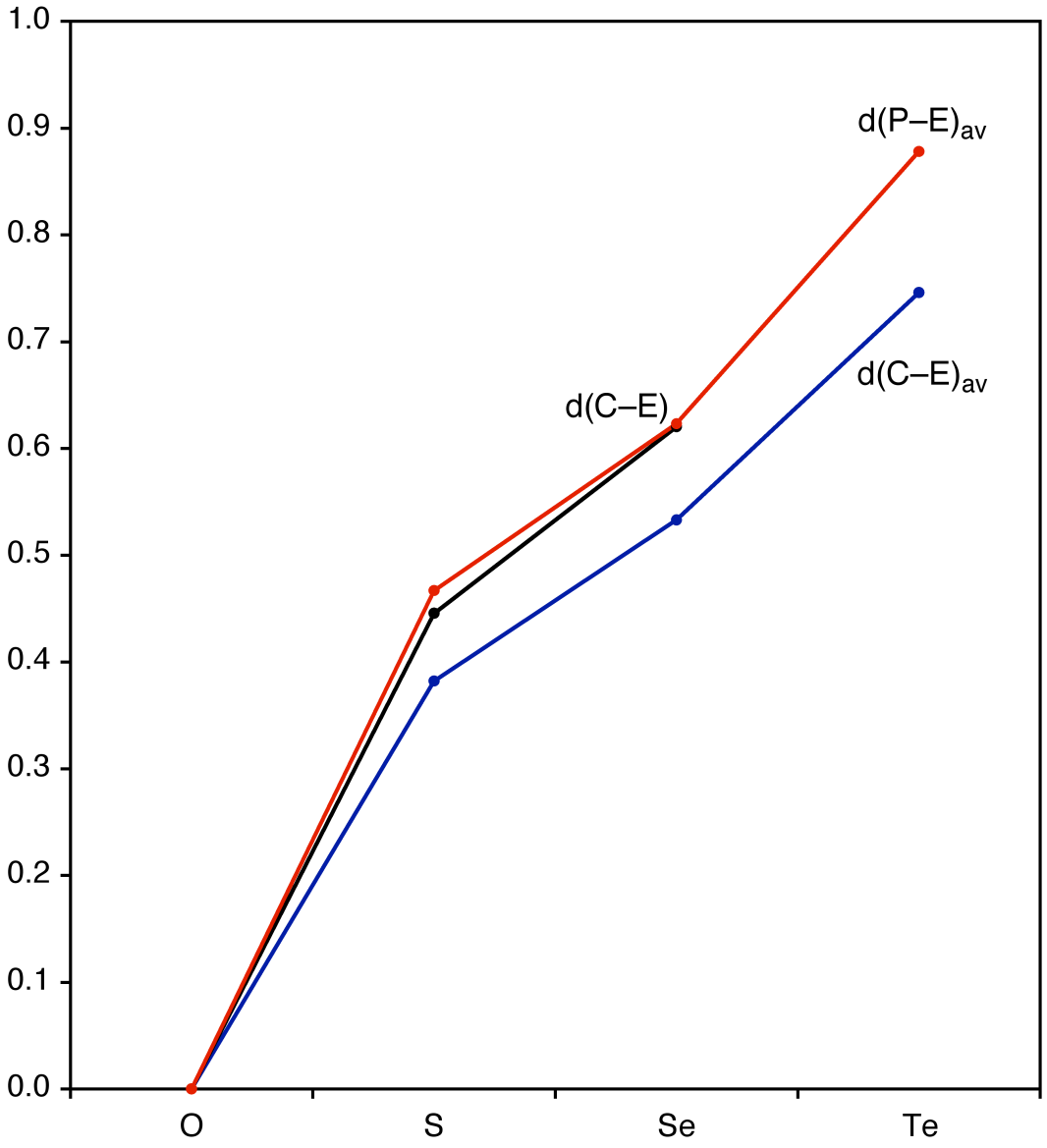

Figure 8. Variation of average C–E bond lengths in H(oim^{But}) and H(*x*benzim^{R}), normalized to the C–O bond length (black line). For comparison, analogous data for CSD average data for C–E single bonds, together with P–E data for R_3PE compounds, are also included. Note that the C–S and C–Se bond lengths in H(*x*benzim^{R}) are longer than would be expected if the trend were to follow the variation in C–E single bond lengths (blue line); correspondingly, the C–O bond lengths in H(oim^{But}) and H(*x*benzim^{R}) are shorter than would be anticipated.

2.3.3 Natural Bond Orbital (NBO) Analysis on Chalcogenones

To better understand this issue, the bonding in the chalcogenones has been investigated by using Natural Bond Orbital (NBO) analysis.[33, 35] As a result, the analysis of the natural localized molecular orbitals (NLMO's) indicates that the amount of π–overlap is most significant for the oxygen derivative and the polarization of the C–E bond is also the greatest for the oxygen derivative, as illustrated in Figure 9 and Table 6. Therefore the combination of a substantial π–component and an ionic component to the bonding results in an exceptionally short C–O bond relative to the C–S bond and C–Se bond.

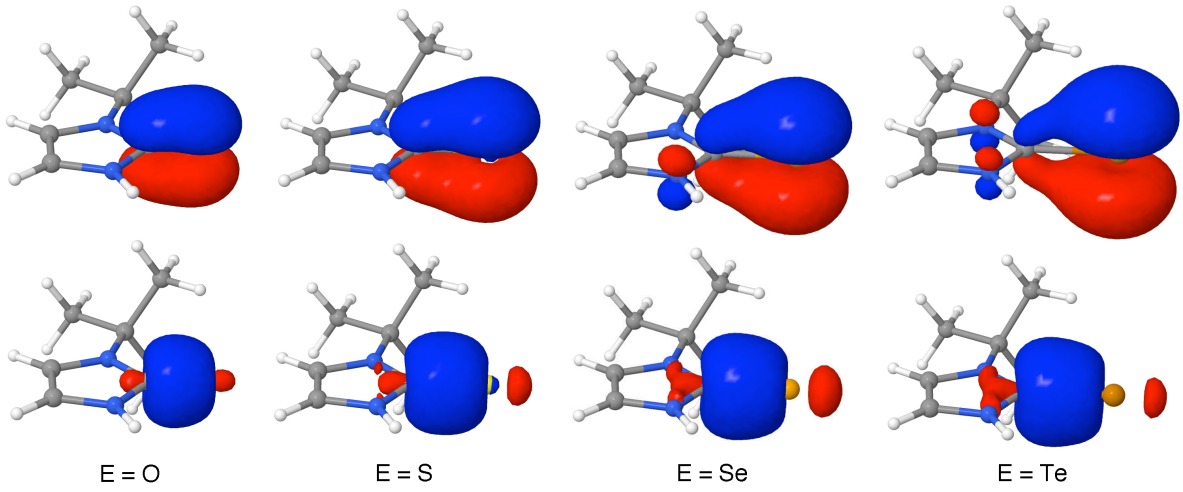

Figure 9. σ and π–NLMOs for H(*x*im^{But}).

Table 6. NLMO composition, atomic charges (Q) and ionicities (i_{CE})[a] for C~E moieties of H($x$im$^{Bu^t}$).

	σ–orbital		π–orbital							
	$\sigma_{\%C}$	$\sigma_{\%E}$	$\pi_{\%C}$	$\pi_{\%E}$	Q_C/e	Q_E/e	$Q_E–Q_C/e$	$i_{CE}(\sigma)$	$i_{CE}(\pi)$	$i_{CE}(\sigma) + i_{CE}(\pi)$
O	35.8%	64.0%	26.8%	73.0%	0.79	-0.68	-1.47	-0.28	-0.46	-0.74
S	60.0%	39.2%	24.8%	74.8%	0.22	-0.30	-0.52	0.21	-0.50	-0.29
Se	65.5%	33.5%	13.1%	82.4%	0.16	-0.26	-0.42	0.32	-1.00[b]	-0.68
Te	71.3%	27.4%	7.1%	87.9%	0.10	-0.23	-0.33	0.45	-1.00[b]	-0.55

(a) $i_{CE} = (c_C^2 – c_E^2)/(c_C^2 + c_E^2)$, where c_X is the NBO polarization coefficient for atom X. A negative value of i_{CE} indicates that the chalcogen atom possesses a negative charge. Values listed are calculated for the dominant resonance structures.

(b) $i_{CE}(\pi)$ is assigned a value of –1 because the NBO is localized on the chalcogen atom.

Interesting differences were observed when comparing the bonding in H(*x*im$^{\mathrm{But}}$) with those of the formaldehyde derivatives, H_2CE. Firstly, whereas the π–bonds of H(*x*im$^{\mathrm{But}}$) become progressively localized on the chalcogen in the sequence O < S < Se < Te (*i.e.* approaching a lone pair orbital for the latter),[36] the π-bonds for H_2CE retain a significant contribution from carbon (36% – 46%) for all of the chalcogen derivatives, as illustrated in Table 7.[37] Secondly, the two series of compounds have opposite polarizations for the C–S, C–Se and C–Te bonds, *i.e.* the chalcogens are negative for H(*x*im$^{\mathrm{But}}$) but positive for H_2CE compounds, as shown in Table 7 and Figure 10. An explanation for this difference in polarization is provided by considering the σ and π ionicities, which is defined as $(c_C^2 - c_E^2)/(c_C^2 + c_E^2)$, where c_X is the NBO polarization coefficient for atom X. To be specific, the variation in σ ionicities for both H(*x*im$^{\mathrm{But}}$) and H_2CE reflects the differences in electronegativity, *i.e.* the chalcogen becomes less negative in the sequence O > S > Se > Te, as illustrated in Figure 11. On the other hand, the π ionicities vary in such a manner that the chalcogen becomes less negative for H_2CE, but more negative for H(*x*im$^{\mathrm{But}}$) (Figure 11).[38] The latter is a consequence of the fact that the zwitterionic structures, as shown in Figure 7, becoming more dominant for the heavier chalcogen derivatives of H(*x*im$^{\mathrm{But}}$), thus resulting in a polarization that opposes simple electronegativity considerations. It is worth noting that the electronegativity, as expressed in the context of natural bond orbital theory, is the property of an orbital, such that the σ and π-electronegativities of an atom are not required to have the same value.[33] To summarize this issue, despite the fact that the zwitterionic C^+–E^- resonance structures[31] are most dominant for the tellurium derivative, the most negatively charged chalcogen within the H(*x*im$^{\mathrm{But}}$) series is that of the oxygen derivative due to the ionicity associated with the σ-bonding.

Table 7. NLMO composition, atomic charges (Q) and ionicities (i_{CE})[a] for C~E moieties of H_2CE.

	σ–orbital		π–orbital							
	$\sigma_{\%C}$	$\sigma_{\%E}$	$\pi_{\%C}$	$\pi_{\%E}$	Q_C/e	Q_E/e	$Q_E–Q_C/e$	$i_{CE}(\sigma)$	$i_{CE}(\pi)$	$i_{CE}(\sigma) + i_{CE}(\pi)$
O	33.7%	66.3%	35.6%	64.4%	0.22	-0.49	-0.71	-0.33	-0.29	-0.62
S	56.1%	43.9%	44.0%	56.0%	-0.52	0.08	0.60	0.12	-0.12	0.00
Se	61.1%	38.9%	45.1%	54.9%	-0.65	0.18	0.83	0.22	-0.10	0.12
Te	66.5%	33.5%	46.2%	53.8%	-0.77	0.30	1.07	0.33	-0.08	0.25

(a) $i_{CE} = (c_C^2 – c_E^2)/(c_C^2 + c_E^2)$, where c_X is the NBO polarization coefficient for atom X. A negative value of i_{CE} indicates that the chalcogen atom possesses a negative charge. Values listed are calculated for the dominant resonance structures.

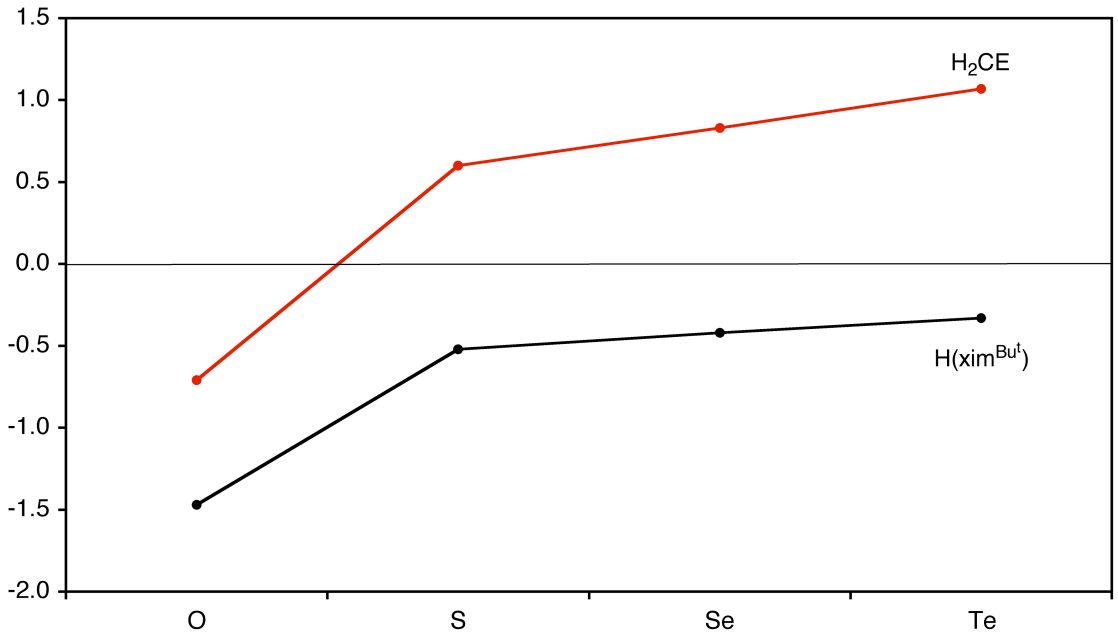

Figure 10. Polarization of the C–E bonds in H(*x*im^{But}) and H_2CE as expressed by Q_E–Q_C. Note that the chalcogen is negatively charged for all of the H(*x*im^{But}) series, whereas only the oxygen atom is negatively charged for the H_2CE series.

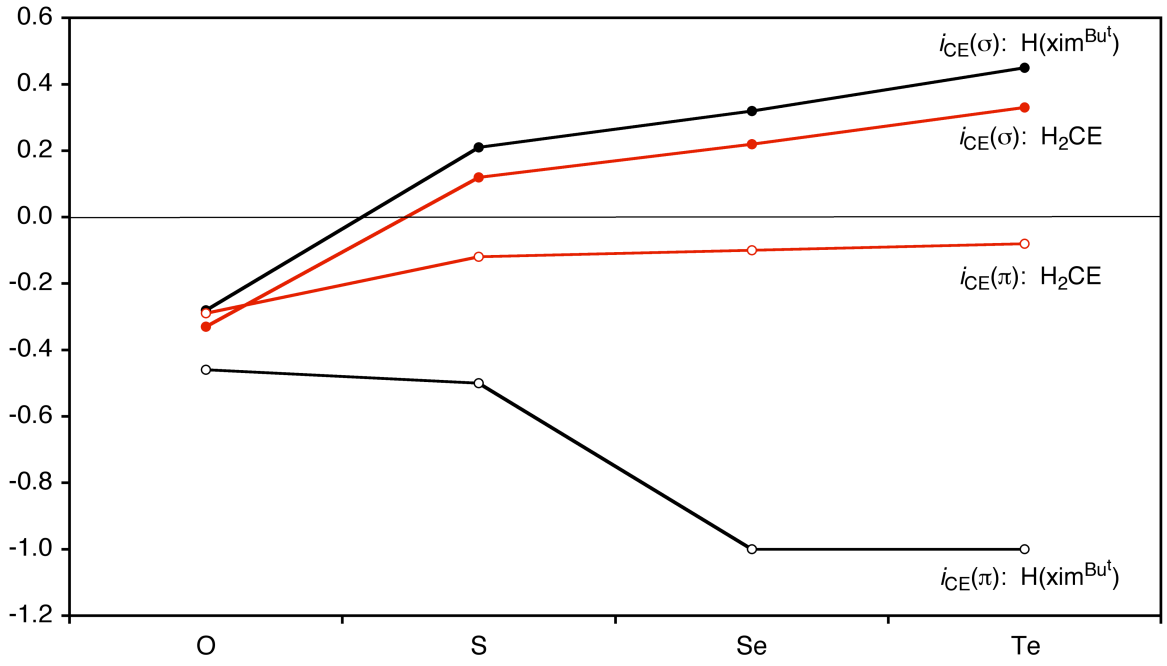

Figure 11. σ and π-components of the ionicity of the C–E bonds in the dominant resonance structures of H(*x*im^{But}) and H_2CE, as expressed in a form in which the sign of i_{CE} refers to the charge on the chalcogen. Note that the σ components of H(*x*im^{But}) and H_2CE result in a less negative charge for the heavier chalcogens and are actually positive for sulfur, selenium and tellurium derivatives. While the π components are all negative, the two series of compounds exhibit opposing trends, with the charge on the chalcogen becoming less negative for the heavier chalcogens in the H_2CE series, but more negative in the H(*x*im^{But}) series. The latter trend is in accord with an increased contribution from the zwitterionic C^+–E^- resonance structure for the heavier chalcogen derivatives of H(*x*im^{But}).

Table 8. Principal resonance structures for H(*x*im$^{Bu^t}$) and their contribution (%), together with the total contributions of resonance structures with C–E single and C=E double bonds.

	O	**S**	**Se**	**Te**
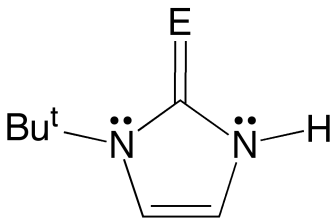	32.60*	25.32*	21.30	16.48
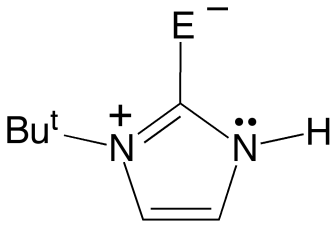	16.20	20.78	21.76*	23.60*
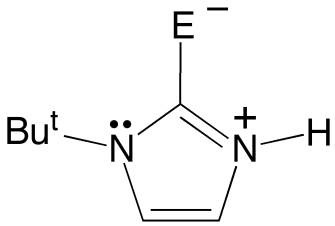	14.78	17.33	20.37	22.87
Total contribution of resonance structures with C=E double bonds	47.74	36.23	29.99	21.11
Total contribution of resonance structures with C–E single bonds	43.95	58.38	63.51	72.16

* dominant resonance structure

Table 9. Principal resonance structures for H_2CE and their contribution (%).

	O	**S**	**Se**	**Te**
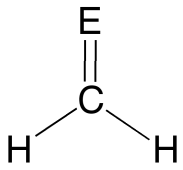	94.23*	96.40*	97.30*	98.07*
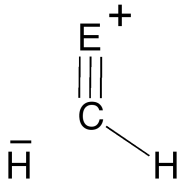	2.88	1.80	1.35	0.96
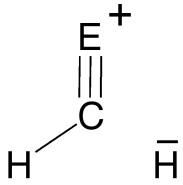	2.88	1.80	1.35	0.96

*dominant resonance structure

Natural bond orbital (NBO) analysis also provides information on resonance structures for the compounds we studied. Several principal resonance structures of H(*x*im^{But}) are summarized in Table 8, and there are a couple of noteworthy features regarding the data listed. First of all, the total contribution of C=E resonance structures for H(*x*im^{But}), which is 47.7 % for E = O, 36.23% for E = S, 29.99% for E = Se and 21.1 % for E = Te, is much less significant than the corresponding forms for both H_2CE (from 94.2 % for E = O to 98.1 % for E = Te as listed in Table 9) and $H_2NC(E)H$ (from 58.6 % for E = O to 56.1 % for E = Te).[39] Second, the prevalence of zwitterionic resonance structures featuring C–E single

bonds for H(*x*im$^{Bu^t}$) increases in the sequence of O < S < Se < Te. In the sulfur, selenium and tellurium derivatives, the dominant resonance structures are not the doubly bonded C=E resonance structures any more but rather the zwitterionic C^+–E^- forms.[40] This result seems to be opposite to the trend that one would expect on the basis of electronegativity differences. Similar observations have been made for (*i*) urea, thiourea and selenourea derivatives, also for (*ii*) formamide, thioformamide, selenoformamide and telluroformamide and related derivatives.[39,41–46] For example, the atomic charges and polarization of the C–E bond decrease in the sequence O > S > Se, but the $n_N \rightarrow \pi^*_{C-E}$ delocalization was observed to increase in the sequence O < S < Se.[41] Therefore, it has been suggested that orbital interactions rather than electronegativities play the more important role in determining the electron delocalization.[41] Naturally, the orbital interactions are more favorable for the heavier chalcogen derivatives because of the fact that the antibonding π^*_{C-E} orbital is lower in energy and so it serves as a better acceptor for the nitrogen lone pair.[41,47] Compared with H(*x*im$^{Bu^t}$) and $XC(E)NH_2$ derivatives, the C–E bonds of chalcogenoformaldehyde compounds, H_2CE, have little zwitterionic character, as illustrated in Table 9, since there is no adjacent nitrogen substituent with a lone pair. In fact, the most dominant zwitterionic component of H_2CE, albeit very small, is a triply bonded resonance structure, $C^-{\equiv}E^+$, such that the polarization actually opposes to those of H(*x*im$^{Bu^t}$) and $XC(E)NH_2$.

2.4 Summary and Conclusions

In summary, structure of 1-t-butyl-1,3-dihydro-2*H*-benzimidazole-2-thione has been determined by X-ray diffraction. The compound exists in the chalcogenone form instead of chalcogenol form, which is similar to its oxo and

selone counterparts. Comparison of 2-imidazolone, 2-imidazolethione and 2-imidazoleselone compounds shows that two N–C–E bond angles in the chalcogenone forms are not symmetric, and the differences between the two angles decrease in the sequence of Se > S > O. This trend can be reproduced by density functional theory calculations. Additionally, H(mbenzim^{But}) has intermolecular hydrogen bonding interactions, whereas its selenium counterpart does not.

Another interesting observation is that the C–E bond lengths of 2-imidazolone, 2-imidazolethione and 2-imidazoleselone compounds are intermediate between those of formal C–E single and double bonds. This observation is in accord with the notion that zwitterionic structures that feature single C^+–E^- dative covalent bonds provide an important contribution in such molecules. Furthermore, NBO analysis of the bonding in H(*x*im^{But}) derivatives demonstrates that the doubly bonded C=E resonance structure is most significant for the oxygen derivative, whereas singly bonded C^+–E^- resonance structures dominate for the tellurium derivative. This result appears to be counterintuitive, based on the fact that it opposes the trend that one would expect on the basis of electronegativity difference, however, studies on XC(E)NH_2 derivatives provide solid support for it. In this regard, the C~E bonding in these compounds is significantly different to that in chalcogenoformaldehyde derivatives for which the bonding is well represented by a H_2C=E double bonded resonance structure.

We also compared the C–E bond lengths of the imidazole-chalcogenones with those of C–E single bonds. Data obtained indicates that the C–O bonds are anomalously short. This observation can be explained in terms of oxygen derivatives having not only the most significant π–component, but also a significant ionic component. Thus, large ionic component for the C–O bond is a consequence of the σ and π-bonds being polarized in the same direction. In

contrast, the σ-polarization for the heavier chalcogens opposes the π-polarization, thereby reducing the negative charge on the chalcogen that is implied by the zwitterionic C^+–E^- contribution, despite the fact that this contribution increases as the chalcogen becomes heavier.

2.5 Experimental Sections

2.5.1 General Considerations

1-t-butylbenzimidazole-2-thione was synthesized according to literature method[25a] and crystals suitable for X-ray diffraction were obtained by crystallization from solution in CH_2Cl_2.

2.5.2 X-ray Structure Determinations

Single crystal X-ray diffraction data were collected on a Bruker Apex II diffractometer and crystal data, data collection and refinement parameters are summarized in Table 10. The structures were solved using direct methods and standard difference map techniques, and were refined by full-matrix least-squares procedures on F^2 with SHELXTL (Version 2008/4).[48]

2.5.3 Computational Details

Calculations were carried out using DFT as implemented in the Jaguar 7.6 (release 110) suite of *ab initio* quantum chemistry programs.[49] Geometry optimizations were performed with the B3LYP density functional[50] using the 6-31G** (C, H, N, O, S) and LAV3P (Se, Te) basis sets.[51] The energies of the optimized structures were reevaluated by additional single point calculations on each optimized geometry using cc-pVTZ(-f) correlation consistent triple-ζ (C, H,

N, O, S) and LAV3P (Se, Te) basis sets. NBO and NRT calculations were performed with NBO 5.0[52] as implemented in the Jaguar suite of programs using the 6-31G** and LAV3P basis sets.

2.6 Crystallographic Data

Table 10. Crystal, intensity collection and refinement data.

	H(mbenzim^{But})
lattice	monoclinic
formula	$C_{11}H_{14}N_2S$
formula weight	206.3
space group	$P2_1/c$
a / Å	7.7333(5)
b / Å	16.9079(10)
c / Å	8.4588(5)
α / °	90
β / °	106.2250(10)
γ / °	90
V / Å^3	1061.97(11)
Z	4
temperature (K)	150(2)
radiation (λ, Å)	0.71073
ρ (calcd.), g cm^{-3}	1.290
μ (Mo Kα), mm^{-1}	0.266
θ max, deg.	32.66
no. of data collected	18173
no. of data used	3753
no. of parameters	130
R_1 [$I > 2\sigma(I)$]	0.0375
wR_2 [$I > 2\sigma(I)$]	0.0983
R_1 [all data]	0.0447
wR_2 [all data]	0.1033
GOF	1.047
R_{int}	0.0293

2.7 References and Notes

(1) (a) Zav'yalov, S. I.; Ezhova, G. I.; Kravchenko, N. E.; Kulikova, L. B.; Dorofeeva, O. V.; Rumyantseva, E. E.; Zavozin, A. G. *Pharm. Chem. J.* **2004**, *38*, 256-260.

(b) Wong, O.; Tsuzuki, N.; Richardson, M.; Rytting, H.; Konishi, R.; Higuchi, T. *Heterocycles* **1987**, *26*, 3153-3158.

(2) (a) Devor, D. C.; Singh, A. K.; Frizzell, R. A.; Bridges, R. J. *Am. J. Physiol. (Lung Cell. Mol. Physiol.)* **1996**, *271*, L775-L784.

(b) Devor, D. C.; Singh, A. K.; Bridges, R. J.; Frizzell, R. A. *Am. J. Physiol. (Lung Cell. Mol. Physiol.)* **1996**, *271*, L785-L795.

(c) Kusama, N.; Kajikuri, J.; Yamamoto, T.; Watanabe, Y.; Suzuki, Y.; Katsuya, H.; Itoh, T. *Br. J. Pharmacol.* **2005**, *146*, 487-497.

(d) Adeagbo, A. O. S. *Eur. J. Pharmacol.* **1999**, 379, 151-159.

(e) Anderson, N. J.; Slough, S.; Watson, W. P. *Eur. J. Pharmacol.* **2006**, *546*, 48-53.

(f) Garduno, J.; Galvan, E.; de Sevilla, D. F.; Buno, W. *Neuropharmacology* **2005**, *49*, 376-388.

(g) Large, C. H.; Terstappen, G. C. *US Patent* #0029773 A1 (2004).

(h) Bezensek, J.; Groselj, U.; Stare, K.; Svete, J.; Stanovnik, B. *Tetrahedron* **2012**, *68*, 516-522.

(i) Dandepally, S. R.; Williams, A. L. *Tetrahedron Lett.* **2009**, *50*, 1395-1398.

(3) (a) Abramov, N. D.; Trzhtsinskaya, B. V. *Chem. Heterocycl. Compd.* **1988**, *24*, 1309-1321.

(b) Kister, J.; Assef, G.; Mille, G.; Metzger, J. *Can. J. Chem.* **1979**, *57*, 813-821.

(c) Van Lommen, G.; Doyon, J.; Coesemans, E.; Boeckx, S.; Cools, M.; Buntinx, M.; Hermans, B.; VanWauwe, J. *Bioorg. Med. Chem. Lett.* **2005**, *15*, 497-500.

(d) Kruse, L. I.; Kaiser, C.; DeWolf, W. E., Jr.; Frazee, J. S.; Ross, S. T.;

Wawro, J.; Wise, M.; Flaim, K. E.; Sawyer, J. L.; Erickson, R. W.; Ezekiel, M.; Ohlstein, E. H.; Berkowitz, B. A. *J. Med. Chem.* **1987**, *30*, 486-494.

(e) Wolfe, D. M.; Schreiner, P. R. *Synthesis* **2007**, 2002-2008.

(f) Laufer, S.; Wagner, G.; Kotschenreuther, D. *Angew. Chem. Int. Edit.* **2002**, *41*, 2290-2293.

(g) Phillips, B. T.; Claremon, D. A.; Varga, S. L. *Synthesis* **1990**, 761-763.

(4) (a) Cooper, D. S. *New Engl. J Med.* **2005**, *352*, 905-917.

(b) Fumarola, A.; Di Fiore, A.; Dainelli, M.; Grani, G.; Calvanese, A. *Exp. Clin. Endocrinol. Diabet.* **2010**, *118*, 678-684.

(5) (a) Guziec, L. J.; Guziec, F. S. Jr. *J. Org. Chem.* **1994**, *59*, 4691-4692.

(b) Taurog, A.; Dorris, M. L.; Guziec, L. J.; Guziec, F. S., Jr. *Biochem. Pharm.* **1994**, *48*, 1447-1453.

(c) Roy, G.; Mugesh, G. *J. Am. Chem. Soc.* **2005**, *127*, 15207-15217.

(d) Roy, G.; Das, D.; Mugesh, G. *Inorg. Chim. Acta* **2007**, *360*, 303-316.

(e) Cristiani, F.; Devillanova, F. A.; Diaz, A.; Verani, G. *Phos. Sulf. Rel. Elem.* **1984**, *20*, 231-240.

(f) Cristiani, F.; Devillanova, F. A.; Diaz, A.; Verani, G. *J. Chem. Soc., Perkin Trans. 2* **1984**, 1383-1386.

(g) Mammadova, G. Z.; Matsulevich, Z. V.; Osmanov, V. K.; Borisov, A. V.; Khrustalev, V. N. *Acta Crystallogr.* **2012**, *E68*, o1381.

(6) (a) Landry, V. K.; Minoura, M.; Pang, K.; Buccella, D.; Kelly, B. V.; Parkin, G. *J. Am. Chem. Soc.* **2006**, *128*, 12490-12497.

(b) Palmer, J. H.; Parkin, G. *Polyhedron* **2013**, *52*, 658–668.

(7) 1,3-dialkyl-2-imidazolechalcogenone and saturated imidazolidine-2-chalcogenone compounds have also been investigated with respect to their use as ligands. See, for example:

(a) Kimani, M. M.; Wang, H. C.; Brumaghim, J. L. *Dalton Trans.* **2012**, *41*, 5248–5259.

(b) Arduengo, A. J., III; Davidson, F.; Dias, H. V. R.; Goerlich, J. R.;

Khasnis, D.; Marshall, W. J.; Prakasha, T. K. *J. Am. Chem. Soc.* **1997**, *119*, 12742–12749.

(c) Kim, H. R.; Jung, I. G.; Yoo, K.; Jang, K.; Lee, E. S.; Yun, J.; Son, S. U. *Chem. Commun.* **2010**, *46*, 758–760.

(d) Williams, D. J.; Pennington, W. T.; VanDerveer, D.; Anderton, J. T.; White, K. M. *J. Chem. Crystallogr.* **2003**, *33*, 465–472.

(e) Isab, A. A.; Wazeer, M. I. M.; Fettouhi, M.; Ahmad, S.; Ashraf, W. *Polyhedron* **2006**, *25*, 2629-2636.

(f) Al-Amri, A. H. D.; Fettouhi, M.; Wazeer, M. I. M.; Isab, A. A. *Inorg. Chem. Commun.* **2005**, *8*, 1109-1112.

(8) (a) Roy, G.; Mugesh, G. *Phosphorus Sulfur Silicon Relat. Elem.* **2008**, *183*, 908-923.

(b) Roy, G.; Mugesh, G. *Chem. Biodivers.* **2008**, *5*, 414-439.

(c) Roy, G.; Bhabak, K. P.; Mugesh, G. *Crys. Growth Des.* **2011**, *11*, 2279-2286.

(d) Roy, G.; Mugesh, G. *Bioinorg. Chem. Appl.* **2006**, 1-9.

(e) Roy, G.; Mugesh, G. *J. Chem. Sci.* **2006**, *118*, 619-625.

(9) Yamashita, Y.; Yamashita, M. *J. Biol. Chem.* **2010**, *285*, 18134-18138.

(10) The term "chalcogenone" is simply used to describe the presence of a CE functional group and is not intended to convey any distinction between C=E and zwitterionic C^{+}–E^{-} resonance structures.

(11) For this reason, these compounds are also referred to in the literature by a variety of other names, *e.g.* mercaptoimidazoles and selenoimidazoles.

(12) While the compounds illustrated in Figure 1 are often commonly referred to as 2-imidazolones, 2-imidazolethiones and 2-imidazoleselones (or imidazol-2-ones, imidazole-2-thiones and imidazole-2-selones), their systematic names are 1-R-1,3-dihydro-2*H*-imidazol-2-one, 1-R-1,3-dihydro-2*H*-imidazole-2-thione and 1-R-1,3-dihydro-2*H*-imidazole-2-selone, respectively. However, it should be noted that these compounds have also been given a plethora of other names. For example, the most commonly encountered compound in this class, 1-methyl-1,3-dihydro-2*H*-imidazole-2-thione, is not only described by its trivial name, methimazole, but also by 1-methylimidazole-2-thione, 1-methylimidazole-2(3*H*)-thione, 1-methyl-3*H*-imidazole-2-thione, 1-methyl-1*H*-imidazole-2(3*H*)-thione, 3-

methyl-imidazole-2-thione and 1-methyl-4-imidazoline-2-thione. In addition, meth-imazole has also been given names that actually correspond to its tautomer, *e.g.* 1-methyl-1*H*-imidazole-2-thiol, 1-methyl-2-mercapto-1*H*-imidazole, 2-mercapto-1-methyl-1*H*-imidazole, 2-mercapto-1-methylimidazole. For brevity, we refer to the compounds described herein as 2-imidazolones, 2-imidazolethiones and 2-imidazoleselones.

(13) (a) Minkin, V. I.; Garnovskii, A. D.; Elguero, J.; Katritzky, A. R.; Denisko, O. V. *Adv. Heterocycl. Chem.* **2000**, *76*, 157-323.

(b) Shtefan, E. D.; Vvedenskii, V. Y. *Russ. Chem. Rev.* **1996**, *65*, 307-314.

(c) Elguero, J.; Marzin, C.; Katritzky, A. R.; Linda, P. *Adv. Heterocycl. Chem.*, Suppl. 1 (1976).

(14) (a) Ren, Y.; Li, M.; Wong, N. B. *J. Mol. Model.* **2005**, *11*, 167-173.

(b) Contreras, J. G.; Madariaga, S. T. *J. Phys. Org. Chem.* **2003**, *16*, 47-52.

(c) Öğretir, C.; Yarligan, S. *J. Mol. Struc.* **1996,** *366*, 227-231.

(15) (a) Flakus, H. T.; Miros, A.; Jones, P. G. *Spectrochim. Acta Part A* **2002**, *58*, 225-237.

(b) Vampa, G.; Benvenuti, S.; Severi, F.; Malmusi, L.; Antolini, L. *J. Heterocyclic Chem.* **1995**, *32*, 227-234.

(c) Raper, E. S.; Creighton, J. R.; Oughtred, R. E.; Nowell, I. W. *Acta Crystallogr.* **1983**, *B39*, 355–360.

(d) Balestrero, R. S.; Forkey, D. M.; Russell, J. G. *Magn. Reson. Chem.* **1986**, *24*, 651-655.
(e) Garner, M.; Armstrong, D. R.; Reglinski, J.; Smith, W. E.; Wilson, R.; McKillop, J. H. *Bioorg. Med. Chem. Lett.* **1994**, *4*, 1357-1360.

(f) Raper, E. S. *Coord. Chem. Rev.* **1985**, *61*, 115-184.

(g) Form, G. R.; Raper, E. S.; Downie, T. C. *Acta Crystallogr.* **1976**, *B32*, 345-348.

(h) Simanek, E. E.; Tsoi, A.; Wang, C. C. C.; Whitesides, G. M.; McBride, M. T.; Palmore, G. T. R. *Chem. Mat.* **1997**, *9*, 1954-1961.

(i) McBride, M. T.; Luo, T. J. M.; Palmore, G. T. R. *Cryst. Growth Des.* **2001**, *1*, 39-46.

(j) Zhu, H.-J.; Ren, Y.; Ren, J.; Chu, S.-Y. *J. Mol. Struct.* **2005**, *730*, 199-205.

(k) Guo, Y.; Li, B. *Acta Chim. Sin.* **2007**, *65*, 1561-1567.

(l) Bojarska-Olejnik, E.; Stefaniak, L.; Witanowski, M.; Hamdi, B. T.; Webb, G. A. *Magn. Res. Chem.* **1985**, *23*, 166-169.

(16) Hu, Y.-C.; Liang, C.-F.; Tsai, J.-H.; Yap, G. P. A.; Chang, Y.-T.; Ong, T.-G. *Organometallics* **2010**, *29*, 3357-3361.

(17) (a) White, J. L.; Tanski, J. M.; Churchill, D. G.; Rheingold, A. L.; Rabinovich, D. *J. Chem. Crystallogr.* **2003**, *33*, 437-445.

(b) Pang, K.; Figueroa, J. S.; Tonks, I. A.; Sattler, W.; Parkin, G. *Inorg. Chim. Acta* **2009**, *362*, 4609-4615.

(c) Cingolani, A.; Effendy; Marchetti, F.; Pettinari, C.; Pettinari, R.; Skelton, B. W.; White, A. H. *Inorg. Chem.* **2002**, *41*, 1151-1161.

(d) Fisher, M. G.; Gale, P. A.; Light, M. E.; Quesada, R. *CrystEngComm* **2008**, *10*, 1180-1190.

(e) Aggarwal, V.; Kumar, V. R.; Singh, U. P. *J. Chem. Crystallogr.* **2011**, *41*, 121-126.

(f) Norris, A. R.; Taylor, S. E.; Buncel, E.; Bélanger-Gariépy, F.; Beauchamp, A. L. *Can. J. Chem.* **1983**, *61*, 1536-1541.

(g) Bell, N. A.; Branston, T. N.; Clegg, W.; Creighton, J. R.; Cucurull-Sánchez, L.; Elsegood, M. R. J.; Raper, E. S. *Inorg. Chim. Acta* **2000**, *303*, 220-227.

(h) Sultana, R.; Lobana, T. S.; Sharma, R.; Castineiras, A.; Akitsu, T.; Yahagi, K.; Aritake, Y. *Inorg. Chim. Acta* **2010**, *363*, 3432-3441.

(i) Dodds, C. A.; Lehmann, M.-A.; Ojo, J. F.; Reglinski, J.; Spicer, M. D. *Inorg. Chem.* **2004**, *43*, 4927-4934.

(j) Butler, L. M.; Creighton, J. R.; Oughtred, R. E.; Raper, E. S.; Nowell, I. W. *Inorg. Chim. Acta* **1983**, *75*, 149-154.

(k) Oughtred, R. E.; Raper, E. S.; Nowell, I. W. *Inorg. Chim. Acta* **1984**, *84*, L5-L8.

(l) Isaia, F.; Aragoni, M. C.; Arca, M.; Caltagirone, C.; Castellano, C.; Demartin, F.; Garau, A.; Lippolis, V.; Pintus, A. *Dalton Trans.* **2011**, *40*, 4505-4513.

(m) Isaia, F.; Aragoni, M. C.; Arca, M.; Demartin, F.; Devillanova, F. A.; Floris, G.; Garau, A.; Hursthouse, M. B.; Lippolis, V.; Medda, R.; Oppo, F.; Pira, M.; Verani, G. *J. Med. Chem.* **2008**, *51*, 4050-4053.

(n) Atkinson, E. R.; Gardiner, D. J.; Jackson, A. R. W.; Raper, E. S. *Inorg. Chim. Acta* **1985**, *98*, 35-41.

(o) Ibrahim, M. M.; Shaban, S. Y. *Inorg. Chim. Acta* **2009**, *362*, 1471-1477.

(p) Bristow, S.; Harrison, J. A.; Farrugia, L. J. *Polyhedron* **1987**, *6*, 2177-2180.

(q) Docrat, A.; Morlok, M. M.; Bridgewater, B. M.; Churchill, D. G.; Parkin, G. *Polyhedron* **2004**, *23*, 481-488.

(r) Morlok, M. M.; Docrat, A.; Janak, K. E.; Tanski, J. M.; Parkin, G. *Dalton Trans.* **2004**, 3448-3452.

(s) Matsunaga, Y.; Fujisawa, K.; Amir, N.; Miyashita, Y.; Okamoto, K.-I. *J. Coord. Chem.* **2005**, *58*, 1047-1061.

(18) Melnick, J. G.; Yurkerwich, K.; Parkin, G. *Inorg. Chem.* **2009**, *48*, 6763-6772.

(19) Al-Harbi, A.; Sattler, W.; Sattler, A.; Parkin, G. *Chem. Commun.* **2011**, *47*, 3123-3125.

(20) Garner, M.; Reglinski, J.; Cassidy, I.; Spicer, M. D.; Kennedy, A. R. *Chem. Commun.* **1996**, 1975-1976.

(21) (a) Spicer, M. D.; Reglinski, J. *Eur. J. Inorg. Chem.* **2009**, 1553-1574.

(b) Parkin, G. *New J. Chem.* **2007**, *31*, 1996-2014.

(c) Smith, J. M. *Comments. Inorg. Chem.* **2008**, *29*, 189-233.

(22) Minoura, M.; Landry, V. K.; Melnick, J. G.; Pang, K.; Marchiò, L.; Parkin, G. *Chem. Commun.* **2006**, 3990-3992.

(23) Landry, V. K.; Pang, K.; Quan, S. M.; Parkin, G. *Dalton Trans.* **2007**, 820-824.

(24) *Bis*(2-mercaptoimidazolyl)hydroborato and *bis*(2-selenoimidazolyl)hydroborato ligands are also known. See, for example:

(a) Kimblin, C.; Bridgewater, B. M.; Hascall, T.; Parkin, G. *J. Chem. Soc., Dalton Trans.* **2000**, 891-897.

(b) Kimblin, C.; Hascall, T.; Parkin, G. *Inorg. Chem.* **1997**, *36*, 5680-5681.

(c) Landry, V. K.; Buccella, D.; Pang, K.; Parkin, G. *Dalton Trans.* **2007**, 866-870.

(d) Landry, V. K.; Parkin, G. *Polyhedron* **2007**, *26*, 4751-4757.

(25) (a) Ellsworth, E. L.; Domagala, J.; Prasad, J.V.N.V.; Hagen, S.; Ferguson, D.; Holler, T.; Hupe, D.; Graham, N.; Nouhan, C.; Tummino, P. J.; Zeikus, G.; Lunney, E. A. *Bioorg. Med. Chem. Lett.* **1999**, *9*, 2019-2024.

(b) Kawauchi, I. *U. S. Patent* 2008/0081291 A1.

(c) Bäuerlein, E.; Trasch, H. *Liebigs Ann. Chem.* **1979**, 1818-1827.

(26) Prakash, O.; Batra, H.; Kaur, H.; Sharma, P. K.; Sharma, V.; Singh, S. P.; Moriarty, R. M. *Synthesis* **2001**, 541-543.

(27) (a) Zhang, P.; Terefenko, E. A.; Bray, J.; Deecher, D.; Fensome, A.; Harrison, J.; Kim, C.; Koury, E.; Mark, L.; McComas, C. C.; Mugford, C. A.; Trybulski, E. J.; Vu, A. T.; Whiteside, G. T.; Mahaney, P. E. *J. Med. Chem.* **2009**, *52*, 5703-5711.

(b) Olofson, R. A.; Vandermeer, R. K.; Hoskin, D. H.; Bernheim, M. Y.; Stournas, S.; Morrison, D. S. *J. Org. Chem.* **1984**, *49*, 3367-3372.

(28) The molecular structure of H(obenzim^{But}) has been determined by Ahmed Al-Harbi. See Rong, Y.; Al-Harbi, A.; Kriegel, B.; Parkin, G. *Inorg. Chem.* **2013**, *52*, 7172–7182

(29) See, for example, references 17a, 15b,c,g,i and

(a) Steiner, T. "The hydrogen bond in the solid state" *Angew. Chem. Int. Edit.* **2002**, *41*, 48-76.

(b) Allen, F. H.; Bird, C. M.; Rowland, R. S.; Raithby, P. R. *Acta Crystallogr.* **1997**, *B53*, 696-701.

(c) Allen, F. H.; Bird, C. M.; Rowland, R. S.; Raithby, P. R. *Acta Crystallogr.* **1997**, *B53*, 680-695.

(30) Cambridge Structural Database (Version 5.34). *3D Search and Research Using the Cambridge Structural Database*, Allen, F. H.; Kennard, O. *Chemical Design Automation News* **1993**, *8* (1), pp 1 & 31-37.

(31) The C^+–E^- abbreviation is being used simply to convey any resonance structure that has a C–E single bond and not specifically one in which the formal positive charge is localized on carbon.

(32) For a discussion of the most appropriate Lewis structures in representing molecules, see: Suidan, L.; Badenhoop, J. K.; Glendening, E. D.; Weinhold, F. *J. Chem. Educ.* **1995**, *72*, 583-586.

(33) Weinhold, F.; Landis, C. R. Valency and Bonding: A Natural Bond Orbital Donor-Acceptor Perspective; Cambridge University Press: New York, 2005.

(34) For studies which discuss the fact that transition metal oxo bond lengths are also exceptionally short, see:

(a) Howard, W. A.; Parkin, G. *J. Am. Chem. Soc.* **1994,** *116*, 606-615.

(b) Parkin, G. *Prog. Inorg. Chem.* **1998**, *47*, 1-165.

(c) Trnka, T. M.; Parkin, G. *Polyhedron* **1997**, *16*, 1031-1045.

(35) (a) Glendening, E. D.; Landis, C. R.; Weinhold, F. *WIREs Comput. Mol. Sci.* **2012**, *2*, 1-42.

(b) Weinhold, F. *J. Comput. Chem.* **2012**, *33*, 2363-2379.

(36) The contribution of zwitterionic resonance structures has also been reported to be more significant for the heavier chalcogen in 6-membered heterocyclic compounds. See, for example: Mautner, H. G.; Chu, S.-H.; Lee, C. M. *J. Org. Chem.* **1962**, *27*, 3671-3673.

(37) For related studies on H_2CO, H_2CS and H_2CSe, see reference 33.

(38) It has previously been noted that the σ and π electrons exhibit opposite polarizations to minimize electron repulsion. See reference 41.

(39) Glendening, E. D.; Hrabal, J. A., II. *J. Am. Chem. Soc.* **1997**, *119*, 12940-12946.

(40) Note that zwitterionic resonance structures in which the positive formal charge is localized on carbon contribute very little to the overall bonding because of the availability of lone pairs on the adjacent nitrogen atoms. As such, the formal positive charge of the zwitterionic structures is more appropriately localized on the nitrogen atoms.

(41) (a) Moudgil, R.; Bharatam, P. V.; Kaur, R.; Kaur, D. *Proc. Indian Acad. Sci. (Chem. Sci.)* **2002**, *114*, 223-230.

(b) Bharatam, P. V.; Moudgil, R.; Kaur, D. *J. Phys. Chem. A* **2003**, *107*, 1627-1634.

(42) Wiberg, K. B. *Acc. Chem. Res* **1999**, *32*, 922-929.

(43) Mo, Y.; Schleyer, P. v. R.; Wu, W.; Lin, M.; Zhang, Q.; Gao, J. *J. Phys. Chem. A* **2003**, *107*, 10011-10018.

(44) Lauvergnat, D.; Hiberty, P. C. *J. Am. Chem. Soc.* **1997**, *119*, 9478-9482.

(45) (a) Kaur, D.; Sharma, P.; Bharatam, P. V.; Dogra, N. *J. Mol. Struct.: Theochem.* **2006**, *759*, 41-49.

(b) Kaur, D.; Sharma, P.; Bharatam, P. V. *J. Mol. Struct.: Theochem.* **2005**, *757*, 149-153.

(46) Huang, Y.; Jahreis, G.; Fischer, G.; Lücke, C. *Chem. Eur. J.* **2012**, *18*, 9841-9848.

(47) It has also been suggested that the greater polarisability of the heavier chalcogen allows it to accommodate a greater charge. See reference 39.

(48) (a) Sheldrick, G. M. SHELXTL, An Integrated System for Solving, Refining and Displaying Crystal Structures from Diffraction Data; University of Göttingen, Göttingen, Federal Republic of Germany, 1981.

(b) Sheldrick, G. M. *Acta Crystallogr.* **2008**, *A64*, 112-122.

(49) Jaguar 7.6, Schrödinger, LLC, New York, NY 2009.

(50) (a) Becke, A. D. *J. Chem. Phys.* **1993**, *98*, 5648-5652.

(b) Becke, A. D. *Phys. Rev. A* **1988**, *38*, 3098-3100.

(c) Lee, C. T.; Yang, W.; Parr, R. G. *Phys. Rev. B* **1988**, *37*, 785-789.

(d) Vosko, S. H.; Wilk, L.; Nusair, M. *Can. J. Phys.* **1980**, *58*, 1200-1211.

(e) Slater, J. C. *Quantum Theory of Molecules and Solids, Vol. 4: The Self-Consistent Field for Molecules and Solids*; McGraw-Hill: New York, 1974.

(51) (a) Hay, P. J.; Wadt, W. R. *J. Chem. Phys.* **1985**, *82*, 270-283.

(b) Wadt, W. R.; Hay, P. J. *J. Chem. Phys.* **1985**, *82*, 284-298.

(c) Hay, P. J.; Wadt, W. R. *J. Chem. Phys.* **1985**, *82*, 299-310.

(52) Glendening, E. D.; Badenhoop, J. K.; Reed, A. E.; Carpenter, J. E.; Bohmann, J. A.; Morales, C. M.; Weinhold, F. (Theoretical Chemistry Institute,

University of Wisconsin, Madison, WI, 2001);
http://www.chem.wisc.edu/~nbo5.

CHAPTER 3

Synthesis, Structural Characterization and Computational Study on [Tm^{R}] Sodium and Thallium Complexes

Table of Contents

Reproduced in part from:

Al-Harbi, A.; Rong, Y.; Parkin, G. *Dalton Trans.* **2013**, *42*, 11117–11127.

3.1 Introduction

Scorpionate ligands, as first defined by Trofimenko, provide two groups (claws) to coordinate a metal ion, allowing the third group to arch over and "sting" the metal ion.[1,2] The original scorpionate ligand is *tris*(pyrazolyl)hydroborate, which was first introduced in 1966.[3] [Tp^R] has often been compared to cyclopentadienyl ligands [Cp], since both ligand systems are anionic, L_2X type,[4] face-capping ligands. As a tripodal [N_3] donor ligand, Tp ligands are a highly successful class of supporting ligands and its versatility has inspired the development of new scorpionate ligands, in which either the pyrazolyl donors or the bridgehead boron atom is replaced. Specifically, the formal replacement of pyrazolyl by a mercaptoimidazolyl group gives *tris*(mercaptoimidazolyl)hydroborato ligands, [Tm^R] (Figure 1), first reported by Reglinski and Spicer in 1996.[5] Comparison to [Cp] and [Tp^R] indicates that [Tm^R] is a stronger electron donor and a more flexible ligand. For example, in six-coordinate $L_2XMn(CO)_3$ (L_2X = Cp*, Tp*, Tm^{Me})[6,7] derivatives, the C–O stretching frequencies in the IR spectra decrease in the order of Cp* > Tp* > Tm^{Me} (Table 1). The fact that $Tm^{Me}Mn(CO)_3$ has the lowest stretching frequency implies that the ligand has the greatest electron donating ability. When coordinated to metal centers, [Tm^R] ligand forms bicyclic [3, 3, 3] cages, instead of [2, 2, 2] as in [Tp^R], resulting in an eight-membered chelating ring, and thus more flexible than [Tp^R] or cyclopentadienyl ligands. Examination of structural characterized compounds listed in the Cambridge Structural Database[8] indicates that the coordination modes of [Tm^R] include κ^3-S_3, κ^3-S_2H, κ^2-S_2, κ^1-S and κ^0. So far, [Tm^R] derivatives that feature Me, Et, Bu^t, 1-Ad, Bz, Cy, Ph, *p*-Tol, *o*-Tol, *p*-$C_6H_4Pr^i$, 2,6-$C_6H_3Me_2$, 2,6-$C_6H_3Pr^i_2$, Mes and 2-biphenyl substituents are known.[9] Also, our group has recently reported the benzannulated version, namely [Tm^{MeBenz}].[10]

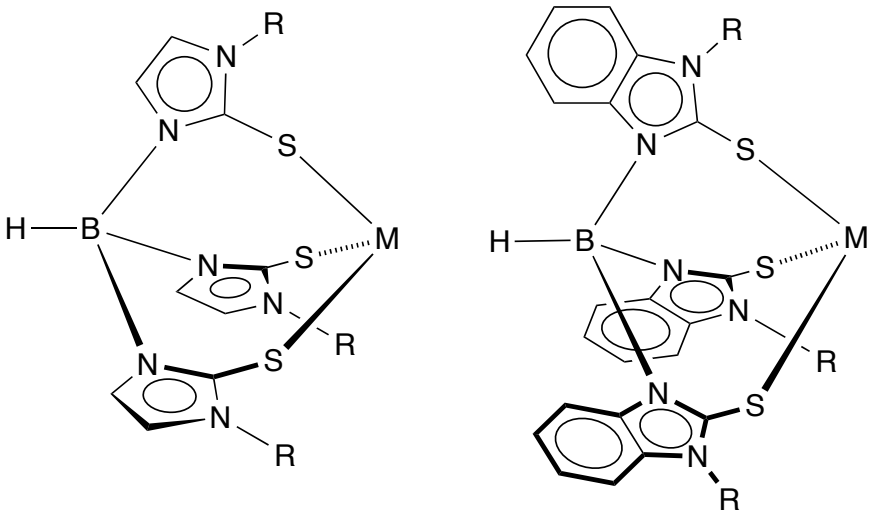

Figure 1. [Tm^{R}] and [Tm^{RBenz}] ligands, as illustrated in a κ^3-coordination mode.

Table 1. IR spectroscopic data of $[L_2X]Mn(CO)_3$ complexes.

Ligand	A_1 / cm^{-1}	E / cm^{-1}	Reference
Cp*	2032	1927	6
Tp*	2017	1929	6
Tm	2003	1905	7

In this chapter, we discuss the computational study on [Tm^{MeBenz}]Na,[10] and the syntheses and structural characterizations of three new compounds, namely [Tm$^{Bu^tBenz}$]Na, [Tm^{MeBenz}]Tl and [Tm$^{Bu^tBenz}$]Tl. It is of note that the [Tm^{MeBenz}]Tl and [Tm$^{Bu^tBenz}$]Tl are the first structurally characterized monovalent, monomeric [Tm^{R}]Tl compounds.

3.2 Computational Analysis on [Tm^{MeBenz}]Na: Benzannulation Promotes κ^3-Coordination

The benzannulated *tris*(mercaptoimidazolyl)borohydride compound, [Tm^{MeBenz}]Na[10] has been synthesized *via* the reactions of $NaBH_4$ with three equivalents of 1-methyl-1,3-dihydro-2*H*-benzimidazole-2-thione (Scheme 1). We are interested in the structure for the reason that there are few structurally characterized sodium complexes of these ligands, despite the fact that [Tm^R] ligands are commonly synthesized in their sodium form. Of all the structurally characterized [Tm^R]Na complexes that are listed in the Cambridge Structural Database,[8] none exhibits the κ^3-S_3 coordination motif that is observed for {[Tm^{MeBenz}]Na}$_2$(μ–THF)$_3$. For instance, the non-benzo analogue, [Tm^{Me}]Na, has been structurally characterized in several solvated forms, namely [Tm^{Me}]Na•4.5H_2O,[5b] [Tm^{Me}]Na•DMF,[11] and [Tm^{Me}]Na•3.25H_2O•0.5DMF,[11] however, none of the [Tm^{Me}] anion in these compounds exhibits a κ^3-S_3 coordination mode. Specifically, [Tm^{Me}]Na•4.5H_2O is composed of discrete [Tm^{Me}]$^-$ anions (*i.e.* κ^0), such that there is no interaction between sodium and the [Tm^{Me}] moiety.[5b,12] In the DMF adduct, {[Tm^{Me}]Na(μ–DMF)}$_2$, the [Tm^{Me}] ligand does not coordinate in a κ^3–S_3 mode, but rather binds in a κ^3–S_2H manner.[11] Thus, only two of the sulfur atoms of the [Tm^{Me}] ligand bind to sodium, with the coordination being supplemented by a Na•••H–B interaction. In contrast to [Tm^{Me}]Na•4.5H_2O and [Tm^{Me}]Na•DMF, the mixed solvate of composition [Tm^{Me}]Na•3.25H_2O•0.5DMF[11] contains [Tm^{Me}] moieties in two different environments, namely an uncoordinated [Tm^{Me}]$^-$ anion (*i.e.* κ^0) and one that is κ^1-coordinated to sodium.

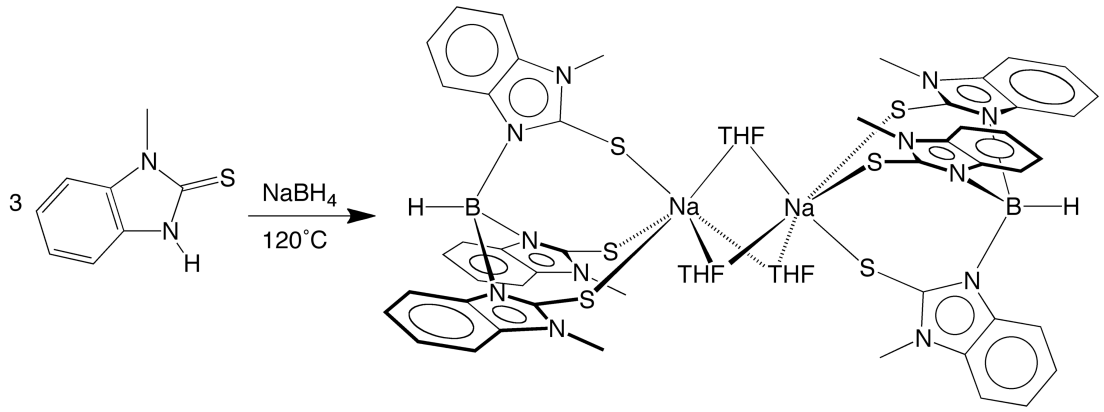

Scheme 1. Synthesis of $\{[Tm^{MeBenz}]Na\}_2(\mu\text{–}THF)_3$

In these complexes, $[Tm^{Me}]$ ligand does not prefer to coordinate in a κ^3-S_3 manner, and one possible explanation is that the Na–S interactions are insufficiently strong to cause the $[Tm^{Me}]$ moiety to adopt a conformation that is different to its conformation in an uncoordinated state.[5b,11,13] To be specific, the conformation of the $[Tm^{Me}]^-$ anion in the above compounds is one in which the three sulfur donors are in a plane on the same side of the molecule as the hydride,[5b,11] and while this conformation allows coordination *via* a κ^4-S_3H coordination mode,[14] it is not appropriate for κ^3-S_3 coordination. Since $\{[Tm^{MeBenz}]Na\}_2(\mu\text{–}THF)_3$ exhibits well defined κ^3-S_3 coordination, it is inferred that benzannulation has the effect of promoting κ^3-S_3 coordination, at least with respect to binding sodium.

To obtain further insight about the observation that benzannulation enables κ^3-S_3 coordination in the sodium complex, density functional theory (DFT) geometry optimization calculations on anions $[Tm^{MeBenz}]^-$ and $[Tm^{Me}]^-$ were carried out. The energies of different conformations are shown in Figure 2. Specifically, the lowest energy conformation for both $[Tm^{MeBenz}]^-$ and $[Tm^{Me}]^-$ is not actually the one that has been observed for $[Tm^{Me}]^-$ in ionic compounds, but is the one in

which one of the sulfur donors points away from the B–H group (Figure 2, center).[15,16] With respect to this lowest energy conformation, the conformation required for κ^3-S_3 coordination of $[Tm^{MeBenz}]^-$, *i.e.* one in which the three sulfur donors point away from the B–H group (Figure 2, right), has an energy difference of 4.9 kcal mol^{-1}, which is much more stable than that for $[Tm^{Me}]^-$ (14.7 kcal mol^{-1}). As such, there is a greater tendency for $[Tm^{MeBenz}]$ to adopt a κ^3-S_3 coordination mode. However, in view of the variety of structures observed for $[Tm^{Me}]$Na, which indicates that the coordination mode of the $[Tm^{Me}]$ ligand is influenced by the nature of coligands, it is possible that $[Tm^{MeBenz}]$Na could also exhibit different coordination modes in different crystalline forms.

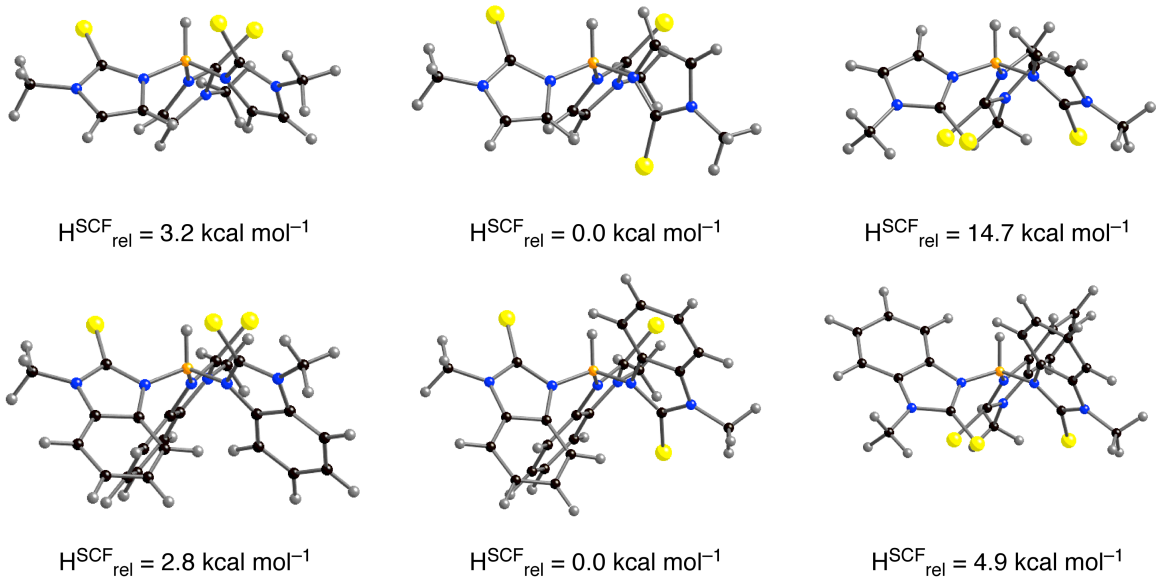

Figure 2. Geometry optimized (B3LYP and 6-31G** basis set) structures of $[Tm^{MeBenz}]^-$ and $[Tm^{Me}]^-$; the energies of the optimized structures were reevaluated by additional single point calculations using the cc-pVTZ(-f) correlation consistent triple-ζ basis set.

3.3 Synthesis and Structure of [Tm$^{Bu^tBenz}$]Na

The benzannulated *tris*(mercaptoimidazolyl)borohydride compound, [Tm$^{Bu^tBenz}$]Na has been synthesized *via* the reactions of $NaBH_4$ with three equivalents of 1-tert-butyl-1,3-dihydro-2*H*-benzimidazole-2-thione, as illustrated in Scheme 2. The molecular structure has been determined by X-ray diffraction (Figure 3). In contrast to the κ^3-S_3 coordination mode presented in [Tm^{MeBenz}]Na, [Tm$^{Bu^tBenz}$]Na prefers a κ^3–S_2H manner, which is characterized by two Na–S bond lengths of 2.945(3) Å and 3.078(3) Å,[17] and a Na•••H–B distance of 2.12(5) Å. It is worth noting that the [Tm$^{Bu^tBenz}$] anion adopts a geometry in which the three thione moities point towards the B–H group, which is different from the geometry of the [Tm^{MeBenz}] anion in the sodium salt, where the three thione moieties point away from the B–H group. Furthermore, while both complexes are dinuclear and each sodium is attached to three THF ligands, the sodium centers of {[Tm^{MeBenz}]Na}$_2$(μ-THF)$_3$ are attached to three bridging THF, the sodium centers of {[Tm$^{Bu^tBenz}$]Na(THF)}$_2$(μ-THF)$_2$ are attached to one terminal and two bridging THF ligands.

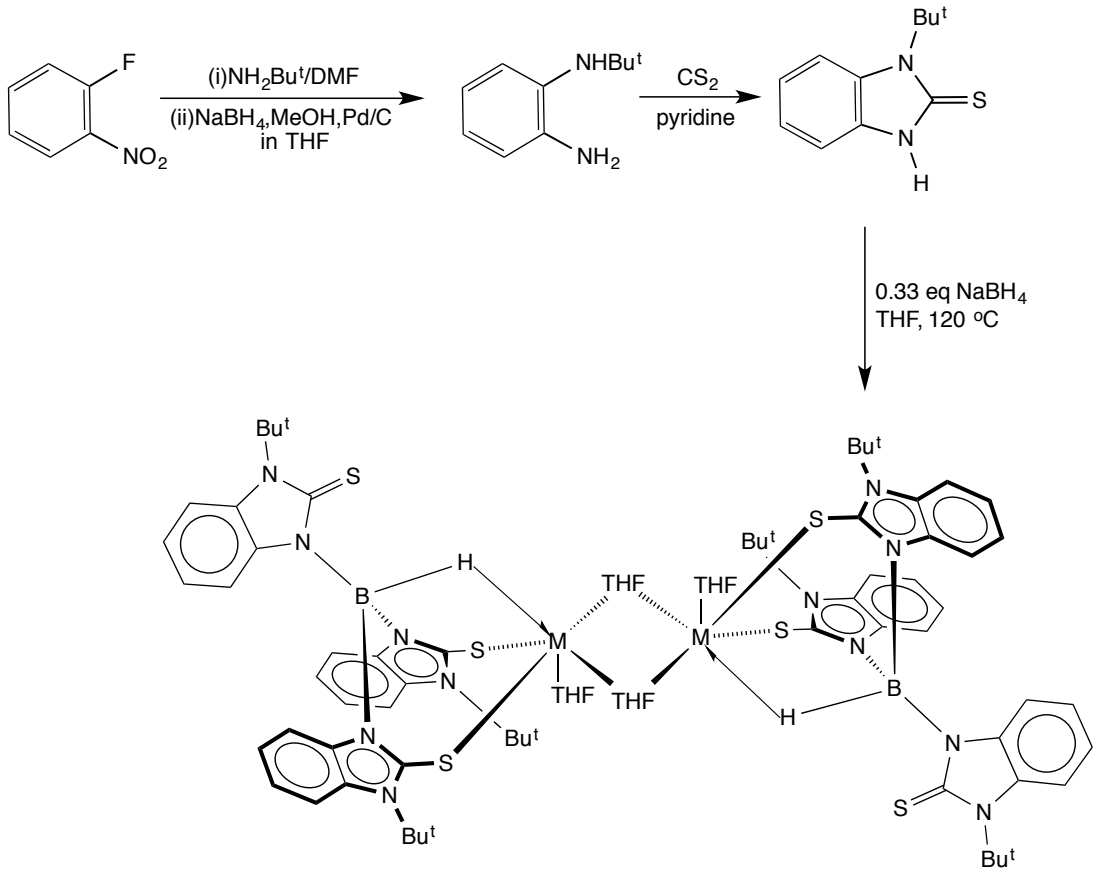

Scheme 2. Synthesis of $\{[Tm^{Bu^tBenz}]Na(THF)\}_2(\mu\text{–}THF)_2$

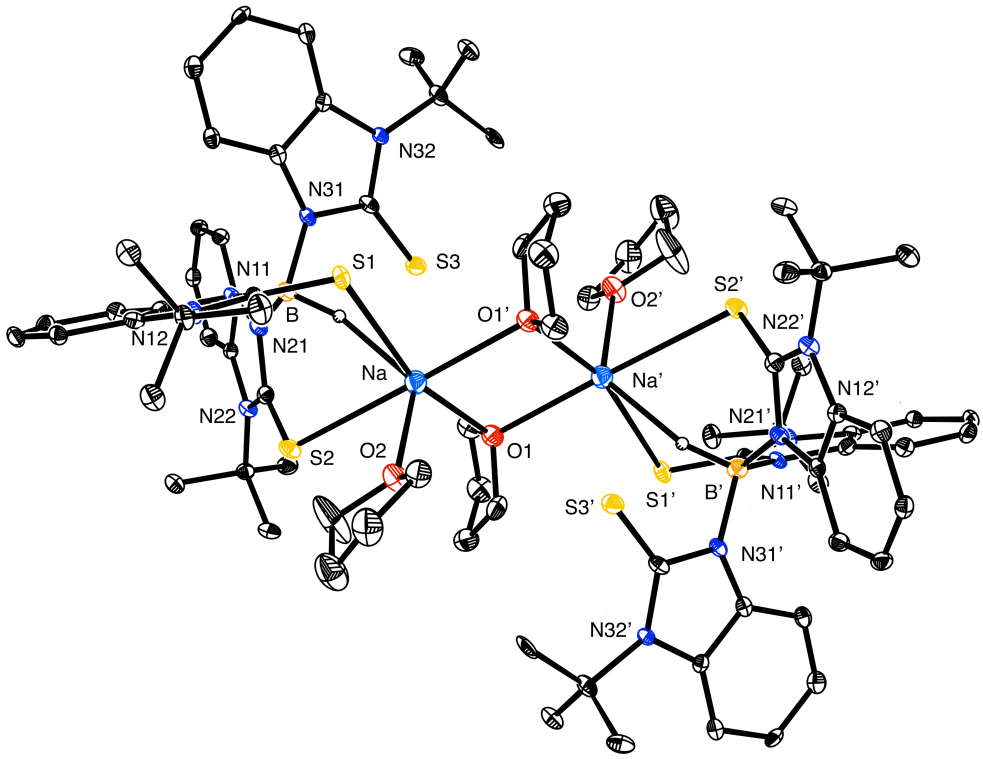

Figure 3. Molecular structure of $\{[Tm^{Bu^tBenz}]Na(THF)\}_2(\mu\text{–}THF)_2$

We also obtained another crystal form of $\{[Tm^{Bu^tBenz}]Na\}_2$, which is a dimer and has no coordinated solvent, as illustrated in Figure 4. With respect to this structure, it is worth noting that firstly, the three sulfur atoms in $[Tm^{Bu^tBenz}]$ ligand bridge in two different manners: (*i*) one sulfur atom acts as the bridgehead by connecting to both Na centers; (*ii*) the other two sulfur atoms in the same $[Tm^{Bu^tBenz}]$ unit bond to the two Na centers via a [*SCNBNCS*] linker, as shown in Figure 5. Secondly, the hydrogen atom attached to the boron bridges the two Na centers. As far as we know, no such bridging modes for $[Tm^R]$ ligand have been observed in compounds listed in the Cambridge Structural Database.[8] However, there is one structure reported by our group, $\{[To^{Bu^t}]Na\}_2$,[10] which shows a similar coordination mode. The values of two shorter Na–S bond lengths are [2.701(4) Å]

and [2.710(3) Å], shorter than the minimum of Na–S distance according to the Cambridge Structural Database (2.81 – 2.98 Å),[8] while the third one [2.894(4)Å] is well within the range.

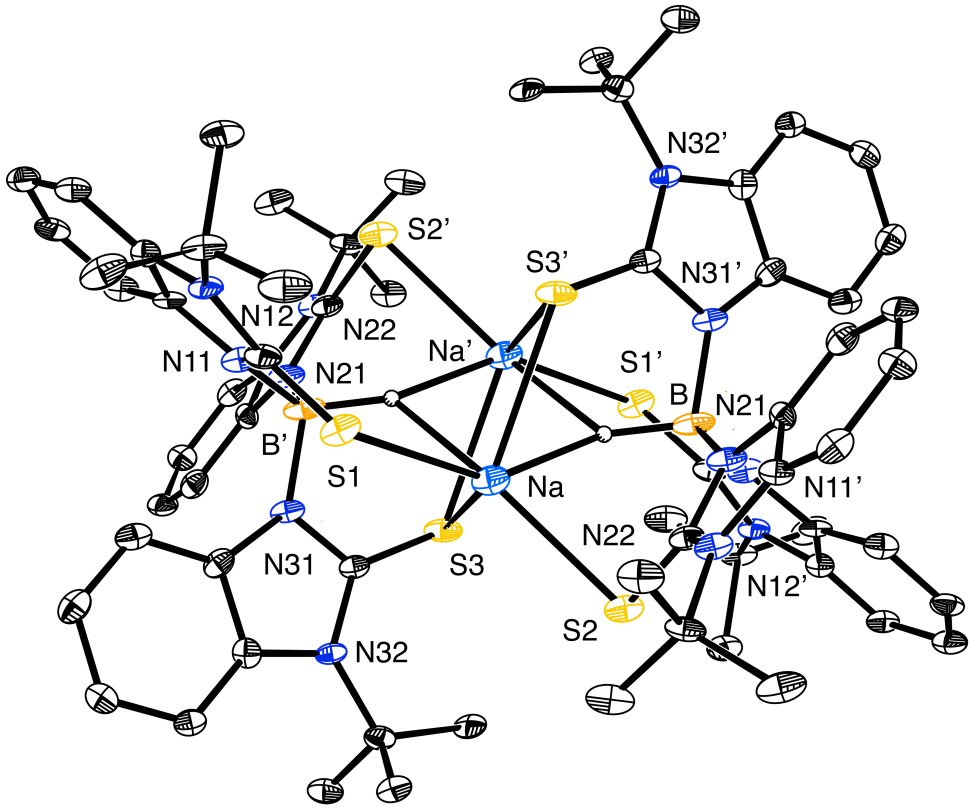

Figure 4. Molecular structure of {[Tm$^{Bu^tBenz}$]Na}$_2$

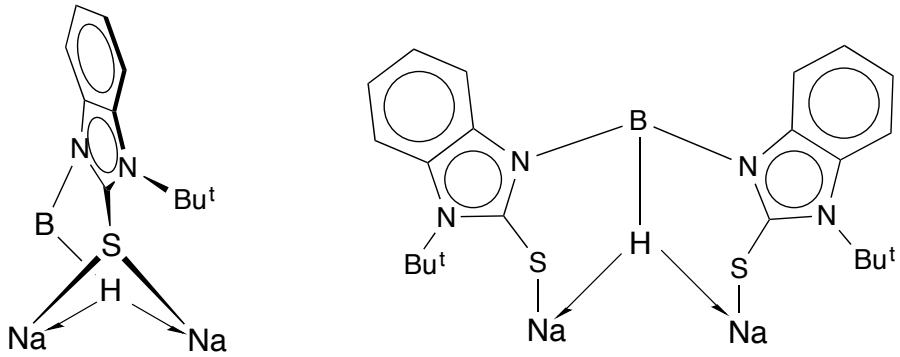

Figure 5. Coordination modes of sulfur atoms in {[Tm$^{Bu^tBenz}$]Na}$_2$. The rest of the molecule is omitted for clarity.

3.4 Synthesis and Structures of Monovalent [Tm^{R}]Tl (R = MeBenz, Bu^{t}Benz)

[Tm^{MeBenz}]Tl and [Tm$^{Bu^{t}Benz}$]Tl were prepared as transfer reagents for introducing [Tm^{R}] ligands to other metals. The compounds were synthesized in a similar way as that for [Tm$^{Bu^{t}}$].[18] The molecular structures have been determined by X-ray diffraction, as illustrated in Figure 6 and Figure 7. As far as we know, they are the first structurally characterized monovalent, monomeric thallium in a sulfur-rich coordination environment.[19] Structural data are summarized in Table 2. Specifically, the average S–Tl–S bond angles in [Tm^{MeBenz}]Tl and [Tm$^{Bu^{t}Benz}$]Tl are acute, such that the thallium centers are highly pyramidal. An indication of the degree of the pyramidality (*P*) of a MX_3 center is provided by the deviation of the sum of the X–M–X bond angles from 360˚, *i.e.* $P = 360^{\circ} - \Sigma(X–M–X)$,[20] and the values observed for [Tm^{MeBenz}]Tl (103.4) and [Tm$^{Bu^{t}Benz}$]Tl (93.6) indicate that the Tl centers are highly pyramidal. The distance between the center of the benzene and Tl atom is 3.386 Å, while that between each carbon in benzene and Tl atom is 3.66 Å, which is not only significantly longer than Tl–C bonds for monovalent thallium (2.31 Å – 2.49 Å),[21] but are also longer than the mean Tl•••C distance (3.31 Å) pertaining to intramolecular Tl–arene interactions for compounds listed in the Cambridge Structural Database. As such, the contact between [Tm$^{Bu^{t}Benz}$]Tl and benzene is not considered to represent a significant bonding interaction. Interestingly, [Tm$^{Bu^{t}Benz}$]Tl does exhibit intermolecular interactions with a benzene molecule that bridges two [Tm$^{Bu^{t}Benz}$]Tl moieties, as illustrated in Figure 8.

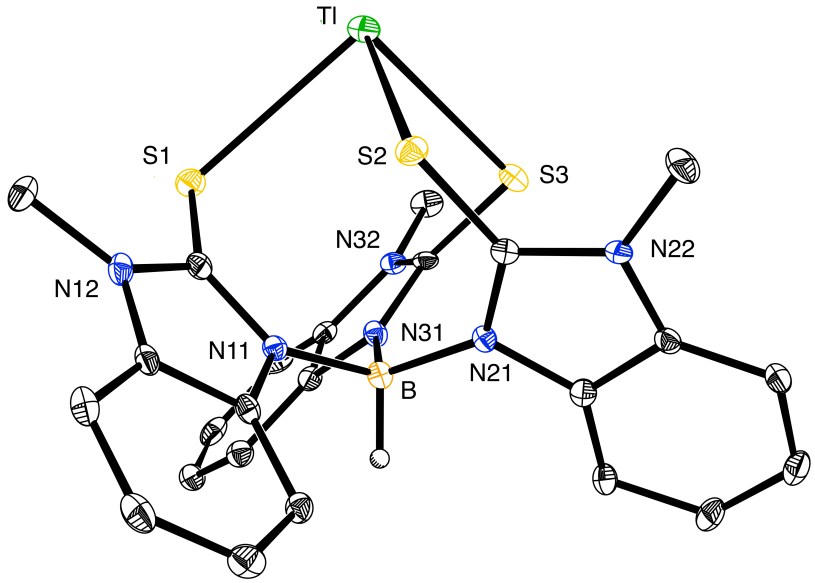

Figure 6. Molecular structure of [Tm^{MeBenz}]Tl. The closest contact is a sulfur atom from an adjacent molecule, with a Tl•••S distance of 3.37 Å.

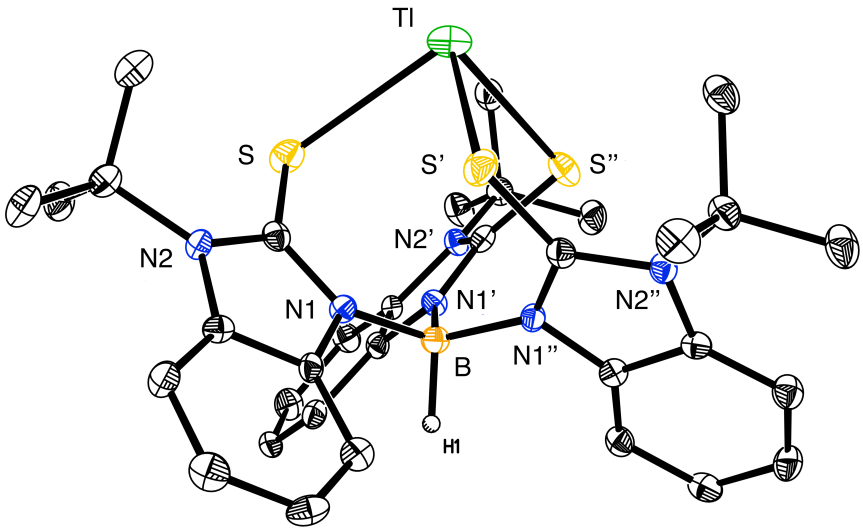

Figure 7. Molecular structure of [Tm$^{Bu^tBenz}$]Tl•C_6H_6.

Table 2. Metric data for [Tm$^{Bu^tBenz}$]Tl and [Tm^{MeBenz}]Tl

	[Tm^{MeBenz}]Tl	[Tm$^{Bu^tBenz}$]Tl
Tl–S / Å	2.926(1), 2.951(1) and 3.112(1)	2.895(1)
Tl•••B / Å	4.39	4.14
S–Tl–S / °	93.55(4), 81.94(4) and 81.11(3)	88.81(3)
Pyramidality $P = 360° - \Sigma(S–Tl–S)$	103.4	93.6

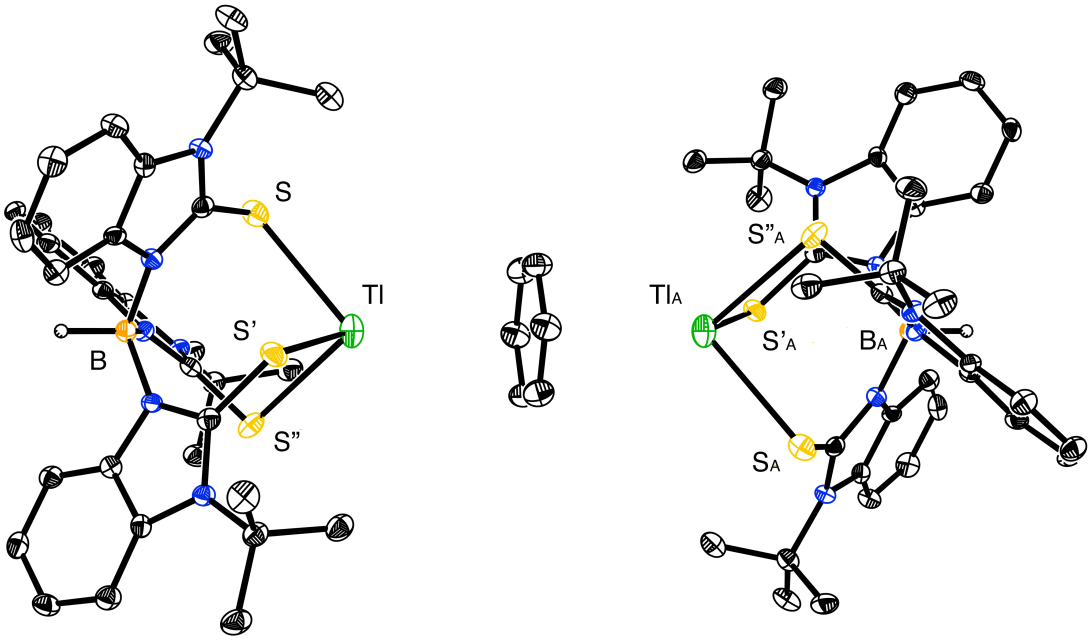

Figure 8. {[Tm$^{Bu^tBenz}$]Tl}$_2$•C_6H_6 unit. The distance between two Tl atoms is 6.77 Å.

3.5 Summary and Conclusion

In summary, computational analysis on [Tm^{MeBenz}] anion demonstrates that benzannulation promotes a κ^3-cooridination mode in [Tm^{MeBenz}]Na. The t-butyl counterpart of [Tm^{MeBenz}]Na, namely [Tm$^{Bu^tBenz}$]Na, was synthesized and

characterized. The compound can be crystallized as a dimer with solvents such as tetrahydrofuran or without solvents coordination. Both [Tm^{MeBenz}]Na and [Tm^{Bu^tBenz}]Na can be converted to the thallium complexes *via* reactions with TlOAc. The two thallium compounds obtained, namely [Tm^{MeBenz}]Tl and [Tm^{Bu^tBenz}]Tl, are the first structurally characterized monovalent, monomeric [Tm^{R}]Tl species.

3.6 Experimental Section

3.6.1 General Considerations

All manipulations were performed using a combination of glovebox, high vacuum, and Schlenk techniques under a nitrogen or argon atmosphere.[22] Solvents were purified and degassed by standard procedures. NMR spectra were measured on Bruker 300 DRX, Bruker Avance III 400, Bruker Avance III 400SL and Bruker Avance III 500 DMX spectrometers. ^{1}H NMR spectra are reported in ppm relative to $SiMe_4$ ($\delta = 0$) and were referenced internally with respect to the protio solvent impurity (δ 7.26 for $CDCl_3$, δ 5.32 for CD_2Cl_2 and δ 2.50 for *d*$_6$-DMSO).[23] ^{13}C NMR spectra are reported in ppm relative to $SiMe_4$ (δ = 0) and were referenced internally with respect to the solvent (δ 77.36 for $CDCl_3$ and δ 39.51 for *d*$_6$-DMSO).[23] Coupling constants are given in hertz. IR spectra were recorded on a PerkinElmer Spectrum Two spectrometer, of which the latter was used in attenuated total reflectance (ATR) mode. IR data are reported in reciprocal centimeters (cm^{-1}). Mass spectra were obtained on Voyager DE pro (MALDI-TOF) mass spectrometer using matrix assisted laser desorption ionization. $NaBH_4$ (Aldrich) and TlOAc (Aldrich) were obtained commercially and used as received.

3.6.2 X-ray Structure Determinations

Single crystal X-ray diffraction data were collected on a Bruker Apex II diffractometer and crystal data, data collection and refinement parameters are summarized in Table 3. The structures were solved using direct methods and standard difference map techniques, and were refined by full-matrix least-squares procedures on F^2 with SHELXTL (Version 2008/4).[24]

3.6.3 Computational Details

Calculations were carried out using DFT as implemented in the Jaguar 7.6 (release 110) and 7.7 (release 107) suite of *ab initio* quantum chemistry programs.[25] Geometry optimizations were performed with the B3LYP density functional[26] using the 6-31G** basis set.[27]

3.6.4 Synthesis of [Tm$^{Bu^tBenz}$]Na(THF)

A mixture of 1-*t*-butyl-2-benzimidazole-2-thione (515 mg, 2.50 mmol)[28] and $NaBH_4$ (32 mg, 0.83 mmol) was placed in an ampoule and treated with THF (*ca.* 6 mL). The mixture was heated at 160 °C for 4 days. After this period, the mixture was filtered and the precipitate was washed with toluene (2 mL) then pentane (3 × 4 mL) and dried *in vacuo* to give [Tm$^{Bu^tBenz}$]Na(THF) (200 mg, 33%) as a white powder. Anal. calcd. for [Tm$^{Bu^tBenz}$]Na•THF: C, 61.5%; H, 6.7%; N,11.6%. Found: C, 60.3%; H, 7.0%; N, 10.5%. ^{1}H NMR (d_6-DMSO): 1.76 [m, 4H of HB{(C_4H_4)C_2N_2(CH_3)CS}$_3$Na($C_4\underline{H}_8O$)], 2.03 [s, 27H of HB{(C_4H_4)C_2N_2($C_4\underline{H}_9$)CS}$_3$Na(C_4H_8O)], 3.61 [m, 4H of HB{(C_4H_4)C_2N_2(C_4H_9)CS}$_3$Na($C_4\underline{H}_8O$)], 6.63 [broad, 3H of HB{($C_4\underline{H}_4$)C_2N_2(C_4H_9)CS}$_3$Na(C_4H_8O)], 6.76 [t, $^3J_{H\text{-}H}$ = 8Hz, 3H of HB{($C_4\underline{H}_4$)C_2N_2(C_4H_9)CS}$_3$Na(C_4H_8O)], 7.58 [d, $^3J_{H\text{-}H}$ = 8 Hz, 3H of

$HB\{(C_4\underline{H}_4)C_2N_2(C_4H_9)CS\}_3Na(C_4H_8O)]$, 6.5 ~ 7.2 [broad, 3H of $HB\{(C_4\underline{H}_4)C_2N_2(C_4H_9)CS\}_3Na(C_4H_8O)]$. $^{13}C\{^1H\}$ NMR (d_6-DMSO): 25.1 [2C of $HB\{(C_4H_4)C_2N_2(C_4H_9)CS\}_3Na(\underline{C}_4H_8O)]$, 30.0 [9C of $HB\{(C_4H_4)C_2N_2(\underline{C}_4H_9)CS\}_3Na(C_4H_8O)]$, 60.8 [3C of $HB\{(C_4H_4)C_2N_2(\underline{C}_4H_9)CS\}_3Na(C_4H_8O)]$, 67.0 [2C of $HB\{(C_4H_4)C_2N_2(C_4H_9)CS\}_3Na(\underline{C}_4H_8O)]$, 111.6 [3C of $HB\{(\underline{C}_4H_4)C_2N_2(C_4H_9)CS\}_3Na(C_4H_8O)]$, 113.0 [3C of $HB\{(\underline{C}_4H_4)C_2N_2(C_4H_9)CS\}_3Na(C_4H_8O)]$, 119.3 [3C of $HB\{(\underline{C}_4H_4)C_2N_2(C_4H_9)CS\}_3Na(C_4H_8O)]$, 119.9 [3C of $HB\{(\underline{C}_4H_4)C_2N_2(C_4H_9)CS\}_3Na(C_4H_8O)]$, 133.8 [3C of $HB\{(C_4H_4)\underline{C}_2N_2(C_4H_9)CS\}_3Na(C_4H_8O)]$, 137.6 [3C of $HB\{(C_4H_4)\underline{C}_2N_2(C_4H_9)CS\}_3Na(C_4H_8O)]$, 173.3 [3C of $HB\{(C_4H_4)C_2N_2(C_4H_9)\underline{C}S\}_3Na(C_4H_8O)]$. Crystals of $\{[Tm^{Bu^tBenz}]Na(THF)\}_2(\mu\text{–}THF)_2$, suitable for X-ray diffraction, were obtained by allowing a hot THF solution to cool to room temperature.

3.6.5 Synthesis of $[Tm^{MeBenz}]Tl$

A solution of $[Tm^{MeBenz}]Na\bullet 1.5THF$ (135 mg, 0.21 mmol) in diglyme (2 mL) was treated with a solution of TlOAc (68 mg, 0.26 mmol) in distilled water (3 mL), resulting in the formation of a white precipitate in a light yellow solution. The mixture was stirred at room temperature for 1 hour and then treated with distilled water (10 mL). The mixture was filtered and the precipitate was washed with water (*ca*. 15 mL) to give $[Tm^{MeBenz}]Tl$ as a white solid obtained was dried in air overnight and then dried *in vacuo* (126 mg, 84%). Crystals of $[Tm^{MeBenz}]Tl$ suitable for X-ray diffraction were obtained by slow evaporation of a concentrated CH_2Cl_2 solution in air. Anal. calcd. for $[Tm^{MeBenz}]Tl$: C, 40.8%; H, 3.1%; N,11.9%. Found:

C, 41.0%; H, 3.2%; N, 11.7%. ^{1}H NMR (CD_2Cl_2): 3.74 [s, 9H of $HB\{(C_4\underline{H}_4)C_2N_2(C\underline{H}_3)CS\}_3Tl$], 7.13 [t, $^{3}J_{H-H}$ = 8 Hz, 3H of $HB\{(C_4\underline{H}_4)C_2N_2(CH_3)CS\}_3Tl$], 7.23 [m, 6H of $HB\{(C_4\underline{H}_4)C_2N_2(CH_3)CS\}_3Tl$], 7.31 [d, $^{3}J_{H-H}$ = 8 Hz, 3H of $HB\{(C_4\underline{H}_4)C_2N_2(CH_3)CS\}_3Tl$]. IR (ATR, cm^{-1}): 2932 (vw), 2414 (vw), 2243 (vw), 1612 (vw), 1484 (m), 1430 (m), 1393 (m), 1370 (w), 1339 (vs), 1296 (m), 1232 (m), 1194 (m), 1142 (m), 1123 (m), 1090 (m), 1014 (m), 914 (w), 858 (m), 814 (w), 739 (vs), 619 (m), 570 (w), 557 (m), 532 (w). FAB-MS: m/z = 704.8 $[M\text{-}1]^+$, M = $[Tm^{MeBenz}]Tl$.

3.6.6 Synthesis of $[Tm^{Bu^tBenz}]Tl$

A solution of $[Tm^{Bu^tBenz}]Na\bullet THF$ (150 mg, 0.21 mmol) in diglyme (2 mL) was treated with a solution of TlOAc (65 mg, 0.25 mmol) in distilled water (3 mL), resulting in the formation of a white precipitate in a light pink solution. The mixture was stirred at room temperature for 1 hour and then treated with distilled water (10 mL). The mixture was filtered and the precipitate was washed with water (*ca*. 15 mL) to give $[Tm^{Bu^tBenz}]Tl$ as a white solid that was dried in air overnight and then dried *in vacuo* (159 mg, 92%). Crystals suitable for X-ray diffraction were obtained by slow evaporation of a concentrated CH_2Cl_2 solution containing one drop of benzene in air. Anal. calcd. for $[Tm^{Bu^tBenz}]Tl$: C, 47.6%; H, 4.8%; N, 10.1%. Found: C, 48.4%; H, 4.7%; N, 10.1%. ^{1}H NMR ($CDCl_3$): 2.02 [s, 27H of $HB\{(C_4H_4)C_2N_2(C_4\underline{H}_9)CS\}_3Tl$], 7.05 [m, 6H of $HB\{(C_4\underline{H}_4)C_2N_2(C_4H_9)CS\}_3Tl$], 7.24 [m, 3H of $HB\{(C_4\underline{H}_4)C_2N_2(C_4H_9)CS\}_3Tl$], 7.78 [m, 3H of $HB\{(C_4\underline{H}_4)C_2N_2(C_4H_9)CS\}_3Tl$]. $^{13}C\{^{1}H\}$ NMR ($CDCl_3$): 31.3 [s, 9C of $HB\{(C_4H_4)C_2N_2(\underline{C}_4H_9)CS\}_3Tl$], 62.9 [s, 3C of $HB\{(C_4H_4)C_2N_2(\underline{C}_4H_9)CS\}_3Tl$], 113.3 [s, 3C of $HB\{(\underline{C}_4H_4)C_2N_2(C_4H_9)CS\}_3Tl$], 113.7 [s, 3C of $HB\{(\underline{C}_4H_4)C_2N_2(C_4H_9)CS\}_3Tl$], 121.9 [s, 3C of $HB\{(\underline{C}_4H_4)C_2N_2(C_4H_9)CS\}_3Tl$], 122.0 [s, 3C of

HB{(C$_4$H$_4$)C$_2$N$_2$(C$_4$H$_9$)CS}$_3$Tl], 134.2 [s, 3C of HB{(C$_4$H$_4$)C$_2$N$_2$(C$_4$H$_9$)CS}$_3$Tl], 136.9 [s, 3C of HB{(C$_4$H$_4$)C$_2$N$_2$(C$_4$H$_9$)CS}$_3$Tl], not observed [3C of HB{(C$_4$H$_4$)C$_2$N$_2$(C$_4$H$_9$)CS}$_3$Tl]. IR (ATR, cm^{-1}): 2968 (w), 2584 (w), 1595 (w), 1474 (m), 1367 (m), 1319 (vs), 1275 (m), 1226 (m), 1188 (m), 1117 (m), 1066 (w), 1031 (m), 975 (m), 929 (w), 823 (m), 786 (m), 742 (s), 633 (m), 583 (m), 554 (m). FAB-MS: *m*/z = 830.9 [M-1]$^+$, M = [Tm$^{Bu^tBenz}$]Tl.

3.7 Crystallographic Data

Table 3. Crystal, intensity collection and refinement data.

	{[Tm$^{Bu^tBenz}$]Na(THF)}$_2$(μ–THF)$_2$	**{[Tm$^{Bu^tBenz}$]Na}$_2$**
lattice	Triclinic	Triclinic
formula	$C_{82}H_{112}B_2N_{12}Na_2O_4S_6$	$C_{66}H_{80}B_2N_{12}Na_2S_6$
formula weight	1589.80	1301.38
space group	*P-1*	*P-1*
a / Å	11.523(5)	11.597(5)
b / Å	11.542(5)	11.630(5)
c / Å	17.423(8)	13.903(6)
α / °	88.111(7)	85.543(7)
β / °	83.839(7)	86.359(7)
γ / °	59.901(6)	60.667(6)
V / Å^3	1992.7(15)	1629.0(13)
Z	1	1
temperature (K)	130(2)	130(2)
radiation (λ, Å)	0.71073	0.71073
ρ (calcd.), g cm^{-3}	1.325	1.327
μ (Mo Kα), mm^{-1}	0.242	0.275
θ max, deg.	26.48	30.90
no. of data collected	34362	31278
no. of data used	8186	10025
no. of parameters	500	411
R_1 [$I > 2\sigma(I)$]	0.0802	0.1152
wR_2 [$I > 2\sigma(I)$]	0.1650	0.1893
R_1 [all data]	0.1378	0.2893
wR_2 [all data]	0.1901	0.2358
GOF	1.033	1.026
R_{int}	0.1380	0.2083

Table 3. (cont.) Crystal, intensity collection and refinement data.

	$[Tm^{MeBenz}]Tl$	$\{[Tm^{Bu^tBenz}]Tl\}_2 \cdot C_6H_6$
lattice	Monoclinic	Rhombohedral
formula	$C_{24}H_{22}BN_6S_3Tl$	$C_{72}H_{86}B_2N_{12}S_6Tl_2$
formula weight	705.84	1742.25
space group	$P2_1/n$	$R\text{-}3$
a / Å	9.3299(7)	17.793(4)
b / Å	12.4112(10)	17.793(4)
c / Å	21.2348(17)	20.084(5)
α / °	90	90
β / °	94.2250(10)	90
γ / °	90	120
V / Å^3	2452.2(3)	5506.3(16)
Z	4	3
temperature (K)	150(2)	150(2)
radiation (λ, Å)	0.71073	0.71073
ρ (calcd.), g cm^{-3}	1.912	1.576
μ (Mo Kα), mm^{-1}	6.869	4.605
θ max, deg.	30.65	30.61
no. of data collected	39361	29619
no. of data used	7560	3778
no. of parameters	322	146
R_1 [$I > 2\sigma(I)$]	0.0435	0.0409
wR_2 [$I > 2\sigma(I)$]	0.0727	0.0597
R_1 [all data]	0.0869	0.1486
wR_2 [all data]	0.0850	0.0747
GOF	1.019	1.103
R_{int}	0.1004	0.2199

3.8 References and Notes

(1) Trofimenko, S. Scorpionates. The Coordination Chemistry of Polypyrazolylborate Ligands, Imperial College Press, London, 1999.

(2) Pettinari, C. Scorpionates II: Chelating Borate Ligands, Imperial College Press, London, 2008.

(3) Trofimenko, S. Boron-Pyrazole Chemistry. *J. Am. Chem. Soc.* **1966**, *88*, 1842–1844.

(4) (a) Green, M. L. H. *J. Organomet. Chem*. **1995**, *500*, 127-148.

(b) Parkin, G. in Comprehensive Organometallic Chemistry III, Volume 1, Chapter 1.01; Crabtree, R. H. and Mingos, D. M. P. (Eds), Elsevier, Oxford, 2006.

(c) Green, J. C.; Green, M. L. H.; Parkin, G. *Chem. Commun*. **2012**, *48*, 11481-11503.

(5) (a) Garner, M.; Reglinski, J.; Cassidy, I.; Spicer, M. D.; Kennedy, A. R. *J. Chem. Soc., Chem. Commun*. **1996**, 1975-1976.

(b) Reglinski, J.; Garner, M.; Cassidy, I. D.; Slavin, P. A.; Spicer, M. D.; Armstrong, D. R. *J. Chem. Soc., Dalton Trans*. **1999**, 2119-2126.

(6) Tellers, D. M., S. J. Skoog, R. G. Bergman, T. B. Gunnoe, and W. D. Harman Organometallics, **2000**, *19*, 2428–2432.

(7) Bailey, P. J.; Lorono-Gonzales, D. J.; McCormack, C.; Parsons, S.; Price, M. *Inorg. Chim. Acta* **2003**, *354*, 61–67.

(8) Cambridge Structural Database (Version 5.34). *3D Search and Research Using the Cambridge Structural Database*, Allen, F. H.; Kennard, O. *Chemical Design Automation News* **1993**, *8* (1), pp 1 & 31-37.

(9) See for example:
(a) Yurkerwich, K.; Yurkerwich, M.; Parkin, G. *Inorg. Chem.* **2011**, *50*, 12284-12295.

(b) Santini, C.; Lobbia, G. G.; Pettinari, C.; Pellei, M.; Valle, G.; Calogero, S. *Inorg. Chem*. **1998**, *37*, 890-900.

(c) Kimblin, C.; Bridgewater, B. M.; Churchill, D. G.; Parkin, G. *Chem. Commun.* **1999**, 2301-2302.

(d) Tesmer, M.; Shu, M.; Vahrenkamp, H. *Inorg. Chem*. **2001**, *40*, 4022-4029.

(e) Bakbak, S.; Bhatia, V. K.; Incarvito, C. D.; Rheingold, A. L.; Rabinovich, D. *Polyhedron* **2001**, *20*, 3343-3348.

(f) Bailey, P. J.; Dawson, A.; McCormack, C.; Moggach, S.; Oswald, I. D. H.; Parsons, S.; Rankin, D.W. H.; Turner, A. *Inorg. Chem*. **2005**, *44*, 8884-8898.

(g) Ibrahim, M. M.; Shu, M.; Vahrenkamp, H. *Eur. J. Inorg. Chem*. **2005,** 1388–1397.

(h) Mihalcik, D. J.; White, J. L.; Tanski, J. M.; Zakharov, L. N.; Yap, G. P. A.; Incarvito, C. D.; Rheingold, A. L.; Rabinovich, D. *Dalton Trans.* **2004**, 1626-1634.

(10) Al-Harbi, A.; Sattler, W.; Sattler, A.; Parkin, G. *Chem. Commun.* **2011**, *47*, 3123–3125.

(11) Biernat, A.; Schwalbe, M.; Wallace, D.; Reglinski, J.; Spicer, M. D. *Dalton Trans.* **2007**, 2242-2244.

(12) The calcium compound $[Tm^{Me}]Ca{\bullet}6H_2O$ also exists as ions in the solid state,[a] whereas the potassium compound $[Tm^{Me}]K{\bullet}4H_2O$ adopts a polymeric structure in which the $[Tm^{Me}]$ ligand bridges potassium centers.

(a) Çetin, A.; Ziegler, C. J. *Dalton Trans*. **2006**, 1006-1008.

(b) Soares, L. F.; Silva, R. M.; Doriguetto, A. C.; Ellena, J.; Mascarenhas, Y. P.; Castellano, E. E. *J. Braz. Chem. Soc.* **2004**, *15*, 695-700.

(13) Evidently, the observation that k^3-S_3 coordination is prevalent for $\{[Tm^R]M\}$ complexes is a reflection of the M–S bonds being sufficiently strong to compensate for the energetic penalty associated with the $[Tm^R]$ ligand adopting a conformation that is not favored in the gas phase anion.

(14) Bridgewater, B. M.; Parkin, G. *Inorg. Chem. Commun*. **2000**, *3*, 534-536.

(15) Rajasekharan-Nair, R.; Moore, D.; Chalmers, K.; Wallace, D.; Diamond, L. M.; Darby, L.; Armstrong, D. R.; Reglinski, J.; Spicer, M. D. *Chem. Eur. J.* **2013**, *19*, 2487-2495.

(16) The energies reported here correspond to the cc-pVTZ(-f) correlation consistent triple-z basis and the values for $[Tm^{Me}]^-$ compare favorably with recently reported calculations that employ the 6-311G** basis set. See reference 15.

(17) The Na•••S distance associated with the uncoordinated thione is 3.552(3) Å.

(18) Mihalcik, D. J.; White, J. L.; Tanski, J. M.; Zakharov, L. N.; Yap, G. P. a; Incarvito, C. D.; Rheingold, A. L.; Rabinovich, D. *Dalton Trans.* **2004**, 1626–34.

(19) Examination of $[Tm^R]Tl$ compounds in Cambridge Structural Database (version 5.34) shows no other monomeric structures.

(20) An out of plane parameter, ϕ, has also been used to indicate the degree of pyramidality. However, in asymmetric structures in which the three Y–X–Y′ angles are not equal, the value of ϕ depends on which three atoms are selected to constitute the plane.[a] For this reason, the deviation of the sum of the three Y–X–Y′ angles from 360° provides a simple gauge of the pyramidality.[b-d]

(a) Ruhlandt-Senge, K.; Bartlett, R. A.; Olmstead, M. M.; Power, P. P. *Angew. Chem. Int. Edit. Engl.* **1993**, *32*, 425-427.

(b) Wright, R. J.; Phillips, A. D.; Hardman, N. J.; Power, P. P. *J. Am. Chem. Soc.* **2002**, *124*, 8538-8539.

(c) Hardman, N. J.; Wright, R. J.; Phillips, A. D.; Power, P. P. *J. Am. Chem. Soc.* **2003**, *125*, 2667-2679.

(d) Rivard, E.; Power, P. P. *Inorg. Chem.* **2007**, *46*, 10047-10064.

(21) Al-Harbi, A.; Rong, Y.; Parkin, G. *Dalton Trans. Accepted.*

(22) (a) McNally, J. P.; Leong, V. S.; Cooper, N. J. in Experimental Organometallic Chemistry, Wayda, A. L.; Darensbourg, M. Y., Eds.; American Chemical Society: Washington, DC, 1987; Chapter 2, pp 6-23.

(b) Burger, B.J.; Bercaw, J. E. in Experimental Organometallic Chemistry; Wayda, A. L.; Darensbourg, M. Y., Eds.; American Chemical Society: Washington, DC, 1987; Chapter 4, pp 79-98.

(c) Shriver, D. F.; Drezdzon, M. A.; The Manipulation of Air-Sensitive Compounds, 2nd Edition; Wiley-Interscience: New York, 1986.

(23) Fulmer, G. R.; Miller, A. J. M.; Sherden, N. H.; Gottlieb, H. E.; Nudelman, A.; Stoltz, B. M.; Bercaw, J. E.; Goldberg, K. I. *Organometallics* **2010**, *29*, 2176–2179.

(24) (a) Sheldrick, G. M. SHELXTL, An Integrated System for Solving, Refining and Displaying Crystal Structures from Diffraction Data; University of Göttingen, Göttingen, Federal Republic of Germany, 1981.

(b) Sheldrick, G. M. *Acta Cryst*. **2008**, *A64*, 112-122.

(25) Jaguar 7.6 and 7.7, Schrödinger, LLC, New York, NY 2009 and 2010.

(26) (a) Becke, A. D. *J. Chem. Phys*. **1993**, *98*, 5648-5652.

(b) Becke, A. D. *Phys. Rev. A* **1988**, *38*, 3098-3100.

(c) Lee, C. T.; Yang, W. T.; Parr, R. G. *Phys. Rev. B* **1988**, *37*, 785-789.

(d) Vosko, S. H.; Wilk, L.; Nusair, M. *Can. J. Phys*. **1980**, *58*, 1200-1211.

(e) Slater, J. C. Quantum Theory of Molecules and Solids, Vol. 4: The Self-Consistent Field for Molecules and Solids; McGraw-Hill: New York, 1974.

(27) (a) Hay, P. J.; Wadt, W. R. *J. Chem. Phys*. **1985**, *82*, 270-283.

(b) Wadt, W. R.; Hay, P. J. *J. Chem. Phys*. **1985**, *82*, 284-298.

(c) Hay, P. J.; Wadt, W. R. *J. Chem. Phys*. **1985**, *82*, 299-310.

(28) Zhang, P.; Terefenko, E. A.; Bray, J.; Deecher, D.; Fensome, A.; Harrison, J.; Kim, C.; Koury, E.; Mark, L.; McComas, C. C.; Mugford, C. A.; Trybulski, E. J.; Vu, A. T.; Whiteside, G. T.; Mahaney, P. E. *J. Med. Chem*. **2009**, *52*, 5703-5711.

CHAPTER 4

Synthesis and Structural Characterization of [Tm^{R}]M (M = Ti, Zr, Hf) Complexes

Table of Contents

4.1 Introduction

The *tris*(mercaptoimidazolyl)hydroborato ligand, as mentioned in the previous chapter, belongs to the same L_2X class[1] as the ubiquitous [Tp^R] and cyclopentadienyl ligands. It is anticipated that [Tm^R] will serve as an ancillary ligand for an extensive and diverse series of organotransition metal compounds. Indeed, [Tm^R] ligand has been widely applied to both main group metals and transition metals.[2] To date, the majority of studies employing [Tm^R] ligands has been largely focused on the group 6 – 10 transition metals, with the first examples of group 5 derivatives, namely [Tm^{Me}]M(NR)Cl_2 (M = Nb, Ta), having been reported only recently.[3] Furthermore, despite the apparent mismatch between the "hard" group-4 elements and the soft sulfur-donor ligands, a number of Ti and Zr compounds incorporated with [Tm^R] ligands had been reported.[4] However, as far as we know, no Hf complexes with [Tm^R] ligand are reported.

Therefore, in this chapter, we report the synthesis and structural characterization of a few [Tm^R]M (M = Ti, Zr, Hf) compounds, including (*i*) Cp[Tm^{Bu^t}]$TiCl_2$ and Cp[Tm^{Bu^t}]$ZrCl_2$, which are analogues of Cp_2TiCl_2 and Cp_2ZrCl_2, and (*ii*) [Tm^{Bu^t}]$Zr(CH_2Ph)_3$ and the first structurally characterized [Tm^R]Hf complexes, [Tm^{Bu^t}]$Hf(CH_2Ph)_3$ and [Tm^{Ad}]$Hf(CH_2Ph)_3$.

4.2 Synthesis and Structure of Cp[Tm^{Bu^t}]$TiCl_2$

Tris(2-mercapto-1-R-imidazolyl)hydroborato titanium compounds are currently unknown. The only structure of a [Tm^R] titanium compound listed in the Cambridge Structural Database,[5] is a Ti^{III} complex, {Ti[Tm^{Me}]$_2$}{Ti(THF)$_2$Cl$_4$}.[4a] Attempts to synthesize [Tm^{Me}]$_x$TiCl$_{4-x}$ derivatives via reaction of $TiCl_4$ or $TiCl_4(THF)_2$ with [Tm^{Me}]Na were reported to be unsuccessful due to redox/ligand

cleavage processes interfering with a simple halide metathesis reaction.[6] Therefore, it is notable that the titanium complex Cp[Tm$^{Bu^t}$]TiCl$_2$ can be obtained by treatment of CpTiCl$_3$ with [Tm$^{Bu^t}$]K in benzene (Scheme 1). The molecular structure has been determined by X-ray diffraction, as illustrated in Figure 1.

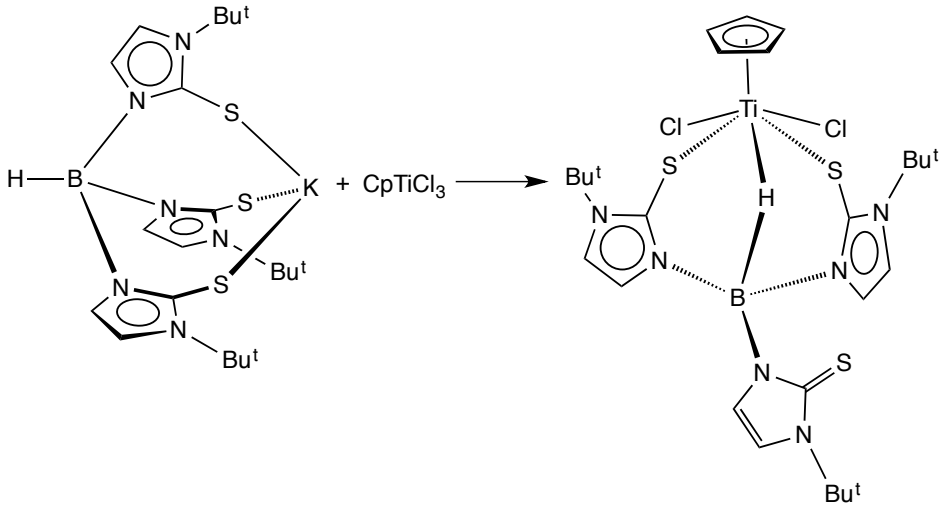

Scheme 1. Synthesis of Cp[Tm$^{Bu^t}$]TiCl$_2$

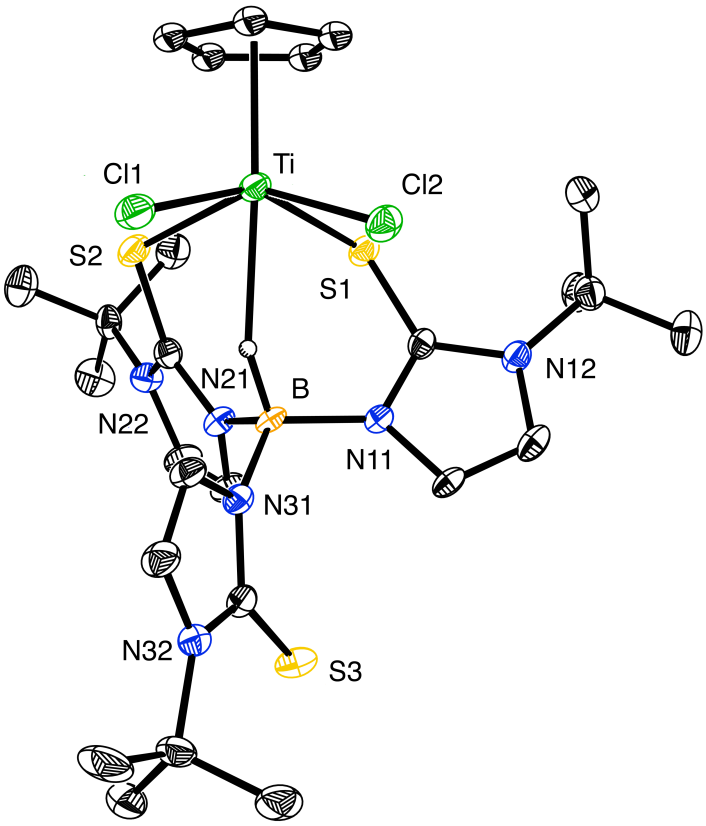

Figure 1. Molecular structure of Cp[Tm$^{Bu^t}$]TiCl$_2$

The most noteworthy structural feature of Cp[Tm$^{Bu^t}$]TiCl$_2$ is that the [Tm$^{Bu^t}$] coordinates in a κ^3-*S*$_2$*H* manner, with the third mercaptoimidazolyl arm pointing away from the B–H group. Thus, the molecule closely resembles Cp$_2$TiCl$_2$ in the sense that [Tm$^{Bu^t}$] and Cp are both L$_2$X type ligands. The Ti–S bond lengths are [2.477(2) Å] and [2.560(2) Å] respectively and are close to the average value [2.45 Å] of Ti–S bond length according to Cambridge Structural Database. The Ti•••H–B distance is [2.23(3) Å], which is at the long end of the distribution.[7] As seen in crystal structure, the molecule is chiral due to the propeller-like twist caused by the t-butyl substituents attached to the mercaptoimidazolyl groups. In the ^{1}H NMR spectrum, the t-butyl groups are characterized by a 2:1 set of signals.

The compound has limited stability at room temperature and decomposes to a mixture of compounds within one hour, one of which is identified by X-ray diffraction as $[CpTiClO]_4$.[8]

4.3 Synthesis and Structures of Tris(mercaptoimidazolyl)hydroborato Complexes of Zirconium

4.3.1 $Cp[Tm^{Bu^t}]ZrCl_2$: an Analogue of $Cp[Tm^{Me}]ZrCl_2$

The first structurally characterized $[Tm^{Me}]$ zirconium compound $Cp[Tm^{Me}]ZrCl_2$ was reported by our group.[4c] The molecule closely resembles the bent-metallocene geometry of Cp_2ZrCl_2. The three methimazole rings are inequivalent in the ^1H NMR spectrum, resulting in a set of 2:1 signals.

Here we report the t-butyl analogue, namely $Cp[Tm^{Bu^t}]ZrCl_2$, by following a similar synthetic method, as illustrated in Scheme 2. It is worth noting that the reaction of $CpZrCl_3$ and $[Tm^{Bu^t}]K$ always produces a small amount of impurity, which has been identified as $Cp(\kappa^2\text{-}S,N\text{-}mim^{Bu^t})(\kappa^1\text{-}S\text{-}Hmim^{Bu^t})ZrCl_2$. The molecular structures of $Cp[Tm^{Bu^t}]ZrCl_2$ and $Cp(\kappa^2\text{-}S,N\text{-}mim^{Bu^t})(\kappa^1\text{-}S\text{-}Hmim^{Bu^t})ZrCl_2$ have been determined by X-ray diffraction, as illustrated in Figure 2 and Figure 3, respectively. Significantly, the $[Tm^{Bu^t}]$ ligand in $Cp[Tm^{Bu^t}]ZrCl_2$ coordinates in the same way as that in $Cp[Tm^{Bu^t}]TiCl_2$, *i.e.* $\kappa^3\text{-}S_2H$ rather than a $\kappa^3\text{-}S_3$ face-capping manner as in $Cp[Tm^{Me}]ZrCl_2$. Density functional theory geometry optimization calculations[9] on $\kappa^3\text{-}S_2H$ and $\kappa^3\text{-}S_3$ coordination modes show that, in $Cp[Tm^{Bu^t}]ZrCl_2$, the $\kappa^3\text{-}S_2H$ mode is favored by 6.3 kcal/mol while that for $Cp[Tm^{Me}]ZrCl_2$ is only 1.5 kcal/mol.

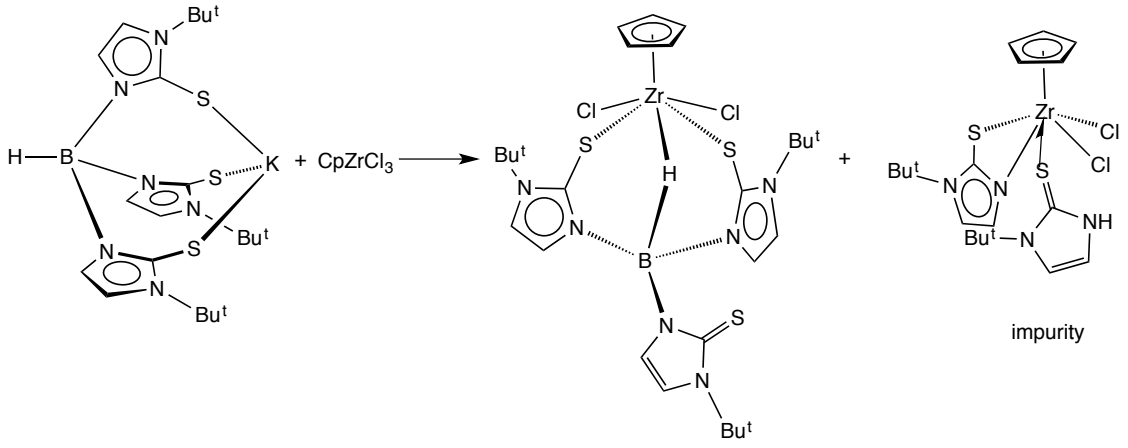

Scheme 2. Synthesis of Cp[Tm$^{Bu^t}$]ZrCl$_2$ *via* reaction of CpZrCl$_3$ and [Tm$^{Bu^t}$]K

Metrical data of Cp[Tm$^{Bu^t}$]ZrCl$_2$, Cp$_2$ZrCl$_2$ and Cp[Tm^{Me}]ZrCl$_2$ are summarized in Table 1. It is worth noting that although [Tm^R] ligand coordinates in a κ^3-*S$_2$H* mode instead of face-capping in Cp[Tm$^{Bu^t}$]ZrCl$_2$, the metrical data of this compound are closer to the values in Cp$_2$ZrCl$_2$ than those in Cp[Tm^{Me}]ZrCl$_2$. In addition, Cp[Tm$^{Bu^t}$]ZrCl$_2$ has the smallest Cl–Zr–Cl angle among the three compounds. The Zr–S bond lengths for Cp[Tm$^{Bu^t}$]ZrCl$_2$ are [2.601 (1)Å] and [2.665(1) Å] respectively, which are within the range of compounds listed in the Cambridge Structural Database (2.31 – 2.95 Å). The distance between Zr and H atom attached to B atom is 2.25 Å, which is also in the range for distance of Zr•••H–B interactions.[10]

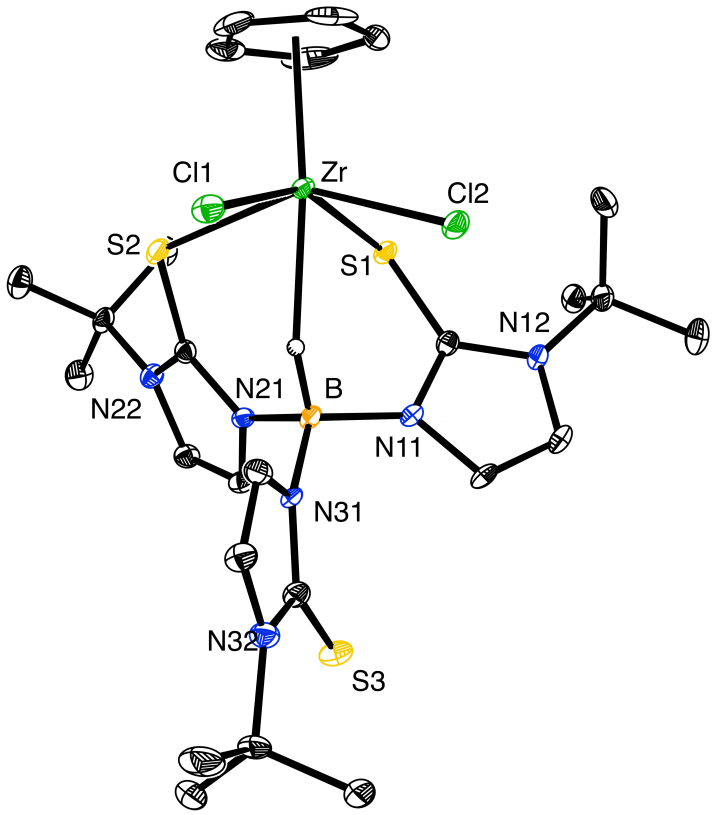

Figure 2. Molecular structure of Cp[Tm$^{Bu^t}$]ZrCl$_2$

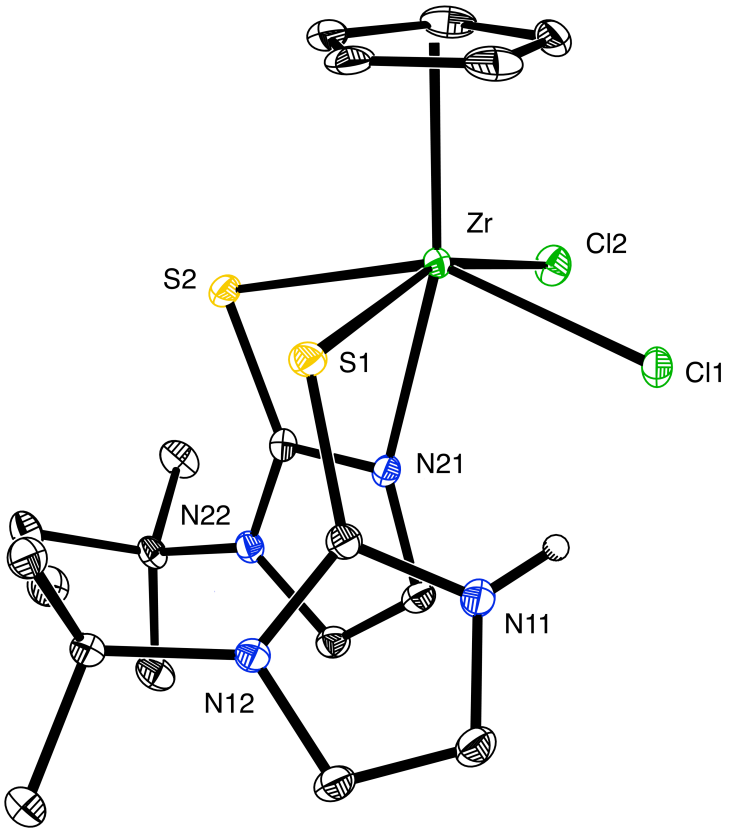

Figure 3. Molecular structure of Cp(κ²-*S*,*N*-mim$^{Bu^t}$)(κ¹-*S*-Hmim$^{Bu^t}$)ZrCl$_2$

Table 1. Metrical Data for Cp[Tm$^{Bu^t}$]ZrCl$_2$, Cp[Tm^{Me}]ZrCl$_2$ and Cp$_2$ZrCl$_2$

	Cp[Tm$^{Bu^t}$]ZrCl$_2$	Cp[Tm^{Me}]ZrCl$_2$[a]	Cp$_2$ZrCl$_2$[a]
Zr-C$_{range}$/Å	2.46 – 2.50	2.51 – 2.57	2.47 –2.52
Zr-C$_{av}$/Å	2.48	2.54	2.50
Zr-Cp$_{cent}$/Å	2.20	2.26	2.20
Zr-Cl/Å	2.45 and 2.48	2.52	2.45
Cl – Zr – Cl/deg	89.4	97.9	97.0

(a) data taken from reference 4c.

Similar to Cp[Tm^{Me}]ZrCl$_2$, Cp[Tm$^{Bu^t}$]ZrCl$_2$ also serves as a precursor for the polymerization of ethylene. Thus a combination of Cp[Tm$^{Bu^t}$]ZrCl$_2$ and methylalumoxane (MAO) produces a catalyst that is capable of polymerizing ethylene with an activity of 104 kg of PE [mol Zr]$^{-1}$ [h]$^{-1}$ [atm C_2H_4]$^{-1}$ at room temperature, which is close to that obtained from Cp_2ZrCl_2 and MAO under comparable conditions (180 kg of PE [mol Zr]$^{-1}$ [h]$^{-1}$ [atm C_2H_4]$^{-1}$).

4.3.2 Synthesis and Structure of a [Tm$^{Bu^t}$]Zr Benzyl Complex

The first [Tm^{R}] zirconium alkyl complex, [Tm$^{Bu^t}$]Zr(CH_2Ph)$_3$ was synthesized by treating [Tm$^{Bu^t}$]Tl with Zr(CH_2Ph)$_3$ in benzene (Scheme 3). The molecular structure of [Tm$^{Bu^t}$]Zr(CH_2Ph)$_3$ has been determined by X-ray diffraction, as illustrated in Figure 4. The most noteworthy structural feature of [Tm$^{Bu^t}$]Zr(CH_2Ph)$_3$ is that it resembles the geometry of [Tp^{Me_2}]Zr(CH_2Ph)$_3$.[11] However, the structure has a C_3 symmetry which is different from the C_{3v} symmetry of [Tp^{Me_2}]Zr(CH_2Ph)$_3$. The Zr–CH_2–Ph angle is 120.7°, therefore, the benzyl ligand coordinates in an η^1-manner according to the discussion in Chapter 1.[12] The Zr–S bond length is [2.648(3) Å], which is close to the average value ([2.63 Å]) obtained from the Cambridge Structural Database. In the ^{1}H NMR spectrum, two methylene protons are inequivalent and appear as two doublets with $^2J_{H\text{-}H}$ value of 10 Hz. The compound has limited stability and decomposes to an unidentified species and bibenzyl within a couple hours at room temperature.

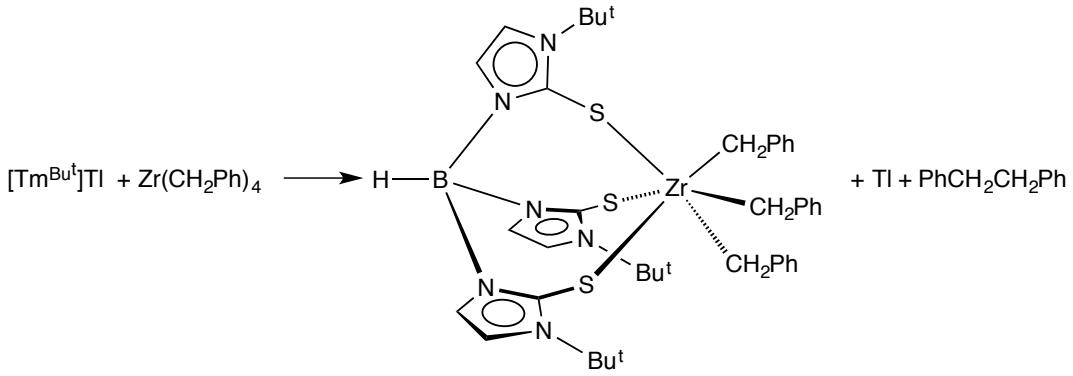

Scheme 3. Synthesis of $[Tm^{Bu^t}]Zr(CH_2Ph)_3$

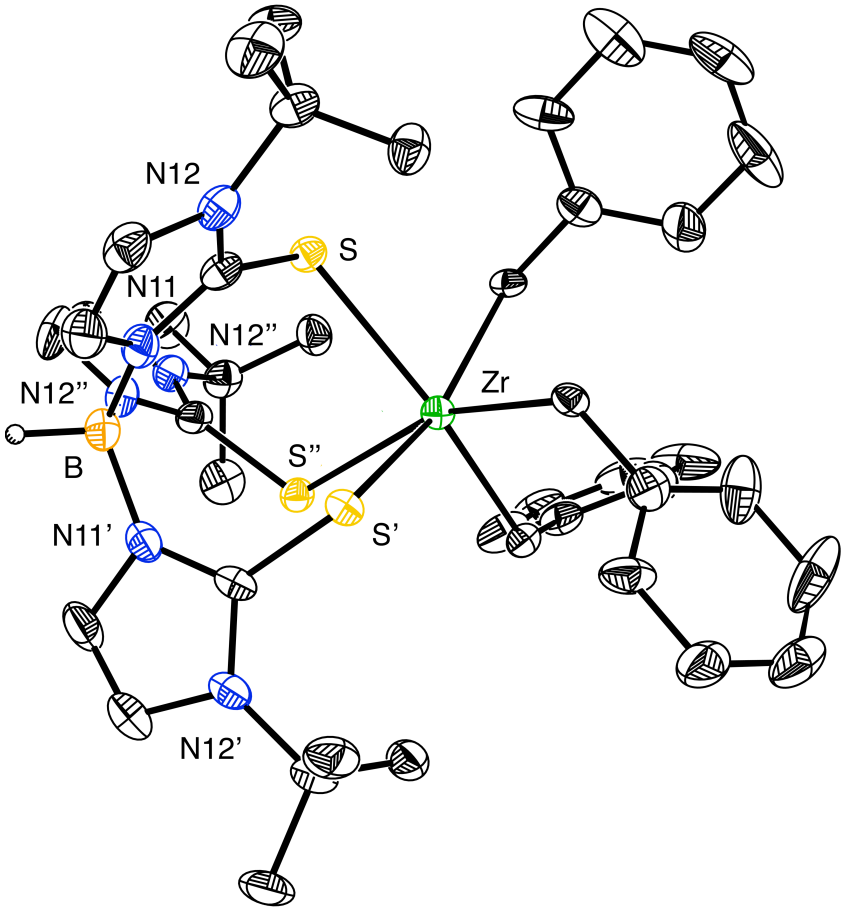

Figure 4. Molecular structure of $[Tm^{Bu^t}]Zr(CH_2Ph)_3$

4.4 Synthesis and Structures of [Tm$^{Bu^t}$]Hf complexes

Similar to the synthesis of [Tm$^{Bu^t}$]Zr(CH$_2$Ph)$_3$, we were able obtain [Tm$^{Bu^t}$]Hf(CH$_2$Ph)$_3$, [Tm^{Ad}]Hf(CH$_2$Ph)$_3$ and [Tm^{MeBenz}]Hf(CH$_2$Ph)$_3$ successfully. Furthermore, the molecular structures of [Tm$^{Bu^t}$]Hf(CH$_2$Ph)$_3$ and [Tm^{Ad}]Hf(CH$_2$Ph)$_3$ have been determined by X-ray diffraction (Figure 5 and Figure 6), therefore, representing the first structurally characterized examples of [Tm^{R}]Hf complexes.

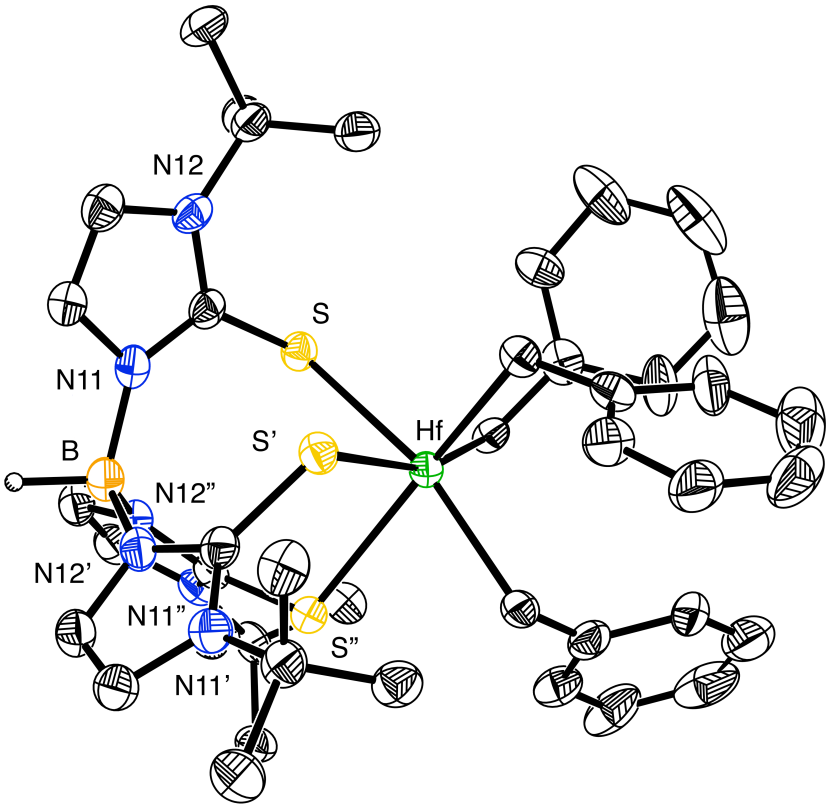

Figure 5. Molecular structure of [Tm$^{Bu^t}$]Hf(CH$_2$Ph)$_3$

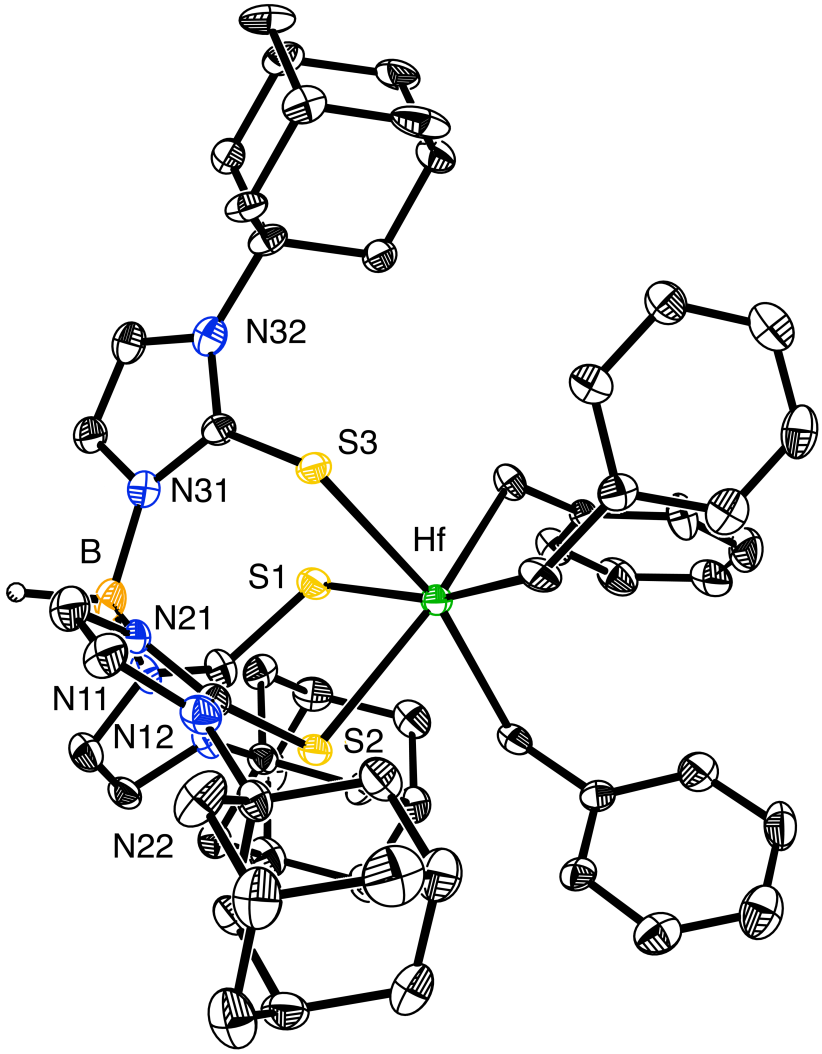

Figure 6. Molecular structure of $[Tm^{Ad}]Hf(CH_2Ph)_3$

The geometries of $[Tm^{Bu^t}]Hf(CH_2Ph)_3$ and $[Tm^{Ad}]Hf(CH_2Ph)_3$ are similar to $[Tm^{Bu^t}]Zr(CH_2Ph)_3$ with C_3 symmetry and η^1- coordinated benzyl groups. The average Hf–S bond length in $[Tm^{Bu^t}]Hf(CH_2Ph)_3$ is 2.63 Å, while that for $[Tm^{Ad}]Hf(CH_2Ph)_3$ is 2.65 Å. Both values are within the range based on data from the Cambridge Structural Database.[13] Similar to $[Tm^{Bu^t}]Zr(CH_2Ph)_3$, all three hafnium complexes have a set of two doublets for their methylene protons in ^1H NMR spectra, as illustrated in Table 2.

Table 2. ^{1}H NMR data for methylene protons

	Hf–C<u>*H*</u>$_2$ #1/ppm	Hf–C<u>*H*</u>$_2$ #2/ppm	Coupling constant/Hz
[Tm$^{Bu^t}$]Hf(CH$_2$Ph)$_3$	1.84	2.25	11
[Tm^{Ad}]Hf(CH$_2$Ph)$_3$	2.52	2.68	11
[Tm^{MeBenz}]Zr(CH$_2$Ph)$_3$	2.31	2.39	11

Additionally, [Tm$^{Bu^t}$]Hf(CH$_2$Ph)$_3$ is able to serve as a precatalyst for ethylene polymerization. Thus, activated by [PhNHMe$_2$][B(C$_6$F$_5$)$_4$], [Tm$^{Bu^t}$]Hf(CH$_2$Ph)$_3$ has an activity of 6 kg of PE [mol Hf]$^{-1}$ [h]$^{-1}$ [atm C$_2$H$_4$]$^{-1}$ at room temperature.

4.5 Summary and Conclusion

In summary, a few [Tm^{R}]M (M = Ti, Zr, Hf) complexes are synthesized and characterized, including (*i*) Cp[Tm$^{Bu^t}$]TiCl$_2$ and Cp[Tm$^{Bu^t}$]ZrCl$_2$, which are analogues of Cp$_2$TiCl$_2$ and Cp$_2$ZrCl$_2$; (*ii*) [Tm$^{Bu^t}$]Zr(CH$_2$Ph)$_3$; (*iii*) [Tm$^{Bu^t}$]Hf(CH$_2$Ph)$_3$ and [Tm^{Ad}]Hf(CH$_2$Ph)$_3$, which are the first structurally characterized [Tm^{R}]Hf complexes.

4.6 Experimental Section

4.6.1 General Considerations

All manipulations were performed using a combination of glovebox, high vacuum, and Schlenk techniques under a nitrogen or argon atmosphere.[14] Solvents were purified and degassed by standard procedures. NMR spectra

were measured on Bruker 300 DRX, Bruker Avance III 400, Bruker Avance III 400SL and Bruker Avance III 500 DMX spectrometers. ^{1}H NMR spectra are reported in ppm relative to $SiMe_4$ ($\delta = 0$) and were referenced internally with respect to the protio solvent impurity (δ 7.16 for C_6D_5H, and δ 5.32 for $CDHCl_2$).[15] ^{13}C NMR spectra are reported in ppm relative to $SiMe_4$ ($\delta = 0$) and were referenced internally with respect to the solvent (δ 128.06 for C_6D_6 and δ 53.84 for CD_2Cl_2).[15] Coupling constants are given in hertz. $CpTiCl_3$ and $CpZrCl_3$ are purchased from SigmaAldrich. $HfCl_4$ was purchased from Strem Chemicals, and converted to $Hf(CH_2Ph)_4$ in a way that is similar to $Zr(CH_2Ph)_4$.[12]

4.6.2 X-ray Structure Determinations

Single crystal X-ray diffraction data were collected on a Bruker Apex II diffractometer and crystal data, data collection and refinement parameters are summarized in Table 3. The structures were solved using direct methods and standard difference map techniques, and were refined by full-matrix least-squares procedures on F^2 with SHELXTL (Version 2008/4).[16]

4.6.3 Computational Details

Calculations were carried out using DFT as implemented in the Jaguar 7.6 (release 110) and 7.7 (release 107) suite of *ab initio* quantum chemistry programs.[9] Geometry optimizations were performed with the B3LYP density functional[17] using the 6-31G** basis set.[18]

4.6.4 Synthesis of $Cp[Tm^{Bu^t}]TiCl_2$

$[Tm^{Bu^t}]K$ (13mg, 0.03 mmol) was added slowly to a $CpTiCl_3$ (5mg, 0.02 mmol) benzene solution in an NMR tube equipped with a J. Young valve,

resulting in a green-brown solution. The reaction completed immediately upon mixing and the mixture was lyophilized. The product was extracted into benzene and big black crystals of Cp[Tm^{Bu^t}]$TiCl_2$ were formed within half an hour after diffusing pentane to the benzene solution. The crystals (6 mg, 45%) were collected immediately and characterized by X-ray diffraction. ^{1}H NMR (C_6D_6): 1.22 [s, 18H of HB{$H_2C_2N_2(C_4\underline{H}_9)CS$}$_3$Ti($C_5H_5$)$Cl_2$], 1.70 [s, 9H of HB{$H_2C_2N_2(C_4\underline{H}_9)CS$}$_3$Ti($C_5H_5$)$Cl_2$], 6.14 [d, $^3J_{H-H}$ = 2 Hz, 2H of HB{$\underline{H}_2C_2N_2(C_4H_9)CS$}$_3$Ti($C_5H_5$)$Cl_2$], 6.24 [d, $^3J_{H-H}$ = 2 Hz, 1H of HB{$\underline{H}_2C_2N_2(C_4H_9)CS$}$_3$Ti($C_5H_5$)$Cl_2$], 6.42 [s, 4H of HB{$H_2C_2N_2(C_4H_9)CS$}$_3$Ti($C_5\underline{H}_5$)$Cl_2$], 6.49 [s, 1H of HB{$H_2C_2N_2(C_4H_9)CS$}$_3TiC_5\underline{H}_5$)$Cl_2$], 9.00 [d, $^3J_{H-H}$ = 2 Hz, 1H of HB{$\underline{H}_2C_2N_2(C_4H_9)CS$}$_3$Ti($C_5H_5$)$Cl_2$], 9.32 [d, $^3J_{H-H}$ = 2 Hz, 2H of HB{$\underline{H}_2C_2N_2(C_4H_9)CS$}$_3$Ti($C_5H_5$)$Cl_2$], the proton attached to the boron atom is not observed.

4.6.5 Synthesis of Cp[Tm^{Bu^t}]$ZrCl_2$

$CpZrCl_3$ (21.4 mg, 0.08 mmol) and [Tm^{Bu^t}]K (30.0 mg, 0.06 mmol) were dissolved in CH_2Cl_2 in a vial. After stirring at room temperature for 3h, the mixture was filtered and pumped down to give a yellow solid. The product was extracted with benzene, and hexane was added to induce precipitation. The solid phase was collected by filtration and dried under vacuum to give Cp[Tm^{Bu^t}]$ZrCl_2$ (15 mg, 35%). Crystals suitable for X-ray diffraction were obtained from slow evaporation of a concentrated benzene solution at room temperature. ^{1}H NMR (C_6D_6): 1.23 [s, 18H of HB{$H_2C_2N_2(C_4\underline{H}_9)CS$}$_3$Zr($C_5H_5$)$Cl_2$], 1.65 [s, 9H of HB{$H_2C_2N_2(C_4\underline{H}_9)CS$}$_3$Zr($C_5H_5$)$Cl_2$], 6.15 [d, $^3J_{H-H}$ = 2 Hz, 2H of HB{$\underline{H}_2C_2N_2(C_4H_9)CS$}$_3$Zr($C_5H_5$)$Cl_2$], 6.20 [d, $^3J_{H-H}$ = 2 Hz, 1H of HB{$\underline{H}_2C_2N_2(C_4H_9)CS$}$_3$Zr($C_5H_5$)$Cl_2$], 6.53 [s, 1H of

$HB\{H_2C_2N_2(C_4H_9)CS\}_3Zr(C_5\underline{H}_5)Cl_2]$, 6.55 [s, 4H of $HB\{H_2C_2N_2(C_4H_9)CS\}_3Zr(C_5\underline{H}_5)Cl_2]$, 8.74 [d, $^3J_{H-H}$ = 2 Hz, 1H of $HB\{\underline{H}_2C_2N_2(C_4H_9)CS\}_3Zr(C_5H_5)Cl_2]$, 9.10 [d, $^3J_{H-H}$ = 2 Hz, 2H of $HB\{\underline{H}_2C_2N_2(C_4H_9)CS\}_3Zr(C_5H_5)Cl_2]$, the proton attached to the boron atom is not observed.

4.6.6 Synthesis of $[Tm^{Bu^t}]Zr(CH_2Ph)_3$

$[Tm^{Bu^t}]Tl$ (10.8 mg, 0.02 mmol) and $Zr(CH_2Ph)_4$ (8.5 mg, 0.02 mmol) were dissolved in toluene and stirred for 1 hour at room temperature. The solution was filtered and the filtrate was collected. Yellow needle crystals (5 mg, 37.6%) were obtained after diffusing pentane to the toluene solution at –15°C. Crystals suitable for X-ray diffraction were obtained from slow evaporation of a concentrated benzene solution at room temperature. ^1H NMR (C_6D_6): 1.34 [s, 27H of $HB\{H_2C_2N_2(C_4\underline{H}_9)CS\}_3Zr\{(CH_2)C_6H_5\}_3]$, 2.82 [d, $^3J_{H-H}$ = 10 Hz, 3H of $HB\{H_2C_2N_2(C_4H_9)CS\}_3Zr\{(C\underline{H}_2)C_6H_5\}_3]$, 3.43 [d, $^3J_{H-H}$ = 10 Hz, 3H of $HB\{H_2C_2N_2(C_4H_9)CS\}_3Zr\{(C\underline{H}_2)C_6H_5\}_3]$, 6.29 [d, $^3J_{H-H}$ = 2 Hz, 3H of $HB\{\underline{H}_2C_2N_2(C_4H_9)CS\}_3Zr\{(CH_2)C_6H_5\}_3]$, 6.49 [d, $^3J_{H-H}$ = 2 Hz, 3H of $HB\{\underline{H}_2C_2N_2(C_4H_9)CS\}_3Zr\{(CH_2)C_6H_5\}_3]$, 6.94 [m, 3H of $HB\{H_2C_2N_2(C_4H_9)CS\}_3Zr\{(CH_2)C_6\underline{H}_5\}_3]$, 7.33 [t, $^3J_{H-H}$ = 7 Hz, 6H of $HB\{H_2C_2N_2(C_4H_9)CS\}_3Zr\{(CH_2)C_6\underline{H}_5\}_3]$, 7.56 [d, $^3J_{H-H}$ = 7 Hz, 6H of $HB\{H_2C_2N_2(C_4H_9)CS\}_3Zr\{(CH_2)C_6\underline{H}_5\}_3]$, the proton attached to the boron atom is not observed. $^{13}C\{^1H\}$ NMR (C_6D_6): 29.0 [s, 9C of $HB\{H_2C_2N_2(\underline{C}_4H_9)CS\}_3Zr\{(CH_2)C_6H_5\}_3]$, 59.7 [s, 3C of $HB\{H_2C_2N_2(\underline{C}_4H_9)CS\}_3Zr\{(CH_2)C_6H_5\}_3]$, 83.0 [s, 3C of $HB\{H_2C_2N_2(C_4H_9)CS\}_3Zr\{(\underline{C}H_2)C_6H_5\}_3]$, 117.2 [s, 3C of $HB\{H_2\underline{C}_2N_2(C_4H_9)CS\}_3Zr\{(CH_2)C_6H_5\}_3]$, 120.5 [s, 3C of

$HB\{H_2C_2N_2(C_4H_9)CS\}_3Zr\{(CH_2)\underline{C}_6H_5\}_3]$, 122.7 [s, 3C of $HB\{H_2\underline{C}_2N_2(C_4H_9)CS\}_3Zr\{(CH_2)C_6H_5\}_3]$, 126.4 [s, 6C of $HB\{H_2C_2N_2(C_4H_9)CS\}_3Zr\{(CH_2)\underline{C}_6H_5\}_3]$, 128.0 [s, 6C of $HB\{H_2C_2N_2(C_4H_9)CS\}_3Zr\{(CH_2)\underline{C}_6H_5\}_3]$, 152.1 [s, 3C of $HB\{H_2C_2N_2(C_4H_9)CS\}_3Zr\{(CH_2)\underline{C}_6H_5\}_3]$, 160.2 [s, 3C of $HB\{H_2C_2N_2(C_4H_9)\underline{C}S\}_3Zr\{(CH_2)C_6H_5\}_3]$.

4.6.7 Synthesis of $[Tm^{Bu^t}]Hf(CH_2Ph)_3$

A solution of $Hf(CH_2Ph)_4$ (15 mg, 0.027 mmol) in CH_2Cl_2 (1 mL) was added to $[Tm^{Bu^t}]Tl$ (18.8 mg, 0.027 mmol) solid in a vial. The mixture was stirred at room temperature for 20 min and then filtered. The solvent was removed from the filtrate *in vacuo* to give a yellow solid that was washed sequentially with pentane (3 × 3 mL), benzene (3 mL) then pentane (2 mL) again. The light yellow solid (14.0 mg, 55%) was dried in the Ar box. ^{1}H NMR (CD_2Cl_2): 1.64 [s, 27H of $HB\{H_2C_2N_2(C_4\underline{H}_9)CS\}_3Hf\{(CH_2)C_6H_5\}_3]$, 1.84 [d, $^2J_{H\text{-}H}$ = 11 Hz, 3H of $HB\{H_2C_2N_2(C_4H_9)CS\}_3Hf\{(C\underline{H}_2)C_6H_5\}_3]$, 2.25 [d, $^2J_{H\text{-}H}$ = 11 Hz, 3H of $HB\{H_2C_2N_2(C_4H_9)CS\}_3Hf\{(C\underline{H}_2)C_6H_5\}_3]$, 6.64 [t, $^3J_{H\text{-}H}$ = 8 Hz, $3H_{para}$ of $HB\{H_2C_2N_2(C_4H_9)CS\}_3Hf\{(CH_2)C_6\underline{H}_5\}_3]$, 6.80 [d, $^3J_{H\text{-}H}$ = 2 Hz, 3H of $HB\{\underline{H}_2C_2N_2(C_4H_9)CS\}_3Hf\{(CH_2)C_6H_5\}_3]$, 6.97 [d, $^3J_{H\text{-}H}$ = 8 Hz, $6H_{ortho}$ of $HB\{H_2C_2N_2(C_4H_9)CS\}_3Hf\{(CH_2)C_6\underline{H}_5\}_3]$, 7.04 [d, $^3J_{H\text{-}H}$ = 2 Hz, 3H of $HB\{\underline{H}_2C_2N_2(C_4H_9)CS\}_3Hf\{(CH_2)C_6H_5\}_3]$, 7.07 [d, $^3J_{H\text{-}H}$ = 8 Hz, $6H_{meta}$ of $HB\{H_2C_2N_2(C_4H_9)CS\}_3Hf\{(CH_2)C_6\underline{H}_5\}_3]$. ^{1}H NMR ($C_6D_6$): 1.35 [s, 27H of $HB\{H_2C_2N_2(C_4\underline{H}_9)CS\}Hf\{(CH_2)C_6H_5\}_3]$, 2.45 [d, $^2J_{H\text{-}H}$ = 11 Hz, 3H of $HB\{H_2C_2N_2(C_4H_9)CS\}_3Hf\{(C\underline{H}_2)C_6H_5\}_3]$, 2.97 [d, $^2J_{H\text{-}H}$ = 11 Hz, 3H of $HB\{H_2C_2N_2(C_4H_9)CS\}_3Hf\{(C\underline{H}_2)C_6H_5\}_3]$, 6.27 [d, $^3J_{H\text{-}H}$ = 2 Hz, 3H of $HB\{\underline{H}_2C_2N_2(C_4H_9)CS\}_3Hf\{(CH_2)C_6H_5\}_3]$, 6.48 [d, $^3J_{H\text{-}H}$ = 2 Hz, 3H of

$HB\{\underline{H}_2C_2N_2(C_4H_9)CS\}_3Hf\{(CH_2)C_6H_5\}_3]$, 6.91 [t, $^3J_{H\text{-}H}$ = 7 Hz, 3H*para* of $HB\{H_2C_2N_2(C_4H_9)CS\}_3Hf\{(CH_2)C_6\underline{H}_5\}_3]$, 7.37 [t, $^3J_{H\text{-}H}$ = 8 Hz, 6H*meta* of $HB\{H_2C_2N_2(C_4H_9)CS\}_3Hf\{(CH_2)C_6\underline{H}_5\}_3]$, 7.54 [d, $^3J_{H\text{-}H}$ =7 Hz, 6H*ortho* of $HB\{\underline{H}_2C_2N_2(C_4H_9)CS\}_3Hf\{(CH_2)C_6H_5\}_3]$. $^{13}C\{^1H\}$ NMR (CD_2Cl_2): 29.4 [9C of $HB\{H_2C_2N_2(\underline{C}_4H_9)CS\}_3Hf\{(CH_2)C_6H_5\}_3]$, 60.2 [3C of $HB\{H_2C_2N_2(\underline{C}_4H_9)CS\}_3Hf\{(CH_2)C_6H_5\}_3]$, 84.7 [3C of $HB\{H_2C_2N_2(C_4H_9)CS\}_3Hf\{(\underline{C}H_2)C_6H_5\}_3]$, 117.5 [3C of $HB\{H_2\underline{C}_2N_2(C_4H_9)CS\}_3Hf\{(CH_2)C_6H_5\}_3]$, 120.3 [3C*para* of $HB\{H_2C_2N_2(C_4H_9)CS\}_3Hf\{(CH_2)\underline{C}_6H_5\}_3]$, 123.5 [3C of $HB\{H_2\underline{C}_2N_2(C_4H_9)CS\}_3Hf\{(CH_2)C_6H_5\}_3]$, 126.6 [6C*ortho* of $HB\{H_2C_2N_2(C_4H_9)CS\}_3Hf\{(CH_2)\underline{C}_6H_5\}_3]$, 127.4 [6C*meta* of $HB\{H_2C_2N_2(C_4H_9)CS\}_3Hf\{(CH_2)\underline{C}_6H_5\}_3]$, 152.3 [3C*ipso* of $HB\{H_2C_2N_2(C_4H_9)CS\}_3Hf\{(CH_2)\underline{C}_6H_5\}_3]$, 158.4 [3C of $HB\{H_2C_2N_2(C_4H_9)\underline{C}S\}_3Hf\{(CH_2)C_6H_5\}_3]$.

4.6.8 Synthesis of $[Tm^{Ad}]Hf(CH_2Ph)_3$

A solution of $Hf(CH_2Ph)_4$ (5 mg, 0.01 mmol) in CH_2Cl_2 (1mL) was added to $Tm^{Ad}Na$ (8 mg, 0.01 mmol) solid in a vial. The mixture was stirred at room temperature for 5 min and then filtered. To the solution, pentane was added. Yellow solid crashed out immediately. The solution was filtered again. The obtained light yellow solid (3 mg, 28.0%) was washed with pentane and dried in Ar box. Crystals suitable for X-ray diffraction were obtained from slow evaporation of a toluene solution at –15°C. ^1H NMR (C_6D_6): 1.46 [m, 18H of $HB\{H_2C_2N_2(C_{10}\underline{H}_{15})CS\}_3Hf\{(CH_2)C_6H_5\}_3]$, 1.88 [s, 9H of $HB\{H_2C_2N_2(C_{10}\underline{H}_{15})CS\}_3Hf\{(CH_2)C_6H_5\}_3]$, 2.32 [m, 18H of $HB\{H_2C_2N_2(C_{10}\underline{H}_{15})CS\}_3Hf\{(CH_2)C_6H_5\}_3]$, 2.52 [d, $^2J_{H\text{-}H}$ = 11 Hz, 3H of

$HB\{H_2C_2N_2(C_{10}H_{15})CS\}_3Hf\{(C\underline{H}_2)C_6H_5\}_3]$, 2.68 [d, $^2J_{H\text{-}H}$ = 11 Hz, 3H of $HB\{H_2C_2N_2(C_{10}H_{15})CS\}_3Hf\{(C\underline{H}_2)C_6H_5\}_3]$, 6.46 [s, 3H of $HB\{\underline{H}_2C_2N_2(C_{10}H_{15})CS\}_3Hf\{(CH_2)C_6H_5\}_3]$, 6.62 [s, 3H of $HB\{\underline{H}_2C_2N_2(C_{10}H_{15})CS\}_3Hf\{(CH_2)C_6H_5\}_3]$, 6.92 [t, $^3J_{H\text{-}H}$ = 8 Hz, 3H of $HB\{H_2C_2N_2(C_{10}H_{15})CS\}_3Hf\{(CH_2)C_6\underline{H}_5\}_3]$, 7.38 [t, $^3J_{H\text{-}H}$ = 8 Hz, 6H of $HB\{H_2C_2N_2(C_{10}H_{15})CS\}_3Hf\{(CH_2)C_6\underline{H}_5\}_3]$, 7.48 [d, $^3J_{H\text{-}H}$ = 8 Hz, 6H of $HB\{H_2C_2N_2(C_{10}H_{15})CS\}_3Hf\{(CH_2)C_6\underline{H}_5\}_3]$. $^{13}C\{^1H\}$ NMR (C_6D_6): 30.2 [s, 9C of $HB\{H_2C_2N_2(\underline{C}_{10}H_{15})CS\}_3Hf\{(CH_2)C_6H_5\}_3]$, 35.9 [s, 9C of $HB\{H_2C_2N_2(\underline{C}_{10}H_{15})CS\}_3Hf\{(CH_2)C_6H_5\}_3]$, 40.8 [s, 9C of $HB\{H_2C_2N_2(\underline{C}_{10}H_{15})CS\}_3Hf\{(CH_2)C_6H_5\}_3]$, 86.5 [s, 3C of $HB\{H_2C_2N_2(C_{10}H_{15})CS\}_3Hf\{(\underline{C}H_2)C_6H_5\}_3]$, 116.9 [s, 3C of $HB\{H_2\underline{C}_2N_2(C_{10}H_{15})CS\}_3Hf\{(CH_2)C_6H_5\}_3]$, 120.8 [s, 3C of $HB\{H_2C_2N_2(C_{10}H_{15})CS\}_3Hf\{(CH_2)\underline{C}_6H_5\}_3]$, 123.1 [s, 3C of $HB\{H_2\underline{C}_2N_2(C_{10}H_{15})CS\}_3Hf\{(CH_2)C_6H_5\}_3]$, 127.2 [s, 6C of $HB\{H_2C_2N_2(C_{10}H_{15})CS\}_3Hf\{(CH_2)\underline{C}_6H_5\}_3]$, overlapped with benzene peak [s, 6C of $HB\{H_2C_2N_2(C_{10}H_{15})CS\}_3Hf\{(CH_2)\underline{C}_6H_5\}_3]$, 152.7 [s, 3C of $HB\{H_2C_2N_2(\underline{C}_{10}H_{15})CS\}_3Hf\{(CH_2)C_6H_5\}_3]$, 158.8 [s, 3C of $HB\{H_2C_2N_2(C_{10}H_{15})\underline{C}S\}_3Hf\{(CH_2)C_6H_5\}_3]$.

4.6.9 Synthesis of $[Tm^{MeBenz}]Hf(CH_2Ph)_3$

A solution of $Hf(CH_2Ph)_4$ (5 mg, 0.01 mmol) in CH_2Cl_2 (1 mL) was added to $[Tm^{MeBenz}]Tl$•diglyme (7 mg, 0.01 mmol) solid in a vial. The mixture was stirred at room temperature for 5 min and then filtered. The DCM solution was concentrated and pentane was added. A yellow solid percipitated immediately. The solution was filtered again. The light yellow solid (3 mg, 29.5%) was washed with pentane and dried in Ar box. ^1H NMR (CD_2Cl_2): 2.31 [d, $^2J_{H\text{-}H}$ = 11, 3H of

$HB\{(C_4H_4)C_2N_2(CH_3)CS\}_3Hf\{(C\underline{H}_2)C_6H_5\}_3]$, 2.39 [d, $^2J_{H\text{-}H}$ = 11, 3H of

$HB\{(C_4H_4)C_2N_2(CH_3)CS\}_3Hf\{(C\underline{H}_2)C_6H_5\}_3]$, 3.40 [s, 9H of

$HB\{(C_4H_4)C_2N_2(C\underline{H}_3)CS\}_3Hf\{(CH_2)C_6H_5\}_3]$, 3.62 [broad, 1H of

$\underline{H}B\{(C_4H_4)C_2N_2(CH_3)CS\}_3Hf\{(CH_2)C_6H_5\}_3]$, 6.71 [t, $^2J_{H\text{-}H}$ = 7 Hz, 3H$_{para}$ of

$HB\{(C_4H_4)C_2N_2(CH_3)CS\}_3Hf\{(CH_2)C_6\underline{H}_5\}_3]$, 6.79 [d, $^2J_{H\text{-}H}$ = 8 Hz, 6H$_{ortho}$ of

$HB\{(C_4H_4)C_2N_2(CH_3)CS\}_3Hf\{(CH_2)C_6\underline{H}_5\}_3]$, 7.07 [t, $^2J_{H\text{-}H}$ = 8 Hz, 6H$_{meta}$ of

$HB\{(C_4H_4)C_2N_2(CH_3)CS\}_3Hf\{(CH_2)C_6\underline{H}_5\}_3]$, 7.23 – 7.27 [m, 3H of

$HB\{(C_4\underline{H}_4)C_2N_2(CH_3)CS\}_3Hf\{(CH_2)C_6H_5\}_3]$, 7.31 – 7.38 [m, 6H of

$HB\{(C_4\underline{H}_4)C_2N_2(CH_3)CS\}_3Hf\{(CH_2)C_6H_5\}_3]$, 7.43 [d, 3H of

$HB\{(C_4\underline{H}_4)C_2N_2(CH_3)CS\}_3Hf\{(CH_2)C_6H_5\}_3]$. $^{13}C\{^1H\}$ NMR (CD_2Cl_2): 31.1 [3C of

$HB\{(C_4H_4)C_2N_2(\underline{C}H_3)CS\}_3Hf\{(CH_2)C_6H_5\}_3]$, 86.1 [3C of

$HB\{(C_4H_4)C_2N_2(CH_3)CS\}_3Hf\{(\underline{C}H_2)C_6H_5\}_3]$, 110.4 [3C of

$HB\{(\underline{C}_4H_4)C_2N_2(CH_3)CS\}_3Hf\{(CH_2)C_6H_5\}_3]$, 114.0 [3C of

$HB\{(\underline{C}_4H_4)C_2N_2(CH_3)CS\}_3Hf\{(CH_2)C_6H_5\}_3]$, 121.0 [3C$_{para}$ of

$HB\{(C_4H_4)C_2N_2(CH_3)CS\}_3Hf\{(CH_2)\underline{C}_6H_5\}_3]$, 124.3 [6C of

$HB\{(\underline{C}_4H_4)C_2N_2(CH_3)CS\}_3Hf\{(CH_2)C_6H_5\}_3]$, 126.9 [6C$_{ortho}$ of

$HB\{(C_4H_4)C_2N_2(CH_3)CS\}_3Hf\{(CH_2)\underline{C}_6H_5\}_3]$, 127.9 [6C$_{meta}$ of

$HB\{(C_4H_4)C_2N_2(CH_3)CS\}_3Hf\{(CH_2)\underline{C}_6H_5\}_3]$, 133.9 [3C of

$HB\{(C_4H_4)\underline{C}_2N_2(CH_3)CS\}_3Hf\{(CH_2)C_6H_5\}_3]$, 135.9 [3C of

$HB\{(C_4H_4)\underline{C}_2N_2(CH_3)CS\}_3Hf\{(CH_2)C_6H_5\}_3]$, 150.5 [3C$_{ipso}$ of

$HB\{(C_4H_4)C_2N_2(CH_3)CS\}_3Hf\{(CH_2)\underline{C}_6H_5\}_3]$, 167.4 [3C of

$HB\{(C_4H_4)C_2N_2(CH_3)\underline{C}S\}_3Hf\{(CH_2)C_6H_5\}_3]$.

4.6.10 Ethylene Polymerization by Cp[Tm$^{Bu^t}$]ZrCl$_2$/MAO

A sample of Cp[Tm$^{Bu^t}$]ZrCl$_2$ (3 mg, 4.8 × 10^{-3} mmol) was treated with MAO (19 mL, 10 wt % in toluene, 28.8 mmol), corresponding to an Al:Zr ratio of ~6000.

The solution was then degassed and treated with ethylene (1 atm). The reaction vessel was placed in a water bath at room temperature for 7 hours, while the pressure of ethylene was maintained at 1 atm. After this period, the reaction was quenched by slow addition of methanol then diluted HCl. The polymer was collected by filtration and washed with MeOH, water and MeOH, and dried *in vacuo* to get 3.483 g PE, corresponding to an activity of 104 kg PE [mol Zr]$^{-1}$ [h]$^{-1}$ [atm C_2H_4]$^{-1}$. Under identical conditions, a catalyst derived from Cp_2ZrCl_2 yields 6.451 g PE, corresponding to an activity of 180 kg PE [mol Zr]$^{-1}$ [h]$^{-1}$ [atm C_2H_4]$^{-1}$.

4.6.11 Ethylene Polymerization by [Tm$^{Bu^tBenz}$]Hf(CH_2Ph)$_3$

A sample of [Tm$^{Bu^tBenz}$]Hf(CH_2Ph)$_3$ (9.3 mg, 0.01 mmol) was dissolved in benzene and added to [$PhNHMe_2$][$B(C_6F_5)_4$] (8 mg, 0.01 mmol), resulting in a dark yellow solution with a little bit of precipitate. The solution was filtered and transferred to an NMR tube equipped with a J. Young valve. Ethylene gas (1 atm) was applied to the sample for a period of 20 min at room temperature, generating 20 mg PE, which corresponds to an activity of 6 kg PE [mol Hf]$^{-1}$ [h]$^{-1}$ [atm C_2H_4]$^{-1}$.

4.7 Crystallographic Data

Table 3. Crystal, intensity collection and refinement data.

	Cp[Tm$^{Bu^t}$]TiCl$_2$·0.5C$_6$H$_6$	**Cp[Tm$^{Bu^t}$]ZrCl$_2$·0.5C$_6$H$_6$**
lattice	Monoclinic	Monoclinic
formula	$C_{29}H_{42}BCl_2N_6S_3Ti$	$C_{29}H_{42}BCl_2N_6S_3Zr$
formula weight	700.48	743.80
space group	$P2_1/n$	$P2_1/n$
a/Å	14.720(7)	14.716(3)
b/Å	11.327(5)	11.358(2)
c/Å	20.422(10)	20.73(4)
α/°	90	90
β/°	102.593(7)	102.130(3)
γ/°	90	90
V/Å^3	3323(3)	3397.8(12)
Z	4	4
temperature (K)	150(2)	125(2)
radiation (λ, Å)	0.71073	0.71073
ρ (calcd.), g cm^{-3}	1.400	1.454
μ (Mo Kα), mm^{-1}	0.637	0.695
θ max, deg.	30.62	30.51
no. of data collected	52398	53472
no. of data used	10177	10340
no. of parameters	435	391
R_1 [$I > 2\sigma(I)$]	0.0831	0.0570
wR_2 [$I > 2\sigma(I)$]	0.1026	0.0816
R_1 [all data]	0.2854	0.1455
wR_2 [all data]	0.1415	0.1017
GOF	1.008	1.001
R_{int}	0.3164	0.1704

Table 3. (cont.) Crystal, intensity collection and refinement data.

	Cp(κ²-*S,N*-mim$^{Bu^t}$)(κ¹-*S*-Hmim$^{Bu^t}$)ZrCl$_2$·C$_6$H$_6$	**[Tm$^{Bu^t}$]Hf(CH$_2$Ph)$_3$ ·2C$_6$H$_6$**
lattice	Triclinic	Cubic
formula	$C_{25}H_{34}Cl_2N_4S_2Zr$	$C_{66}H_{79}BN_6S_3Hf$
formula weight	616.80	1241.83
space group	*P-1*	*Pa-3*
a/Å	10.5741(17)	23.1441(13)
b/Å	10.7222(17)	23.1441(13)
c/Å	14.246 (4)	23.1441(13)
α/°	93.930(3)	90
β/°	92.095(3)	90
γ/°	118.274(2)	90
V/Å^3	1414.7(5)	12397.1(12)
Z	2	8
temperature (K)	125(2)	150(2)
radiation (λ, Å)	0.71073	0.71073
ρ (calcd.), g cm^{-3}	1.448	1.331
μ (Mo Kα), mm^{-1}	0.746	1.828
θ max, deg.	30.53	26.36
no. of data collected	22462	143844
no. of data used	8562	4234
no. of parameters	313	261
R_1 [$I > 2\sigma(I)$]	0.0491	0.0607
wR_2 [$I > 2\sigma(I)$]	0.0857	0.1765
R_1 [all data]	0.0941	0.1359
wR_2 [all data]	0.0979	0.2250
GOF	1.001	1.130
R_{int}	0.0706	0.2679

4.8 References and Notes

(1) (a) Green, M. L. H. *J. Organomet. Chem.* **1995**, *500*, 127-148.

(b) Parkin, G. in *Comprehensive Organometallic Chemistry III*, Volume 1, Chapter 1.01; Crabtree, R. H. and Mingos, D. M. P. (Eds), Elsevier, Oxford, 2006.

(c) Green, J. C.; Green, M. L. H.; Parkin, G. *Chem. Commun.* **2012**, *48*, 11503.

(2) (a) Spicer, M. D.; Reglinski, J. *Eur. J. Inorg. Chem*. **2009**, 1553-1574.

(b) Parkin, G. *New J. Chem*. **2007**, *31*, 1996-2014.

(c) Smith, J. M. *Comments. Inorg. Chem*. **2008**, *29*, 189-233.

(d) Soares, L. F.; Silva, R. M. *Inorg. Synth*. **2002**, *33*, 199-202.

(3) (a) Hill, A. F.; Rae, A. D.; Smith, M. K. *Inorg. Chem*. **2005**, *44*, 7316-7318.

(b) Hill, A. F.; Smith, M. K. *Organometallics* **2007**, *26*, 4688–4691.

(4) (a) Hill, A. F.; Smith, M. K. *Dalton Trans*. **2007**, 3363–3364.

(b) Hill, A. F.; Smith, M. K. *Organometallics* **2007**, *26*, 3900–3903.

(c) Buccella, D.; Shultz, A.; Melnick, J. G.; Konopka, F.; Parkin, G. *Organometallics* **2006**, *25*, 5496–5499.

(5) Cambridge Structural Database (Version 5.34). *3D Search and Research Using the Cambridge Structural Database*, Allen, F. H.; Kennard, O. *Chemical Design Automation News* **1993**, *8* (1), pp 1 & 31-37.

(6) Hill, A. F.; Smith, M. K. *Dalton Trans*. **2006**, 28-30.

(7) The range of Ti•••H–B interactions is 1.611 ~ 2.285Å according to Cambridge Structural Database (version 5.34).

(8) For the crystal structure of $[CpTiClO]_4$, see: Skapski, A. C.; Troughton, P. G. H. *Acta Cryst. B.* **1970**, *26*, 716–722.

(9) Jaguar 7.6, Schrödinger, LLC, New York, NY 2009.

(10) The range of Zr•••H–B interactions is 1.746 ~ 3.294 Å according to Cambridge Structural Database (version 5.34).

(11) Lee, H.; Jordan, R. F. *J. Am. Chem. Soc.* **2005**, *127*, 9384–9385.

(12) Rong, Y.; Al-Harbi, A.; Parkin, G. *Organometallics* **2012**, *31*, 8208–8217.

(13) The range of Hf–S bond length is 2.31 – 2.92 Å according to Cambridge Structural Database (version 5.34).

(14) (a) McNally, J. P.; Leong, V. S.; Cooper, N. J. in Experimental Organometallic Chemistry, Wayda, A. L.; Darensbourg, M. Y., Eds.; American Chemical Society: Washington, DC, 1987; Chapter 2, pp 6-23.

(b) Burger, B.J.; Bercaw, J. E. in Experimental Organometallic Chemistry; Wayda, A. L.; Darensbourg, M. Y., Eds.; American Chemical Society: Washington, DC, 1987; Chapter 4, pp 79-98.

(c) Shriver, D. F.; Drezdzon, M. A.; The Manipulation of Air-Sensitive Compounds, 2nd Edition; Wiley-Interscience: New York, 1986.

(15) Fulmer, G. R.; Miller, A. J. M.; Sherden, N. H.; Gottlieb, H. E.; Nudelman, A.; Stoltz, B. M.; Bercaw, J. E.; Goldberg, K. I. *Organometallics* **2010**, *29*, 2176–2179.

(16) (a) Sheldrick, G. M. SHELXTL, An Integrated System for Solving, Refining and Displaying Crystal Structures from Diffraction Data; University of Göttingen, Göttingen, Federal Republic of Germany, 1981.

(b) Sheldrick, G. M. *Acta Cryst*. **2008**, *A64*, 112-122.

(17) (a) Becke, A. D. *J. Chem. Phys*. **1993**, *98*, 5648-5652.

(b) Becke, A. D. *Phys. Rev. A* **1988**, *38*, 3098-3100.

(c) Lee, C. T.; Yang, W. T.; Parr, R. G. *Phys. Rev. B* **1988**, *37*, 785-789.

(d) Vosko, S. H.; Wilk, L.; Nusair, M. *Can. J. Phys*. **1980**, *58*, 1200-1211.

(e) Slater, J. C. Quantum Theory of Molecules and Solids, Vol. 4: The Self-Consistent Field for Molecules and Solids; McGraw-Hill: New York, 1974.

(18) (a) Hay, P. J.; Wadt, W. R. *J. Chem. Phys*. **1985**, *82*, 270-283.
(b) Wadt, W. R.; Hay, P. J. *J. Chem. Phys*. **1985**, *82*, 284-298.
(c) Hay, P. J.; Wadt, W. R. *J. Chem. Phys.* **1985**, *82*, 299-310.

CHAPTER 5

Zinc and Cadmium Compounds Supported by Multidentate Ligands featuring [CN_3] and [CNO_2] donors: Synthesis and Structural Characterization

Table of Contents

Reproduced in part from:

Rong, Y.; Parkin, G. *Aust. J. Chem.* http://dx.doi.org/10.1071/CH13263

5.1 Introduction

5.1.1 Application of The *Tris*(2-pyridylthio)methyl Ligand, [Tptm], in Zinc Chemistry

Our group has recently reported a tetradentate tripodal ligand, namely *tris*(2-pyridylthio)methyl, [Tptm], as a useful supporting ligand for zinc. A variety of [Tptm]ZnX complexes which feature reactive functionalities such as hydride, methyl, *bis*(trimethylsilyl)amido and siloxide ligands[1] have been made. Among these compounds, the hydride complex is of particular interest as an effective catalyst for *(i)* the release of hydrogen by protolytic cleavage of phenylsilane and *(ii)* the hydrosilylation of aldehydes, ketones and carbon dioxide.[1c] To expand the family of [CN_3] donor ligands, we report here the synthesis of the selenium analogue of [Tptm], the *tris*(2-pyridylseleno)methyl ligand, [Tpsem].

5.1.2 The *Tris*(2-pyridylseleno)methyl Ligand, [Tpsem]

As an analogue of [Tptm]H, [Tpsem]H was first reported in 2002.[2] The original synthesis involves reduction of dipyridyl diselenide to pyridylselenolate using hydrazine hydrate, in the presence of NaOH, followed by addition of halomethanes (Scheme 1). However, we developed a new one-pot synthetic method, as illustrated in Scheme 1. The molecular structure of [Tpsem]H has been reported[2a] and is similar to that of [Tptm]H with all three nitrogen atoms facing the hydrogen attached to the carbon. Thus, replacement of this hydrogen with a metal forms an atrane motif.[3] In this chapter, we report the synthesis and structural characterization of some zinc compounds that incorporate [Tpsem] ligand, thereby revealing the multiple coordination modes that it may adopt.

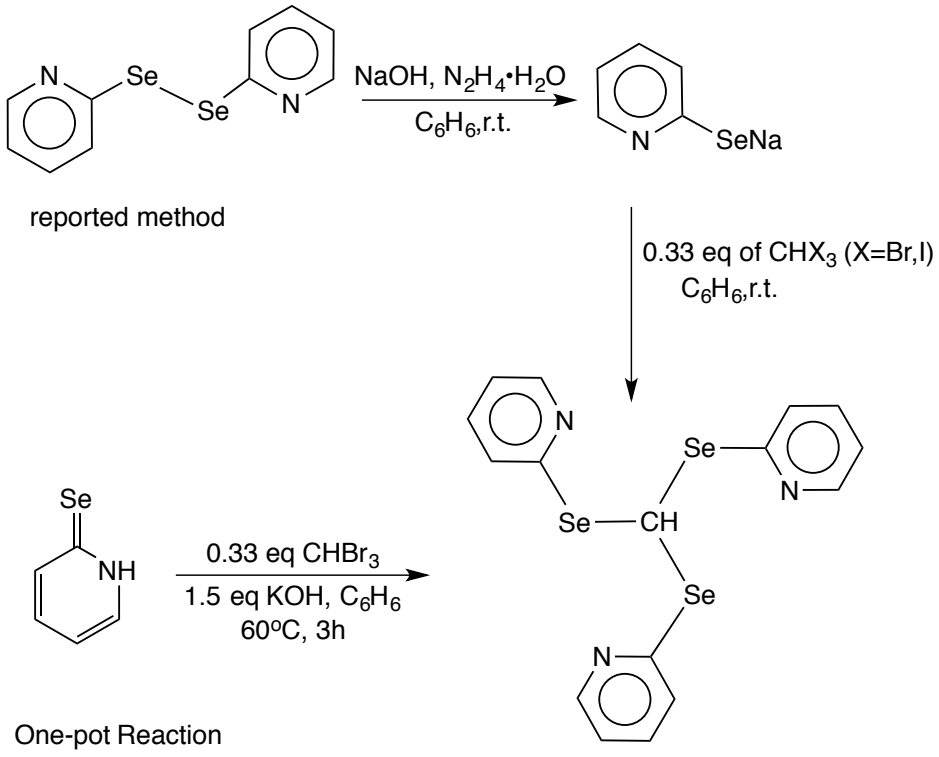

Scheme 1. Synthesis of [Tpsem]H

5.1.3 The *Bis*(2-pyridonyl)(pyridin-2-yloxy)methyl Ligand, [*O*-poBpom]

In addition, we also synthesized *bis*(2-pyridonyl)(pyridin-2-yloxy)methane, [*O*-poBpom]H *via* isomerization of *tris*(pyridin-2-yloxy)methane (Scheme 2).[4] The molecular structure has been determined by X-ray diffraction (Figure 1). One structural feature, which is worth noting, is that the molecule resembles closely [Tptm]H and [Tpsem]H with all three donor atoms (O, N) facing towards the H attached to the central carbon. Therefore, upon replacing the specific H with a metal atom, the ligand could form a unique [CNO_2] coordination environment. In this chapter, zinc and cadmium amide complexes incorporating this ligand were prepared and structurally characterized by X-ray diffraction.

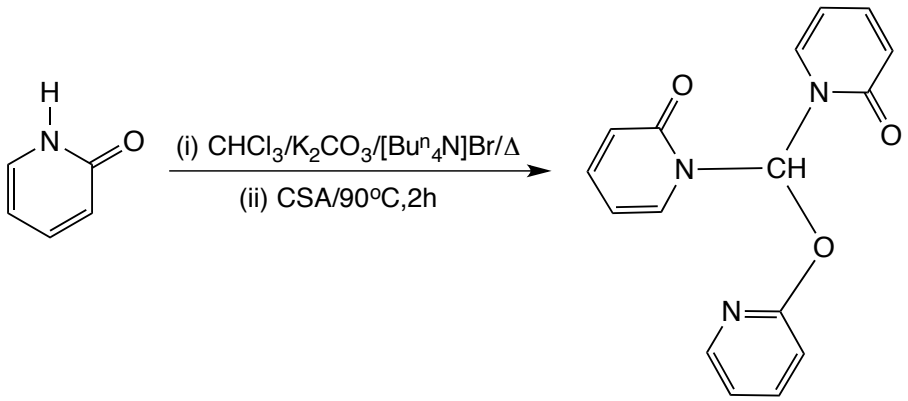

Scheme 2. Synthesis of [*O*-poBpom]H

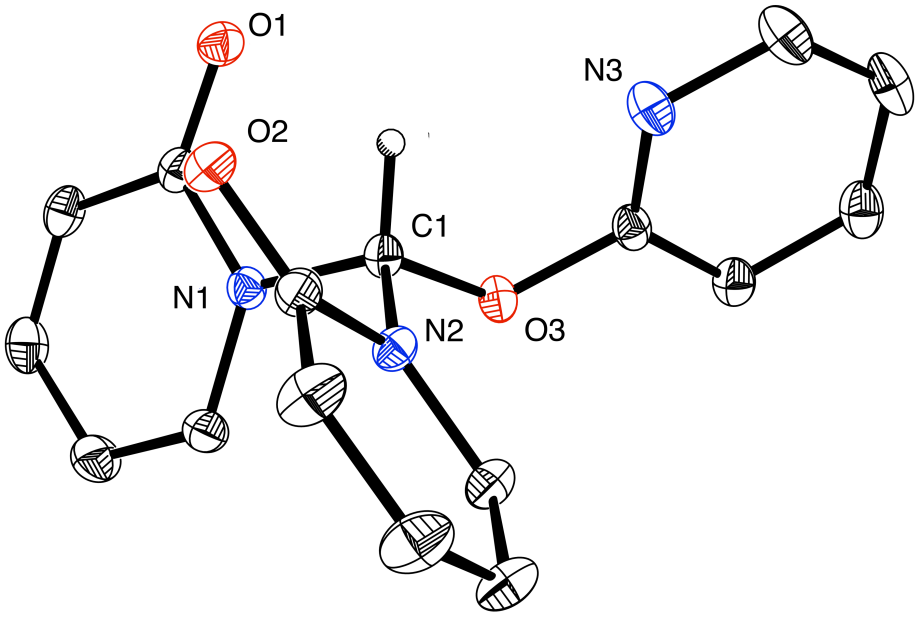

Figure 1. Molecular structure of *bis*(2-pyridonyl)(pyridin-2-yloxy)methane.

5.2 Synthesis and Structures of *Tris*(2-pyridylseleno)methyl Zinc Compounds with κ^2-, κ^3- and κ^4-Coordination Modes

5.2.1 Synthesis and NMR Study of [κ^3-Tpsem]ZnN(SiMe$_3$)$_2$

Tris(2-pyridylseleno)methane, [Tpsem]H reacts with Zn[N(SiMe$_3$)$_2$]$_2$ to give the *bis*(trimethylsilyl)amido derivative, [κ^3-Tpsem]ZnN(SiMe$_3$)$_2$, as illustrated in Scheme 3. Although the molecular structure of [κ^3-Tpsem]ZnN(SiMe$_3$)$_2$ has not been determined by X-ray diffraction, variable temperature ^{1}H NMR spectroscopic studies demonstrate that the [Tpsem] ligand coordinates in a κ^3-manner and that the molecule is fluxional at room temperature. The ^{1}H NMR spectrum of [κ^3-Tpsem]ZnN(SiMe$_3$)$_2$ exhibits a 2:1 pattern consistent with κ^3-coordination, which merges at *ca*. –35˚C, although three chemically equivalent pyridyl groups were observed at room temperature, as illustrated in Figure 2. In this regard, it is worth noting that the *tris*(2-pyridylthio)methyl counterpart, [κ^3-Tptm]-ZnN(SiMe$_3$)$_2$ has similar NMR spectroscopic properties, but the spectrum corresponding to the static molecule starts to merge at *ca*. -10˚C.[1a]

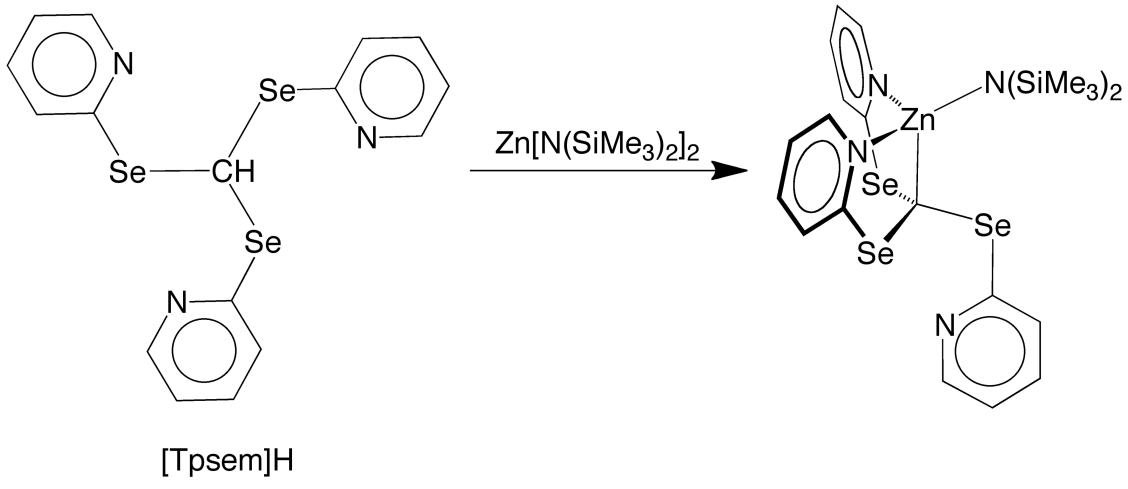

Scheme 3. Synthesis of [κ^3-Tptm]ZnN(SiMe$_3$)$_2$.

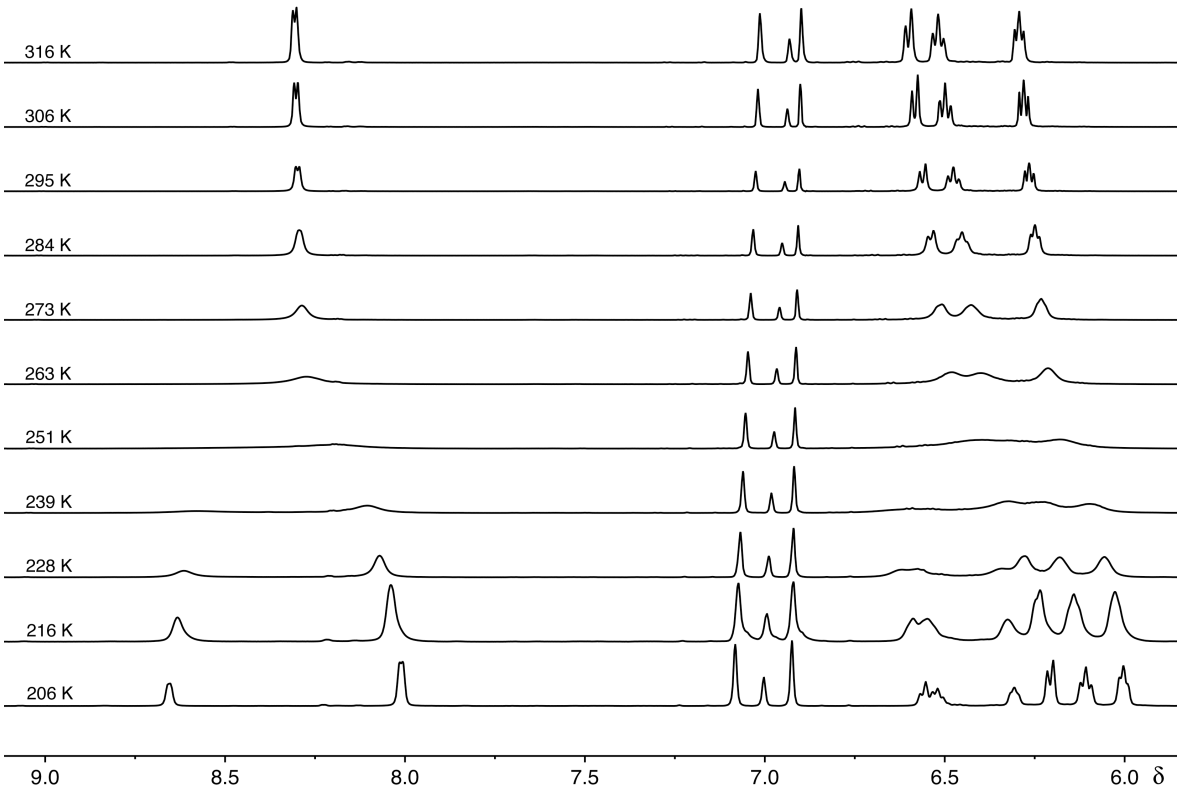

Figure 2. Variable temperature ^{1}H NMR spectra of [κ^3-Tpsem]ZnN(SiMe$_3$)$_2$ in d_8-toluene.

5.2.2 Reactivity of [κ^3-Tpsem]ZnN(SiMe$_3$)$_2$ Towards Carbon Dioxide

[κ^3-Tpsem]ZnN(SiMe$_3$)$_2$ is a useful precursor for other zinc derivatives. For example, it reacts with CO_2 to form the isocyanate complex, [κ^4-Tpsem]ZnNCO, as illustrated in Scheme 4. The molecular structure of [κ^4-Tpsem]ZnNCO has been determined by X-ray diffraction, as shown in Figure 3. Although the reactions between CO_2 and *bis*(trimethylsilyl)amido complexes have received little attention,[5,6] the reactivity observed for [κ^3-Tpsem]ZnN(SiMe$_3$)$_2$ is similar to that of [κ^3-Tptm]ZnN(SiMe$_3$)$_2$.[1a]

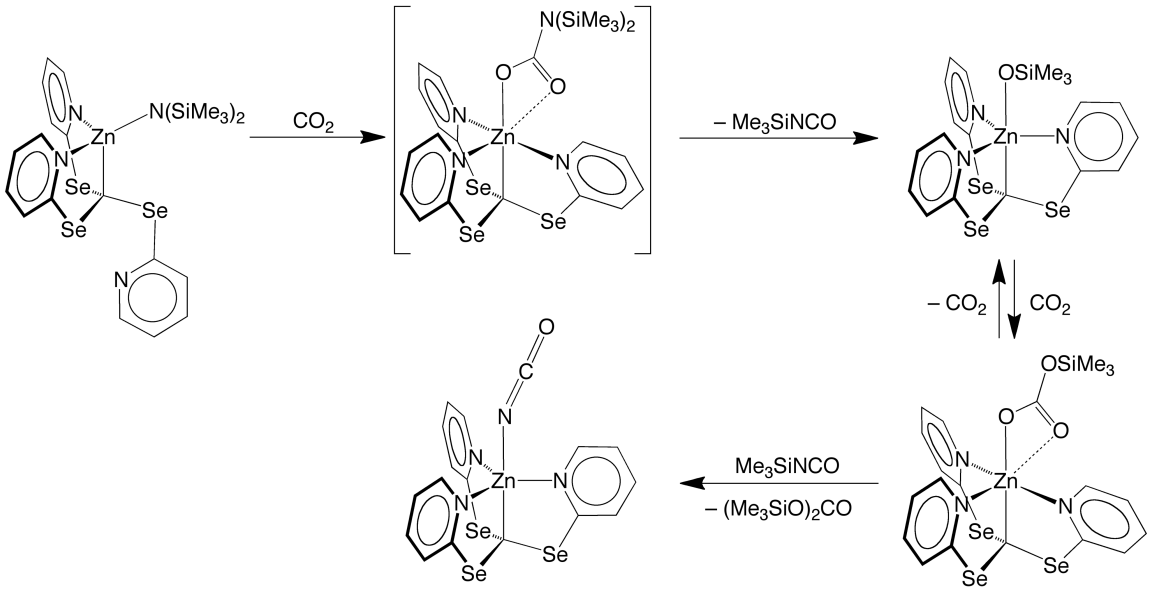

Scheme 4. Reactivity of [κ^3-Tpsem]ZnN(SiMe$_3$)$_2$ towards CO_2.

We propose that the formation of the isocyanate compound [κ^4-Tpsem]-ZnNCO occurs *via* an initial sequence that involves insertion of CO_2 into the Zn–N(SiMe$_3$)$_2$ bond to give [Tpsem]Zn[O_2CN(SiMe$_3$)$_2$], which subsequently converts to the trimethysiloxide derivative [κ^4-Tptm]ZnOSiMe$_3$ and Me$_3$SiNCO (Scheme 4). The final steps of this transformation involve another insertion of CO_2 into the Zn–OSiMe$_3$ bond to give the carbonate derivative, [Tpsem]ZnO_2COSiMe$_3$, which undergoes metathesis with Me$_3$SiNCO to give [κ^4-Tpsem]ZnNCO. This proposed mechanism is similar to the reaction of [Tptm]ZnN(SiMe$_3$)$_2$ with CO_2 and supported by the following two observations: *(i)* Me$_3$SiNCO is observed by ^{1}H NMR spectroscopy during the course of the reaction, and *(ii)* the byproduct accompanying the formation of [κ^4-Tpsem]ZnNCO is the silyl carbonate, (Me$_3$SiO)$_2$CO, a compound whose formation is the most easily rationalized by a sequence that involves insertion of CO_2 into the Zn-OSiMe$_3$ bond.

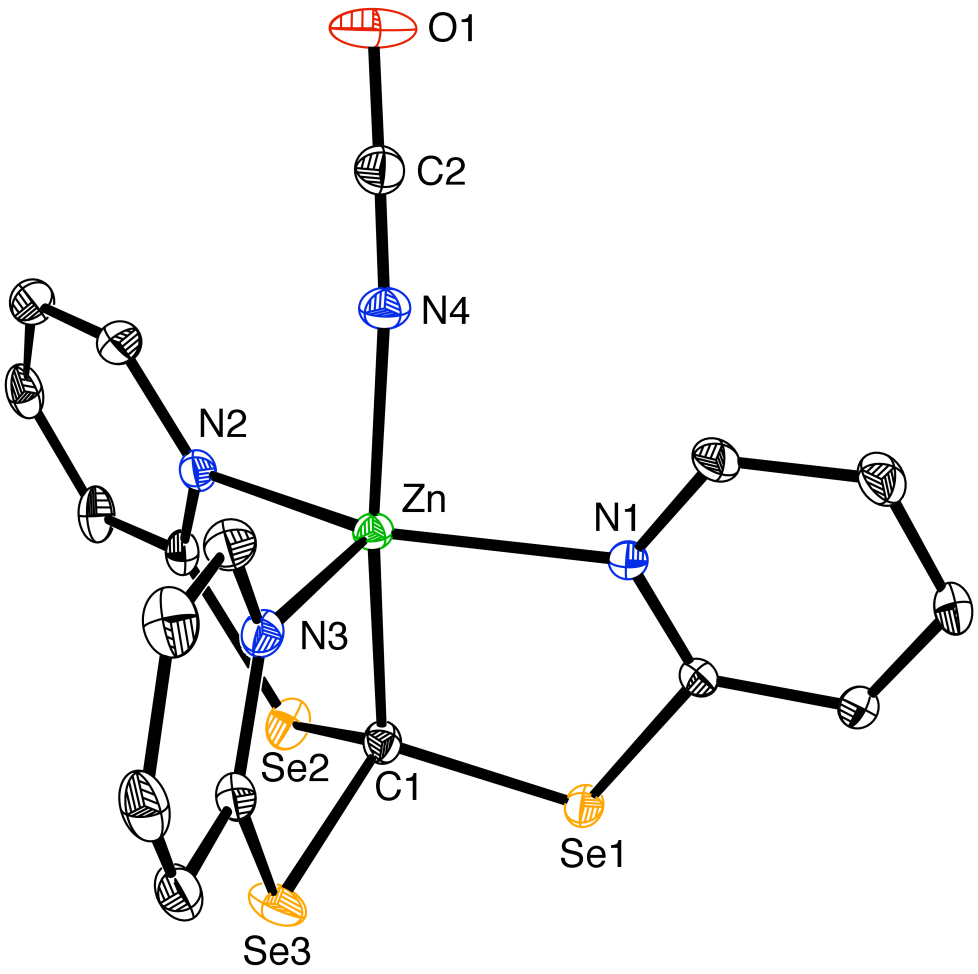

Figure 3. Molecular structure of [κ^4-Tpsem]ZnNCO.

5.2.3 Structural Study of [κ^4-Tpsem]ZnNCO

As the first structurally characterized [Tpsem]-metal complex, [κ^4-Tpsem]ZnNCO provides a means to compare the coordination of the [Tpsem] ligand with that of the sulfur counterpart. The structural data for [κ^4-Tpsem]ZnNCO and [κ^4-Tptm]ZnNCO are summarized in Table 1.

Table 1. Selected bond lengths (Å) and angles (°) for [κ^4-Tpsem]ZnNCO and [κ^4-Tptm]ZnNCO.

	[κ^4-Tpsem]ZnNCO	**[κ^4-Tptm]ZnNCO**[a]
Zn–N	2.085(3), 2.203(3), 2.220(3)	2.073(3), 2.132(3), 2.142(3)
Zn-N_{av}	2.169	2.116
Zn–C	2.123(3)	2.194(3)
C–E	1.946(3)	1.779(3)
C–E	1.941(3)	1.798(3)
C–E	1.959(4)	1.804(3)
Zn–NCO	1.997(3)	2.007(3)
Zn–N–C	161.5(3)	158.7(3)
C–E–C	99.06(14), 99.76(15), 100.81(15)	104.13(15), 104.59(15) 104.64(15)
E–C–E	106.31(16), 109.05(17), 109.49(16)	108.21(17), 110.42(17), 110.23(17)
C–Zn–NCO	169.95(13)	174.12(12)
C–Zn–N	86.47(11), 87.06(12), 92.33(12)	84.88(11), 85.18(11), 87.76(11)
N–Zn–N	104.43(11), 108.36(11), 146.79(10)	105.28(10), 114.27(10), 138.69(10)
N–Zn–NCO	90.28(11), 90.49(11), 97.69(12)	92.90(11), 92.96(11), 98.09(11)

(a) Data taken from reference 1a

The principal differences in the coordination environment of the zinc center are that the average Zn–N bond length associated with the [κ^4-Tpsem] ligand [2.169 Å] is 0.053 Å longer than that for the [κ^4-Tptm] ligand [2.116 Å], while the Zn–C bond for the former [2.123(3) Å] is 0.071 Å shorter than that for the latter [2.194(3) Å]. Density functional theory geometry optimization calculations on both structures provide support for these bond length differences, *i.e*. the Zn–N and Zn–C bonds of geometry optimized [κ^4-Tpsem]ZnNCO are respectively longer by 0.053 Å and shorter by 0.10 Å, than those of [κ^4-Tptm]ZnNCO.

In addition to the differences in Zn–N and Zn–C bond lengths, the coordination geometries at zinc center in [κ^4-Tpsem]ZnNCO and [κ^4-Tptm]ZnNCO are also different. Specifically, although in both [κ^4-Tptm]ZnNCO and [κ^4-Tpsem]ZnNCO, the zinc centers adopt an approximately trigonal bipyramidal geometry, the one for the [κ^4-Tpsem] selenium ligand is distorted more towards a square pyramidal geometry. Here we adopt the five coordinate geometry index τ_5[7] as a criterion for the comparison. In an idealized trigonal bipyramidal structure, the index τ_5 equals to 1.00, whereas in an idealized square pyramid, τ_5 is 0.00. In our case, the value for [κ^4-Tpsem]ZnNCO is 0.39, but that for [κ^4-Tptm]ZnNCO is 0.59. The differences in structures could be rationalized by the following two facts: (*i*) selenium atom is larger than sulfur atom[8] and (*ii*) the bond angles at two-coordinate selenium are smaller than those at sulfur. [9] To be specific, the average H–C–Se bond length in [Tpsem]H[2] [1.939(4) Å] is 0.128 Å longer than the H–C–S bond length in [Tptm]H[10] [1.8108(9) Å], whereas the average C–Se–C bond angle in [Tpsem]H[2] [100.3(3)°] is 2.6° smaller than that for [Tptm]H[10] [102.85(7)°].

5.2.4 Reactivity of [κ³-Tpsem]ZnN(SiMe$_3$)$_2$ Towards Hydrogen Sulfide

[κ³-Tpsem]ZnN(SiMe$_3$)$_2$ also reacts with H_2S to form the terminal hydrosulfido and bridging sulfido compounds, [κ³-Tpsem]ZnSH and {[κ³-Tpsem]Zn}$_2$(μ–S), as illustrated in Scheme 5. Molecular structures of both compounds have been determined by X-ray diffraction and are shown in Figure 4 and Figure 5. Additionally, the two compounds readily interconvert. Thus, addition of H_2S to {[κ³-Tpsem]Zn}$_2$(μ–S) forms [κ³-Tpsem]ZnSH, while removal of the H_2S *in vacuo* regenerates {[κ³-Tpsem]Zn}$_2$(μ–S). The interconversion process is monitored by ^{1}H NMR spectroscopy, and a detailed description is provided in the experimental section.

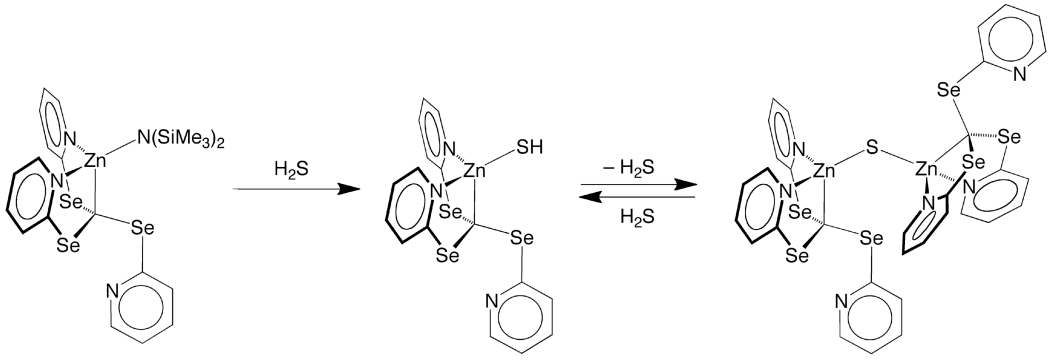

Scheme 5. Reactivity of [κ³-Tptm]ZnN(SiMe$_3$)$_2$ towards H_2S.

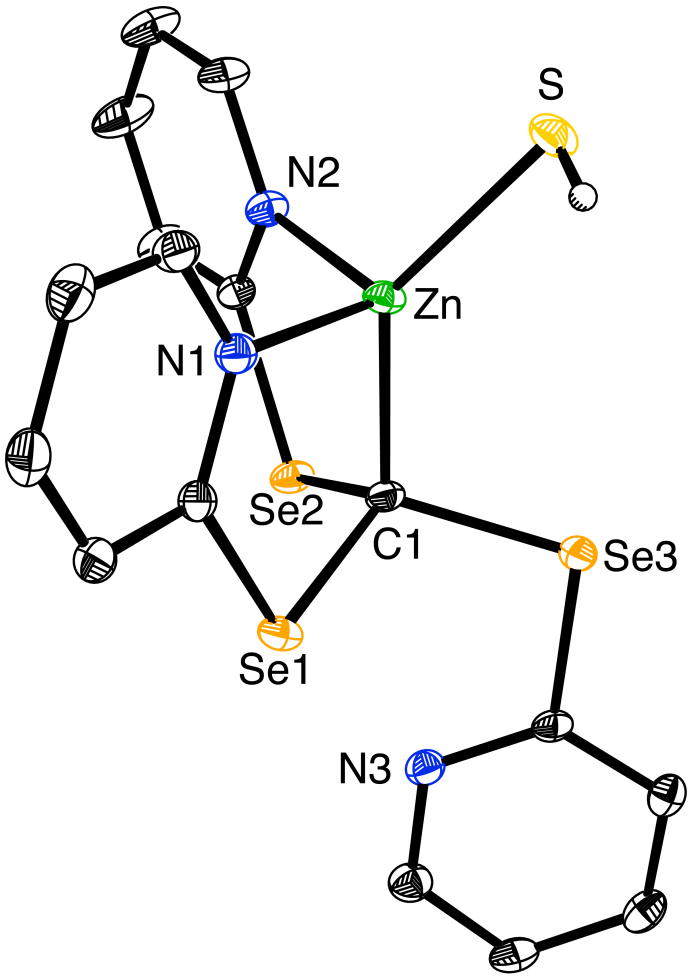

Figure 4. Molecular structure of [κ^3-Tpsem]ZnSH.

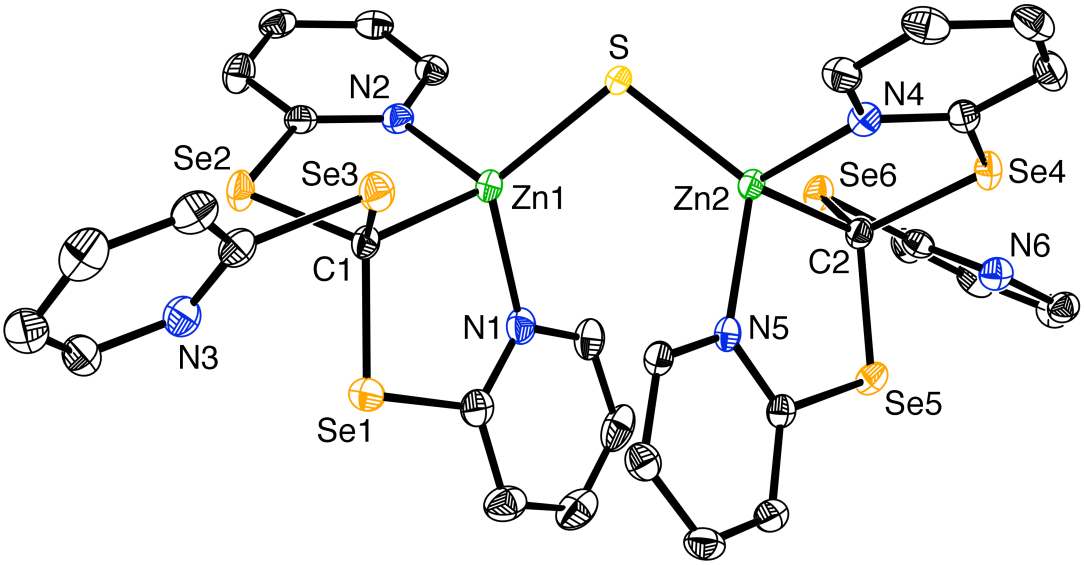

Figure 5. Molecular structure of $\{[\kappa^3\text{-Tpsem}]Zn\}_2S$.

5.2.5 Structural Study of $[\kappa^3\text{-Tpsem}]ZnSH$ and $\{[\kappa^3\text{-Tpsem}]Zn\}_2(\mu\text{–S})$

$[\kappa^3\text{-Tpsem}]ZnSH$ and $\{[\kappa^3\text{-Tpsem}]Zn\}_2(\mu\text{–S})$ are of interest because zinc compounds that feature hydrosulfido[11,12,13] and bridging sulfido[14,15] ligands are uncommon. As far as we know, $[\kappa^3\text{-Tpsem}]ZnSH$ is the only structurally characterized example of an alkylzinc hydrosulfido compound,[16] and with respect to $\{[\kappa^3\text{-Tpsem}]Zn\}_2(\mu\text{–S})$, there is only one structurally characterized dinuclear zinc compound that features a μ–sulfido bridge listed in the Cambridge Structural Database (CSD),[17] namely $\{[Tp^{Cum,Me}]Zn\}_2(\mu\text{–S})$.[14] Even though the two compounds both feature a bridging μ–sulfide motif, there is a significant difference regarding the Zn–S–Zn bond angle. Specifically, $\{[Tp^{Cum,Me}]Zn\}_2(\mu\text{–S})$ exhibits a large Zn–S–Zn angle of (138.9°), whereas that for $\{[\kappa^3\text{-Tpsem}]Zn\}_2(\mu\text{–S})$ is only (103.5°). One explanation for this large difference in bond angles is that the different steric demands of the $[Tp^{Cum,Me}]$ and $[\kappa^3\text{-Tpsem}]$ ligands, such that the less sterically demanding $[\kappa^3\text{-Tpsem}]$ ligand allows for a smaller angle at sulfur. A density

functional theory geometry optimization calculation on $\{[\kappa^3\text{-Tpsem}]Zn\}_2(\mu\text{–}S)$ was carried out and the result is in accord with a highly bent angle at sulfur (110.6°).

The Zn–S bond lengths of $[\kappa^3\text{-Tpsem}]ZnSH$ [2.242(1) Å and $\{[\kappa^3\text{-Tpsem}]Zn\}_2(\mu\text{–}S)$ [2.215(1) Å and 2.202(1) Å] are similar to each other and are comparable to the values in related compounds, as illustrated in Table 2.[11a-f] Interestingly, in both structures, the [Tpsem] ligand coordinates in a κ^3 rather than κ^4 manner (Figure 4 and Figure 5). Therefore, the four-coordinate structure of $[\kappa^3\text{-Tpsem}]ZnSH$ is quite distinct from that of the *tris*(2-pyridylmethyl)amine (TPA) compound $\{[\kappa^4\text{-TPA}]ZnSH\}[BPh_4]$[11b,d] in which the structurally related TPA

Table 2. Zn–S Bond lengths in structurally characterized zinc hydrosulfido and μ–sulfido compounds.

	***d*(Zn–SH)/Å**	**Reference**
$[\kappa^3\text{-Tpsem}]ZnSH$	2.242(1)	this work
$[(TPA)ZnSH][BPh_4]$	2.306	11b
$[(TPA)ZnSH][BF_4]$	2.3207(14)	11d
$[Tm^{Bu^t}]ZnSH$	2.265(1)	11a
$[Tp^{Pr^i_2}]ZnSH$	2.2300(4)	11c
$[Tp^{Cum,Me}]ZnSH$	2.210(3)	11e
$[Tp^{Cum,Me*}]ZnSH$	2.209(3)	11e
$[Tp^{Ph,Me}]ZnSH$	2.219(2)	11f
$[Tp^{3\text{-}py,Me}]ZnSH$	2.21(1)	11f
$[Tp^{4\text{-}pic,Me}]ZnSH$	2.214(1)	11f
$\{[\kappa^3\text{-Tpsem}]Zn\}_2(\mu\text{–}S)$	2.215(1), 2.202(1)	this work
$\{[Tp^{Cum,Me}]Zn\}_2(\mu\text{–}S)$	2.186(2), 2.189(2)	14

ligand coordinates in a tetradentate tripodal manner. Similar to [κ^3-Tpsem]ZnN(SiMe$_3$)$_2$ discussed above, the hydrosulfido and sulfido compounds [κ^3-Tpsem]ZnSH and {[κ^3-Tpsem]Zn}$_2$(μ–S) are also fluxional, and spectra which are in accord with a static structure start to merge at *ca.* –55˚C. (Figure 6 and Figure 7). In addition, although the [Tpsem] ligands of [κ^3-Tpsem]ZnSH and {[κ^3-Tpsem]Zn}$_2$(μ–S) bind in a κ^3-manner, the coordination geometries deviate considerably from tetrahedral. For example, the four coordinate geometry indices[18] τ_4 of [κ^3-Tpsem]ZnSH (0.79) and {[κ^3-Tpsem]Zn}$_2$(μ–S) (0.76) [19] are intermediate between the values for a trigonal monopyramid (0.85) and an idealized see-saw geometry with bond angles of 180˚ and 90˚ (0.64).

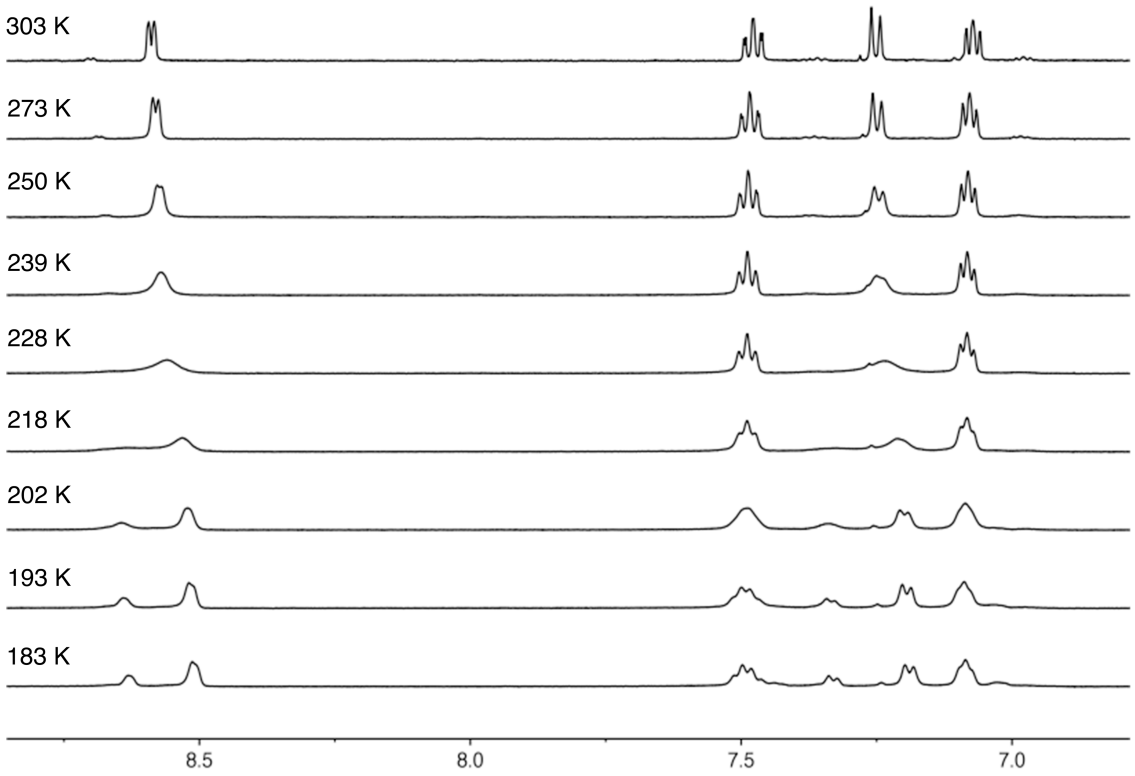

Figure 6. Variable temperature ^{1}H NMR spectra of [κ^3-Tpsem]ZnSH in CD_2Cl_2.

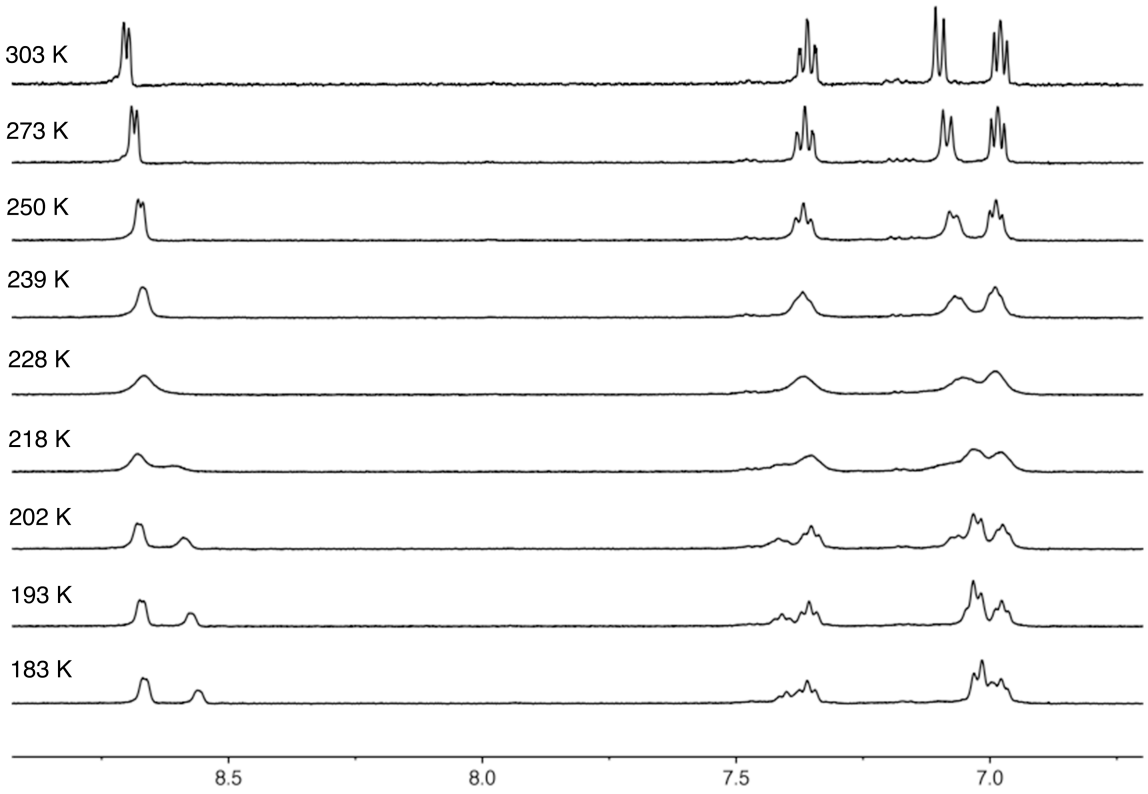

Figure 7. Variable temperature ^{1}H NMR spectra of {[κ^3-Tpsem]Zn}$_2$(μ–S) in CD_2Cl_2.

5.2.6 Decomposition of [κ^3-Tpsem]ZnN(SiMe$_3$)$_2$: [κ^2-Tpsem]$_2$Zn and [κ^4-Tpsem]Zn(κ^2–SeC$_6$H$_4$N)

[κ^3-Tpsem]ZnN(SiMe$_3$)$_2$ exhibits limited stability and decomposes in solution to give, [κ^2-Tpsem]$_2$Zn and [κ^4-Tpsem]Zn(κ^2–SeC$_6$H$_4$N), as illustrated in Scheme 6. The molecular structures of [κ^2-Tpsem]$_2$Zn and [κ^4-Tpsem]Zn(κ^2–SeC$_6$H$_4$N) have been determined by X-ray diffraction, as shown in Figure 8 and Figure 9 respectively. The four coordinate τ_4 geometry index[18] is 0.73[19] for [κ^2-Tpsem]$_2$Zn, which adopts a distorted tetrahedral geometry. One interesting feature of [κ^2-Tpsem]$_2$Zn is the κ^2-coordination mode for the [Tpsem] ligand, which complements the κ^3- and κ^4-coordination modes observed in the above

compounds. Therefore, it is evident that the [Tpsem] ligand exhibits considerable flexibility in its ability to bind metals. Table 3 shows all the metric details for coordination of the [Tpsem] ligand as a function of kapticity. According to the table, the κ^4-coordination mode is associated with a longer Zn–C bond length although the variation is not large. Compared with [Tptm] ligand, it is worth noting that, while the [Tpsem] ligand can have κ^2-, κ^3- and κ^4-coordination modes, there is presently no [Tptm] compounds listed in the CSD[17] that feature κ^2-coordination modes.[20]

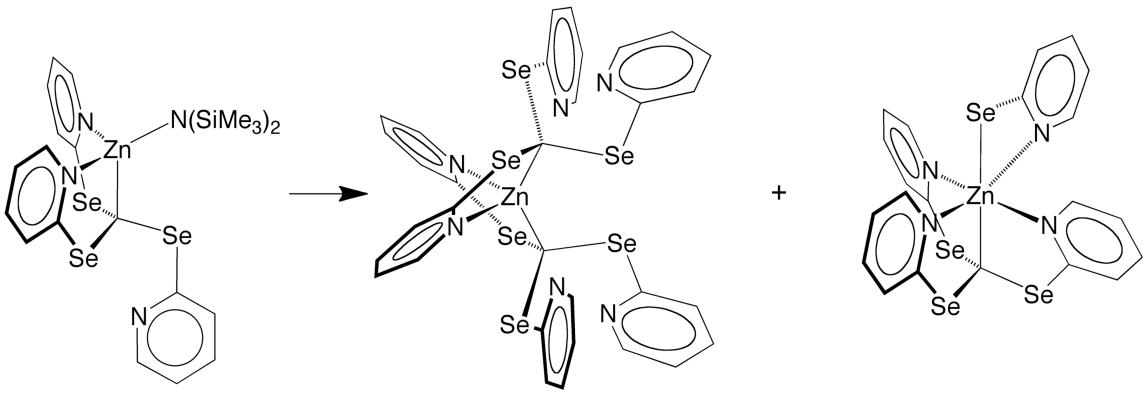

Scheme 6. Decomposition of [κ^3-Tpsem]ZnN($SiMe_3$)$_2$

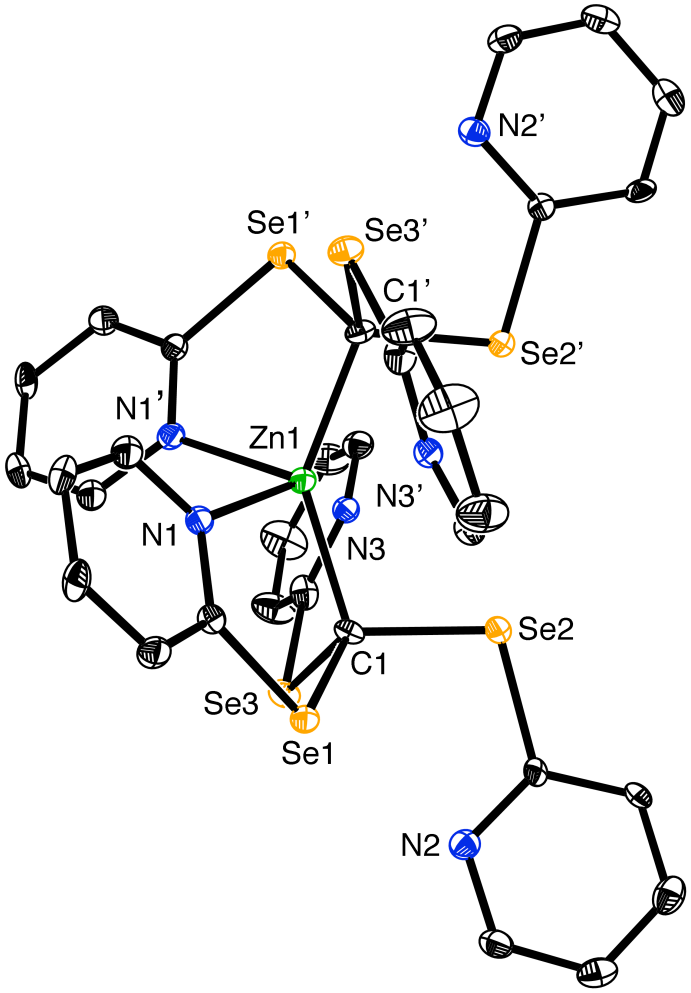

Figure 8. Molecular structure of $[\kappa^2\text{-Tpsem}]_2Zn$

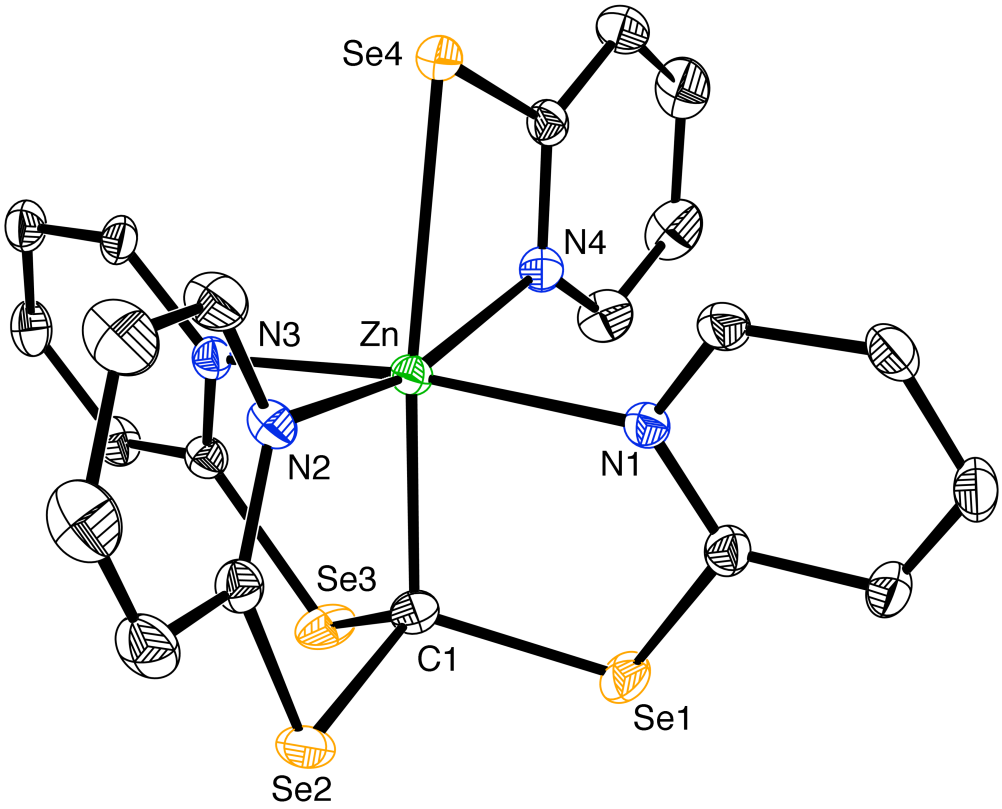

Figure 9. Molecular structure of [κ^4-Tpsem]Zn(κ^2–SeC_6H_4N).

Table 3. Zn–N and Zn–C bond lengths for coordination of [Tpsem] as a function of kapticity.

	***d*(Zn–C)/Å**	***d*(Zn–N)$_{av}$/Å**
[κ^4-Tpsem]ZnNCO	2.123(3)	2.169
[κ^4-Tpsem]Zn(κ^2–SeC_6H_4N)	2.120(3)	2.210
[κ^3-Tpsem]ZnSH	2.049(3)	2.048
{[κ^3-Tpsem]Zn}$_2$(μ–S)	2.060(4), 2.061(5)	2.086
[κ^2-Tpsem]$_2$Zn	2.070(6)	2.138

[κ^4-Tpsem]Zn(κ^2–SeC_6H_4N) has an approximately octahedral structure, and the selenium of the κ^2–SeC_6H_4N ligand is located *trans* to the carbon atom. We also obtained the sulfur counterpart [κ^4-Tptm]Zn(κ^2–SC_6H_4N), as a decomposition product of the reaction of [κ^4-Tptm]$ZnOSiMe_3$ with $P(SiMe_3)_3$. The molecular structure was determined by X-ray diffraction, as illustrated in Figure 10. Similar to the selenium counterpart, the sulfur of the κ^2–SC_6H_4N ligand is located *trans* to the carbon atom. Related structurally characterized compounds for the sulfur system include {[κ^4-Tptm]Fe(κ^2–SC_6H_4N)}[OTf][21] and {[κ^4-Tptm]Co(κ^2–SC_6H_4N)}$[ClO_4]$,[22] both of which have been isolated as isomers in which the atom *trans* to carbon may be either nitrogen or sulfur. The observations of both [κ^4-Tptm]Zn(κ^2–SC_6H_4N) and [κ^4-Tpsem]Zn(κ^2–SeC_6H_4N) are noteworthy, because although pyridyl-2-thiolate compounds have been studied extensively,[23] the selenium counterparts have received comparatively little attention.[24,25,26] As such compounds have, nevertheless, found applications as single source precursors for semiconductor materials[25] and in the formation of metal selenide nanoparticles.[26]

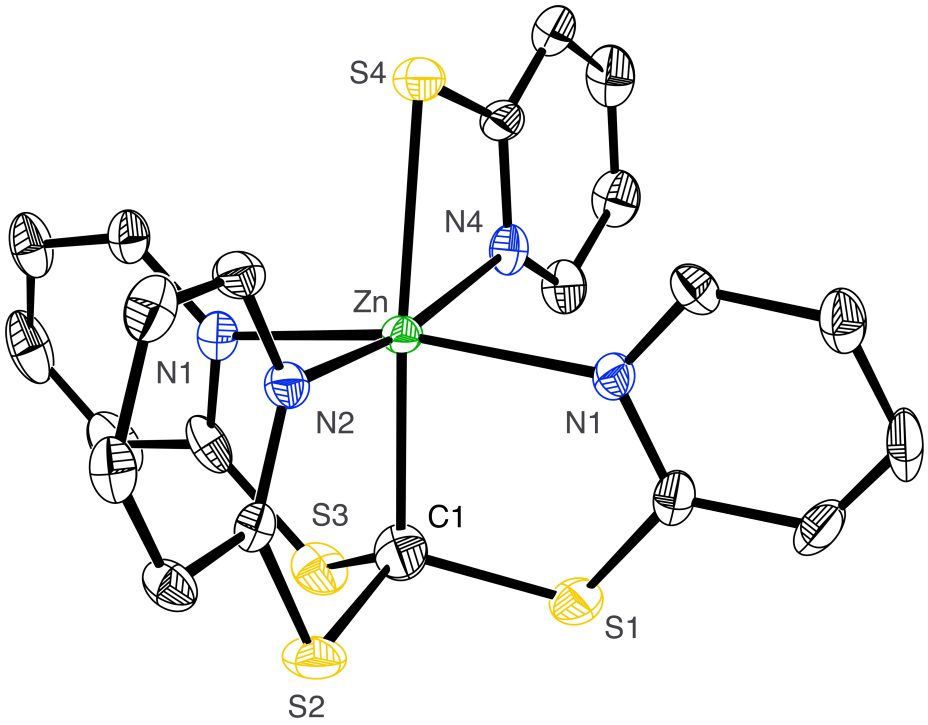

Figure 10. Molecular structure of [κ^4-Tptm]Zn(κ^2–SC_6H_4N).

5.3 Synthesis and Structures of *Bis*(2-pyridonyl)(pyridin-2-yloxy)methyl Zinc and Cadmium Complexes

5.3.1 Synthesis and Structure of *Bis*(2-pyridonyl)(pyridin-2-yloxy)methyl Zinc Amide

[κ^4-*O*-poBpom]ZnN(SiMe$_3$)$_2$ could be made *via* reaction of Zn[N(SiMe$_3$)$_2$]$_2$ with *bis*(2-pyridonyl)(pyridin-2-yloxy)methane, which was obtained from isomerization of *tris*(pyridin-2-yloxy)methane, or by directly reacting *tris*(pyridin-2-yloxy)methane with Zn[N(SiMe$_3$)$_2$]$_2$, as illustrated in Scheme 7. The molecular structure of [κ^4-*O*-poBpom]ZnN(SiMe$_3$)$_2$ has been determined by X-ray diffraction (Figure 11). It is worth noting that there is no such mixed donors ligand featuring a [*CNO*$_2$] coordination mode in the Cambridge Structural Database.[17]

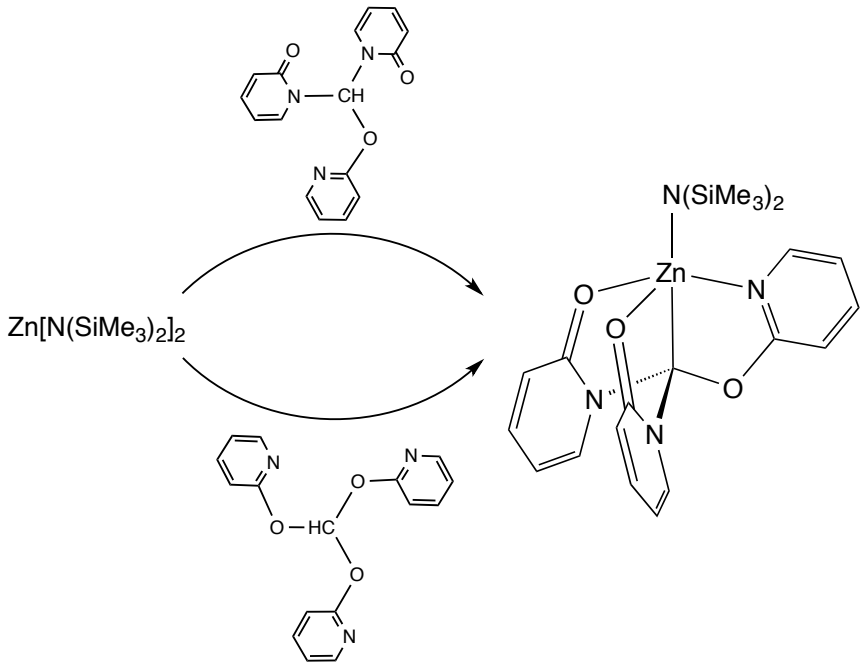

Scheme 7. Synthesis of [κ^4-*O*-poBpom]ZnN(SiMe$_3$)$_2$

Structural data of [κ^4-*O*-poBpom]ZnN(SiMe$_3$)$_2$ and its isomer [κ^3-Tpom]ZnN(SiMe$_3$)$_2$][4] are summarized in Table 4. It is worth noting that the Zn–C bond length in both structures are comparable, with that in [κ^4-*O*-poBpom]ZnN(SiMe$_3$)$_2$ being slightly shorter. The Zn–O bond lengths in [κ^3-Tpom]ZnN(SiMe$_3$)$_2$ are close to each other, while those in [κ^4-*O*-poBpom]ZnN(SiMe$_3$)$_2$ are different by 0.470 Å ([2.082(2) Å] and [2.552(2) Å]). All of these values are within the range for Zn–O (carbonyl oxygen) bond lengths (1.881 ~ 2.898 Å) according to CSD data.[17] Density functional theory[27] geometry optimization calculation on [κ^4-*O*-poBpom]ZnN(SiMe$_3$)$_2$ reproduces the difference in bond lengths ([2.126 Å] and [2.329 Å]). One simple explanation for this difference is the coordination of pyridin-2-yloxy arm in [κ^4-*O*-poBpom]ZnN(SiMe$_3$)$_2$ increases the steric effect, thus elongates one of the Zn–O bonds. However, variable temperature ^{1}H NMR spectroscopic studies indicate that

the two pyridine-2-yloxy groups of [κ^4-*O*-poBpom]ZnN(SiMe$_3$)$_2$ remain chemically equivalent on the NMR time scale at -70 ˚C.

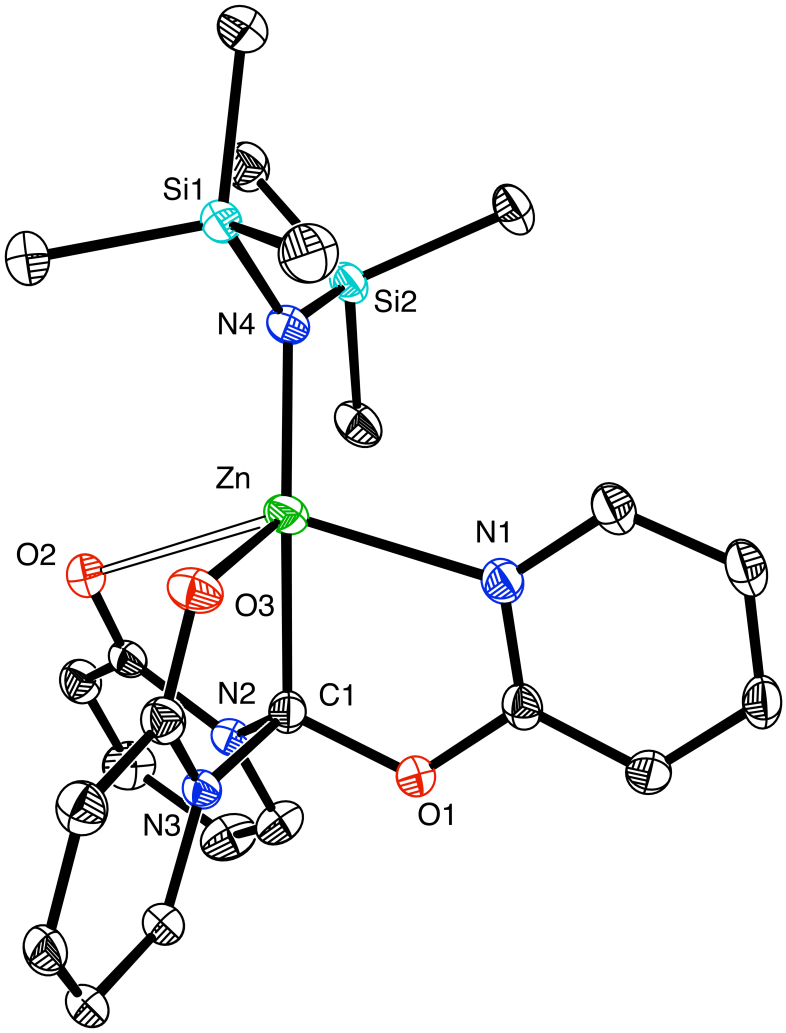

Figure 11. Molecular structure of [κ^4-*O*-poBpom]ZnN(SiMe$_3$)$_2$.

Table 4. Metrical data of [κ^3-Tpom]ZnN(SiMe$_3$)$_2$ and [κ^4-*O*-poBpom]ZnN(SiMe$_3$)$_2$.

	***d*(Zn–C)/Å**	***d*(Zn–O)/Å**
[κ^3-Tpom]ZnN(SiMe$_3$)$_2$	2.064(2)	2.095(2) and 2.104(2)
[κ^4-*O*-poBpom]ZnN(SiMe$_3$)$_2$	2.032(3)	2.082(2) and 2.552(2)

5.3.2 Synthesis and Structure of *Bis*(2-pyridonyl)(pyridin-2-yloxy)methyl Cadmium Amide

Bis(2-pyridonyl)(pyridin-2-yloxy)methane reacts with $Cd[N(SiMe_3)_2]_2$ to give the *bis*(trimethylsilyl)amido derivative, [κ^4-*O*-poBpom]$CdN(SiMe_3)_2$, as illustrated in Scheme 8. The molecular structure of [κ^4-*O*-poBpom]$CdN(SiMe_3)_2$ has been determined by X-ray diffraction (Figure 12). Similar to [κ^4-*O*-poBpom]$ZnN(SiMe_3)_2$, the two Cd–O bond lengths ([2.276(2)] Å and [2.565(2)] Å) are different by 0.289 Å, while both values are within the range (2.170 ~ 2.916 Å) of the Cd–O (carbonyl oxygen) bond length according to Cambridge Structural Database.[17] DFT calculations results are consistent with this observation ([2.313 Å] and [2.480 Å]). The Cd–C bond length [2.225(3) Å] in the crystal structure is also comparable to the average value (2.36 Å) for compounds listed in CSD.[17] Structural data of [κ^4-*O*-poBpom]$ZnN(SiMe_3)_2$ and [κ^4-*O*-poBpom]$CdN(SiMe_3)_2$ are summarized in Table 5. It is worth noting: (*i*) the M–C bond and the M–N bond are longer in the cadmium amide complex by 0.19 Å and 0.28 Å respectively; (*ii*) the difference between two M–O bond length is less significant in the cadmium compound. Furthermore, the five coordinate geometry index τ_5 for [κ^4-*O*-poBpom]$CdN(SiMe_3)_2$ is 0.41, while that for [κ^4-*O*-poBpom]$ZnN(SiMe_3)_2$ is 0.26. Therefore, the zinc center adopts a geometry that is closer to square pyramidal.

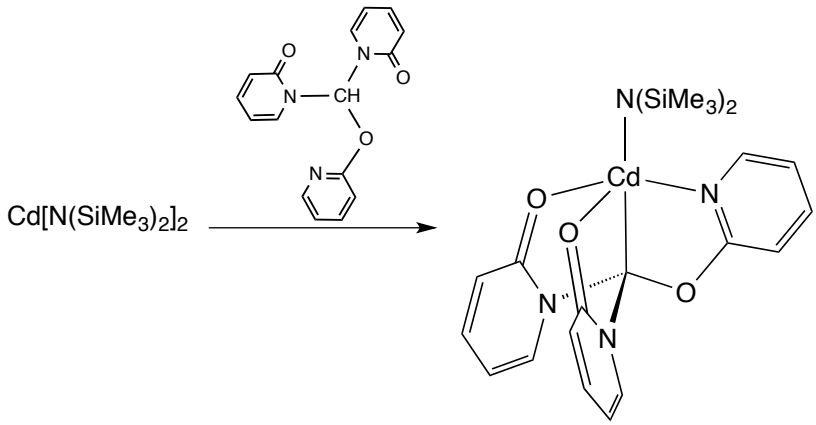

Scheme 8. Synthesis of [κ^4-*O*-poBpom]CdN(SiMe$_3$)$_2$.

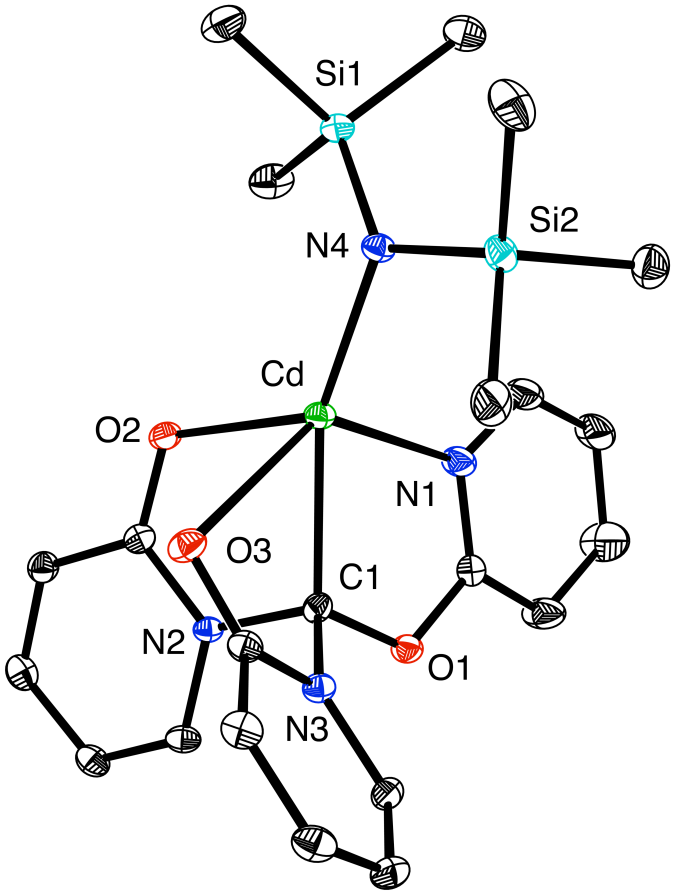

Figure 12. Molecular structure of [κ^4-*O*-poBpom]CdN(SiMe$_3$)$_2$.

Table 5. Metrical data of [κ⁴-*O*-poBpom]ZnN(SiMe$_3$)$_2$ and [κ⁴-*O*-poBpom]CdN(SiMe$_3$)$_2$.

	[κ⁴-*O*-poBpom]ZnN(SiMe$_3$)$_2$	**[κ⁴-*O*-poBpom]CdN(SiMe$_3$)$_2$**
d(Zn–C)/Å	2.032(3)	2.225(3)
d(Zn–O)/Å	2.082(2) and 2.552(2)	2.276(2) and 2.565(2)
d(Zn–N)/Å	2.244(3)	2.524(2)
d(Zn–N(SiMe$_3$)$_2$/Å	1.902(2)	2.091(2)
O–M–O/°	93.1	83.8
O–M–N/°	95.9 and 142.5	93.3 and 135.0

5.4 Summary and Conclusion

In summary, two multidentate, L$_3$X type ligands, which feature [*CN*$_3$] and [*CNO*$_2$] donors, have been synthesized and characterized, namely *tris*(2-pyridylseleno)methane, [Tpsem]H, and *Bis*(2-pyridonyl)(pyridin-2-yloxy)methane, [*O*-poBpom]H. They have been employed in the synthesis of zinc and cadmium complexes. Specifically, [Tpsem]H has been employed to synthesize the *bis*(trimethylsilyl)amido zinc complex, [κ³-Tpsem]ZnN(SiMe$_3$)$_2$. The latter compound provides access to a variety of other [Tpsem]ZnX derivatives, which include the isocyanate complex [κ⁴-Tpsem]ZnNCO, the hydrosulfido complex [κ³-Tpsem]ZnSH, the sulfido complex {[κ³-Tpsem]Zn}$_2$(μ–S), the 2:1 complex [κ²-Tpsem]$_2$Zn and the pyridyl-2-selenolate complex [κ⁴-Tpsem]Zn(κ²–SeC$_6$H$_4$N), thereby demonstrating that the [Tpsem] ligand can exhibit κ²-, κ³- and κ⁴-coordination modes. Variable temperature ^{1}H NMR spectroscopic studies demonstrate that [κ³-Tpsem]ZnN(SiMe$_3$)$_2$, [κ³-Tpsem]ZnSH and {[κ³-Tpsem]Zn}$_2$(μ–S) are fluxional on the NMR time scale. Similarly, [*O*-

poBpom]H has been employed to synthesize the *bis*(trimethylsilyl)amido zinc complex, [κ^4-*O*-poBpom]ZnN(SiMe$_3$)$_2$, and the *bis*(trimethylsilyl)amido cadmium complex, [κ^4-*O*-poBpom]CdN(SiMe$_3$)$_2$. Both structures were characterized by X-ray diffraction, which demonstrate a new [CNO_2] coordination environment.

5.5 Experimental Section

5.5.1 General Considerations

All manipulations were performed using a combination of glovebox, high vacuum, and Schlenk techniques under a nitrogen or argon atmosphere.[28] Solvents were purified and degassed by standard procedures. NMR spectra were measured on Bruker 300 DRX, Bruker Avance III 400, Bruker Avance III 400SL and Bruker Avance III 500 DMX spectrometers. ^{1}H NMR spectra are reported in ppm relative to SiMe$_4$ (δ = 0) and were referenced internally with respect to the protio solvent impurity (δ 7.16 for C_6D_5H, δ 5.32 for $CDHCl_2$ and δ 7.26 for $CHCl_3$).[29] ^{13}C NMR spectra are reported in ppm relative to SiMe$_4$ (δ = 0) and were referenced internally with respect to the solvent (δ 128.06 for C_6D_6 and δ 53.84 for CD_2Cl_2).[29] Coupling constants are given in hertz. Pyridine-2(1*H*)-selone[30], Zn[N(SiMe$_3$)$_2$]$_2$[31] and Cd[N(SiMe$_3$)$_2$]$_2$[31] were prepared by the literature methods. Mass spectra were obtained on a JEOL JMS-HX110HF tandem mass spectrometer using fast atom bombardment (FAB). Infrared spectra were recorded on PerkinElmer Spectrum Two spectrometer and are reported in cm^{-1}.

5.5.2 X-ray Structure Determinations

Single crystal X-ray diffraction data were collected on a Bruker Apex II diffractometer and crystal data, data collection and refinement parameters are summarized in Table 6. The structures were solved using direct methods and standard difference map techniques, and were refined by full-matrix least-squares procedures on F^2 with SHELXTL (Version 2008/4).[32]

5.5.3 Computational Details

Calculations were carried out using DFT as implemented in the Jaguar 7.6 (release 110) and 7.7 (release 107) suite of *ab initio* quantum chemistry programs.[27] Geometry optimizations were performed with the B3LYP density functional[33] using the 6-31G** (H, C, O, N, S) and LAV3P (Se, Zn, Cd) basis sets.[34]

5.5.4 Synthesis of Pyridine-2(1*H*)-selone

Pyridine-2(1*H*)-selone was prepared from Na_2Se_2[35] by a modification of the literature method.[36] A mixture of Se (15 g, 0.19 mol) and $NaBH_4$ (5 g, 0.13 mol) in a large Schlenk tube (*ca*. 600 mL) under an atmosphere of N_2 was cooled in an ice bath and treated with degassed ethanol (250 mL) *via* a cannula over a period of 20 minutes ("smoking" was observed at the beginning). After the addition was complete, the reaction vessel was allowed to warm to room temperature and then heated at 40 ˚C for 2 h. The reaction mixture was allowed to cool and N_2 was bubbled through the reaction mixture for 25 minutes to remove H_2Se. The volatile components were removed *in vacuo* to give a purple-grey residue, to which was added 2-ethoxy ethanol (250 mL) *via* cannula, followed by 2-bromopyridine (6.5 mL, 68 mmol) *via* syringe. The reaction mixture was refluxed for 23 hours and then allowed to cool to room temperature. The volatile

components were removed *in vacuo* from the red-brown solution at 70 ˚C giving a black solid, which was dried *in vacuo* overnight. Degassed water (160 mL) was added *via* syringe to the residue under N_2. The mixture was stirring vigorously and the black residue slowly dissolved over a period of *ca.* 10 minutes to give a red solution. Glacial acetic acid (40 mL) was added to the solution *via* syringe, thereby resulting in the immediate formation of a red precipitate (Se). The mixture was stirred for 1 h at room temperature, resulting in the formation of a yellow solution with a grey-black precipitate over which period the precipitate became grey-black. The mixture was filtered under N_2 and the volatile components were removed *in vacuo* from the yellow filtrate to give an orange residue. The orange residue was extracted with CH_2Cl_2 (2 × 100 mL) and the volatile components were removed from the yellow extracts *in vacuo* to give pyridine-2(1*H*)-selone as a yellow solid that was washed with pentane and dried *in vacuo* (6.78 g, 68%).

5.5.5 Synthesis of [Tpsem]H

Tris(2-pyridylseleno)methane has been previously reported[2] but was synthesized by an alternative method based on that for *tris*(2-pyridylthio)methane.[10] A mixture of $CHBr_3$ (184 μL, 2.1 mmol), KOH (529 mg, 9.5 mmol) and pyridine-2(1*H*)-selone (1.0 g, 6.3 mmol) was treated with benzene (6 mL) and heated at 60 ˚C for 3 hours, resulting in the formation of a red-brown solution with an oily layer that contained a brown solid, both of which were removed by filtration. The volatile components were removed from the filtrate by lyophilization to give a brown solid that was washed with benzene and dried *in vacuo* to give [Tpsem]H as a brown solid (642 mg, 63%) that is pure according to ^{1}H NMR spectroscopy. The compound may be obtained as pale

yellow crystals from toluene and has been authenticated by X-ray diffraction.[2a] ^{1}H NMR ($CDCl_3$): 7.06 [m, 3H, HC(SeC$_5$H$_4$N)$_3$], 7.37 [d, $^3J_{H–H}$ = 4 Hz, 3H, HC(SeC$_5$H$_4$N)$_3$], 7.39 [s, 1H, HC(SeC$_5$H$_4$N)$_3$], 7.49 [dt, $^4J_{H–H}$ = 2 Hz, $^3J_{H–H}$ = 8 Hz, 3H, HC(SeC$_5$H$_4$N)$_3$], 8.53 [d, $^3J_{H–H}$ = 4 Hz, 3H, HC(SeC$_5$H$_4$N)$_3$]. ^{1}H NMR (C_6D_6): 6.36 [m, 3H, HC(SeC$_5$H$_4$N)$_3$], 6.69 [dt, $^4J_{H–H}$ = 2 Hz, $^3J_{H–H}$ = 8 Hz, 3H, HC(SeC$_5$H$_4$N)$_3$], 6.98 [d, $^3J_{H–H}$ = 8 Hz, 3H, HC(SeC$_5$H$_4$N)$_3$], 7.99 [s, 1H, HC(SeC$_5$H$_4$N)$_3$], 8.36 [d, $^3J_{H–H}$ = 4 Hz, 3H, HC(SeC$_5$H$_4$N)$_3$]. ^{13}C{^{1}H} NMR (C_6D_6): 22.5 [s, 1C, HC(SeC$_5$H$_4$N)$_3$], 120.6 [s, 3C, HC(SeC$_5$H$_4$N)$_3$], 125.2 [s, 3C, HC(SeC$_5$H$_4$N)$_3$], 136.3 [s, 3C, HC(SeC$_5$H$_4$N)$_3$], 150.3 [s, 3C, HC(SeC$_5$H$_4$N)$_3$], 158.1 [s, 3C, HC(SeC$_5$H$_4$N)$_3$]. MS: m/z = 486.0 $[M]^+$, M = [Tpsem]H.

5.5.6 Synthesis of [κ^3-Tpsem]ZnN(SiMe$_3$)$_2$

A mixture of [Tpsem]H (10 mg, 0.02 mmol) and Zn[N(SiMe$_3$)$_2$]$_2$ (8 mg, 0.02 mmol) in an NMR tube equipped with a J. Young valve was dissolved in benzene-d_6 (1 mL) and heated at 60 ˚C. The reaction was monitored by ^{1}H NMR spectroscopy, thereby demonstrating the formation of [κ^3-Tpsem]ZnN(SiMe$_3$)$_2$ over a period of 6 hours. ^{1}H NMR (C_6D_6): 0.47 [s, 18H, [(CH$_3$)$_3$Si]$_2$NZn-C(SeC$_5$H$_4$N)$_3$], 6.28 [t, $^3J_{H–H}$ = 6 Hz, 3H, (Me$_3$Si)$_2$NZnC(SeC$_5$H$_4$N)$_3$], 6.48 [t, $^3J_{H–H}$ = 7 Hz, 3H, (Me$_3$Si)$_2$NZnC(SeC$_5$H$_4$N)$_3$], 6.66 [d, $^3J_{H–H}$ = 8 Hz, 3H, (Me$_3$Si)$_2$N-ZnC(SeC$_5$H$_4$N)$_3$], 8.39 [d, $^3J_{H–H}$ = 4 Hz, 3H, (Me$_3$Si)$_2$NZnC(SeC$_5$H$_4$N)$_3$]. ^{1}H NMR (THF-d_8): -0.04 [s, 18H, [(CH$_3$)$_3$Si]$_2$N-ZnC(SeC$_5$H$_4$N)$_3$], 7.11 [m, 3H, (Me$_3$Si)$_2$N-ZnC(SeC$_5$H$_4$N)$_3$], 7.34 [d, $^3J_{H–H}$ = 8 Hz, 3H, (Me$_3$Si)$_2$NZnC(SeC$_5$H$_4$N)$_3$], 7.54 [m, 3H, (Me$_3$Si)$_2$NZnC(SeC$_5$H$_4$N)$_3$], 8.62 [dt, $^3J_{H–H}$ = 5 Hz, $^4J_{H–H}$ = 1 Hz, 3H, (Me$_3$Si)$_2$N-ZnC(SeC$_5$H$_4$N)$_3$]. ^{13}C{^{1}H} NMR (C_6D_6): 6.7 [s, 6C, [(CH$_3$)$_3$Si]$_2$N-ZnC(SeC$_5$H$_4$N)$_3$], not observed [1C, (Me$_3$Si)$_2$NZnC(SeC$_5$H$_4$N)$_3$], 119.7 [s, 3C, (Me$_3$Si)$_2$NZnC(SeC$_5$H$_4$N)$_3$], 124.5 [s, 3C, (Me$_3$Si)$_2$NZnC(SeC$_5$H$_4$N)$_3$], 136.6 [s, 3C, (Me$_3$Si)$_2$NZnC(SeC$_5$H$_4$N)$_3$],

148.3 [s, 3C, $(Me_3Si)_2NZnC(Se\underline{C}_5H_4N)_3$], 163.4 [s, 3C, $(Me_3Si)_2NZnC(Se\underline{C}_5H_4N)_3$]. $^{13}C\{^1H\}$ NMR (THF- d_8): 6.4 [s, 6C, $[(\underline{C}H_3)_3Si]_2N\text{-}ZnC(SeC_5H_4N)_3$], not observed [1C, $(Me_3Si)_2NZn\underline{C}(SeC_5H_4N)_3$], 120.8 [s, 3C, $(Me_3Si)_2N\text{-}ZnC(Se\underline{C}_5H_4N)_3$], 124.7 [s, 3C, $(Me_3Si)_2NZnC(Se\underline{C}_5H_4N)_3$], 137.9 [s, 3C, $(Me_3Si)_2N\text{-}ZnC(Se\underline{C}_5H_4N)_3$], 149.3 [s, 3C, $(Me_3Si)_2NZnC(Se\underline{C}_5H_4N)_3$], 163.9 [s, 3C, $(Me_3Si)_2N\text{-}ZnC(Se\underline{C}_5H_4N)_3$].

5.5.7 Synthesis of [κ⁴-Tpsem]ZnNCO

A mixture of [Tpsem]H (10 mg, 0.02 mmol) and $Zn[N(SiMe_3)_2]_2$ (8 mg, 0.02 mmol) in an NMR tube equipped with a J. Young valve was dissolved in benzene-d_6 (1 mL) and heated at 60 ˚C for 2 hours to generate $[\kappa^3\text{-Tpsem}]ZnN(SiMe_3)_2$. The solution was frozen and the atmosphere removed *in vacuo*. The sample was treated with CO_2 (1 atm) and allowed to stand at room temperature for 2 days. The reaction was monitored by ^1H NMR spectroscopy, thereby demonstrating the quantitative conversion to $[\kappa^4\text{-Tpsem}]ZnNCO$, together with the formation of $(Me_3SiO)_2CO$ (δ 0.21).[1a] The sample was lyophilized and the solid obtained was dissolved in benzene (*ca.* 1 mL) and allowed to evaporate, thereby depositing colorless crystals of $[\kappa^4\text{-Tpsem}]ZnNCO$ suitable for X-ray diffraction (5 mg, 40%). ^1H NMR (C_6D_6): 6.24 [m, 3H, $OCNZnC(SeC_5\underline{H}_4N)_3$], 6.42 [dt, $^3J_{H-H}$ = 7 Hz, $^4J_{H-H}$ = 2 Hz, 3H, $OCNZnC(SeC_5\underline{H}_4N)_3$], 6.47 [d, $^3J_{H-H}$ = 8 Hz, 3H, $OCNZnC(SeC_5\underline{H}_4N)_3$], 9.13 [d, $^3J_{H-H}$ = 6 Hz, 3H, $OCNZnC(SeC_5\underline{H}_4N)_3$]. $^{13}C\{^1H\}$ NMR (C_6D_6): not observed [1C, $OCNZn\underline{C}(SeC_5H_4N)_3$], 120.5 [s, 3C, $OCNZnC(Se\underline{C}_5H_4N)_3$], 124.0 [s, 3C, $OCN\text{-}ZnC(Se\underline{C}_5H_4N)_3$], not observed [1C, $O\underline{C}NZnC(Se\underline{C}_5H_4N)_3$], 137.7 [s, 3C, $OCN\text{-}ZnC(Se\underline{C}_5H_4N)_3$], 149.6 [s, 3C, $OCNZnC(Se\underline{C}_5H_4N)_3$], 158.6 [s, 3C, $OCN\text{-}ZnC(Se\underline{C}_5H_4N)_3$]. MS: m/z = 591.9 $[M]^+$. IR Data (cm^{-1}): 3056 (w), 2951 (w), 2205 (s), 1655 (w), 1584 (s), 1553 (s), 1452 (s), 1413 (s), 1340 (m), 1277 (m), 1244 (w), 1152 (m), 1116 (s), 1085 (m), 1044 (m), 1002 (m), 891 (m), 836 (m), 752 (s), 729 (m), 700 (m), 679 (m), 651 (w), 620 (m), 569 (m), 469 (s), 406 (s).

5.5.8 Synthesis of [κ³-Tpsem]ZnSH

A mixture of [Tpsem]H (25 mg, 0.05 mmol) and $Zn[N(SiMe_3)_2]_2$ (20 mg, 0.05 mmol) in an NMR tube equipped with a J. Young valve was dissolved in benzene-d_6 (3 mL) and heated at 60 ˚C for 5 hours to generate [κ³-Tpsem]ZnN(SiMe₃)₂. The solution was transferred to a small Schlenk tube and treated with H_2S, slowly allowing the pressure to reach 1 atm(started from 8 cmHg to 60 cmHg for 5 min), thereby depositing [κ³-Tpsem]ZnSH as a microcrystalline solid. The H_2S was removed *in vacuo* and the mixture was filtered to give [κ³-Tpsem]ZnSH as a light yellow solid that was washed with hexane (2 × 3 mL) and dried *in vacuo* (16 mg, 53%). Crystals suitable for X-ray diffraction were obtained by treating a frozen solution of [κ³-Tpsem]ZnN(SiMe₃)₂ in benzene with H_2S (*ca*. 24cm Hg) H_2S for 15 minutes, during which period the solution was allowed to warm to room temperature slowly. Anal. calcd. for [κ³-Tpsem]ZnSH: C, 33.0%; H, 2.3%; N, 7.2%. Found: C, 33.1%; H, 1.9%; N, 6.8%. ^{1}H NMR (CD_2Cl_2): -1.65 [s, 1H, HS-ZnC(SeC₅H₄N)₃], 7.15 [t, $^3J_{H-H}$ = 6 Hz, 3H, HSZnC(SeC₅H₄N)₃], 7.32 [d, $^3J_{H-H}$ = 8 Hz, 3H, HSZnC(SeC₅H₄N)₃], 7.55 [t, $^3J_{H-H}$ = 7 Hz, 3H, HSZnC(SeC₅H₄N)₃], 8.66 [d, $^3J_{H-H}$ = 5 Hz, 3H, HSZnC(SeC₅H₄N)₃]. ^{13}C{^{1}H} NMR (CD_2Cl_2): not observed [1C, HS-ZnC(SeC₅H₄N)₃], 120.9 [s, 3C, HSZnC(SeC₅H₄N)₃], 124.5 [s, 3C, HSZnC(SeC₅H₄N)₃], 137.9 [s, 3C, HSZnC(SeC₅H₄N)₃], 149.0 [s, 3C, HSZnC(SeC₅H₄N)₃], 161.5 [s, 3C, HSZnC(SeC₅H₄N)₃]. MS: m/z = 549.9 $[M - SH]^+$.

5.5.9 Synthesis of {[κ³-Tpsem]Zn}₂(μ–S)

A solution of [κ³-Tpsem]ZnSH (6 mg, 0.01 mmol) in CH_2Cl_2 (*ca.* 0.5 mL) was allowed to evaporate slowly at room temperature, thereby depositing orange crystals of {[κ³-Tpsem]Zn}₂(μ–S) suitable for X-ray diffraction (2 mg, 31%). ^{1}H NMR (CD_2Cl_2): 7.05 [t, $^3J_{H-H}$ = 6 Hz, 6H, [ZnC(SeC₅H₄N)₃]₂(μ-S)], 7.18 [d, $^3J_{H-H}$ = 8

Hz, 6H, [ZnC(SeC$_5$H$_4$N)$_3$]$_2$(μ-S)], 7.43 [t, $^3J_{H–H}$ = 7 Hz, 6H, [ZnC(SeC$_5$H$_4$N)$_3$]$_2$(μ-S)], 8.78 [d, $^3J_{H–H}$ = 5 Hz, 6H, [ZnC(SeC$_5$H$_4$N)$_3$]$_2$(μ-S)].

5.5.10 Interconversion of [κ^3-Tpsem]ZnSH and {[κ^3-Tpsem]Zn}$_2$(μ–S)

A mixture composed of {[κ^3-Tpsem]Zn}$_2$(μ–S) and [κ^3-Tpsem]ZnSH (2.5:1, *ca.* 5 mg) was dissolved in CD_2Cl_2 in an NMR tube equipped with J. Young valve and treated with H_2S (*ca.* 20 cm Hg) at room temperature. The reaction was monitored by ^{1}H NMR spectroscopy, thereby demonstrating the complete conversion of {[κ^3-Tpsem]Zn}$_2$(μ–S) into [κ^3-Tpsem]ZnSH within a period of 5 minutes. The volatile components were removed *in vacuo* and the resulting yellow solid was redissolved in CD_2Cl_2 and analyzed by ^{1}H NMR spectroscopy, thereby demonstrating that the formation of a mixture of {[κ^3-Tpsem]Zn}$_2$(μ–S) and [κ^3-Tpsem]ZnSH (0.4:1).

5.5.11 Synthesis of [κ^2-Tpsem]$_2$Zn

A solution of [κ^3-Tpsem]ZnN(SiMe$_3$)$_2$ (*ca.* 10 mg, 0.02 mmol) in benzene (*ca.* 1 mL) was allowed to evaporate slowly, thereby depositing colorless crystals of [κ^2-Tpsem]$_2$Zn suitable for X-ray diffraction.

5.5.12 Synthesis of [κ^4-Tpsem]Zn(κ^2–SeC$_6$H$_4$N)

A mixture of [Tpsem]H (10 mg, 0.02 mmol) and Zn[N(SiMe$_3$)$_2$]$_2$ (8 mg, 0.02 mmol) in an NMR tube equipped with a J. Young valve was dissolved in benzene-d_6 (1 mL) and heated at 60 ˚C for a period of 6 hours. The solvent was allowed to evaporate slowly at room temperature, thereby depositing pale yellow crystals of [κ^4-Tpsem]Zn(κ^2–SeC$_6$H$_4$N) suitable for X-ray diffraction.

5.5.13 Synthesis of $HC(OC_5H_4N)(NC_5H_4O)_2$

$HC(OC_5H_4N)_3$[4] (330 mg, 1.12 mmol) and camphorsulfonic acid (35 mg, 0.15 mmol) were dissolved in a mixture of THF (1.5 mL) and toluene (3 mL) in a small ampoule. The reaction was heated at 90 °C for 2 hours resulting in a white precipitate. The mixture was cooled down to room temperature and filtered to give a white solid. The solid was washed with ethyl ether (3 × 1 mL) and dried *in vacuo* overnight (235 mg, 71%). Colorless crystals suitable for X-ray diffraction were obtained from slow evaporation of a benzene solution. Anal. calcd. for $HC(OC_5H_4N)(NC_5H_4O)_2$: C, 65.1%; H, 4.4%; N, 14.2%. Found: C, 64.9 %; H, 4.2 %; N, 14.4 %. ^{1}H NMR ($CDCl_3$): 6.19 [t, $^3J_{H\text{-}H}$ = 7 Hz, 2H of $HC(OC_5H_4N)(NC_5\underline{H}_4O)_2$], 6.50 [d, $^3J_{H\text{-}H}$ = 9 Hz, 2H of $HC(OC_5H_4N)(NC_5\underline{H}_4O)_2$], 6.99 ~ 7.04 [m, 2H of $HC(OC_5\underline{H}_4N)(NC_5H_4O)_2$], 7.32 [m, 2H of $HC(OC_5H_4N)(NC_5\underline{H}_4O)_2$], 7.69 [m, 1H of $HC(OC_5\underline{H}_4N)(NC_5H_4O)_2$], 7.99 [d, $^3J_{H\text{-}H}$ = 7 Hz, 2H of $HC(OC_5H_4N)(NC_5\underline{H}_4O)_2$], 8.15 [d, $^3J_{H\text{-}H}$ = 4 Hz, 1H of $HC(OC_5\underline{H}_4N)(NC_5H_4O)_2$], 8.61 [s, 1H of $\underline{H}C(OC_5H_4N)(NC_5H_4O)_2$. $^{13}C\{^1H\}$ NMR ($CDCl_3$): 88.5 [s, 1C of $H\underline{C}(OC_5H_4N)(NC_5H_4O)_2$], 105.0 [s, 2C of $HC(OC_5H_4N)(N\underline{C}_5H_4O)_2$], 111.5 [s, 1C of $HC(O\underline{C}_5H_4N)(NC_5H_4O)_2$], 119.6 [s, 1C of $HC(O\underline{C}_5H_4N)(NC_5H_4O)_2$], 121.7 [s, 2C of $HC(OC_5H_4N)(N\underline{C}_5H_4O)_2$], 136.3 [s, 2C of $HC(OC_5H_4N)(N\underline{C}_5H_4O)_2$], 139.9 [s, 1C of $HC(O\underline{C}_5H_4N)(NC_5H_4O)_2$], 140.5 [s, 2C of $HC(OC_5H_4N)(N\underline{C}_5H_4O)_2$], 147.2 [s, 1C of $HC(O\underline{C}_5H_4N)(NC_5H_4O)_2$], 160.0 [s, 1C of $HC(O\underline{C}_5H_4N)(NC_5H_4O)_2$], 162.3 [s, 2C of $HC(OC_5H_4N)(N\underline{C}_5H_4O)_2$]. FAB-MS: m/z = 296.2 $[M + H]^+$. IR Data (ATR, cm^{-1}): 3098 (w), 1658 (vs), 1585 (s), 1534 (s), 1468 (m), 1430 (m), 1400 (w), 1358 (w), 1307 (w), 1263 (m), 1232 (s), 1175 (m), 1140 (m), 1113 (s), 1049 (s), 1018 (m), 991 (w), 910 (s), 887 (m), 866 (m), 849 (m), 778 (s), 761 (s), 734 (m), 655 (w), 631 (w), 583 (w), 569 (m), 552 (w), 517 (m), 500 (s).

5.5.14 Synthesis of [κ⁴-*O*-poBpom]ZnN(SiMe$_3$)$_2$

$HC(OC_5H_4N)(NC_5H_4O)_2$ (20 mg, 0.07 mmol) was dissolved in benzene in an NMR tube equipped with a J. Young valve. Excess $Zn[N(SiMe_3)_2]_2$ was added and the mixture was kept in 100°C oil bath, and monitored by ^{1}H NMR. The reaction completed after 4 days. The sample was lyophilized and washed with pentane, then dried *in vacuo* overnight to give off-white solid (16 mg, 46%). Colorless crystals suitable for X-ray diffraction were obtained from slow evaporation of a benzene solution. ^{1}H NMR (C_6D_6): 0.47 [s, 18H of $\{(C\underline{H}_3)_3Si\}_2NZnC\{N(C_4H_4)(CO)\}_2\{OC(C_4H_4)N\}$], 5.62 [t, $^3J_{H-H}$ = 7 Hz, 2H of of $\{(CH_3)_3Si\}_2NZnC\{N(C_4\underline{H}_4)(CO)\}_2\{OC(C_4H_4)N\}$], 6.31 [t, $^3J_{H-H}$ = 6 Hz, 1H of of $\{(CH_3)_3Si\}_2NZnC\{N(C_4H_4)(CO)\}_2\{OC(C_4\underline{H}_4)N\}$], 6.39 [m, 1H of of $\{(CH_3)_3Si\}_2NZnC\{N(C_4H_4)(CO)\}_2\{OC(C_4\underline{H}_4)N\}$ and 2H of $\{(CH_3)_3Si\}_2NZnC\{N(C_4\underline{H}_4)(CO)\}_2\{OC(C_4H_4)N\}$], 6.48 [m, 2H of $\{(CH_3)_3Si\}_2NZnC\{N(C_4\underline{H}_4)(CO)\}_2\{OC(C_4H_4)N\}$], 6.89 [dt, $^3J_{H-H}$ = 3 Hz, $^4J_{H-H}$ = 1 Hz, 1H of of $\{(CH_3)_3Si\}_2NZnC\{N(C_4H_4)(CO)\}_2\{OC(C_4\underline{H}_4)N\}$], 7.46 [dd, $^3J_{H-H}$ = 7 Hz, $^4J_{H-H}$ = 1 Hz, 2H of $\{(CH_3)_3Si\}_2NZnC\{N(C_4\underline{H}_4)(CO)\}_2\{OC(C_4H_4)N\}$], 8.27 [dd, $^3J_{H-H}$ = 6 Hz, $^4J_{H-H}$ = 1 Hz, 1H of $\{(CH_3)_3Si\}_2NZnC\{N(C_4H_4)(CO)\}_2\{OC(C_4\underline{H}_4)N\}$]. ^{13}C $\{^1H\}$ NMR (C_6D_6): 5.7 [6C of $\{(\underline{C}H_3)_3Si\}_2NZnC\{N(C_4H_4)(CO)\}_2\{OC(C_4H_4)N\}$], 91.7 [s, 1C of $\{(CH_3)_3Si\}_2NZn\underline{C}\{N(C_4H_4)(CO)\}_2\{OC(C_4H_4)N\}$], 107.8 [s, 2C of $\{(CH_3)_3Si\}_2NZnC\{N(\underline{C}_4H_4)(CO)\}_2\{OC(C_4H_4)N\}$], 111.1 [s, 1C of $\{(CH_3)_3Si\}_2NZnC\{N(C_4H_4)(CO)\}_2\{OC(\underline{C}_4H_4)N\}$], 118.9 [s, 1C of $\{(CH_3)_3Si\}_2NZnC\{N(C_4H_4)(CO)\}_2\{OC(\underline{C}_4H_4)N\}$], 120.3 [s, 2C of $\{(CH_3)_3Si\}_2NZnC\{N(\underline{C}_4H_4)(CO)\}_2\{OC(C_4H_4)N\}$], 132.5 [s, 2C of $\{(CH_3)_3Si\}_2NZnC\{N(\underline{C}_4H_4)(CO)\}_2\{OC(C_4H_4)N\}$], 139.3 [s, 2C of $\{(CH_3)_3Si\}_2NZnC\{N(\underline{C}_4H_4)(CO)\}_2\{OC(C_4H_4)N\}$], 140.6 [s, 1C of $\{(CH_3)_3Si\}_2NZnC\{N(C_4H_4)(CO)\}_2\{OC(\underline{C}_4H_4)N\}$], 146.5 [s, 1C of

$\{(CH_3)_3Si\}_2NZnC\{N(C_4H_4)(CO)\}_2\{OC(\underline{C}_4H_4)N\}]$, 161.9 [s, 1C of $\{(CH_3)_3Si\}_2NZnC\{N(C_4H_4)(CO)\}_2\{O\underline{C}(C_4H_4)N\}]$, 164.1 [s, 2C of $\{(CH_3)_3Si\}_2NZnC\{N(C_4H_4)(\underline{C}O)\}_2\{OC(C_4H_4)N\}]$.

5.5.15 Synthesis of [κ⁴-*O*-poBpom]CdN(SiMe₃)₂

$HC(OC_5H_4N)(NC_5H_4O)_2$ (25 mg, 0.08 mmol) was dissolved in benzene in an NMR tube equipped with a J. Young valve. Excess $Cd[N(SiMe_3)_2]_2$ was added and the mixture was kept in a 100°C oil bath, and monitored by ^{1}H NMR. The reaction completed after 4 days. The sample was lyophilized and washed with pentane, then dried *in vacuo* overnight to get off-white solid (48 mg, 100%). Colorless crystals suitable for X-ray diffraction were obtained from slow evaporation of a benzene solution. ^{1}H NMR (C_6D_6): 0.50 [s, 18H of $\{(C\underline{H}_3)_3Si\}_2NCdC\{N(C_4H_4)(CO)\}_2\{OC(C_4H_4)N\}]$, 5.59 [dt, $^3J_{H-H}$ = 7 Hz, $^4J_{H-H}$ = 1 Hz, 2H of of $\{(CH_3)_3Si\}_2NCd\text{-}C\{N(C_4\underline{H}_4)(CO)\}_2\{OC(C_4H_4)N\}]$, 6.30 ~ 6.50 [overlapping, m, 4H of $\{(CH_3)_3Si\}_2NCd\text{-}C\{N(C_4\underline{H}_4)(CO)\}_2\{OC(C_4H_4)N\}$ and 2H of $\{(CH_3)_3Si\}_2NCd\text{-}C\{N(C_4H_4)(CO)\}_2\{OC(C_4\underline{H}_4)N\}]$, 6.85 [m, 1H of of $\{(CH_3)_3Si\}_2NCd\text{-}C\{N(C_4H_4)(CO)\}_2\{OC(C_4\underline{H}_4)N\}]$, 7.42 [dd, $^3J_{H-H}$ = 7 Hz, $^4J_{H-H}$ = 1 Hz, 2H of $\{(CH_3)_3Si\}_2NCdC\{N(C_4\underline{H}_4)(CO)\}_2\{OC(C_4H_4)N\}]$, 8.20 [dd, $^3J_{H-H}$ = 5 Hz, $^4J_{H-H}$ = 1 Hz, 1H of $\{(CH_3)_3Si\}_2NCdC\{N(C_4H_4)(CO)\}_2\{OC(C_4\underline{H}_4)N\}]$.

5.6 Crystallographic Data

Table 6. Crystal, intensity collection and refinement data.

	[κ⁴-Tpsem]ZnNCO·0.5C₆H₆	**[κ³-Tpsem]ZnSH**
lattice	Monoclinic	Orthorhombic
formula	$C_{20}H_{15}N_4OSe_3Zn$	$C_{16}H_{13}N_3SSe_3Zn$
formula weight	629.61	581.60
space group	*C2/c*	*Pbca*
a / Å	33.545(5)	8.4549(7)
b / Å	9.1886(14)	17.4460(15)
c / Å	14.125(2)	25.563(2)
α / °	90	90
β / °	102.036(2)	90
γ / °	90	90
V / Å^3	4258.1(11)	3770.6(5)
Z	8	8
temperature (K)	150(2)	130(2)
radiation (λ, Å)	0.71073	0.71073
ρ (calcd.), g cm^{-3}	1.964	2.049
μ (Mo Kα), mm^{-1}	6.301	7.208
θ max, deg.	32.77	30.65
no. of data collected	36250	57778
no. of data used	7522	5819
no. of parameters	271	221
R_1 [$I > 2\sigma(I)$]	0.0430	0.0374
wR_2 [$I > 2\sigma(I)$]	0.0891	0.0772
R_1 [all data]	0.0889	0.0671
wR_2 [all data]	0.1042	0.0878
GOF	1.011	1.029
R_{int}	0.0708	0.0859

Table 6 (cont.) Crystal, intensity collection and refinement data.

	{[κ³-Tpsem]Zn}₂(μ–S)·THF	**[κ²-Tpsem]₂Zn·2C₆H₆**
lattice	Monoclinic	Monoclinic
formula	$C_{36}H_{32}N_6OSSe_6Zn_2$	$C_{44}H_{36}N_6Se_6Zn$
formula weight	1201.24	1187.92
space group	*Cc*	*P2/c*
a / Å	22.1822(19)	20.788(8)
b / Å	16.4386(14)	8.263(3)
c / Å	13.2756(12)	25.940(10)
α / °	90	90
β / °	122.6530(10)	101.114(6)
γ / °	90	90
V / Å³	4075.8(6)	4372(3)
Z	4	4
temperature (K)	130(2)	149(2)
radiation (λ, Å)	0.71073	0.71073
ρ (calcd.), g cm^{-3}	1.958	1.805
μ (Mo Kα), mm^{-1}	6.624	5.596
θ max, deg.	30.75	29.57
no. of data collected	32923	63502
no. of data used	12653	12248
no. of parameters	424	515
R_1 [$I > 2\sigma(I)$]	0.0430	0.0579
wR_2 [$I > 2\sigma(I)$]	0.0803	0.0655
R_1 [all data]	0.0621	0.1860
wR_2 [all data]	0.0847	0.0857
GOF	1.000	1.000
R_{int}	0.0437	0.2340

Table 6 (cont.) Crystal, intensity collection and refinement data.

	[κ⁴-Tpsem]Zn(κ²–SeC₆H₄N)·0.5C₆H₆	**[Tpsem]H**
lattice	Monoclinic	Rhombohedral (hexagonal setting)
formula	$C_{24}H_{19}N_4Se_4Zn$	$C_{16}H_{13}N_3Se_3$
formula weight	744.64	484.17
space group	*C*2/*c*	*R*-3*c*
a / Å	32.015(9)	12.0529(17)
b / Å	9.029(3)	12.0529(17)
c / Å	17.758(5)	39.847(6)
α / °	90	90
β / °	95.383(4)	90
γ / °	90	120
V / Å³	5110(3)	5013.2(12)
Z	8	12
temperature (K)	150(2)	150(2)
radiation (λ, Å)	0.71073	0.71073
ρ (calcd.), g cm^{-3}	1.936	1.924
μ (Mo Kα), mm^{-1}	6.679	6.602
θ max, deg.	31.52	32.64
no. of data collected	42494	26789
no. of data used	8503	2007
no. of parameters	299	67
R_1 [$I > 2\sigma(I)$]	0.0392	0.0266
wR_2 [$I > 2\sigma(I)$]	0.0780	0.0594
R_1 [all data]	0.0769	0.0467
wR_2 [all data]	0.0891	0.0677
GOF	1.013	1.063
R_{int}	0.0598	0.0535

Table 6 (cont.) Crystal, intensity collection and refinement data.

	[κ⁴-Tptm]Zn(κ²–SC$_6$H$_4$N)	**[*O*-poBpom]H·0.5C$_6$H$_6$**
lattice	Monoclinic	Monoclinic
formula	$C_{19}H_{16}N_4Se_4Zn$	$C_{19}H_{16}N_3O_3$
formula weight	517.99	334.35
space group	$P2_1/c$	$P2_1/c$
a / Å	12.914(2)	9.0635(12)
b / Å	13.057(2)	10.1292(13)
c / Å	12.849(2)	17.654(2)
α / °	90	90
β / °	90.127(2)	90.721(2)
γ / °	90	90
V / Å^3	2166.6(6)	1620.6(4)
Z	4	4
temperature (K)	130(2)	130(2)
radiation (λ, Å)	0.71073	0.71073
ρ (calcd.), g cm^{-3}	1.588	1.370
μ (Mo Kα), mm^{-1}	1.536	0.095
θ max, deg.	30.65	30.92
no. of data collected	34236	25979
no. of data used	6672	5109
no. of parameters	271	226
R_1 [$I > 2\sigma(I)$]	0.1012	0.0508
wR_2 [$I > 2\sigma(I)$]	0.2563	0.1020
R_1 [all data]	0.2209	0.0975
wR_2 [all data]	0.3058	0.1190
GOF	1.053	1.043
R_{int}	0.1820	0.0664

Table 6 (cont.) Crystal, intensity collection and refinement data.

	[*O*-poBpom]-$ZnN(SiMe_3)_2$	**[*O*-poBpom]-$CdN(SiMe_3)_2 \cdot 0.5C_6H_6$**
lattice	Triclinic	Orthorhombic
formula	$C_{22}H_{30}N_4O_3Si_2Zn$	$C_{25}H_{33}N_4O_3Si_2Cd$
formula weight	520.05	606.13
space group	*P-1*	*Pbca*
a / Å	9.7373(18)	15.6969(13)
b / Å	10.474(2)	11.9352(10)
c / Å	13.688(3)	29.663(2)
α / °	90.193(3)	90
β / °	91.496(3)	90
γ / °	114.582	90
V / Å^3	1268.9(3)	5557.3(8)
Z	2	8
temperature (K)	130(2)	130(2)
radiation (λ, Å)	0.71073	0.71073
ρ (calcd.), g cm^{-3}	1.361	1.449
μ (Mo Kα), mm^{-1}	1.092	0.905
θ max, deg.	31.56	30.68
no. of data collected	21371	85982
no. of data used	8306	8555
no. of parameters	295	295
R_1 [$I > 2\sigma(I)$]	0.0561	0.0435
wR_2 [$I > 2\sigma(I)$]	0.1109	0.0907
R_1 [all data]	0.13239	0.0732
wR_2 [all data]	0.1364	0.0997
GOF	1.001	1.047
R_{int}	0.0719	0.0851

5.7 References and Notes

(1) (a) Sattler, W.; Parkin, G. *J. Am. Chem. Soc.* **2011**, *133*, 9708-9711.

(b) Sattler, W.; Parkin, G. *Chem. Sci.* **2012**, *3*, 2015-2019.

(c) Sattler, W.; Parkin, G. *J. Am. Chem. Soc.* **2012**, *134*, 17462-17465.

(2) Bhasin, K. K.; Singh, J. *J. Organomet. Chem.* **2002**, *658*, 71-76.

(3) Verkade, J. G. Coord. Chem. Rev. **1994**, *137*, 233-295.

(4) Al-Harbi, A.; Rong, Y.; Parkin, G. manuscript in preparation.

(5) (a) Tsuda, T.; Washita, H.; Saegusa, T. *J. Chem. Soc. Chem. Commun.* **1977**, 468-469.

(b) Sita, L. R.; Babcock, J. R.; Xi, R. *J. Am. Chem. Soc.* **1996**, *118*, 10912-10913.

(c) Wannagat, U.; Kuckertz, H.; Kruger, C.; Pump, J. *Z. Anorg. Allg. Chem.* **1964**, *333*, 54-61.

(d) Cheng, M.; Moore, D. R.; Reczek, J. J.; Chamberlain, B. M.; Lobkovsky, E. B.; Coates, G. W. *J. Am. Chem. Soc.* **2001**, *123*, 8738-8749.

(e) Andersen, R. A. *Inorg. Chem.* **1979**, *18*, 2928-2932.

(f) Phull, H.; Alberti, D.; Korobkov, I.; Gambarotta, S.; Budzelaar, P. H. M. *Angew. Chem. Int. Edit.* **2006**, *45*, 5331-5334.

(g) Dickie, D. A.; Ulibarri-Sanchez, III, R. P.; Jarman, P. J.; Kemp, R. A. *Polyhedron* **2013**, *58*, 92-98.

(6) For a recent example of isocyanate formation from the reaction of a cyclic disilylamide derivative with CO_2, see: Stewart, C. A.; Dickie, D. A.; Parkes, M. V.; Saria, J. A.; Kemp, R. A. *Inorg. Chem.* **2010**, *49*, 11133-11141.

(7) $\tau_5 = [\beta - \alpha]/60$, where α and β are the two largest angles. See: Addison, A. W.; Rao, T. N.; Reedijk, J.; Vanrijn, J.; Verschoor, G. C. *J. Chem. Soc. Dalton Trans.* **1984**, 1349-1356.

(8) For example, the covalent radii of sulfur and selenium are 1.05 Å and 1.20 Å, respectively. See: Cordero, B.; Gómez, V.; Platero-Prats, A. E.; Revés, M.; Echeverría, J.; Cremades, E.; Barragán, F.; Alvarez, S. *Dalton Trans.* **2008**, 2832–2838.

(9) For example, the average C–S–C and C–Se–C bond angles for two coordinate chalcogen derivatives listed in the Cambridge Structural Database (version 5.34) are 97.8˚ and 95.8˚, respectively.

(10) de Castro, V. D.; de Lima, G. M.; Filgueiras, C. A. L.; Gambardella, M. T. P. *J. Mol. Struct.* **2002**, *609*, 199-203.

(11) For examples of zinc hydrosulfido compounds, see:

(a) Melnick, J. G.; Docrat, A.; Parkin, G. *Chem. Commun.* **2004**, 2870-2871.

(b) Galardon, E.; Tomas, A.; Roussel, P.; Artaud, I. *Eur. J. Inorg. Chem.* **2011**, 3797-3801.

(c) Galardon, E.; Tomas, A.; Selkti, M.; Roussel, P.; Artaud, I. *Inorg. Chem.* **2009**, *48*, 5921-5927.

(d) Spiropulos, N. G.; Standley, E. A.; Shaw, I. R.; Ingalls, B. L.; Diebels, B.; Krawczyk, S. V.; Gherman, B. F.; Arif, A. M.; Brown, E. C. *Inorg. Chim. Acta* **2012**, *386*, 83-92.

(e) Ruf, M.; Vahrenkamp, H. *Inorg. Chem.* **1996**, *35*, 6571-6578.

(f) Rombach, M.; Vahrenkamp, H., *Inorg. Chem.* **2001**, *40*, 6144-6150.

(g) Ibrahim, M. M.; Seebacher, J.; Steinfeld, G.; Vahrenkamp, H. *Inorg. Chem.* **2005**, *44*, 8531-8538.

(h) Han, R.; Gorrell, I. B.; Looney, A. G.; Parkin, G., *J. Chem. Soc. Chem. Commun.* **1991**, 717-719.

(i) Looney, A.; Han, R. Y.; Gorrell, I. B.; Cornebise, M.; Yoon, K.; Parkin, G.; Rheingold, A. L. *Organometallics* **1995**, *14*, 274-288.

(12) For a review of metal hydrosulfido compounds, see: Kuwata, S.; Hidai, M. *Coord. Chem. Rev.* **2001**, *213*, 211-305.

(13) For unsuccessful efforts to obtain a zinc hydrosulfido compound using an azamacrocyclic ligand, see: Notni, J.; Görls, H.; Anders, E. *Eur. J. Inorg. Chem.* **2006**, 1444-1455.

(14) (a) Ruf, M.; Vahrenkamp, H. *J. Chem. Soc. Dalton Trans.* **1995**, 1915-1916.

(b) Reference 11i.

(15) For an example of a polynuclear zinc complex that features μ^3–sulfido bridges, see: Khadka, C. B.; Eichhofer, A.; Weigend, F.; Corrigan, J. F. *Inorg. Chem.* **2012**, *51*, 2747-2756.

(16) Structurally characterized alkyl or aryl hydrosulfido compounds are not common. For some examples, see:

(a) Ozawa, Y.; Demiguel, A. V.; Isobe, K. *J. Organomet. Chem.* **1992,** *433*, 183-188.

(b) Goto, K.; Shimo, I.; Kawashima, T. *Bull. Chem. Soc. Jpn.* **2003,** *76*, 2389-2394.

(c) Liang, H. C.; Shapley, P. A. *Organometallics* **1996,** *15*, 1331-1333.

(d) Morton, M. S.; Lachicotte, R. J.; Vicic, D. A.; Jones, W. D. *Organometallics* **1999,** *18*, 227-234.

(e) Singh, S.; Bhattacharya, S. *Inorg. Chim. Acta* **2011,** *367*, 230-232.

(f) Saito, M.; Hashimoto, H.; Tajima, T.; Ikeda, M. *J. Organomet. Chem.* **2007,** *692*, 2729-2735.

(17) Cambridge Structural Database (Version 5.34). *3D Search and Research Using the Cambridge Structural Database*, Allen, F. H.; Kennard, O. *Chemical Design Automation News* **1993**, *8* (1), pp 1 & 31-37.

(18) $\tau_4 = [360 - (\alpha + \beta)]/141$, where $\alpha + \beta$ is the sum of the two largest angles. See: Yang, L.; Powell, D. R.; Houser, R. P. *Dalton Trans.* **2007**, 955-964.

(19) Average value for two crystallographically independent molecules.

(20) Structurally characterized κ^2–*S,S*–{[Tptm]H} coordination modes of the protonated ligand are known. See: Kitano, K.; Kuwamura, N.; Tanaka, R.; Santo, R.; Nishioka, T.; Ichimura, A.; Kinoshita, I. *Chem. Commun.* **2008**, 1314-1316.

(21) Halder, P.; Paine, T. K. *Inorg. Chem.* **2011**, *50*, 708-710.

(22) Halder, P.; Paine, T. K. *Ind. J. Chem.* **2011**, *50*, 1394-1402.

(23) (a) Raper, E. S. *Coord. Chem. Rev.* **1996**, *153*, 199-255.

(b) Raper, E. S. *Coord. Chem. Rev.* **1997**, *165*, 475-567.

(c) Akrivos, P. D. *Coord. Chem. Rev.* **2001**, *213*, 181-210.

(24) (a) Khasnis, D. V. V.; Buretea, M.; Emge, T. J.; Brennan, J. G. *J. Chem. Soc. Dalton Trans.* **1995**, 45-48.

(b) Kienitz, C. O.; Thone, C.; Jones, P. G. *Inorg. Chem.* **1996**, *35*, 3990-3997.

(c) Chopra, N.; Damude, L. C.; Dean, P. A. W.; Vittal, J. J. *Can. J. Chem.* **1996**, *74*, 2095-2105.

(d) Narayan, S.; Jain, V. K.; Varghese, B. *J. Chem. Soc. Dalton Trans.* **1998**, 2359-2366.

(25) (a) Cheng, Y. F.; Emge, T. J.; Brennan, J. G. *Inorg. Chem.* **1994**, *33*, 3711-3714.

(b) Cheng, Y. F.; Emge, T. J.; Brennan, J. G. *Inorg. Chem.* **1996**, *35*, 342-346.

(26) (a) Sharma, R. K.; Kedarnath, G.; Wadawale, A.; Jain, V. K.; Vishwanadh, B. *Inorg. Chim. Acta* **2011**, *365*, 333-339.

(b) Sharma, R. K.; Kedarnath, G.; Wadawale, A.; Betty, C. A.; Vishwanadh, B.; Jain, V. K. *Dalton Trans.* **2012**, *41*, 12129-12138.

(c) Sharma, R. K.; Kedarnath, G.; Jain, V. K.; Wadawale, A.; Pillai, C. G. S.; Nalliath, M.; Vishwanadh, B. *Dalton Trans.* **2011**, *40*, 9194-9201.

(27) Jaguar 7.6 and 7.7, Schrödinger, LLC, New York, NY 2009 and 2010.

(28) (a) McNally, J. P.; Leong, V. S.; Cooper, N. J. in *Experimental Organometallic Chemistry*, Wayda, A. L.; Darensbourg, M. Y., Eds.; American Chemical Society: Washington, DC, 1987; Chapter 2, pp 6-23.

(b) Burger, B.J.; Bercaw, J. E. in *Experimental Organometallic Chemistry*; Wayda, A. L.; Darensbourg, M. Y., Eds.; American Chemical Society: Washington, DC, 1987; Chapter 4, pp 79-98.

(c) Shriver, D. F.; Drezdzon, M. A.; *The Manipulation of Air-Sensitive Compounds*, 2nd Edition; Wiley-Interscience: New York, 1986.

(29) Fulmer, G. R.; Miller, A. J. M.; Sherden, N. H.; Gottlieb, H. E.; Nudelman, A.; Stoltz, B. M.; Bercaw, J. E.; Goldberg, K. I. *Organometallics* **2010**, *29*, 2176–2179.

(30) Laube, J.; Jäger, S.; Thöne, C. *Eur. J. Inorg. Chem.* **2001,** *2001*, 1983–1992.

(31) Bochmann, M.; Bwembya, G. Webb, K. J. *Inorganic Syntheses*; Cowley, A. H., Ed.; John Wiley & Sons, Inc.: Hoboken, NJ, USA, 1996; Vol. 31, pp. 19–24.

(32) (a) Sheldrick, G. M. SHELXTL, An Integrated System for Solving, Refining and Displaying Crystal Structures from Diffraction Data; University of Göttingen, Göttingen, Federal Republic of Germany, 1981.

(b) Sheldrick, G. M. *Acta Cryst.* **2008**, *A64*, 112-122.

(33) (a) Becke, A. D. *J. Chem. Phys.* **1993**, *98*, 5648-5652.

(b) Becke, A. D. *Phys. Rev. A* **1988**, *38*, 3098-3100.

(c) Lee, C. T.; Yang, W. T.; Parr, R. G. *Phys. Rev. B* **1988**, *37*, 785-789.

(d) Vosko, S. H.; Wilk, L.; Nusair, M. *Can. J. Phys.* **1980**, *58*, 1200-1211.

(e) Slater, J. C. *Quantum Theory of Molecules and Solids, Vol. 4: The Self-Consistent Field for Molecules and Solids*; McGraw-Hill: New York, 1974.

(34) (a) Hay, P. J.; Wadt, W. R. *J. Chem. Phys.* **1985**, *82*, 270-283.

(b) Wadt, W. R.; Hay, P. J. *J. Chem. Phys.* **1985**, *82*, 284-298.

(c) Hay, P. J.; Wadt, W. R. *J. Chem. Phys.* **1985**, *82*, 299-310.

(35) Klayman, D. L.; Griffin, T. S. *J. Am. Chem. Soc.* **1973**, *95*, 197–199.

(36) Laube, J.; Jäger, S.; Thöne, C. *Eur. J. Inorg. Chem.* **2001,** *2001*, 1983–1992.

CHAPTER 6

Synthesis, Structure and Reactivity of Allyl-*tris*(3-t-Butylpyrazolyl)borato Lithium

Table of Contents

6.1 Introduction

6.1.1 Development and Application of *Tris*(pyrazolyl)borato Ligands

Since their introduction in 1966,[1] *tris*(pyrazolyl)borato (Tp) ligands have found widespread application in coordination chemistry.[2,3] Their complexes have made important contributions in numerous areas, such as modeling of metallo-enzymes,[4] catalysis,[5] and material science.[6] The popularity of the Tp systems stems from the fact that their electronic and steric features can be tuned easily by attaching different substituents to the 3-, 4- and 5-positions of the pyrazolyl rings.[7] Also, the functional group on the central boron atom is not limited to hydrogen,[8] giving further flexibility to the ligand system.

6.1.2 Immobilization of Tp Complexes

Regarding the various applications of [Tp] compounds in catalysis,[5] it is of interest to graft this particular type of ligand to polymers or substrates, since the immobilization of homogeneous catalysts has its advantages.[9,10] For example, it facilitates the separation of products, simplifies the recovery and recycling process of the catalysts. For this purpose, we synthesized a new [Tp] ligand featuring an allyl functional group on the boron atom in [Tp^{Bu^t}] with the notion that the allyl group would provide a means to connect the [Tp^{Bu^t}] ligand to a polymer, such as mercaptopropyl-terminated polydimethylsiloxane (Scheme 1). For example, we considered that the attachment could be achieved *via* addition of an S–H group, i.e. a thiol-ene reaction, a transformation that is highly efficient and amenable to a variety of substrates.[11]

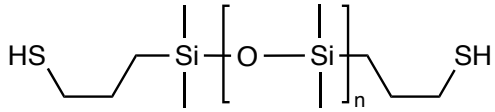

Scheme 1. Structure of mercaptopropyl terminated polydimethylsiloxane (5000 Mw)

Thiol–ene coupling can be achieved by either: (*i*) a free-radical addition to carbon–carbon double bonds; (*ii*) a catalyzed Michael addition to electron-deficient carbon–carbon double bonds (Scheme 2). Both types are very efficient, while the radical pathway is more appealing to us because there are examples in literature[12,13,14] reporting light-mediated thiol–ene radical reactions, which effectively combine the classical benefits of click reactions with the advantages of a photoinitiated process, resulting in a powerful method for chemical synthesis.

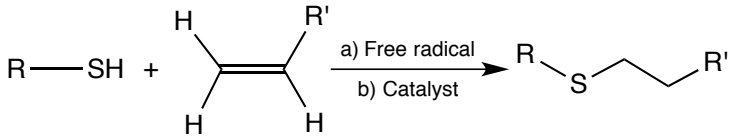

Scheme 2. General thiol–ene coupling reactions.

In this chapter, we report the synthesis and structural characterization of a Tp ligand with an allyl substituent on the boron atom. From examination of compounds in Cambridge Structural Database,[15] the [allylTp$^{Bu^t}$]Li we obtained is the first structurally characterized compound of its kind, though a similar [allylTp] complex, namely [allylTp]K[16,17] has been reported in 2006. We also studied the reactivity of the [allylTp$^{Bu^t}$]Li complex towards ethanethiol, which provides a simple model for immobilization of [Tp] metal compounds to the –SH functionalized polymers or surfaces.

6.2 The Allyl-*Tris*(3-t-Butylpyrazolyl)borato Lithium

Allyl-*tris*(3-t-butylpyrazolyl)borato lithium was synthesized in a way that is illustrated in Scheme 3. The molecular structure has been determined by X-ray diffraction, as illustrated in Figure 1. The three-coordinated lithium center adopts a trigonal pyramidal geometry.[18]

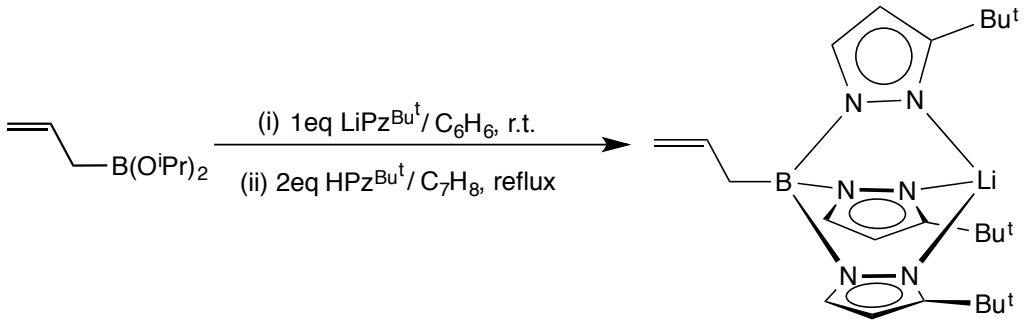

Scheme 3. Synthesis of [allylTp$^{Bu^t}$]Li

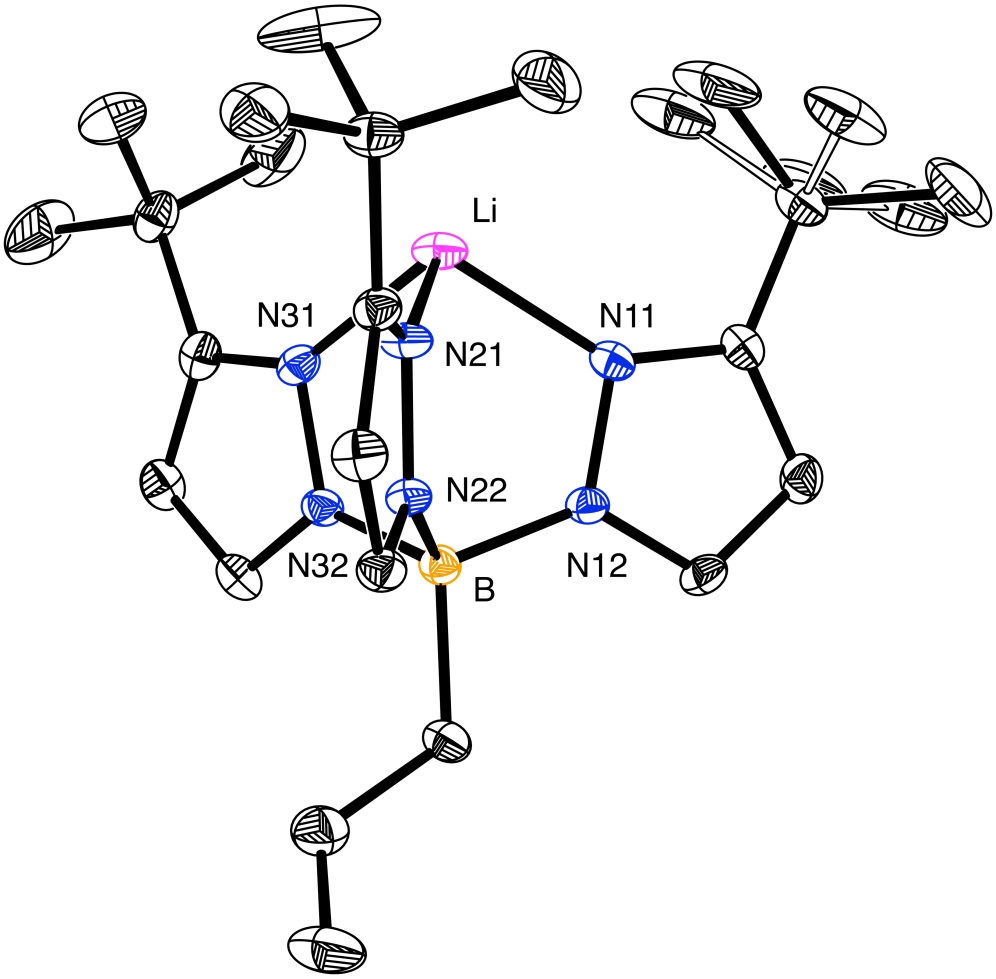

Figure 1. Molecular structure of [allylTp$^{Bu^t}$]Li (one of the t-butyl group on pyrazolyl ring is disordered).

It is of interest to compare the [Tp$^{Bu^t}$] lithium compounds with different substituents on the central boron atom. Therefore, selected bond lengths and bond angles of [RB(pz$^{Bu^t}$)$_3$]Li (R = H, Ph, allyl) are listed in Table 1. It is worth noting that the structural differences among the three compounds are small, *i.e.* the substituent on the boron atom does not have a significant influence on the electronic property of [B(pz$^{Bu^t}$)$_3$] motif. Studies carried out by former group

member, Wesley Sattler, show that [allylTp$^{Bu^t}$]Li can be converted to [allylTp$^{Bu^t}$]Tl and [allylTp$^{Bu^t}$]ZnMe species.[19]

Table 1. Selected bond lengths and angles of [allylTp$^{Bu^t}$]Li, [Tp$^{Bu^t}$]Li and [PhTp$^{Bu^t}$]Li.

	[Tp$^{Bu^t}$]Li	**[allylTp$^{Bu^t}$]Li**	**[PhTp$^{Bu^t}$]Li**
d(Li–N)/Å	1.982(4)	1.933(4)	1.934
	1.994(3)	1.956(4)	1.977
	1.994(3)	1.964(4)	1.979
d_{av}(Li–N)/Å	1.99	1.95	1.96
N–Li–N/°	96.41(16)	96.54(17)	95.12
	98.03(13)	96.58(17)	97.26
	98.03(13)	96.58(17)	97.51
$(N–Li–N)_{av}$/°	97.5	96.6	96.6

6.3 Reactivity of [allylTp$^{Bu^t}$]Li Towards Ethanethiol

To study the reactivity of the carbon–carbon double bond in the allyl group in [allylTp$^{Bu^t}$]Li towards thiols, we use ethanethiol as a model of polymer chains with –SH terminals. Two samples of [allylTp$^{Bu^t}$]Li and excess ethanethiol in benzene solutions were prepared. One of them had 2% of benzophenone, which is a common photoinitiator, and the other one did not. Both samples were placed under a 350 nm UV light for 24 h. The reactions were monitored by ^{1}H NMR spectroscopy, thereby revealing the formation of products. It is interesting to observe that the one with photo initiator actually produced a mixture of different species besides [$CH_3CH_2S(CH_2)_3$Tp$^{Bu^t}$]Li, while the one without photoinitiator only

quantitatively produced $[CH_3CH_2S(CH_2)_3Tp^{Bu^t}]Li$.[20] Therefore, the carbon–carbon double bond in the $[allylTp^{Bu^t}]Li$ complex is reactive towards the –SH group under UV light and no photo initiator is required to initiate the photochemistry reaction. $[CH_3CH_2S(CH_2)_3Tp^{Bu^t}]Li$ could be separated with sufficient purity by removal of volatile components under vacuum. Attempts to crystallize the compound from different solvents were not successful.

6.4 Reactivity of $[CH_3CH_2S(CH_2)_3Tp^{Bu^t}]Li$ towards ZnI_2

$[CH_3CH_2S(CH_2)_3Tp^{Bu^t}]Li$ reacts with ZnI_2 at room temperature and the reaction was monitored by ^1H NMR spectroscopy, thereby revealing the formation of a product, which is assigned as $[CH_3CH_2S(CH_2)_3Tp^{Bu^t}]ZnI$ based on ^1H NMR spectra.

A comparison of ^1H NMR spectra before and after the reaction is shown in Figure 2. The top spectrum is the pure $[CH_3CH_2S(CH_2)_3Tp^{Bu^t}]Li$ starting material and the bottom is the one after the treatment of excess ZnI_2 to the sample at room temperature for 30 min. The most significant change in the NMR spectrum is that the peak at 1.28 ppm, which represents the protons on the t-butyl group, shifts to 1.61 ppm, thereby indicating a formation of $[CH_3CH_2S(CH_2)_3Tp^{Bu^t}]ZnI$. Attempts to crystallize the compound from different solvents were not successful.

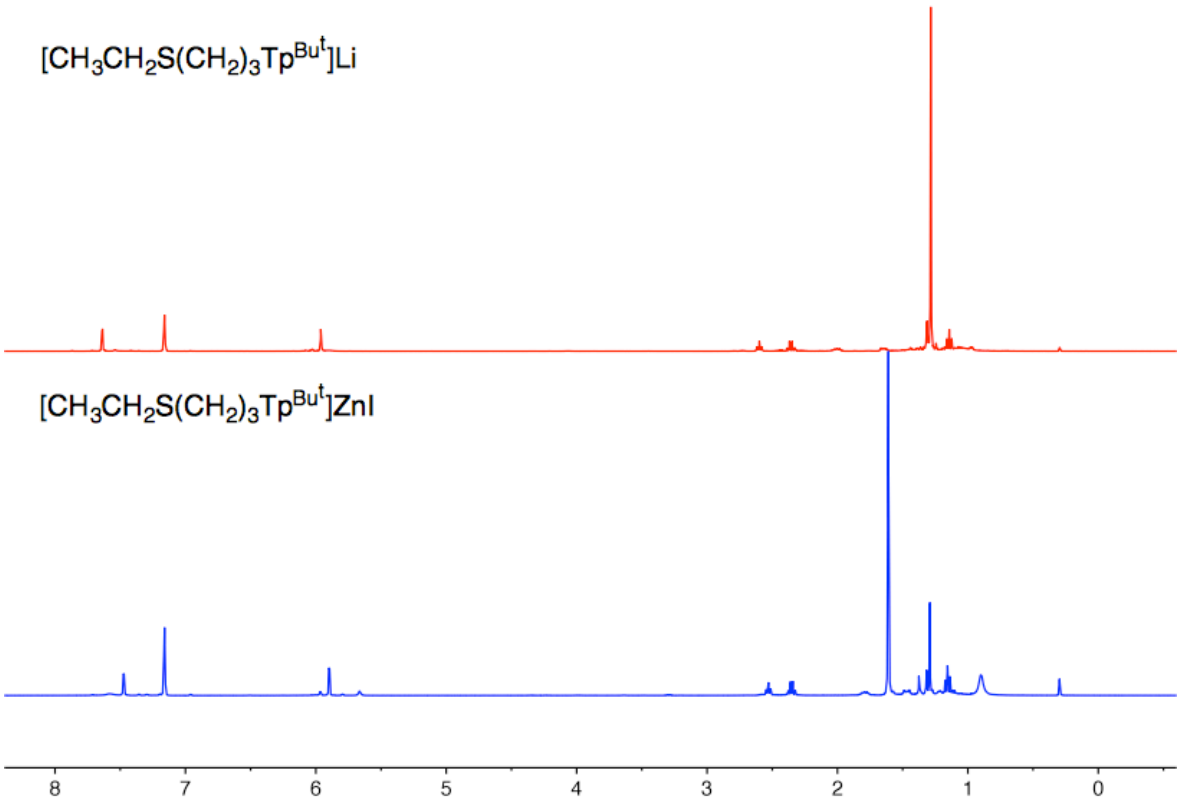

Figure 2. Comparison of ^{1}H NMR spectrum of $[CH_3CH_2S(CH_2)_3Tp^{But}]Li$ and $[CH_3CH_2S(CH_2)_3Tp^{But}]ZnI$.

6.5 Reactivity of $[CH_3CH_2S(CH_2)_3Tp^{But}]Li$ towards Polymers

The reactivity of $[CH_3CH_2S(CH_2)_3Tp^{But}]Li$ towards polyethylene glycol (PEG) and polydimethylsiloxane (PDMS) with terminal –SH group was investigated (Scheme 4). However, the attempt to graft $[CH_3CH_2S(CH_2)_3Tp^{But}]Li$ to the polymer chains were not successful. The reactions either caused decomposition of [Tp] ligand or degradation of polymer chains.

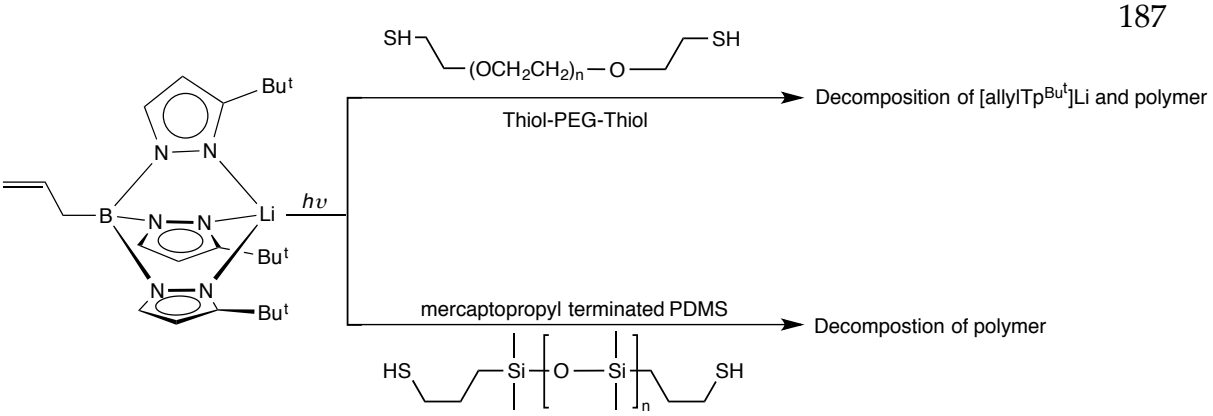

Scheme 4. Reactivity of $[CH_3CH_2S(CH_2)_3Tp^{Bu^t}]Li$ towards polymers

6.6 Summary and Conclusion

In summary, we reported the synthesis and structural characterization of a new [Tp] ligand featuring an allyl substituent on the central boron atom, namely $[allylTp^{Bu^t}]Li$. The compound reacted steadily with CH_3CH_2SH under 350 nm UV light *via* a thiol-ene click reaction. The resulting $[CH_3CH_2S(CH_2)_3Tp^{Bu^t}]Li$ complex can further react with metal halide. For example reaction of $[CH_3CH_2S(CH_2)_3Tp^{Bu^t}]Li$ with ZnI_2 produced $[CH_3CH_2S(CH_2)_3Tp^{Bu^t}]ZnI$ at room temperature. Our study provided a simple model on the immobilization of [Tp] metal complexes to the polymer chains with –SH terminals.

6.7 Experimental Section

6.7.1 General Considerations

All manipulations were performed using a combination of glovebox, high vacuum, and Schlenk techniques under a nitrogen or argon atmosphere.[21] Solvents were purified and degassed by standard procedures. NMR spectra were measured on Bruker Avance III 400 and Bruker Avance III 400SL ^1H NMR

spectra are reported in ppm relative to $SiMe_4$ ($\delta = 0$) and were referenced internally with respect to the protio solvent impurity (δ 7.16 for C_6D_5H).[22] Coupling constants are given in hertz. Mercaptopropyl terminated PDMS (5000 Mw) was purchased from Gelest. Thiol-PEG-Thiol (2kDa) was purchased from Creative PEGworks and allylB(O^iPr)$_2$ was purchased from TCI America by United Technologies Research Center, ZnI_2 (anhydrous) was purchased from Strem Chemicals. Photochemistry reactions were carried out in Professor Turro's research laboratory.

6.7.2 X-ray Structure Determinations

Single crystal X-ray diffraction data were collected on a Bruker Apex II diffractometer and crystal data, data collection and refinement parameters are summarized in Table 2. The structures were solved using direct methods and standard difference map techniques, and were refined by full-matrix least-squares procedures on F^2 with SHELXTL (Version 2008/4).[23]

6.7.3 Synthesis of AllylTp$^{Bu^t}$Li

(a) Lipz$^{Bu^t}$: 3-t-butylpyrazole (3 g, 0.024 mol) was dissolved in toluene in a medium sized Schlenk and cooled down in dry ice/acetone bath. LiBu^n (10 mL, 2.5 M in hexane) was added slowly to the toluene solution, resulting formation of white solid. The mixture was then warmed up to room temperature and stirred for 40 min. The solid was separated by filtration and dried *in vacuo*.

(b) Li[allylB(O^iPr)$_2$(pz$^{Bu^t}$)]: Lipz$^{Bu^t}$ (2.32 g, 17.8 mmol) and allylB(O^iPr)$_2$ (3.01 g, 17.9 mmol) were placed in a medium sized Schlenk and benzene (8 mL) was added slowly *via* a pipet. The Schlenk was kept in a 50°C water bath and the mixture was

stirred till all the Lipz$^{Bu^t}$ was dissolved. After that, the solution was pumped down to give a white solid, which was good for use without further purification. (c) [allylTp$^{Bu^t}$]Li: pz$^{Bu^t}$ (4.67 g, 3.7 mmol) was added to Schlenk with the Li[allylB(O^{i}Pr)$_2$(pz$^{Bu^t}$)] solid obtained from step (b). Toluene (80 mL) was added to the mixture and a Dean-Stark trap containing a KH (1.5 g, 3.8 mmol) bag was connected to the Schlenk. The reaction vessel was kept in a 130°C oil bath and reflux for 12.5 h under N_2. After this period, the mixture was cooled to room temperature and volatile components were removed under vacuum. The solid (6.85 g, 90%) obtained was light yellow and ^{1}H NMR showed that there was no impurity. ^{1}H NMR (C_6D_6): 1.28 [s, 27 H of {$CH_2CHCH_2B[N_2(CH)_2C(C_4\underline{H}_9)]_3Li$}], 2.55 [d, $^3J_{H-H}$ = 7 Hz, 2 H of {$CH_2CHC\underline{H}_2B[N_2(CH)_2C(C_4H_9)]_3Li$}], 5.13 [dd, $^3J_{H-H}$ = 2 Hz, $^4J_{H-H}$ = 10 Hz, 1 H of {$C\underline{H}_2CHCH_2B[N_2(CH)_2C(C_4H_9)]_3Li$}], 5.28 [dd, $^3J_{H-H}$ = 2 Hz, $^4J_{H-H}$ = 17 Hz, 1 H of {$C\underline{H}_2CHCH_2B[N_2(CH)_2C(C_4H_9)]_3Li$}], 5.92 [d, $^3J_{H-H}$ = 2 Hz, 3 H of {$CH_2CHCH_2B[N_2(C\underline{H})_2C(C_4H_9)]_3Li$}], 6.37 [m, 1 H of {$CH_2C\underline{H}CH_2B[N_2(CH)_2C(C_4H_9)]_3Li$}], 7.70 [d, $^3J_{H-H}$ = 2 Hz, 3 H of {$CH_2CHCH_2B[N_2(C\underline{H})_2C(C_4H_9)]_3Li$}].

6.7.4 Synthesis of [$CH_3CH_2S(CH_2)_3Tp^{Bu^t}$]Li

[allylTp$^{Bu^t}$]Li (10 mg, 0.02 mmol) and ethanethiol (1.73 μL, 0.02 mmol) were dissolved in benzene in an NMR tube equipped with a J. Young valve. The reaction mixture was placed under 350 nm UV light for 24 h. After this period, the sample was lyophilized, resulting in a sticky oil. ^{1}H NMR (C_6D_6): 1.14 [s, 3 H of {$C\underline{H}_3CH_2SCH_2CH_2CH_2B[N_2(CH)_2C(C_4H_9)]_3Li$}], 1.28 [s, 27 H of {$CH_3CH_2SCH_2CH_2CH_2B[N_2(CH)_2C(C_4\underline{H}_9)]_3Li$}], 1.64 [m, 2 H of {$CH_3CH_2SCH_2C\underline{H}_2CH_2B[N_2(CH)_2C(C_4H_9)]_3Li$}], 2.01 [m, 2 H of {$CH_3CH_2SCH_2CH_2C\underline{H}_2B[N_2(CH)_2C(C_4H_9)]_3Li$}], 2.36 [q, $^3J_{H-H}$ = 7 Hz, 2 H of

{$CH_3C\underline{H}_2SCH_2CH_2CH_2B[N_2(CH)_2C(C_4H_9)]_3Li$}], 2.60 [t, $^3J_{H–H}$ = 7 Hz, 2 H of {
$CH_3CH_2SC\underline{H}_2CH_2CH_2B[N_2(CH)_2C(C_4H_9)]_3Li$}], 5.96 [d, $^3J_{H–H}$ = 2 Hz, 3 H of
{$CH_3CH_2SCH_2CH_2CH_2B[N_2(C\underline{H})_2C(C_4H_9)]_3Li$}], 7.64 [d, $^3J_{H–H}$ = 2 Hz, 3 H of
{$CH_3CH_2SCH_2CH_2CH_2B[N_2(C\underline{H})_2C(C_4H_9)]_3Li$}].

6.7.5 Synthesis of $[CH_3CH_2S(CH_2)_3Tp^{Bu^t}]ZnI$

[allylTp^{Bu^t}]Li (10 mg, 0.02 mmol) and ethanethiol (1.73 μL, 0.02 mmol) were dissolved in benzene in an NMR tube equipped with a J. Young valve. The reaction mixture was placed under 350 nm UV light for 24 h. After this period, the sample was lyophilized, resulting in a sticky oil. ZnI_2 (5 mg, 0.02 mmol) was dissolved in d_6-benzene (*ca.* 1mL) and added to the NMR tube with $[CH_3CH_2S(CH_2)_3Tp^{Bu^t}]Li$. The reaction was monitored by ^1H NMR spectroscopy, thereby demonstrating a formation of $[CH_3CH_2S(CH_2)_3Tp^{Bu^t}]ZnI$ at room temperature. The reaction completed in *ca.* 30 min. The mixture was filtered and the solution was lyophilized to give a white greasy solid. ^1H NMR (C_6D_6): 1.16 [s, 3 H of {$C\underline{H}_3CH_2SCH_2CH_2CH_2B[N_2(CH)_2C(C_4H_9)]_3ZnI$}], 1.36 [m, 2 H of
{$CH_3CH_2SCH_2C\underline{H}_2CH_2B[N_2(CH)_2C(C_4H_9)]_3ZnI$}], 1.61 [s, 27 H of
{$CH_3CH_2SCH_2CH_2CH_2B[N_2(CH)_2C(C_4\underline{H}_9)]_3ZnI$}], 1.78 [m, 2 H of
{$CH_3CH_2SCH_2CH_2C\underline{H}_2B[N_2(CH)_2C(C_4H_9)]_3ZnI$}], 2.35 [q, $^3J_{H–H}$ = 7 Hz, 2 H of
{$CH_3C\underline{H}_2SCH_2CH_2CH_2B[N_2(CH)_2C(C_4H_9)]_3ZnI$}], 2.53 [t, $^3J_{H–H}$ = 7 Hz, 2 H of {
$CH_3CH_2SC\underline{H}_2CH_2CH_2B[N_2(CH)_2C(C_4H_9)]_3ZnI$}], 5.90 [d, $^3J_{H–H}$ = 2 Hz, 3 H of
{$CH_3CH_2SCH_2CH_2CH_2B[N_2(C\underline{H})_2C(C_4H_9)]_3ZnI$}], 7.48 [d, $^3J_{H–H}$ = 2 Hz, 3 H of
{$CH_3CH_2SCH_2CH_2CH_2B[N_2(C\underline{H})_2C(C_4H_9)]_3ZnI$}].

6.8 Crystallographic Data

Table 2. Crystal, intensity collection and refinement data.

	AllylTp$^{Bu^t}$Li
lattice	Monoclinic
formula	$C_{24}H_{38}BLiN_6$
formula weight	428.35
space group	$P2_1/n$
a / Å	10.3772(13)
b / Å	16.235(2)
c / Å	15.3682(18)
α / °	90
β / °	90.707(2)
γ / °	90
V / Å^3	2589.0(5)
Z	4
temperature (K)	150(2)
radiation (λ, Å)	0.71073
ρ (calcd.), g cm^{-3}	1.099
μ (Mo Kα), mm^{-1}	0.066
θ max, deg.	30.58
no. of data collected	41573
no. of data used	7934
no. of parameters	329
R_1 [$I > 2\sigma(I)$]	0.0602
wR_2 [$I > 2\sigma(I)$]	0.0899
R_1 [all data]	0.17.76
wR_2 [all data]	0.1040
GOF	0.975
R_{int}	0.1370

6.9 References and Notes

(1) Trofimenko, S. *J. Am. Chem. Soc.* **1966**, *3*, 1842–1844.

(2) Trofimenko, S. Scorpionates. The Coordination Chemistry of Polypyrazolylborate Ligands, Imperial College Press, London, 1999.

(3) Pettinari, C. Scorpionates II: Chelating Borate Ligands, Imperial College Press, London, 2008.

(4) (a) Kitajima, N.; Fujisawa, K.; Moro-oka, Y.; Toriumi, K. *J. Am. Chem. Soc.* **1989**, *111*, 8975;

(b) Siewert, I.; Limberg, C. *Angew. Chem., Int. Ed.* **2008**, *47*, 7953

(c) Ruth, K.; Tu̇llmann, S.; Vitze, H.; Bolte, M.; Lerner, H.-W.; Holthausen, M.C.; Wagner, M. *Chem. Eur. J.* **2008**, *14*, 6754.

(5) (a) DiÅLaz-Requejo, M.M.; Pérez, P.J. *Chem. Rev.* **2008**, *108,* 3379 and references cited therein

(b) Despagnet-Ayoub, E.; Jacob, K.; Vendier, L.; Etienne, M.; Alvarez, E.; Caballero, A.; Diaz-Requejo, M.M.; Pérez, P.J. *Organometallics* **2008,** *27*, 4779

(6) McCleverty, J. A.; Ward, M. D. *Acc. Chem. Res*, **1998**, *31*, 842.

(7) Trofimenko, S. *Chem. Rev*. **1993**, *93*, 943.

(8) According to Cambridge Structural Database, 92.7% of structurally characterized compounds incorporating Tp ligands are tris(pyrazolyl)hydroborates.

(9) For examples of immobilizations of Tp metal complexes, see (a) Gil, M. P.; dos Santos, J. H. Z.; Casagrande, O. L. *J. Mol. Catal. A: Chem.* **2004**, *209*, 163–169.

(b) Casagrande, A. C. .; Tavares, T. T. D. R.; Kuhn, M. C. a; Casagrande, O. L.; dos Santos, J. H. .; Teranishi, T. *J. Mol. Catal. A: Chem.* **2004**, *212*, 267–275.

(10) Jones, C., and Yu, K., *Organometallics,* **2003**, 22, 2571-2580.

(11) Hoyle, C. E.; Bowman, C. N. *Angew. Chem. Int. Ed. Engl.* **2010**, *49*, 1540–1573.

(12) Griesbaum, K. *Angew. Chem. Int. Ed. Engl*. **1970**, *9*, 273 – 287.

(13) Jacobine A. F. in Radiation Curing in Polymer Science and Technology III

(Eds.: J. D. Fouassier, J. F. Rabek), Elsevier, London, 1993, chap. 7, pp. 219 – 268

(14) Hoyle, C. E.; Lee, T. Y.; Roper, T. J. *Polym. Sci. Part A* **2004**, *42*,5301 – 5338

(15) Cambridge Structural Database (Version 5.34). *3D Search and Research Using the Cambridge Structural Database*, Allen, F. H.; Kennard, O. *Chemical Design Automation News* **1993**, *8* (1), pp 1 & 31-37.

(16) Camerano, J.; Casado, M.; Ciriano, M.; Oro, L.*Dalton Trans.* **2006**, 5287–93.

(17) As stated in reference 16, attempts to grow crystals of [allylTp]K or [allylTp]Tl were unsuccessful.

(18) Chakrabarti, N.; Sattler, W.; Parkin, G. *Polyhedron* **2013**, *58*, 235–246.

(19) Crystal structures of these compounds have been determined by X-ray diffraction and solved by Dr. Wesley Sattler.

(20) Other photo initiators, *e.g.* 2,2-dimethyloxy-2-phenylacetophenone, were also applied but they all gave mixtures of species under same condition.

(21) (a) McNally, J. P.; Leong, V. S.; Cooper, N. J. in Experimental Organometallic Chemistry, Wayda, A. L.; Darensbourg, M. Y., Eds.; American Chemical Society: Washington, DC, 1987; Chapter 2, pp 6-23.

(b) Burger, B.J.; Bercaw, J. E. in Experimental Organometallic Chemistry; Wayda, A. L.; Darensbourg, M. Y., Eds.; American Chemical Society: Washington, DC, 1987; Chapter 4, pp 79-98.

(c) Shriver, D. F.; Drezdzon, M. A.; The Manipulation of Air-Sensitive Compounds, 2nd Edition; Wiley-Interscience: New York, 1986.

(22) Fulmer, G. R.; Miller, A. J. M.; Sherden, N. H.; Gottlieb, H. E.; Nudelman, A.; Stoltz, B. M.; Bercaw, J. E.; Goldberg, K. I. *Organometallics* **2010**, *29*, 2176–2179.

(23) (a) Sheldrick, G. M. SHELXTL, An Integrated System for Solving, Refining and Displaying Crystal Structures from Diffraction Data; University of Göttingen, Göttingen, Federal Republic of Germany, 1981.

(b) Sheldrick, G. M. *Acta Cryst*. **2008**, *A64*, 112-122.